l. 124 No. 2, March 1, 1981
mpleting Vol. 124

ISSN 0003-2670

ANALYTICA CHIMICA ACTA

International journal devoted to all branches of analytical chemistry

ELSEVIER SCIENTIFIC PUBLISHING COMPANY

ANALYTICA CHIMICA ACTA

International journal devoted to all branches of analytical chemistry
Revue internationale consacrée à tous les domaines de la chimie analytique
Internationale Zeitschrift für alle Gebiete der analytischen Chemie

PUBLICATION SCHEDULE FOR 1981 (incorporating the section on Computer Techniques and Optimization)

	J	F	M	A	M	J	J	A	S	O	N	D
Analytica Chimica Acta	123	124/1	124/2	125	126	127	128	129	130/1	130/2	131	132
Section on Computer Techniques and Optimization		133/1			133/2			133/3			133/4	

Scope. *Analytica Chimica Acta* publishes original papers, short communications, and reviews dealing with every aspect of modern chemical analysis, both fundamental and applied. The section on *Computer Techniques and Optimization* is devoted to new developments in chemical analysis by the application of computer techniques and by interdisciplinary approaches, including statistics, systems theory and operation research. The section deals with the following topics: Computerized acquisition, processing and evaluation of data. Computerized methods for the interpretation of analytical data including chemometrics, cluster analysis, and pattern recognition. Storage and retrieval systems. Optimization procedures and their application. Automated analysis for industrial processes and quality control. Organizational problems.

Submission of Papers. Manuscripts (three copies) should be submitted as designated below for rapid and efficient handling:

Papers from the Americas to: Professor Harry L. Pardue, Department of Chemistry, Purdue University, West Lafayette, IN 47907, U.S.A.

Papers from all other countries to: Dr. A. M. G. Macdonald, Department of Chemistry, The University, P.O. Box 363, Birmingham B15 2TT, England.

For the section on *Computer Techniques and Optimization:* Dr. J. T. Clerc, Universität Bern, Pharmazeutisches Institut, Sahlistrasse 10, CH-3012 Bern, Switzerland.

American authors are recommended to send manuscripts and proofs by INTERNATIONAL AIRMAIL.

Information for Authors. Papers in English, French and German are published. There are no page charges. Manuscripts should conform in layout and style to the papers published in this Volume. Authors should consult Vol. 121, p. 353 for detailed information. Reprints of this information are available from the Editors or from: Elsevier Editorial Services Ltd., Mayfield House, 256 Banbury Road, Oxford OX2 7DE (Great Britain).

Reprints. Fifty reprints will be supplied free of charge. Additional reprints (minimum 100) can be ordered. An order form containing price quotations will be sent to the authors together with the proofs of their article.

Advertisements. Advertisement rates are available from the publisher.

Subscriptions. Subscriptions should be sent to: Elsevier Scientific Publishing Company, P.O. Box 211, 1000 AE Amsterdam, The Netherlands. The section on *Computer Techniques and Optimization* can be subscribed to separately.

Publication. *Analytica Chimica Acta* (including the section on *Computer Techniques and Optimization*) appears in 11 volumes in 1981. The subscription for 1981 (Vols. 123–133) is Dfl. 1639.00 plus Dfl. 198.00 (postage) (total approx. U.S. $942.00). The subscription for the *Computer Techniques and Optimization* section only (Vol. 133) is Dfl. 149.00 plus Dfl. 18.00 (postage) (total approx. U.S. $86.00). Journals are sent automatically by airmail to the U.S.A. and Canada at no extra cost and to Japan, Australia and New Zealand for a small additional postal charge. All earlier volumes (Vols. 1–121) except Vols. 23 and 28 are available at Dfl. 164.00 (U.S. $84.00), plus Dfl. 13.00 (U.S. $6.50) postage and handling, per volume.

Claims for issues not received should be made within three months of publication of the issue, otherwise they cannot be honoured free of charge.

Customers in the U.S.A. and Canada who wish to obtain additional bibliographic information on this and other Elsevier journals should contact Elsevier/North Holland Inc., Journal Information Center, 52 Vanderbilt Avenue, New York, NY 10017. Tel: (212) 867-9040.

Analytica Chimica Acta, 124 (1981) 245—258

DEVELOPMENT AND CHARACTERIZATION OF A 9-mm INDUCTIVELY-COUPLED ARGON PLASMA SOURCE FOR ATOMIC EMISSION SPECTROMETRY

A. D. WEISS, R. N. SAVAGE and G. M. HIEFTJE*

Department of Chemistry, Indiana University, Bloomington, IN 47405 (U.S.A.)

(Received 8th August 1980)

SUMMARY

A new 9-mm (i.d.) inductively-coupled plasma (ICP) torch is described which supports a stable, analytically useful plasma at less than 500 W of r.f. power and 7 l min^{-1} total argon gas flow. Detection limits, working curves and other analytical characteristics of the new device are compared with those of both a miniature (13-mm i.d.) and conventional (19-mm i.d.) ICP. Although temperatures of the new plasma are somewhat lower than those in the larger plasmas, the new system offers promise for future, miniaturized ICP instruments.

The current acceptance of the inductively-coupled plasma (ICP) has been stimulated by a number of favorable performance characteristics [1—6]. However, the high initial and operating costs and large physical dimensions of such devices have limited their use mostly to larger laboratory facilities with high sample throughput. In order to expand the use of ICP systems, numerous workers have focussed upon improving the plasma efficiency by reducing both its power and gas-flow requirements.

Several new torch designs have been introduced which operate on lower power and argon gas consumption without sacrificing the analytical capabilities of the ICP. A substantial reduction in argon consumption has been realized by employing water rather than gas for cooling the outer tube of the torch [7]. The water-cooled plasma could be sustained on as little as 2 l min^{-1} argon, but yielded low sensitivity. Allemand and Barnes [8] used computer modelling to design torches which not only consumed less gas, but also ignited more easily. Genna et al. [9], by modifying the tangential coolant tube inlet of a torch, were able to produce higher swirl velocities and thereby allow the plasma to be sustained at a 30—40% lower argon flow rate. This latter modification also improved the discharge performance of the plasma.

An alternative approach toward reducing the argon consumption and power requirement of an ICP has been to decrease the size of the torch. Savage and Hieftje [1] have described a reduced-size ICP which operates at less than 1 kW of r.f. power and an argon flow of 8 l min^{-1}. Significantly,

these economies have been realized without degrading analytical performance. There appears to be no fundamental reason why a further reduction in the size of the ICP could not be achieved. Allemand et al. [10] have reported the development and characterization of both 13-mm and 9-mm ICP torches. The 13-mm ICP performed similarly to conventional ICP's, but with 20% lower argon consumption and 23% less r.f. power. The 9-mm ICP yielded poorer detection limits, particularly at lower r.f. power levels (700 W). Other performance characteristics of the 9-mm ICP were not discussed in the communication.

In the present study, a new 9-mm torch is reported which supports a plasma at approximately 1/3 the r.f. power and less than half the argon flow of a conventional torch. Although the resulting plasma yields somewhat greater interelement interferences than its larger counterpart, it offers excellent sensitivity and linearity. Moreover, with its low operating requirement (500 W, 7 l Ar min^{-1}), it suggests the future development of compact, inexpensive instrumentation for ICP spectrometry.

Preliminary considerations on the selection of plasma size and operating power

It is appropriate to ask the degree to which the ICP can be reduced in size and yet remain a viable analytical tool. Although several considerations necessary to answer this question have been offered before [8, 9], a fundamental limit is posed by the "skin-effect" exhibited by all high-frequency discharges. According to the skin-effect model, most of the energy in such discharges is introduced near the outer boundary (or skin) of the plasma; the energy introduction decreases in an approximately exponential fashion toward the plasma center. As a result, the conditions (temperature, conductivity, etc.) in the plasma center do not markedly influence the coupling of r.f. energy into the discharge; this feature is responsible in part for the relative immunity of the ICP to changes in sample aerosol composition.

The distance into the plasma penetrated by the energy-coupling field is characterized by the "skin depth" which, by definition, is the depth where the r.f. energy has been reduced to 36.8% (1/e) of its surface (skin) value. For a plasma operating at 27.12 MHz, the skin depth is approximately 2 mm. Therefore, at a distance of 4 mm from the discharge surface, the r.f. energy addition should be only $(0.37)^2 = 0.13$ of its surface value. Stated differently, sample sent into the plasma a distance of 4 mm from its surface should have less than a 13% effect on energy coupling. Taking this degree of perturbation to be the maximum permissible, the plasma must have a diameter at least 8 mm greater than that of the aerosol stream sent into it. Assuming nearly laminar aerosol flow, and given the 0.75—1.0 mm sample tube found in most torches, one then calculates a minimum plasma diameter of 9 mm, the size of torch chosen for the present work.

Because it is desirable that the 9-mm plasma operates as well as a conventional one, the smaller torch was sustained at comparable power density.

Using the toroidal model for plasma volume described earlier [1] and inner and outer toroid radii of 1.5 and 3.5 mm, respectively, a plasma volume of 49 mm^3 was calculated. To produce in this discharge the same power density of 11.7 W mm^{-3} computed for larger (miniature and conventional) plasmas, an r.f. input of approximately 570 W is needed.

An empirical means of establishing the optimal ICP input power was offered by Greenfield and Burns [11] who suggested that sources be compared on the basis of the signal-to-background (S/B) ratios that they provided. Figure 1 shows the relationship between S/B and r.f. power input for the torch used in the present study. From a third-order spline fit to these data, an applied r.f. power of 570 W seems optimal.

The foregoing considerations argue that a 9-mm torch operated at an applied r.f. power near 570 W should provide the most efficient ICP design. However, practical considerations urge that even lower powers be utilized, if they are viable. In particular, extremely inexpensive r.f. power supplies of 500 W capabilities have been developed for use in amateur radio transmissions. Moreover, at power levels of 500 W and below, compact solid-state supplies can be employed. For these reasons, the new 9-mm torch was tested at an applied power of 500 W, with the anticipation that a slight worsening in analytical characteristics might result.

EXPERIMENTAL

Instrumentation

Most of the experimental system used in this study is identical to that described previously [1]. Details concerning slight alterations are discussed below.

Load coils. In order to increase both the electric field strength and the

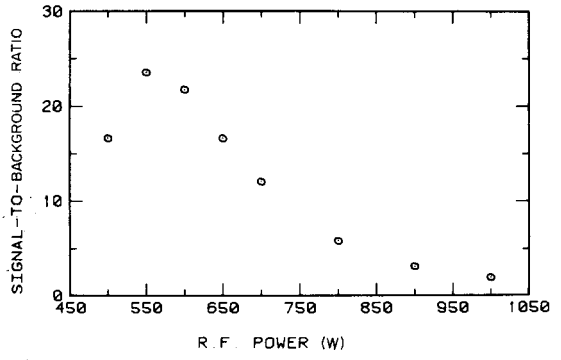

Fig. 1. Effect of applied r.f. power on the signal-to-background ratio of the new torch at the 422.7-nm Ca line. An aqueous solution of calcium (10 $\mu g\ ml^{-1}$) was aspirated into the plasma during all signal measurements; background readings were taken at the same wavelength with a blank being aspirated.

magnetic flux density needed to sustain a smaller plasma [3, 8, 12, 13], a new water-cooled load coil was constructed. The new coil consisted of four turns of 1.6-mm copper tubing, which covered a length of 1 cm in the plasma and had a diameter of 2 cm, to accommodate the smaller plasma torch. A spark from a Tesla coil served as the plasma igniter.

Plasma torch. The basic configuration of the torch used in this study, shown in Fig. 2, is the same as that in both the miniature and conventional ICP [1] except for a reduction in size. In all phases of the development and construction of this device, hydrodynamic techniques were utilized to insure proper function [14].

Several design features of the new torch are critical to its proper operation. The quartz tangential inlet tubes for both the plasma and coolant gases were constricted to 1.5 mm to increase the swirl velocity. Also, the outer diameter of the flared-out portion of the plasma tube was increased to force the coolant gas against the coolant tube and thereby shield the tube from the plasma and further increase the swirl velocity. The length (3 mm), shape, and smooth taper of the flared-out portion also proved to be critical to maintain a stable vortex.

The 0.75-mm center capillary injection tube extended from the base of the torch to the top of the plasma tube to produce a laminar jet of sample aerosol. Injection tube diameters from 0.60 to 0.75 mm were examined successfully with the larger diameter being ultimately selected. This larger diameter permits longer sample residence times in the plasma, but seems not markedly to affect r.f. energy coupling into the discharge. As mentioned earlier, the size of the sample channel is especially critical in this smaller

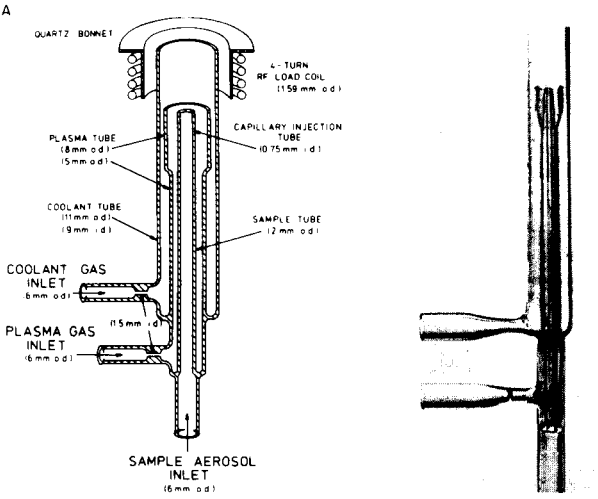

Fig. 2. Design features of 9-mm ICP torch. (A) Torch construction; except for capillary injector, all tubing is of 1-mm wall thickness. (B) Photograph of torch.

ICP because of the likelihood of the sample aerosol intercepting the energy-coupling "skin" region. The coolant tube extended at least 12 mm above the plasma tube to minimize optical background caused by entrained air components.

Nebulizer and spray chamber. Sample was introduced into the plasma by means of a cross-flow nebulizer (Model TN-1, Plasma-Therm Inc., Kresson, NJ). The nebulizer was mounted in a teflon cap which fits over one end of a dual-tube spray chamber similar to type 2C described by Schutyser and Janssens [15]. Sample solution was delivered at a rate of 0.85 ml min^{-1} by a peristaltic pump. No desolvation apparatus was employed.

Procedures

Detection limit calculations and analyses of SRM. The 9-mm ICP was utilized to establish detection limits of various elements and their concentrations in NBS standard reference materials (SRM). Operating parameters for these determinations are given in Table 1. For detection limit investigations, the viewing region in the plasma was optimized for each element by rotating the 150-mm (diameter) collection mirror. During the determination of eight elements in NBS standard 1571, a compromise viewing region was selected for the elements of interest. All standard solutions and blanks were appropriately matrix-matched for SRM analyses.

Nebulizer flow rate was limited in all cases to 0.86 l min^{-1}, above which the plasma had a tendency to extinguish; moreover, below 0.60 l min^{-1} the pneumatic nebulizer was found not to function efficiently. Five measurements of both the sample and blank were used to calculate the detection limit for each element according to the procedure outlined by Winefordner et al. [16].

Plasma excitation temperature measurements. Excitation temperatures in the 9-mm plasma were determined by using the slope or Atomic Boltzmann Plot method [17]. Background-corrected intensities were obtained for three

TABLE 1

General operating conditions for 9-mm ICP

	Plasma ignition	Plasma operation
R.f. power	1.0 kW	500 W
Ar flows (l min^{-1})		
coolant	9.8	6.4
plasma	0.42	—
nebulizer	—	0.75
Sample uptake rate	—	1.2 ml min^{-1}
Monochromator slits	width 50 μm (0.2 Å spectral band width), height 5 mm	
Time constant	1 s	

iron emission lines whose wavelengths, excitation energies, statistical weights, and relative transition probabilities have been documented elsewhere [18]. The iron(III) sulfate solution employed contained 1000 μg Fe ml^{-1}. Conditions used during temperature measurements are identical to those in Table 1 except for a narrowing of the monochromator slits to 40 μm for better resolution. The observation zone was centered at 15.5 mm above the load coils and encompassed a 4.1-mm vertical segment of the plasma.

Plasma spectral background scans. The optical arrangement used for spectral background scans has been described elsewhere [19]. With this design, the viewing region was a rectangle 8 mm high by 80 μm wide centered 11 mm above the load coils. Operating conditions for these scans are listed in Table 1. Spectral background scans were obtained while a solution containing 100 μg Mn ml^{-1} and 10 μg Ca ml^{-1} was being sprayed into the plasma.

Plasma interference experiments. Classical interferences were examined with the modified optical design and silicon intensifier tube (SIT) detection system described previously [20]. A minor alteration was the placement of a neutral-density filter in front of the entrance slit of the monochromator to prevent saturation of the detector.

Reagents

Stock solutions were prepared as described by Dean and Rains [21]. All salts and acids were reagent-grade and water used in dilution was distilled-deionized. Where necessary, solutions and blanks were matrix-matched by addition of the appropriate salt and acid.

RESULTS AND DISCUSSION

Plasma ignition and operating characteristics

Plasma ignition was relatively simple under the conditions listed in Table 1. The best method for ignition was to form initially a filamentary plasma [9, 12] at low r.f. power (300 W). Once the filamentary plasma had been formed, the r.f. power was increased to ca. 1 kW and the now conventional toroidal plasma stabilized. Next, the nebulizer gas flow was initiated [cf. Table 1]; occasionally (30% of the time), initiation of nebulizer gas flow would extinguish the plasma, requiring the ignition procedure to be repeated. Operating conditions were then set for the particular experiment.

During operation, the 9-mm plasma would readily accept sample solutions up to 10000 μg ml^{-1} without difficulty. However, it was found that salt build-up in the tip of the capillary tube occasionally required ultrasonic cleaning in a dilute acid bath.

Excitation temperature

An excitation temperature of 4000 K was measured in the 9-mm plasma at a height of 15.5 mm above the load coils. This temperature is considerably

less than the 5000 K assigned to the conventional (19-mm) ICP [1], but not significantly lower than the 4300 K of the miniature (13-mm) discharge [1]. Partly responsible for this lower temperature is the reduced power density (500 W rather than 570 W) at which the 9-mm plasma operates. Moreover, the uncertainty associated with this method of determining excitation temperatures (± 10%) lessens significantly the difference between the 9-mm ICP and the larger versions.

Background spectrum

As with the miniature and conventional ICP's, the background of the 9-mm discharge (cf. Fig. 3) was found to be complex and consisted of three types of spectral features: (1) continuum, (2) line spectra, and (3) band spectra. The detailed discussion of these features as they relate to the miniature ICP [22] is also applicable to the 9-mm ICP.

Detection limits and calibration curves

Table 2 lists detection limits for a number of elements determined in the 9-mm plasma, the 13-mm ICP, a conventional (19-mm) ICP and literature values. For every element but iron, detection limits obtained with the 9-mm torch are not significantly different from those obtained with the larger plasmas. No explanation can be given for the slightly poorer performance of the smaller discharge for iron determination.

For the conventional ICP the linearity of the calibration curves is over 5—6 orders of magnitude; similar results have been obtained with the miniature ICP [1]. Calibration curves for the 9-mm ICP, shown in Fig. 4, indicate the same wide dynamic range expected from other ICP systems. The straight lines (Fig. 4) were obtained from a least-squares fit to the original data using the equation $\log I = (a + S_a) + (b \pm S_b) \log c$, where I is the measured intensity, C is the analyte concentration (μg ml^{-1}), a and b are the intercept and slope, respectively, of the calculated line, and S_a and S_b are the calculated standard deviations in the intercept and slope. These least-squares parameters, cited in the legend to Fig. 4, reveal the near-unity slope of the calibration curves and their small departure from linearity, even over this extended concentration range. The least squares equation is also included for copper, although no plot is drawn because of overlap with the sodium curve.

Interferences

To examine the susceptibility of the 9-mm ICP to classical solute vaporization interferences, the influence of phosphate on the spatial emission profiles of the Ca I and Ca II lines was investigated. These effects were examined at two different r.f. power levels. Figure 5 (I) illustrates the influence of phosphate on the Ca I (422.7-nm) line; curve A was obtained from a solution containing 50 μg Ca ml^{-1} while curve B is from the same solution but with phosphate added at a molar ratio of 50 to 1 (PO_4^{3-}:Ca).

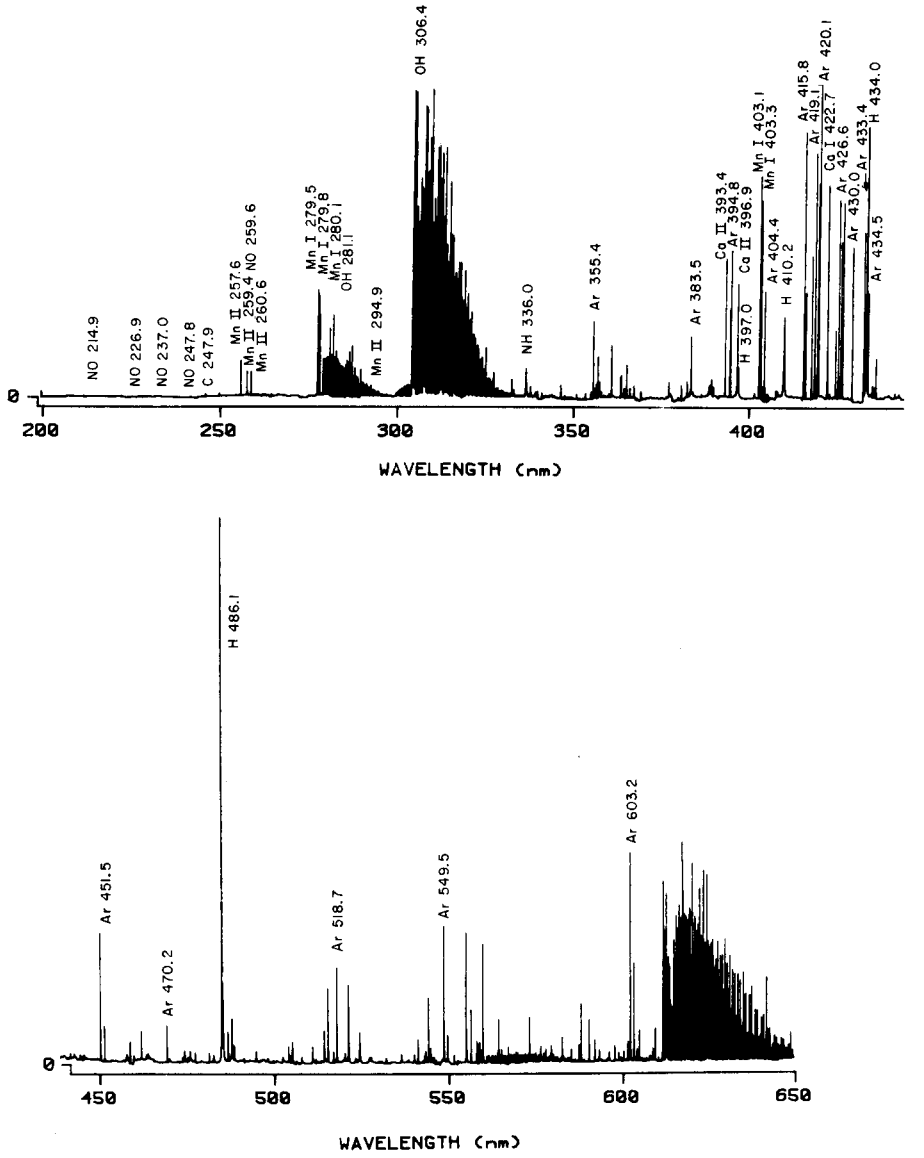

Fig. 3. Typical background spectrum of 9-mm ICP with 100 μg Mn ml^{-1} and 10 μg Ca ml^{-1} aspirated into it.

Profile X was obtained at 500 W r.f. power and profile Y at 750 W. The addition of phosphate as a matrix interference clearly causes a shift in the Ca I emission to regions higher in the plasma. Also, at higher r.f. power the profile shifts toward lower regions of the plasma. From these profiles, it is evident that, at any applied power, phosphate has an effect on Ca I emission,

TABLE 2

Detection limits (ng ml^{-1}) in various ICP sources

Element	Spectral line (nm)	9-mm ICP	13-mm ICP [1]	Conventional (19-mm) ICP [1]	19-mm torch	Reference
Al	396.15	4	5	3	2	[2]
Ba II	455.50	0.6	—[a]	—[a]	0.1	[3]
Ca II	393.37	0.08	0.07	0.04	0.07	[3]
Cd	228.80	10	42	13	30	[2]
Cu	324.75	1	8	2	1	[3]
Fe	371.99	51	10	12	5	[2]
Mg	285.21	2	6	2	0.7	[3]
Na	588.49	0.5	0.7	0.2	0.2	[3]
Ni	352.45	8	4	15	6	[2]
Pb	405.78	25	33	40	8	[2]
Zn	213.86	10	71	23	10	[12]

[a]Not determined.

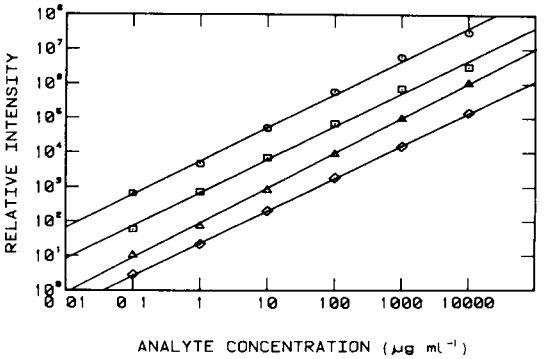

Fig. 4. Calibration curves obtained with the 9-mm ICP. Least-squares equations included for clarity (see text for discussion). (⊙) Ba II (455.4 nm) $\log I = 3.74 \pm 0.06 + (0.96 \pm 0.03) \log C$; $S_{yx} = 0.11$; (⊡) Na I (588.9 nm) $\log I = 2.82 \pm 0.08 + (0.96 \pm 0.03) \log C$; $S_{yx} = 0.14$; (△) Ba I (553.6 nm) $\log I = 1.96 \pm 0.03 + (1.01 \pm 0.02) \log C$; $S_{yx} = 0.06$; (◇) Fe I (371.9 nm) $\log I = 1.36 \pm 0.16 + (0.94 \pm 0.01) \log C$; $S_{yx} = 0.03$; Cu I (324.7 nm) $\log I = 2.77 \pm 0.11 + (0.92 \pm 0.05) \log C$; $S_{yx} = 0.20$.

but that a viewing region can be selected where the influence would be minimal or nonexistent.

The profiles in Fig. 5(II) indicate that phosphate causes a significant depression of the Ca II signal rather than just a spatial shift in intensity. Moreover, changes in applied r.f. power have little effect upon the degree of the depression. Because of this reduction in intensity, the interference of phosphate on Ca II emission cannot be nullified by spatial selection in the plasma, as was possible for the Ca I line. Although no mechanism can be offered here for these findings, the Ca I emission line would clearly offer the

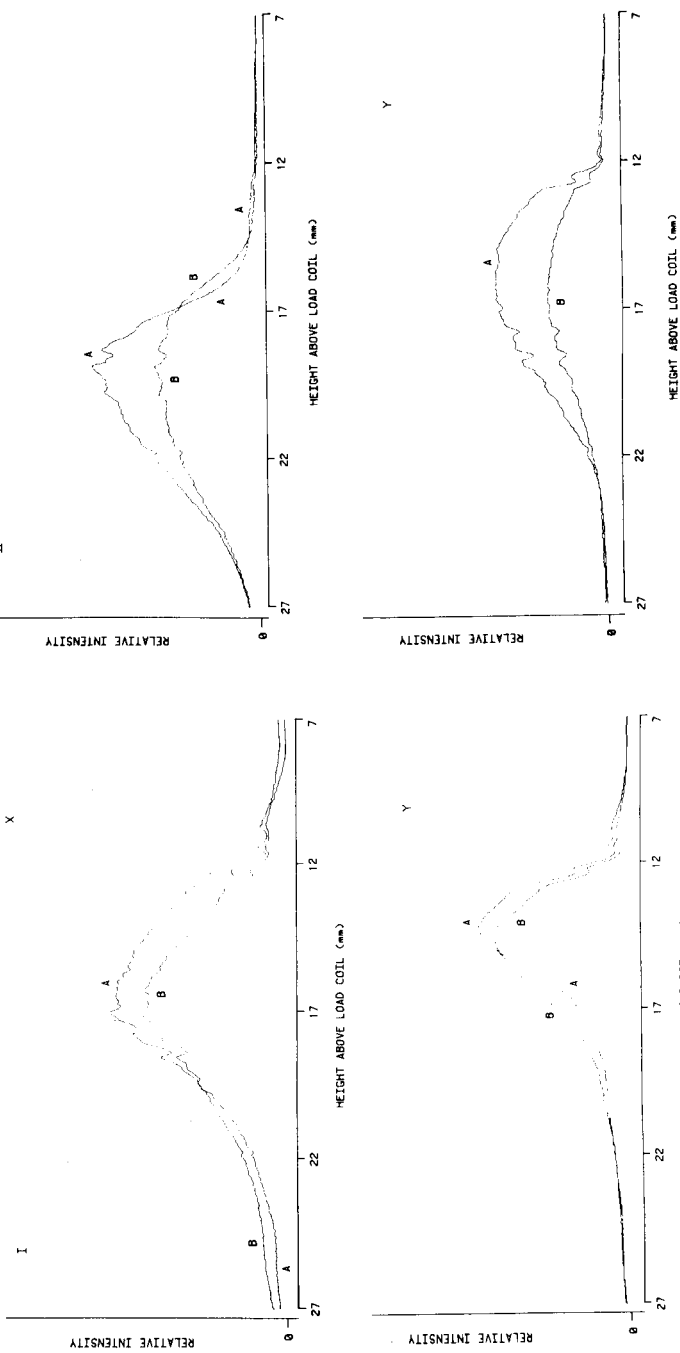

Fig. 5. Effect of phosphate on the emission profiles of (I) the Ca I (422.7 nm) line and (II) the Ca II (393.4 nm) line, with changing r.f. power levels (Frames X, 500 W; Y, 750 W). Curves A represent analyte (50 μg Ca ml^{-1}) signal and curves B analyte plus interferent (50:1 molar ratio PO_4^{3-} : Ca). Relative scales X, 10^4; Y, 10^5.

better conditions for minimizing the interference of phosphate in a practical analysis.

The effects of sodium and cesium on calcium emission were also examined in the 9-mm ICP. Profiles were obtained for both the Ca I and Ca II lines at r.f. powers of 500 W and 750 W. Figure 6(I) shows the influence of cesium on Ca I emission; in the profiles, curve A represents a 5 μg Ca ml^{-1} solution and curve B the same solution but with cesium added at a molar ratio of 140:1 (Cs:Ca). At both 500 W and 750 W, there is a significant enhancement of the Ca I emission when cesium is present although the enhancement at 750 W is somewhat lower. The influence of cesium on Ca II emission is shown in Fig. 6(II). At 500 W there is a significant depression of the Ca II emission while at 750 W there is relatively little effect (a downward shift of emission occurs as power is increased). The influence of sodium on calcium emission follows the same pattern as that discussed for cesium.

Based on these results, viewing regions can be selected to minimize the effect of an easily ionized species upon calcium. The influence on the Ca II emission is considerably less than on Ca I, particularly at higher r.f. power levels and would provide the best analytical conditions. The pattern displayed by these profiles strongly suggests that the smaller ICP suffers a greater degree of "ionization" interference than a larger ICP.

It is interesting in Figs. 5 and 6 that Ca II profiles peak higher in the plasma than Ca I profiles under any given set of operating conditions. Also, although the profiles of both lines are shifted downward by increases in r.f. power, the shift for the ion line is greater. These trends are the same as those expected from experience in an analytical flame, where ionization often lags behind atom formation and is strongly influenced by source temperature. In the ICP, however, it is doubtful that these straightforward mechanisms prevail, and further evidence will be needed to completely explain the observed behavior.

Determination of various elements in NBS SRM 1571 Orchard Leaves

To assess the performance of the 9-mm ICP system, the determination of several elements in a "real" sample was undertaken. Table 3 lists the determined values for eight elements along with the corresponding certified values for NBS SRM 1571. For all elements but manganese the values obtained were within the uncertainty range of the certified values. The manganese determination was only slightly higher than the acceptable certified value. The results indicate that the 9-mm ICP performs with good sensitivity and accuracy in the routine analysis of biological material.

Conclusions

Further reductions in the consumption of argon gas and r.f. power have been achieved through scaling down the ICP torch with little loss of analytical performance. The 9-mm torch can support a stable plasma under more economical operating conditions while accepting sample solution

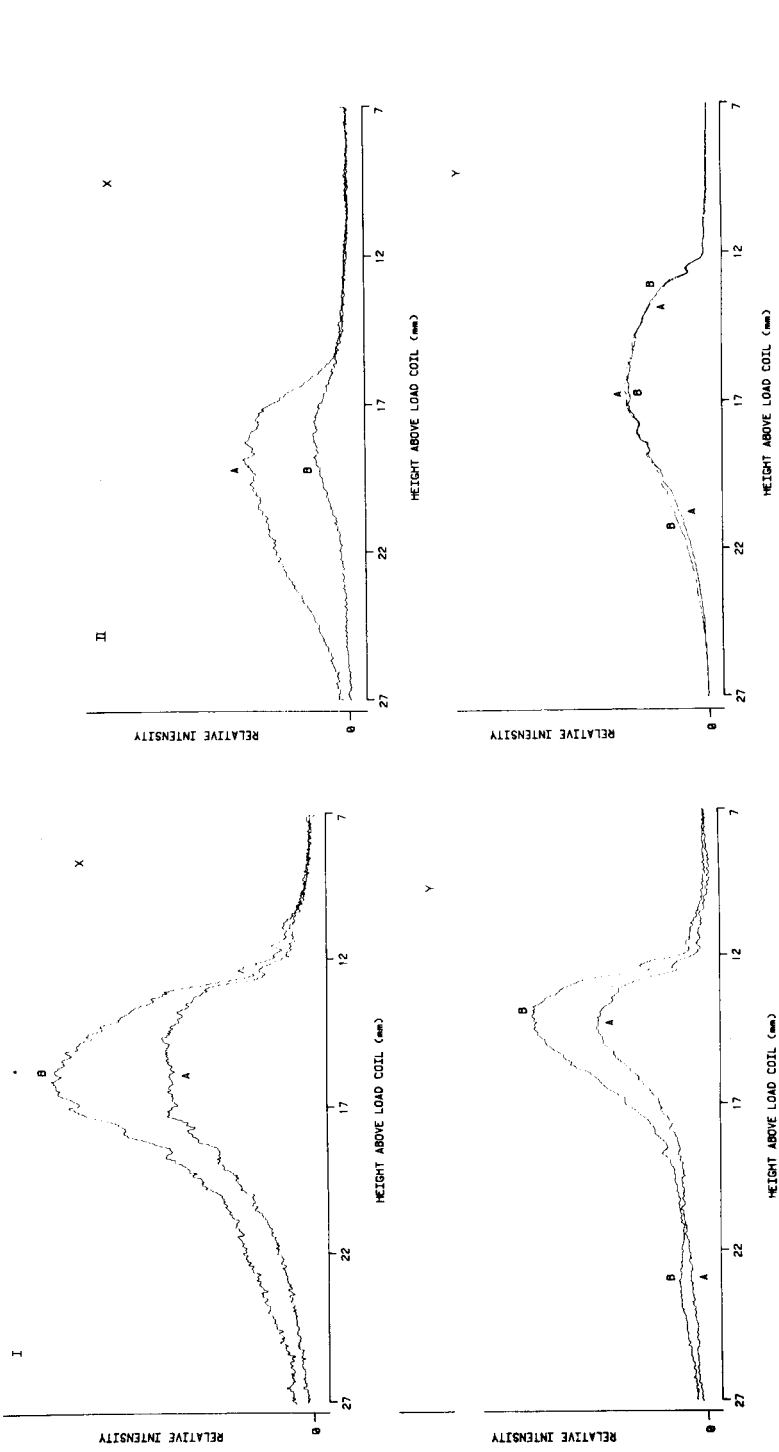

Fig. 6. Effect of cesium on the emission profiles of (I) the Ca I (422.7 nm) line and (II) the Ca II (393.4 nm) line, with changing r.f. power levels (Frames X, 500 W; Y, 750 W). Curves A represent analyte (5 μg Ca ml^{-1}) signal and curves B analyte plus interferent (140:1 molar ratio Cs:Ca). Relative scales (I) X, 10^3; (I) Y, 10^4; (II) X, 10^4; (II) Y, 10^5.

TABLE 3

Results for NBS SRM 1571 Orchard Leaves with 9-mm ICP torch[a]

Element	Present study ($\mu g\ g^{-1}$)	Certified value ($\mu g\ g^{-1}$)	Element	Present study ($\mu g\ g^{-1}$)	Certified value ($\mu g\ g^{-1}$)
Ca	2.11[b]	2.09 ± 0.03[b]	Mn	96	91 ± 4
K	1.48[b]	1.47 ± 0.03[b]	Pb	47	45 ± 3
Mg	0.64[b]	0.64 ± 0.02[b]	Zn	25	25 ± 3
Fe	313	300 ± 20	Cu	11	12 ± 1

[a]Digestion by standard methods [23]. [b]% (w/w).

readily. The ability to operate the smaller ICP stably at 500 W offers the prospect of solid-state ICP r.f. generators, which would reduce both cost and physical size of ICP-AES systems.

However, interferences in the current system are somewhat worse than in conventional plasmas. Because interferences from such disparate concomitants as Al, Cs, Na and phosphate were found to persist in the mini-ICP even at elevated r.f. power levels (750 W), they are believed to arise in part from the effect of sample components on the efficiency of energy coupling into the discharge. If this assumption is correct, operating the 9-mm ICP at higher frequencies (e.g. 40.68 MHz) should improve performace; at this higher frequency, the skin depth would be reduced and intrusion of sample material into the energy-coupling region would be lessened.

This paper is taken in part from the M.S. thesis of A. D. Weiss and from the Ph.D. thesis of R. N. Savage. The work was supported in part by the National Science Foundation through grants CHE 79-18073 and CHE 77-22152 and by the Office of Naval Research.

REFERENCES

1 R. N. Savage and G. M. Hieftje, Anal. Chem., 51 (1979) 408.
2 G. W. Dickinson and V. A. Fassel, Anal. Chem., 41 (1969) 1041.
3 V. A. Fassel and R. N. Kniseley, Anal. Chem., 46 (1974) 1110A.
4 S. Greenfield, I. L. Jones, H. McD. McGeachin and P. B. Smith, Anal. Chim. Acta, 74 (1975) 225.
5 P. W. J. M. Boumans and F. J. de Boer, Spectrochim. Acta, Part B, 27 (1972) 391.
6 P. W. J. M. Boumans, F. J. de Boer, F. J. Dahmer, H. Hoelzel and A. Meir, Spectrochim. Acta, Part B, 30 (1975) 449.
7 G. R. Kornblum, W. van der Waa and L. de Galan, Anal. Chem., 51 (1979) 2378.
8 C. D. Allemand and R. M. Barnes, Appl. Spectrosc., 31 (1977) 434.
9 J. L. Genna, R. M. Barnes and C. D. Allemand, Anal. Chem., 49 (1977) 1450.
10 C. D. Allemand, R. M. Barnes and C. C. Wohlers, Anal. Chem., 51 (1979) 2392.
11 S. Greenfield and D. T. Burns, Spectrochim. Acta, Part B, 34 (1979) 423.
12 C. D. Allemand and R. M. Barnes, Spectrochim. Acta, Part B, 33 (1978) 513.
13 R. C. Miller and R. J. Ayen, J. Appl. Phys., 40 (1969) 5260.
14 E. Sexton, R. N. Savage and G. M. Hieftje, Appl. Spectrosc., 33 (1979) 643.

15 P. Schutyser and E. Janssens, Spectrochim. Acta, Part B, 34 (1979) 443.
16 J. D. Winefordner, P. A. St. John and W. J. McCarthy, Anal. Chem., 39 (1967) 1495.
17 R. H. Tourin, Spectroscopic Gas Temperature Measurements, Elsevier, New York, 1962, pp. 47, 48.
18 I. Reif, V. A. Fassel, R. N. Kniseley and D. J. Kalnicky, Spectrochim. Acta, Part B, 33 (1978) 807.
19 R. N. Savage, Development of Highly Efficient Inductively Coupled Plasma Systems for Multi-element Atomic Emission Spectrometry, Ph.D. Thesis, Indiana University, Bloomington, IN, 1979.
20 R. N. Savage and G. M. Hieftje, Anal. Chem., 52 (1980) 1267.
21 J. A. Dean and T. C. Rains, in J. A. Dean and T. C. Rains (Eds.), Flame Emission and Atomic Absorption Spectrometry, Ch. 13, Vol. 2, M. Dekker, New York, 1971.
22 R. N. Savage and G. M. Hieftje, Anal. Chim. Acta, 123 (1981) 319.
23 J. C. van Loon, Analytical Atomic Absorption Spectrometry, Academic Press, New York, 1980, p. 171.

Analytica Chimica Acta, 124 (1981) 259—266

PERFORMANCE AND APPLICATION OF CONTROLLED TEMPERATURE-GRADIENT LAMPS IN ATOMIC ABSORPTION SPECTROMETRY

D. S. GOUGH and J. V. SULLIVAN*

CSIRO Division of Chemical Physics, P.O. Box 160, Clayton, Victoria 3168 (Australia)

(Received 3rd November 1980)

SUMMARY

An improved design of controlled temperature-gradient lamp (CTGL) is suitable for arsenic, cadmium, phosphorus, potassium, rubidium, selenium, sodium, sulphur and zinc. Intensity and linewidth measurements indicate that the CTGL is significantly more intense than an electrodeless discharge lamp (EDL) at the same linewidth. CTGL's also compare favourably with EDL's when used as light sources for a.a.s. Arsenic and selenium can be determined at very low concentrations (ng ml^{-1}) by the hydride generation technique. Sulphur and phosphorus can be detected in the vacuum ultra-violet region using nitrogen-separated flames; the limits of detection are 13 and 10 $\mu g\ ml^{-1}$, respectively.

In a previous communication [1], the authors described a new type of atomic spectral lamp (CTGL: controlled temperature-gradient lamp) capable of emitting very intense and sharp spectral lines for those elements which are readily volatilized at relatively low temperatures. This lamp was unsuitable for sulphur and phosphorus because the vapour, generated in the anode compartment, reacted with the anode material. The present paper describes an improved version of the CTGL which can be used for sulphur and phosphorus, as well as for other elements which have a vapour pressure of approximately 10^{-5} torr at temperatures in the range 300—500 K. Lamps have been made for arsenic, cadmium, phosphorus, potassium, rubidium, selenium, sodium, sulphur and zinc. Because of their high spectral output, they are particularly suitable for arsenic, selenium, phosphorus and sulphur, whose resonance lines, lying in the region below 200 nm, are strongly absorbed by atmospheric oxygen and by gases in the flames used in atomic and fluorescence spectrometry.

EXPERIMENTAL

Design of the lamp

A schematic diagram of the lamp is shown in Fig. 1. (Patent applications have been made.) The lamp consists essentially of three glass tubes attached to a bulb housing a re-entrant silica exit window. One tube contains an

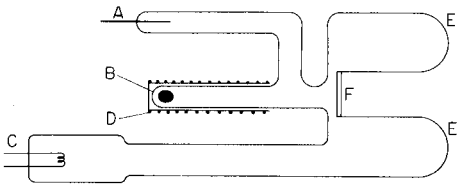

Fig. 1. Schematic diagram of controlled temperature-gradient lamp. A, anode; B, central tube (6 mm i.d.); C, oxide-coated cathode; D, furnace; E, lamp envelope; F, silica exit window (20 mm diameter).

anode, A, and is joined, as shown, to the central tube, B. The material whose resonance line is to be excited is placed in tube B in the form of pure element. A third tube contains the cathode, C, which is an oxide-coated filament. Use of this type of filament permits a low-voltage, high-current discharge to be maintained, resulting in high excitation efficiency for low power dissipation. The anode compartment is connected to the central tube in such a way as to ensure that all the atomic vapour will diffuse into the exciting discharge.

This vapour is produced by heating the element with a furnace, D, which consists of approximately 5Ω of resistance wire wound on a thin cylindrical insulator. The temperature of the furnace can be pre-set and maintained accurately at any desired value by means of a control circuit which incorporates a thermistor (ITT M15) to sense changes in temperature and a triac to regulate the current in the heating coil.

Vapour of the element in the region of the discharge diffuses to the cool portion of the lamp envelope, E, where it condenses. Such condensation must occur in order to ensure that the vapour pressure of the element is kept low in the filament compartment. This is absolutely essential with arsenic, selenium, phosphorus and sulphur, whose vapours are highly corrosive and can quickly poison the coating of the filament, thereby resulting in poor electron emission.

The exit window, F, is attached to a re-entrant tube as shown and its inner surface is positioned very close to the region of the discharge. This keeps the window sufficiently hot to avoid condensation of vapour, which would cause loss of transmission.

The lamp is processed on a vacuum system equipped with a diffusion pump. When the pressure has reached a value of approximately 10^{-6} torr, the filament coating is activated by conventional techniques. The lamp is filled with spectrally pure argon to a pressure of 3 torr and is removed from the pumping system.

The power supply to the lamp incorporates a filament heater (6 V, 10 A) and two outlets which are connected in parallel across the lamp. One outlet is capable of delivering 10 mA at 900 V, and the other up to 750 mA (regulated) at 120 V. The high-voltage supply is used to strike the lamp and provides a continuous current of 10 mA to permit square-wave electronic modulation of the exciting current.

Procedures

Resonance line intensities. Absolute intensities of the resonance lines (As 193.7 nm; Cd 228.8 nm; Se 196.0 nm and Zn 213.9 nm) emitted by CTGL's, EDL's (Westinghouse) and hollow-cathode lamps (HCL; Varian-Techtron Pty. Ltd.) were determined by comparing the intensity of each lamp with that of a calibrated deuterium lamp (Model UV40, Optronic Laboratories Inc., USA). Each spectral line was isolated by using a grating monochromator whose spectral band-pass was 0.075 nm. To ensure that the slit of the monochromator was evenly illuminated, its height was set at 1 mm.

Linewidths. Resonance lines emitted by EDL's and the corresponding CTGL's were scanned at approximately 0.00 nm min^{-1} using a monochromator which was operated in high order (13th to 16th). The recorder traces of intensity versus wavelength obtained from these scans were used to determine the width (full width half maximum) of each line. The focal length of the monochromator was 3.81 m and the grating was 76 mm wide and had 600 grooves/mm. The photomultiplier used in these measurements was the solar-blind type (R166, Hamamatsu TV Company, Japan) which helped to minimize spurious signals arising from scattered light and to reduce the possibility of overlapping orders.

Atomic absorption measurements of arsenic and selenium. The concentrations of arsenic and selenium in aqueous solutions at the ultra-trace level were determined by using a hydride vapor generator accessory (Model 65, Varian-Techtron Pty. Ltd.).

Atomic absorption measurements of phosphorus and sulphur. The concentrations of phosphorus and sulphur in aqueous solutions were determined using the experimental arrangement shown in Fig. 2.

This arrangement provided an easy means of purging the entire light path with dry nitrogen in order to permit transmission of the resonance lines of sulphur (180.7 nm) and phosphorus (177.5 nm). To provide some flexibility for optical alignment, short pieces of plastic hose were used to connect the glass tubes housing the Suprasil lenses, L, to the spectral lamp, S, and monochromator, M, (Model H10 UV-V, Jobin-Yvon, France). The burner, T, described more fully elsewhere [2] was circular in cross-section, had a path length of approximately 2 cm, and was separated by a nitrogen sheath.

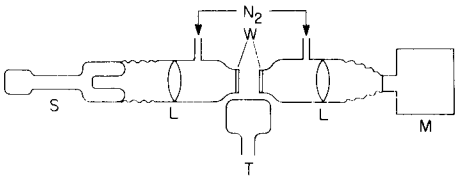

Fig. 2. Experimental arrangement with nitrogen-purged light path for absorption measurements of sulphur and phosphorus. L, silica (Suprasil) lenses; M, monochromator; S, spectral lamp; T, burner; W, silica windows (Suprasil).

Air—acetylene or nitrous oxide—acetylene mixtures could be used with this burner simply by replacing the burner top with one having different size holes [3]. The Suprasil windows, W, which sealed the glass tubes were brought as close as possible to the flame and lay within the nitrogen sheath.

For these measurements, stock solutions of phosphorus and sulphur were made up in distilled water from analytical reagent-grade potassium dihydrogen orthophosphate (KH_2PO_4) and potassium hydrogen sulphate ($KHSO_4$), respectively.

RESULTS AND DISCUSSION

Figure 3 shows warm-up traces for an arsenic CTGL and EDL. In order to shorten its warm-up time, the EDL was first run for 6 min at 9 W. Recorder trace, A, shows that the short-term stability of the CTGL is approximately ±0.25% f.s.d. with the long-term stability approximately ±1% f.s.d. It can be seen that the CTGL has a much faster warm-up time than the EDL.

Table 1 shows the absolute intensities of the resonance lines of arsenic, cadmium, selenium and zinc. These intensities, expressed in terms of radiance, were measured for CTGL's, EDL's and HCL's. The CTGL's were operated to give as high a spectral output as possible. The temperature of the furnace was set to produce maximum elemental vapour pressure consistent with safe operation of the filament. The EDL's and HCL's were run at the powers and currents indicated. All the lamps were modulated at a frequency of 285 Hz. It can be seen from Table 1 that the spectral output of the CTGL's is greater than that of the EDL's when the latter are operated at the power recommended by the manufacturer. There is some self-reversal of the resonance lines emitted by the EDL's. This line broadening is discussed more fully below.

Table 2 shows the linewidths (full width at half maximum) obtained for the resonance lines of arsenic, cadmium, selenium and zinc at the wavelengths indicated. No attempt has been made to correct the linewidths for

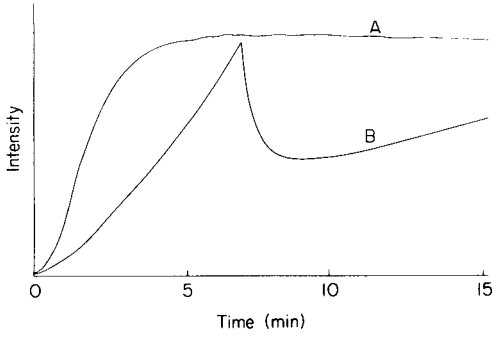

Fig. 3. Recorder traces of lamp intensity versus time for the arsenic resonance line at 193.7 nm: (A) CTGL, (B) EDL, operated initially for 6 min at 9 W.

TABLE 1

Radiance of the resonance lines for arsenic, cadmium, selenium and zinc emitted by the appropriate CTGL, EDL and HCL
(The values are in units of 10^{-4} W sterad^{-1} cm^{-2})

Element	λ (nm)	CTGL	EDL		HCL	
		[a]	7 W	9 W	[b]	[c]
As	193.7	30	2	22	—	1.2
Cd	228.8	69	25	52	3	39
Se	196.0	13	8	15	—	1.2
Zn	213.9	45	42	150	2.4	6.5

[a]Maximum intensities for satisfactory operation. [b]At current recommended (8 mA for Cd and Zn). [c]At maximum current recommended (As, 7 mA; Cd, 20 mA; Se, Zn, 15 mA).

TABLE 2

Linewidths (full width at half maximum) measured for arsenic, cadmium, selenium and zinc
(The CTGL's were operated at furnace temperatures which gave intensities from the lamps comparable with those of the EDL's run at 7 W and 9 W respectively)

Element	λ (nm)	Instrumental width	Measured linewidth		
			CTGL	EDL	
		(nm)	(nm)	(nm)	
As	193.7	0.00031	0.00073	0.0007	(7 W)
			0.0010	0.00089	(9 W)
Cd	228.8	0.00045	0.00077	0.0015[a]	(7 W)
			0.00099	0.00198[a]	(9 W)
Se	196.0	0.00030	0.00066	0.00105[a]	(7 W)
			0.00083	0.00154[a]	(9 W)
Zn	213.9	0.00040	0.00081	0.00131[a]	(7 W)
			0.00119	0.0019[a]	(9 W)

[a]Line is self-reversed.

that component arising from the instrument, but the instrumental width is shown in the Table. The EDL's were operated at 7 W and 9 W whilst the CTGL's were operated at furnace temperatures which gave intensities comparable with those of the EDL's. The resonance line emitted by each CTGL exhibited some broadening as the temperature of the furnace, and hence the elemental vapour pressure in the lamp, was increased, but no self-reversal of the line was detected. However, the resonance lines emitted by the cadmium, selenium and zinc EDL's showed self-reversal even at the recommended operating power.

Figure 4 shows the recorder traces of line profiles of cadmium and selenium

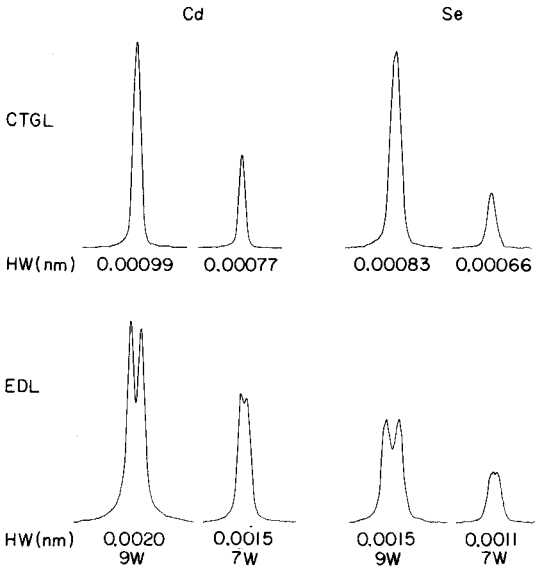

Fig. 4. Recorder traces obtained under high resolution showing the profiles of the resonance lines emitted by CTGL's and EDL's for cadmium and selenium. The lamps were operated to give comparable intensities.

resonance lines emitted by CTGL's and EDL's operated under the conditions indicated in Table 2. The resonance lines emitted by the EDL's were self-reversed even at 7 W, the recommended operating power.

Table 3 shows the results for arsenic and selenium obtained by the hydride generation technique. The absorbance values quoted are each the average of three determinations with background subtracted. The CTGL and the EDL give similar sensitivities for each element and the curves of concentration versus absorbance are linear in the range examined.

TABLE 3

Absorbances measured for arsenic and selenium with CTGL's and EDL's as light sources in conjunction with hydride generation

Element	λ (nm)	Concentration (ng ml^{-1})	Absorbance	
			CTGL	EDL
Se	196.0	10	0.057	0.06
		20	0.12	0.12
		40	0.24	0.233
As	193.7	2.5	0.084	0.073
		5.0	0.172	0.142
		10.0	0.336	0.294

Table 4 gives the limits of detection found from atomic absorption measurements of phosphorus and sulphur using nitrogen-separated, air—acetylene and nitrous oxide—acetylene flames. Kirkbright et al. [4—6] have demonstrated the usefulness of these nitrogen-separated flames for absorption measurement in the spectral region below 200 nm. In particular, they have shown that the nitrous oxide—acetylene flame is remarkably transparent in this region. For the sulphur determinations reported here, both flames were used. The greater transparency of the latter type of flame at 180.7 nm resulted in less noise and therefore a lower limit of detection. Since no EDL for sulphur was available, comparison could not be made with the corresponding CTGL. However, such comparisons could for phosphorus. As Table 4 shows, the CTGL with its better signal-to-noise ratio gave a limit of detection significantly better than that obtained when the EDL was used.

Conclusion

The data show controlled temperature-gradient lamps to be more intense than electrodeless discharge lamps, and the resonance lines to be significantly sharper. Furthermore, the resonance lines are not self-reversed even when the elemental vapour pressure exceeds a value likely to cause deterioration of the cathode because the field of view is one of uniform excitation.

The CTGL has particular application in the determination of arsenic and selenium by a.a.s., because there are no satisfactory hollow-cathode lamps for these elements. Lamps can be made for arsenic, cadmium, cesium, phosphorus, potassium, rubidium, selenium, sulphur and zinc.

The authors are indebted to Mr. P. L. Larkins for help with the measurements of linewidths.

TABLE 4

Limits of detection for sulphur and phosphorus obtained by a.a.s.

Element	λ (nm)	Type of lamp	Flame nitrogen-separated	Limit of detection[a] ($\mu g\ ml^{-1}$)
S	180.7	CTGL	Air—acetylene	33
		CTGL	Nitrous oxide—acetylene	13
P	177.5	EDL	Nitrous oxide—acetylene	20
		CTGL	Nitrous oxide—acetylene	10

[a]The limit of detection is defined as that concentration of analyte for which the signal has a value equal to twice the standard deviation of a series of readings on a sample whose concentration is just above this limit.

REFERENCES

1 D. S. Gough and J. V. Sullivan, Anal. Chim. Acta, 108 (1979) 347.
2 P. L. Larkins, Spectrochim. Acta, Part B, 26 (1971) 477.
3 P. L. Larkins and J. B. Willis, Spectrochim. Acta, Part B, 26 (1971) 491.
4 G. F. Kirkbright, M. Sargent and T. S. West, At. Absorpt. Newsl., 8 (1969) 34.
5 G. F. Kirkbright and L. Ranson, Anal. Chem., 43 (1971) 1238.
6 G. F. Kirkbright and M. Marshall, Anal. Chem., 44 (1972) 1288.

Analytica Chimica Acta, 124 (1981) 267—274

SPUTTERING AND EMISSION INTENSITY OF CAST IRONS WITH DIFFERENT METALLURGICAL STRUCTURES IN A GRIMM GLOW LAMP

M. FUJITA[a] and J. KASHIMA

The Casting Research Laboratory, Waseda University, Nishiwaseda 2-8-26, Shinjuku-ku, Tokyo (Japan)

K. NAGANUMA*

Government Industrial Research Institute, Nagoya, Hirate-machi 1-1, Kita-ku, Nagoya (Japan)

(Received 1st September 1980)

SUMMARY

The cathodic sputtering and emission intensities for the white, gray and malleable cast irons in the Grimm glow lamp are discussed. The intensities of the Fe 247.98-nm line for the samples of the three types depend linearly on the electrical power but the slopes of the plots differ. The intensity of the carbon line at 247.86 nm for malleable cast iron is weaker than those for the others. Sputtering is influenced by the form of the graphite, which can lead to distortion of the electrical field. Graphite on malleable cast iron is sputtered not only as atomic carbon but also as moieties containing several carbon atoms. The higher the supplied voltage, the shorter the time for the intensities of the Fe I and C I lines to reach constant values.

At present, cast iron is mainly analyzed by emission spectrochemical methods with a spark discharge. In the case of discharge on cast iron samples containing graphite, cathode spots are concentrated at the boundaries between the graphite and the matrix; such samples are unsuitable and must be converted to the white cast iron by casting the melt in a copper mould.

Matrix effects caused by the metallurgical structure of samples when the Grimm glow lamp is used as light source in emission spectrometry are usually less than those occurring with the spark discharge. However, selective sputtering of the specific phases on Al—Cu—Si alloy [1] and copper-base alloy [2] has been observed to influence the emission intensities. For cast irons, working curves must be prepared for each type of metallurgical structure [3]. Accordingly, it seems useful, in attempts to improve the accuracy of the analysis of cast irons by the Grimm glow lamp method, to study the sputtering and the emission intensities in this lamp for cast iron samples with different metallurgical structures.

---

[a]Present address: Nissan Motors Ltd., Tokyo, Japan.

EXPERIMENTAL

The Grimm glow lamp, designed and constructed in this laboratory [4], was operated at a constant argon pressure of 6 torr. The anode tube had a fixed inner diameter of 5 mm, and the anode—cathode distance was 0.1 mm. Cross-sections of the surface craters produced by sputtering were recorded with an instrument for measuring surface roughness and waviness. The intensities of spectral lines were measured with a Shimazu GE-340 grating spectroscope. The lines used were: C I (247.86 nm), Fe I (247.98 nm), Si I (251.61 nm) and Fe II (249.33 nm).

To study the effects of different forms of carbon (graphite or compounds with iron), and different shapes of graphite on the cast irons, on sputtering and emission intensities, cast irons of three types, white, gray and malleable, were prepared. White and gray cast irons were obtained from one ingot as follows: the melt was cast into a cylindrical sand mould (30 mm i.d., 90 mm long) on a copper plate for rapid cooling; the white sample was obtained from the bottom surface and the gray sample was prepared by cutting off the top. Malleable cast iron was prepared by a graphitizing treatment for 30 h at 940°C or 50 h at 700°C. The samples were 10 mm thick. The concentrations of the main elements other than iron in the cast iron samples, measured by wet chemical methods are shown in Table 1. The microstructures are shown in Fig. 1; the white cast iron consisted of cementite and perlite, the gray iron of perlite and graphite, and the malleable iron of ferrite and graphite. White, gray and malleable cast irons are designated here by W, G and M, respectively.

RESULTS AND DISCUSSION

Intensity—time curves for white cast iron

The behavior of the emission intensities vs. time for W1 was examined at voltages in the range 700 to 1000 V. The intensities were obtained with stepped integration of an exposure time of 10 s at intervals of 20 s and plotted against the time when the exposure had finished; the results are

TABLE 1

Composition of cast iron samples
(Contents are given as %wt.)

Samples	C	Si	Mn	P	S
W1, M1	3.09	2.69	0.01	0.003	0.013
W2, M2	2.58	2.74	0.01	0.003	0.012
G1	3.14	2.75	0.01	0.003	0.012
G2	2.57	2.76	0.01	0.003	0.014
G3	3.91	2.56	0.01	0.003	0.012

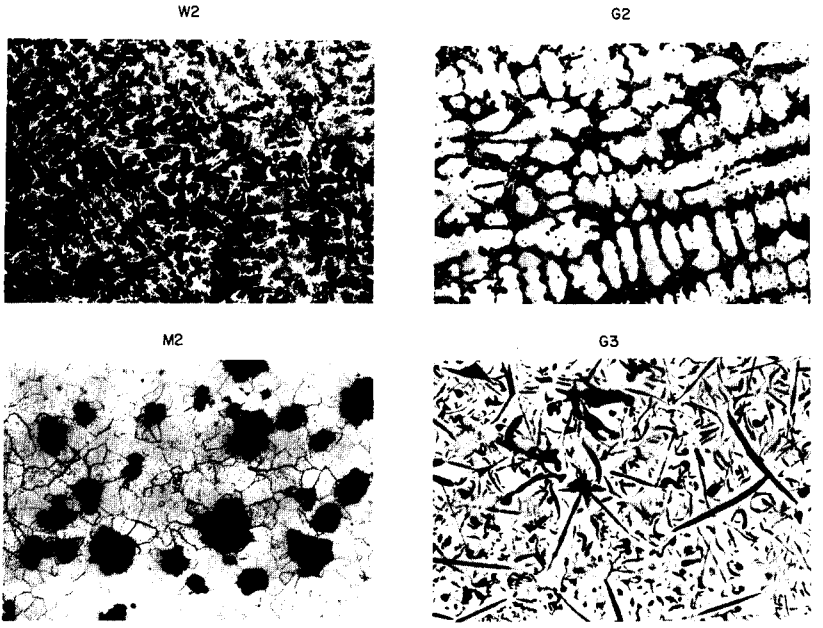

Fig. 1. Cast irons with different metallurgical structures (magnification 200×).

shown in Fig. 2. The intensities of the Fe I and Fe II lines increased gradually with increasing discharge times, whereas the intensity of the C I line was strong immediately after burn-off and then decreased. This different behavior of the Fe I and II and C I intensities was not caused by selective sputtering [1, 2]; a change in the discharge conditions was indicated. The carbon in the W1 sample was present as a compound with iron and not as graphite, and this sample had a fine metallurgical structure. The higher the voltage, the shorter the time to reach constant intensities of the C I line. Furthermore, increase in the voltage reduced the differences in the intensity ratio, I_C/I_{Fe}, i.e. the ratio of the C I intensity at 246.86 nm to the Fe I at 247.98 nm, as shown in Fig. 3.

Figure 2 shows that the shapes of the intensity—time curves for the Fe II and Fe I lines are similar. However, the reproducibility of the intensity of the Fe I line was better. For sample W1 sputtered at 1000 V with a pre-exposure time of 120 s and an exposure time of 60 s, the coefficient of variations (n = 8) were 4.92% on an average reading of 31.12 at 247.98 nm, and 8.62% on an average reading of 25.4 at 249.33 nm. Therefore, the neutral lines should be used in the analysis of cast iron with a Grimm glow lamp.

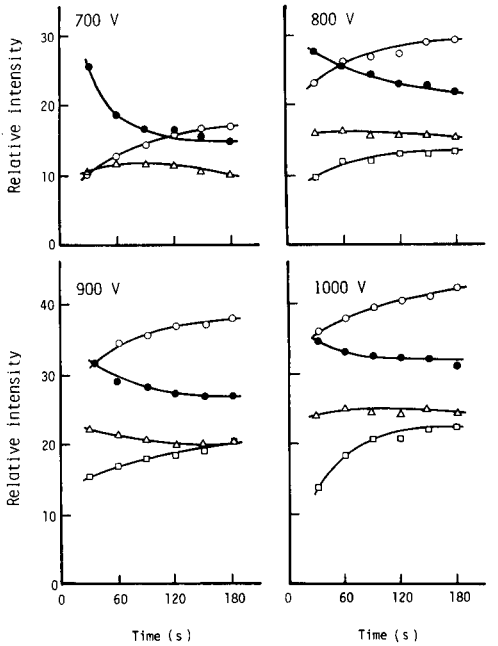

Fig. 2. Intensity—time curves for white cast iron at various voltages: (•) C I; (○) Fe I; (□) Fe II; (△) Si I.

Influence of electrical power

In order to decide the best pre-burn and exposure times, the coefficients of variation for I_C, I_{Fe} and I_C/I_{Fe} were examined using the G1 sample for a fixed pre-burn time of 75 s with various exposure times. The results (Fig. 4) indicated that the reproducibilities of the I_C, I_{Fe} and I_C/I_{Fe} improved at exposure times over 60 s. Therefore, the C I and Fe I were measured under fixed conditions with a pre-burn time of 100 s and an exposure time of 60 s.

The influence of the electrical power on the Fe I and C I intensities and their ratio was examined for the three types of cast iron (W2, G2, and M2). The results are shown in Fig. 5. The Fe I intensity for all cast iron samples depended linearly on the power; but the slopes of the lines were different. At low power, the intensity for the M2 sample was weaker than those for the other samples, but at high power, it was stronger than those for the other samples. In contrast, the C I intensity was clearly influenced by the metallurgical structure: the intensity for the M2 sample was weaker than those for other samples over the whole power range, but the intensity patterns for the G2 and W2 samples differed, although similar values were obtained at powers above about 30 W for these samples (Fig. 5). The I_C/I_{Fe} for the M2 sample decreased gradually only with increasing power. These results show that the malleable cast iron sample differs from the others;

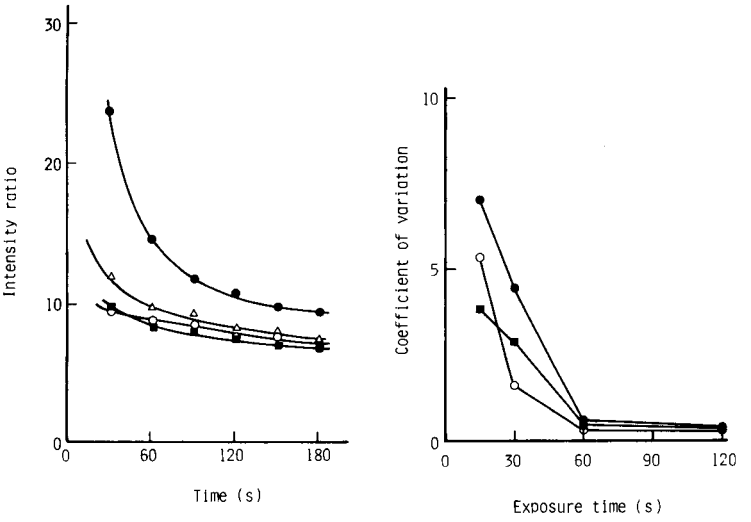

Fig. 3. Intensity ratios (I_c/I_{Fe}) of white cast iron plotted vs. time at various powers: (•) 700 V; (△) 800 V; (▪) 900 V; (○) 1000 V.

Fig. 4. Relations between exposure time and coefficient of variation for the intensities of the spectral lines (I_{Fe} and I_C) and the intensity ratio (I_C/I_{Fe}), with a pre-burn time of 75 s: (○) 247.98 nm; (•) 247.86 nm; (▪) ratio.

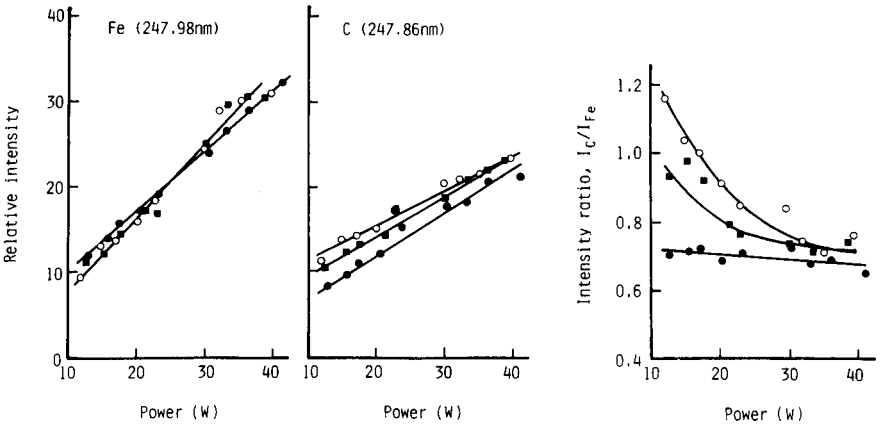

Fig. 5. Intensities of spectral lines (I_{Fe} and I_C) and intensity ratios (I_C/I_{Fe}) plotted vs. power for cast iron samples with different metallurgical structures: (○) W2; (▪) G2; (•) M2.

this happens because the C I intensity is influenced by the form of carbon and the shape of graphite in the sample. Figure 6 shows the C I intensity–time curves for the W2, G2 and M2 samples at 1000 V. The intensity was obtained with stepped integration of an exposure of 5 s at intervals of 5 s, and was plotted vs. the time when the exposure had finished. For all samples

the intensities became nearly constant after 30—60 s, but for the W2 and G2 samples the intensity merely decreased initially, whereas for the M2 sample it showed a minimum about 30 s after burn-off. It is therefore essential that working curves be prepared for each type of cast iron sample, as recommended earlier [4].

It is notable that the electrical currents for the cast irons of the three types were different at a fixed voltage. For instance, at 1000 V, the currents for the W2, G2 and M2 samples were 31.0, 31.4 and 31.9 mA, respectively, at 120 s after burn-off. Furthermore, the current (30.5 mA) for a low carbon steel (BCS-SS435, 0.49% C) was lower than those for all cast iron samples. The differences between the W2, G2 and M2 samples are merely in the metallurgical structure, because the carbon contents are about the same in those samples. However, the W2 sample contains compounds with iron and not graphite, the G2 sample contains graphite and perlite with about 0.5% C, and the M2 sample contains graphite and ferrite with little carbon. Therefore, the current must be affected by the total amount of carbon, the form of the carbon (compounds with iron and graphite), and the amount, size and shape of the graphite in the cast iron. It has been reported for pure copper [1] that the emission intensity and the sputtering yield depend linearly on the current and increase with increasing current. In contrast, for the cast iron, the Fe I and C I intensities for the M2 sample were weaker than those for the other samples; the sputtering yield for M2 was the same as for W2 and G2 (Fig. 7) in spite of the larger current for the M2 sample.

Sputtering of cast irons

Figure 8 shows scanning electron micrographs of the sputtered surfaces for cast irons of the three types. Figure 8C shows the selective sputtering of the perlite; long projections along the flaky graphite particles were formed on the sputtered surface of the gray cast iron and the graphite was visible at the top. The longer the graphite, the higher the height of the projection. On the malleable cast iron, however, the sputtering rate of the graphite was much the same as that of the ferrite grain sputtered slowly; the sputtering rate of the ferrite grain depended on its crystal orientation [5]. Thus, the graphite on the malleable cast iron was less resistant to sputtering than that on the gray sample. Furthermore, the sputtering yields for the malleable and gray cast irons were similar whereas the C I intensity for the malleable sample was weaker than that for the gray sample. These results show that not all the carbon sputtered from the graphite on malleable cast iron contributed to the emission, i.e. the graphite was sputtered not only as atomic carbon but also as species consisting of several carbon atoms.

As mentioned above, projection with graphite cores were found on the sputtered surface of the gray cast iron. Figure 8D is a micrograph of the sputtered surface suitably etched after a discharge of 180 s. It appears that formation of the projection is caused by distortion of the electrical field and not by the difference in sputtering rates of graphite and perlite. It has been

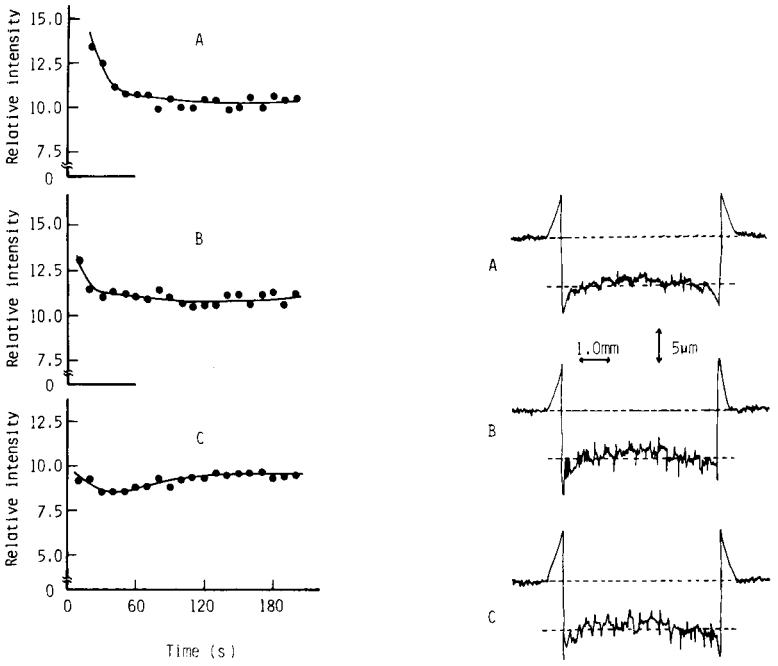

Fig. 6. Intensity—time curves for the C I line with cast iron samples of the three types: (A) white; (B) gray; (C) malleable.

Fig. 7. Cross-sections of craters produced by sputtering during 180 s on cast iron samples of the three types: (A) white; (B) gray; (C) malleable.

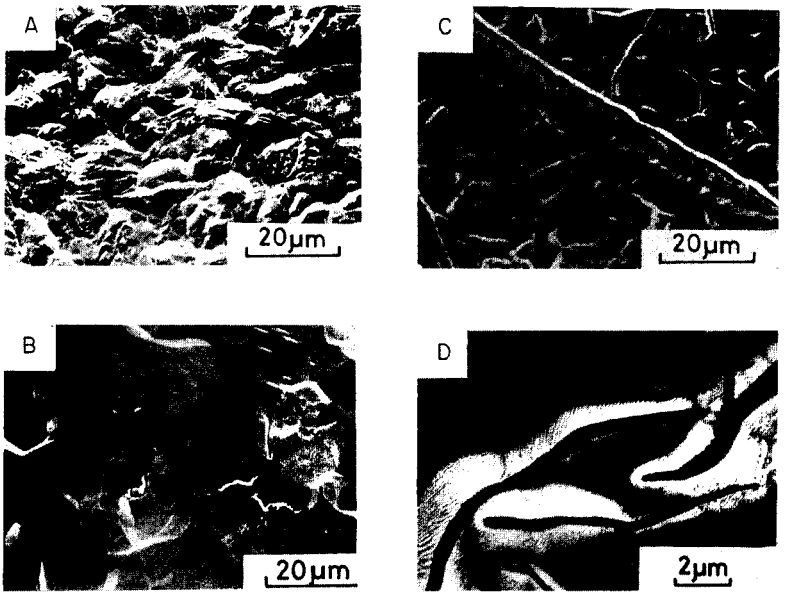

Fig. 8. Scanning electron micrographs of sputtered surfaces (180-s sputtering time) of cast iron sample of the three types: (A) white , W2; (B) malleable, M2; (C and D) gray, G5.

reported that residual lead grains in copper alloys [2] and selective sputtering on Al—Cu—Si alloy [1] are caused by distortion of the electrical field. If the projections were formed merely because of different sputtering rates of graphite and perlite, the sides of the projections would not consist of perlite, because the sputtering rate of a perlite grain does not vary locally and the heights of the projections do not depend on the size of the graphite at the top.

REFERENCES

1 K. Naganuma, M. Kubota and J. Kashima, Anal. Chim. Acta, 98 (1978) 77.
2 H. Jäger and F. Blum, Spectrochim. Acta, Part B, 29 (1974) 73.
3 H. Jung, Giesserei, 64 (1977) 133.
4 K. Naganuma, M. Kubota and J. Kashima, Bunseki Kagaku, 26 (1977) 25.
5 G. K. Wehner, Phys. Rev., 102 (1956) 690.

Analytica Chimica Acta, 124 (1981) 275—280

SPUTTERING AND EMISSION INTENSITY OF COPPER ALLOYS IN A GRIMM GLOW LAMP

T. YAMADA[a] and J. KASHIMA

The Casting Research Laboratory, Waseda University, Nishiwaseda 2-8-26, Shinjuku-ku, Tokyo (Japan)

K. NAGANUMA*

Government Industrial Research Institute, Nagoya, Hirate-machi 1-1, Kita-ku, Nagoya (Japan)

(Received 6th October 1980)

SUMMARY

The effects of the metallurgical structure and the aluminium content of copper—aluminium alloy (1—12% Al) on the sputtering and intensities of spectral lines in the Grimm glow lamp are reported. The electrical current and sputtering yield decreased linearly with increasing aluminium content; the intensities of the Al I lines depended linearly on the amount of aluminium in the sputtering yield at a fixed voltage and argon pressure. The structure affected the intensities of the Al I and Cu I lines but not the intensity ratio (Al I/Cu I) for about 100 s after burn-off. Working curves for aluminium for samples of different structure were very similar.

The matrix effects caused by selective sputtering of the sample phase in the Grimm glow lamp for emission spectrochemical analysis have been reported [1, 2]. However, matrix effects in the Grimm glow lamp are less than those occurring in spark or arc discharges. Copper-base alloys containing wide ranges of alloying elements are used industrially, and the metallurgical structures of the alloys can be changed remarkably by changing the contents of alloying elements, cooling conditions and heat treatments. Accordingly, copper-base alloys should not be analyzed by emission spectrochemical analysis using spark or arc discharges; at present, these alloys are analyzed by such methods only over limited content ranges of alloying elements. In contrast, the Grimm glow lamp has been applied to the determination of alloying elements in copper-base alloys [3]. In order to apply the Grimm glow lamp to the determination of wider content ranges of alloying elements in copper alloys, the effects of aluminium content and metallurgical structure on the sputtering and intensities of spectral lines for Cu—Al alloys were studied.

---

[a]Present address: Mitsui Mining and Smelting Co., Ltd., Tokyo, Japan.

EXPERIMENTAL

The Grimm glow lamp was designed and constructed in this laboratory [4]. The anode tube had a fixed inner diameter of 5.5 mm, and the anode—cathode distance was adjusted to 0.1 mm. The lamp was operated at a constant argon pressure of 6 torr and a fixed voltage of 850 V. The cross-section of a crater produced by cathodic sputtering on a sample surface was recorded with an instrument for measuring surface roughness and waviness. The intensities of spectral lines were measured with a Shimazu GE-340 grating spectroscope. The following spectral lines were used: Al I (265.2 nm), Al I (236.7 nm) and Cu I (244.2 nm).

Copper—aluminium alloys with different structures were prepared by the following methods: (1) BS series: furnace cooling of melts at a rate of 100 K h^{-1}; (2) BQ series: quenching of the BS-series samples at 900°C into water; (3) BU series: annealing of the BQ-series samples for 15 min at 500°C; (4) BL series: annealing of the BQ-series samples for 15 min at 400°C.

The aluminium contents, densities and structures are shown in Table 1 and the microstructures of the samples are shown in Fig. 1.

RESULTS AND DISCUSSION

Sputtering and intensities

Figure 2 shows characteristic voltage—current curves for the Cu—Al alloys of the BQ series, pure copper and pure aluminium samples. In the aluminium content range studied here (1—12%), the currents for the Cu—Al alloy samples decreased with increasing aluminium content in the sample. The differences in the sputtering yields among samples of the BQ series with different aluminium contents are clear from Fig. 3, which shows the cross-sections of the craters produced by sputtering during 180 s. Figure 4A showed the current and the sputtering yield plotted against the aluminium content; the intensities of the spectral lines Al I (265.2 nm and 236.7 nm), plotted against the amount of aluminium in the sputtering yield are shown

TABLE 1

Aluminium contents, densities and metallurgical structures of the Cu—Al alloys

Sample	Al (wt %)	Density (g cm^{-3})	Structure	Sample	Al (wt %)	Density (g cm^{-3})	Structure
BS-1	1.75	8.81	α	BU-3	10.81	—	Upper bainite
BQ-1	1.59	—	α	BL-3	9.98	—	Lower bainite
BS-2	6.14	8.43	α	BS-4	12.22	7.39	$\alpha + \gamma_2$
BQ-2	6.30	—	α	BQ-4	12.45	—	Martensite
BS-3	10.24	7.66	$\alpha + \gamma_2$	BU-4	12.46	—	Upper bainite
BQ-3	10.01	—	Martensite	BL-4	12.30	—	Lower bainite

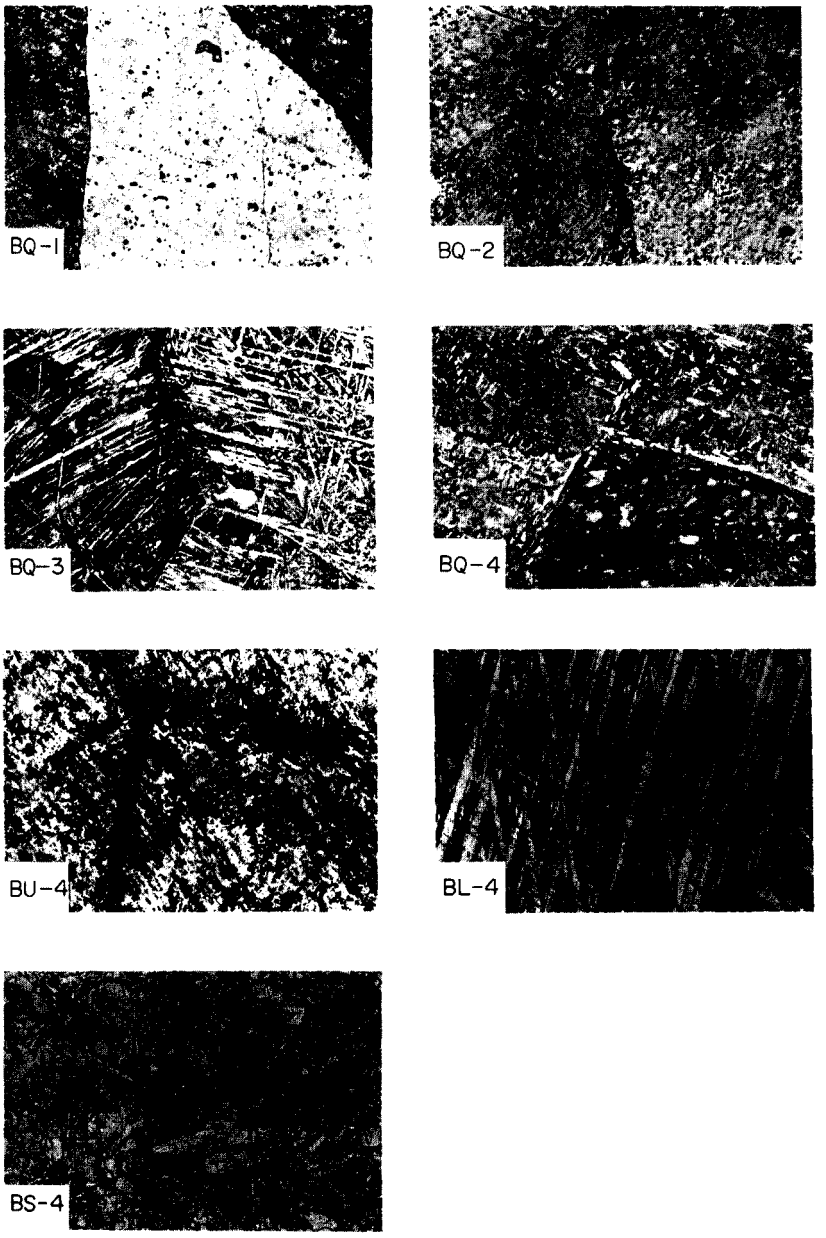

Fig. 1. Microstructures of Cu—Al alloy samples (magnification, 50×).

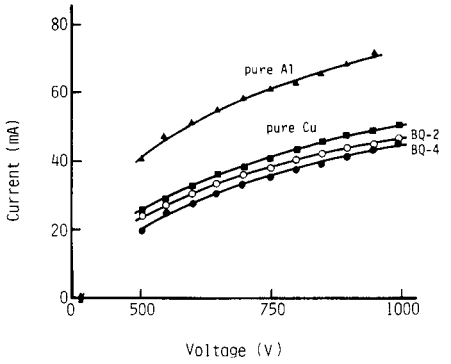

Fig. 2. Voltage—current characteristics for pure copper, pure aluminium and Cu—Al alloys.

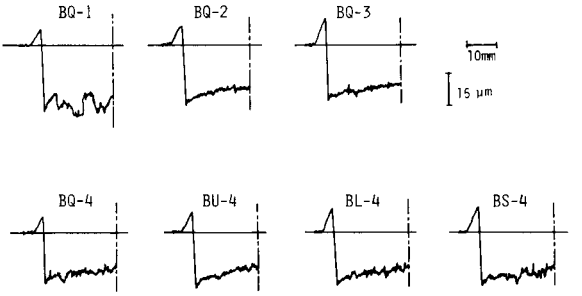

Fig. 3. Cross-sections of craters produced by sputtering for 180 s.

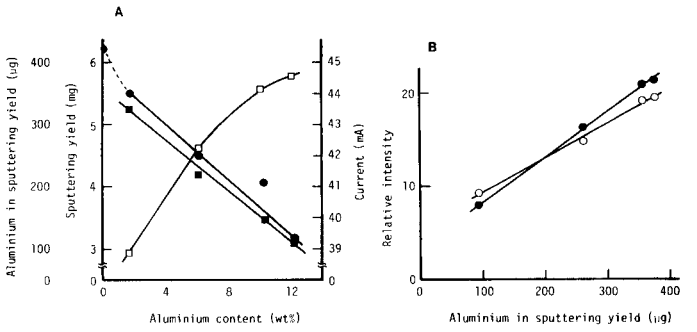

Fig. 4. (A) Sputtering yield (▪), aluminium in the sputtering yield (□), and current plotted vs. aluminium content (•). (B) Relative intensities plotted vs. aluminium in sputtering yield for (•) the Al I line at 265.2 nm, and (○) the Al I line at 236.7 nm.

in Fig. 4B. The intensities were measured at a pre-burn time of 20 s with an exposure time of 40 s, and the sputtering yields were obtained from the cross-sections shown in Fig. 3. Figure 4A shows that the current and the sputtering yield decrease linearly with increasing aluminium content in the sample, and so these results indicate a linear relationship between the current and the sputtering yield. It has been reported that the current and the intensity of the spectral line decrease with increasing thickness of the sample, and have a linear relationship with the sputtering yield for pure copper under fixed conditions of voltage and argon pressure [1]. Clearly, these relationships hold for the Cu—Al alloys in spite of the different cause of changes in the current. However, the amount of aluminium in the sputtering yield increased as the aluminium content in the sample increased, but this relationship was not linear. Yet, the intensities of the Al I lines did depend linearly on the amount of aluminium in the sputtering yield (Fig. 4B).

The sputtered surface of the BQ-1 sample was rough in comparison to that of other samples, probably because the sputtering rate of α-phase grains is influenced by crystal orientation. The influence of crystal orientation on sputtering has been reported for pure silver [5] and also observed for cast iron [6]. As the samples containing more than about 6% aluminium had fine structures, the influence of crystal orientation on the sputtering is not apparent in Fig. 3. Selective sputtering was shown slightly by the sputtered surface of the BS-4 sample but was not apparent on the surfaces of other samples. However, for the BS-4 sample, the intensities of the Cu I and Al I lines were constant with time, i.e., selective sputtering did not influence the intensities [1] although the structure clearly influenced the intensities of the Cu I and Al I lines (Fig. 5). The intensities of both the Cu I and Al I lines for the BS-4 sample were stronger than those for the other three samples tested (Fig. 5). The current for the BS-4 sample (40.7 mA) was larger than those for the other samples (BQ-4, 39.3 mA, BU-4, 39.7 mA) except the BL-4 sample (41.0 mA); it is difficult to find a definite relationship between the intensities and the current. Furthermore, the sputtering yields for the four samples were nearly the same. Further research is needed to explain precisely the influence of structure for Cu—Al alloys.

Working curves

The effect of structure on the intensities of the Cu I and Al I lines for Cu—Al alloy is clear from Fig. 5. All intensities for samples containing 12% Al became constant with time at about 20 s after burn-off, but the intensity ratios for such samples increased linearly with time and the slopes of these intensity ratio—time lines differed. The differences of the intensity ratios among the Cu—12% Al alloy samples with different structures increased with increasing time, but the influence of structure on the intensity ratio was reduced about 100 s after burn-off. Therefore, the intensity ratio should be measured at short pre-burn times. For a pre-burn time of 40 s, the coefficients of variation of the intensities and intensity ratio for various exposure times are

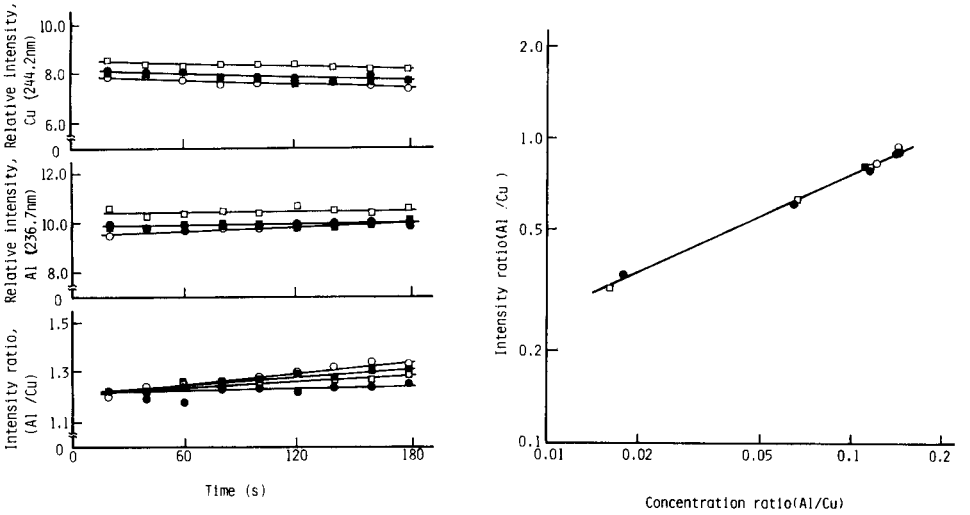

Fig. 5. Relative intensities and intensity ratios for different samples plotted vs. time: (•) BQ-4; (▪) BL-4; (○) BU-4; (□) BS-4.

Fig. 6. Working curve for aluminium in Cu—Al alloys: (•) BQ series; (○) BU series; (▪) BL series; (□) BS series.

TABLE 2

Coefficients of variation of intensities and intensity ratios at various exposure times under the otherwise recommended conditions

Exposure time(s)	20	40	60
Al I (236.71 nm)	1.47	1.80	1.14
Cu I (244.16 nm)	2.18	0.80	0.75
Al I/Cu I	1.52	1.40	1.21

given in Table 2. The longer the exposure time, the greater the repeatabilities of the intensities and intensity ratio. Therefore, the recommended conditions for the working curve are as follows: voltage, 850 V; argon pressure, 6 torr; pre-burn time, 40 s; exposure time, 60 s.

The working curve for aluminium in Cu—Al alloys is shown in Fig. 6; it is clear that the different structures of the Cu—Al alloys do not affect the relationship.

REFERENCES

1 K. Naganuma, M. Kubota and J. Kashima, Anal. Chim. Acta, 98 (1978) 77.
2 H. Jäger and F. Blum, Spectrochim. Acta, Part B, 29 (1974) 73.
3 R. A. Kruger and L. P. Buler, Analyst, 102 (1977) 949.
4 K. Naganuma, M. Kubota and J. Kashima, Bunseki Kagaku, 26 (1977) 25.
5 G. K. Wehner, Phys. Rev., 102 (1956) 690.
6 H. Fujita, K. Naganuma and J. Kashima, Anal. Chim. Acta, 124 (1981) 267.

Analytica Chimica Acta, 124 (1981) 281—294

THE APPLICATION OF GEL FILTRATION AND ELECTROTHERMAL ATOMIC ABSORPTION SPECTROMETRY TO THE SPECIATION OF PROTEIN-BOUND ZINC AND COPPER IN HUMAN BLOOD SERUM

P. E. GARDINER[a] and J. M. OTTAWAY*

Department of Pure and Applied Chemistry, University of Strathclyde, Cathedral Street, Glasgow (Scotland)

G. S. FELL and R. R. BURNS[b]

Department of Clinical Biochemistry, Royal Infirmary, Glasgow (Scotland)

(Received 23rd October 1980)

SUMMARY

Gel filtration with Sephadex G-100 is used to partition zinc- and copper-containing proteins in samples of human sera. The zinc and copper content in the fractions collected are determined by electrothermal (carbon furnace) atomic absorption spectrometry without sample pretreatment. Proteins associated with both metals are measured by immunonephelometry. The results confirm the known association of zinc with α_2-macroglobulin and albumin, but association with other proteins was also found. This combination of techniques provides a method of estimating copper bound to caeruloplasmin and non-caeruloplasmin. Essential clean-up procedures are described.

Most essential trace metals are present at highest concentration inside cells. For reasons of convenience, it is often necessary to attempt diagnosis of deficiency or excess by analysis of an extracellular fluid (serum or urine). Since a variety of non-specific causes unrelated to tissue trace metal concentrations can alter total serum concentrations, interpretation of results is often difficult because of the influence of organic disease, infectious illness or endocrine responses to injury. When the particular metal protein complexes in blood serum can be measured and their function is understood, as in the case of the iron proteins transferrin and ferritin, more reliable diagnosis of iron deficiency or excess can be obtained. Similar information is required for other essential trace metals.

Techniques used for the separation of the serum proteins and subsequent determinations of the trace elements should meet the following four criteria. The fractionation method must not disturb the specific metal—protein associations. Metal contamination from reagents and apparatus should be less than 10% of the initial total metal concentration in the serum sample. The analytical technique chosen for the determination of metal content in

Present addresses: [a]Hahn-Meitner-Institut für Kernforschung, West Berlin, Germany. [b]Biochemistry Department, Royal Inverclyde Hospital, Greenock, Scotland.

the fractions must be able to detect levels 50—100 times less than the normal levels in serum. The resolution of the protein separation technique must be good.

Himmelhoch et al. [1] combined gradient chromatography on a DEAE—cellulose column with spark emission and atomic absorption spectrometry to study the distribution of iron, zinc, manganese, nickel, calcium, magnesium and strontium in dialysed human serum. This work demonstrated the association of zinc with two major protein fractions, and discussed the problem of contamination and steps taken to reduce extraneous trace elements in the gel and buffer. However, the use of ion-exchange for separation has the disadvantage of affecting the weaker metal—protein associations. Fritze and Robertson [2] used neutron activation and gel filtration to study the distribution of various elements that could be determined after irradiation. Recently, Behne et al. [3] combined neutron activation with isoelectric focussing to study the distribution of eight trace elements. Although neutron activation is a very sensitive technique for a wide range of elements, its use is restricted to laboratories that have access to a nuclear reactor. In a study by Falchuk [4], gel filtration combined with flame atomic absorption spectrometry was used to study the effect of the administration of ACTH on the zinc distribution. However, flame atomic absorption spectrometry has inadequate sensitivity to meet the third criterion, and even if the sample size can be increased, zinc levels less than 20 $\mu g\ l^{-1}$ cannot be measured, making accurate assessment of the blank difficult.

In the present study, the combination of gel filtration and carbon-furnace atomic absorption spectrometry is used to study the distribution of zinc- and copper-bound proteins. This combination offers a number of advantages. Only 1 ml of serum sample is required for the fractionation. The analysis of the fractions for proteins and trace elements is semi-automated and thus rapid. Only a 10-μl sample is required for each analysis; therefore a wide range of determinations can be carried out on each fraction. Zinc and copper levels of about 1 $\mu g\ l^{-1}$ can be detected and thus accurate estimates of the blank correction are possible. This combination of techniques, therefore, appears to meet the criteria mentioned earlier.

EXPERIMENTAL

Apparatus

The columns used (2.6 × 100 cm) were supplied by Pharmacia Fine Chemicals Ltd. The eluent from the column was collected in polystyrene vials with an automatic fraction collector, LKB Model 7000 UltraRac.

For the protein measurements and identification, a Technicon Auto-Analyzer II specific protein analyzer, consisting of a pump, cartridge with mixing coils, nephelometer and recorder, was used.

The fractions were analysed for copper and zinc by using a Perkin-Elmer Model 272 spectrophotometer equipped with a Perkin-Elmer HGA500 heated

graphite atomiser and a Perkin-Elmer Model AS-1 autosampler. The atomic absorption signals were recorded with a Perkin-Elmer Model 56 strip-chart recorder. Total serum copper and zinc were determined with Perkin-Elmer Model 403 spectrophotometer with the burner and accessories for use with an air—acetylene flame.

A Wang 600 programmable calculator was used for calibration and sample concentration calculations.

Reagents

Columns were prepared from Chelex-100 (100—200 mesh; Bio-Rad Laboratories) and Sephadex G-100 (40—120 μm; Pharmacia Fine Chemicals Ltd.). The buffer was prepared from tris(hydroxymethyl)aminomethane hydrochloride and tris(hydroxymethyl)aminomethane.

The atomic absorption spectrometry standards were individual 1000 μg ml^{-1} stock metal solutions (British Drug Houses Ltd.) containing zinc and copper nitrates. Intermediate stock solutions (10 μg ml^{-1}) were prepared daily for subsequent preparation of the working standards.

Purification of reagents and columns

Preparation of gel. In order to remove endogenous trace metal contamination the following procedure was adopted. Approximately 400 ml of 0.02 M HCl was measured into a 1-l vacuum flask and 25 g of dry Sephadex G-100 beads were sprinkled into the solution. The beads were allowed to swell for 24 h at room temperature. The supernatant liquid was decanted and a further 400 ml of 0.02 M HCl was added to the gel. This procedure was repeated twice more. Subsequently, the already swollen gel was washed three times with deionised water, left overnight, and then deaerated. At this point extra care was taken to avoid contaminating the already cleaned gel.

Removal of metal contamination in the Tris-HCl buffer. Copper and zinc contamination in the Tris-HCl used in preparing the buffer was removed by passing the solution through a Chelex-100 column; 2 g of resin in its sodium form was mixed with deionised water. The mixture was poured into a glass column (1 × 30 cm). The column was equilibrated by passing through it 100 ml of 1 M HCl followed by 200 ml of deionised water. A solution of 0.1 M Tris-HCl prepared by dissolving 14 g in 1 l of deionised water was passed through the column. The pH of the eluent was monitored and at pH 2.7 the eluent was collected for the subsequent preparation of the buffer; 500 ml of the purified buffer was diluted to 1 l and the pH brought to 7.4 by adding Tris-base.

Packing the column with Sephadex G-100. Before packing, the column was decontaminated by cleaning with 3 M HNO_3. The acid was left in the column and tubing for 3 days and washed out thoroughly with deionised water before use. The prepared gel was poured into the column and packed as prescribed by the manufacturer. The pH of the eluent was monitored until it was the same as that of the starting buffer. The column was operated at 20 ml h^{-1}.

Sample collection

Blood samples were drawn from donors into individual 10-ml glass bottles with no anticoagulant added. The samples were allowed to clot at room temperature, and then centrifuged at 2500 rpm for 15 min. The sera were transferred to 5-ml polystyrene vials using a 500-μl Sherwood pipette with the recommended tip. All stages of this procedure were shown to be free from metal contamination.

Procedures

Chromatography of the serum sample. A 1-ml portion of serum was applied to the column and, after eluting 100 ml of buffer, forty 3.2-ml fractions were collected in polystyrene vials pre-rinsed with deionised water and air-dried.

Determination of zinc and copper in the fractions. The zinc and copper standards used in the analysis of the column fractions were prepared in 0.05 M Tris-HCl buffer. For the copper determination, standards containing 0—80 μg Cu l^{-1} were prepared by measuring 0, 10, 20, 40, 80, 120 and 160 μl-respectively, of the 10 μg ml^{-1} intermediate stock solution into separate polystyrene vials and making up the volumes to 20 ml with buffer. Standards (0—40 μg Zn l^{-1}) for the determination of zinc were prepared by transferring 0, 10, 20, 40, 60 and 80 μl of the 10 μg ml^{-1} solution into vials and making up the volumes to 20 ml. Instrumental conditions for the determination of both elements are given in Table 1.

The total serum zinc and copper were determined by flame atomic absorption spectrometry as described by Peaston [5].

Calculation of the recovery of zinc and copper applied to the column. After the fractions had been analysed for zinc and copper, the amount of each element in each fraction was calculated by using least-squares calibration plots, computed by and stored in the Wang 600 calculator. The use of the programme was feasible because the plots of absorbance versus concentration were linear for both elements.

TABLE 1

Instrumental conditions for the determination of copper and zinc in the gel chromatography column fractions[a]

	Cu	Zn		Temp. (°C)		Ramp time (s)		Hold time (s)
				Cu	Zn	Cu	Zn	Cu and Zn
Wavelength (nm)	324.8	213.8	Dry	100	100	20	20	30
Lamp current (mA)	13.0	15.0	Ash	700	500	10	10	10
Spectral band width (nm)	0.7	0.7	Atomise	2700[b]	2500[c]	1	5	5
Sample size (μl)	20	10	Clean	2700	2700	2	2	3

[a]Background correction used, scale expansion × 2. [b]No gas flow through the tube during atomisation. [c]100 ml min^{-1} gas flow through the tube during atomisation.

The amounts of analyte found in each fraction were added to give the total metal content. The total obtained was corrected for the blank, which was calculated by taking the mean of the amount of analyte in three fractions collected just before any protein emerged from the column and similarly after the last protein had left the column. The mean blank value was then multiplied by the total number of the fractions collected and the figure obtained was regarded as the overall blank.

Protein identification and measurement. A modification of the automated procedure for specific proteins [6] was used for this study; details are available on request.

RESULTS AND DISCUSSION

In the development stage of the protein fractionation technique, experiments were done with a column (2.6 × 40 cm) packed with superfine Sephadex G-150 gel. All the precautions to avoid metal contamination of the fractions were taken, except for purification of the buffer and gel as described above. Figure 1 presents the protein absorbance at 280 nm and the distribution of zinc, copper and iron. The calculated total metal recovered from the column for each element was over 200% of the starting amount. The first protein peak, composed mainly of proteins excluded from the gel, contained a higher proportion of zinc compared to the second peak made up mainly of albumin and known to bind about two-thirds [7] of the zinc in serum. In addition, smaller iron and copper peaks (shown by arrows) were associated with the first protein peak, but could not be explained in terms of any specific interaction with a protein. Evans and Fritze [8] also observed

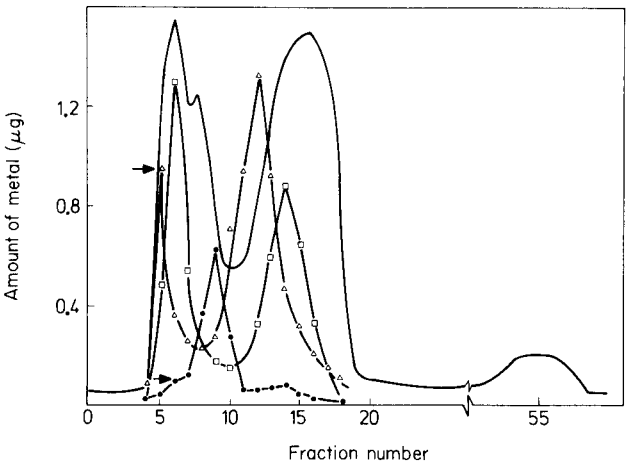

Fig. 1. Distribution of (□) zinc, (•) copper and (△) iron after gel filtration of a serum sample from a healthy donor on a Sephadex G-150 column (2.6 × 40 cm) using a gel of superfine grade beads (1 ml of serum eluted with 0.05 M Tris-HCl buffer, pH 7.4, at 40°C at 10 ml h^{-1}). The continuous line is the serum protein profile at 280 nm.

this behaviour with copper and attributed it to proteins scavenging traces of the metal deposited on the gel. They also suggested that the copper was deposited on the gel after the application of the sample.

There are two possibilities, not necessarily mutually exclusive, that may explain this observation. First, trace metals in the buffer were being deposited on the beads since the beads may act as weak ion-exchangers. Secondly, the beads themselves may contain the metals. In both cases, as the protein front came through the column, the contaminants would be washed down. The first possibility was investigated by increasing the ionic strength of the buffer by the addition of 0.1 M Aristar sodium chloride, which should have overcome any weak ion-exchange effect. This did not give the required improvement in recoveries and the second possibility was therefore investigated. The investigation was carried out in two steps. Superfine Sephadex G-150 (15 g) was soaked in 400 ml of 0.1 M Tris-HCl buffer at pH 7.3 for 3 days. Some of the supernatant liquid was collected and a column was packed with the gel. Buffer was passed continuously through the column and samples of the eluent were collected after 4 h, 24 h and 30 h. The buffer, the gel supernatant solution and the eluent were analysed for copper, zinc and iron. The dry beads were then ashed and the solution of the ash was analysed for the above elements. The results of these experiments (Table 2) show that the batch of beads analysed contained these elements at significant levels, and that it took 30 h of continuous running of buffer through the column before baseline levels were obtained.

The removal of the trace metal contamination in the gel and buffer, therefore, is essential if good trace element recoveries are to be obtained. This was achieved by using the procedures described in the Experimental section. To reduce the risk of incidental contamination, the experimental system consisted only of a column and fraction collector; the flow cell of the u.v. monitor was removed.

TABLE 2

Determination of copper, iron and zinc in Tris-HCl buffer and superfine Sephadex G-150 beads

Material analyzed	Concentration ($\mu g\ l^{-1}$)		
	Cu	Fe	Zn
Buffer	6.5	55.0	3.0
Gel supernatant	15.0	102.0	21.0
Effluent after 4 h	20.0	120.0	37.2
Effluent after 24 h	6.5	41.0	10.0
Effluent after 30 h	6.5	41.0	3.0
Sephadex G-150 beads ($\mu g\ g^{-1}$)	0.58, 0.60	9.0, 8.9	1.48, 1.25

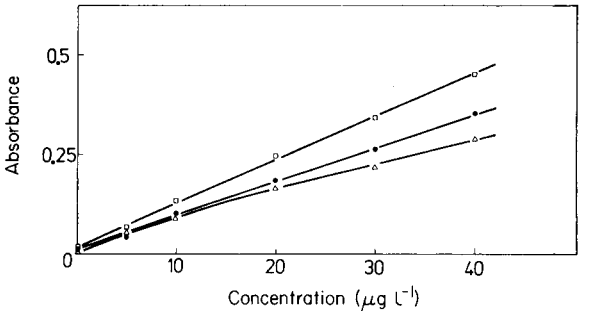

Fig. 2. The effect of gas flow rate through the graphite furnace on the calibration graph for zinc in 0.05 M Tris-HCl. Gas flow: (□) 80; (●) 100; (△) 120 ml min^{-1}.

Optimisation of the carbon-furnace atomic absorption spectrometric (c.f.a.a.s) measurements

Both the inorganic and organic components of the serum matrix have an effect on the absorbances of the metal analytes by c.f.a.a.s. The extent of any interference is determined by the instrumental conditions and the presence of other salts and proteins. Earlier experiments with serum fractions eluted from a Sephadex column showed that the inorganic part of the matrix is eluted later than the serum proteins. The fractions collected, therefore, only contained protein dissolved in the buffer. The depressive effect of 0.05 M Tris-HCl buffer on the zinc signal is about 40% over the range 5—40 μg Zn l^{-1}. A similar effect was observed for copper. This effect was allowed for by preparing the standards in 0.05 M Tris-HCl. It has been reported that the presence of protein can enhance the absorbance of some analytes. However, in the investigation described here, the high dilution of the protein by the buffer rendered such effects unlikely.

An important feature of the Perkin-Elmer HGA500 heated graphite atomiser is its flexibility in the choice of gas flow through the carbon furnace during the atomisation stage. The facility enables the sensitivity to be selected

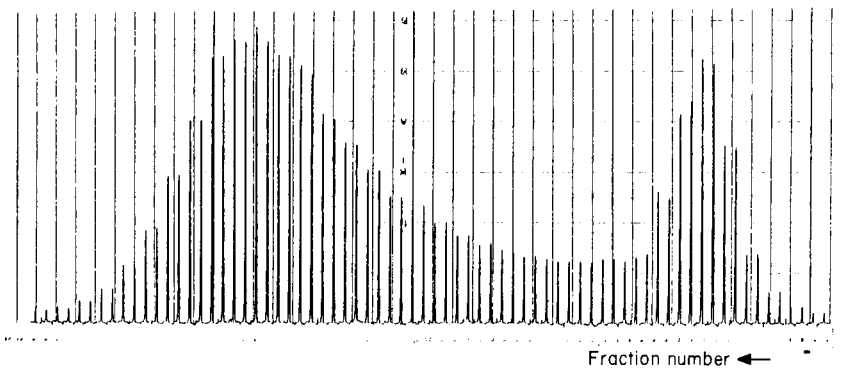

Fig. 3. Typical c.f.a.a.s readout of the zinc distribution in normal serum. Each fraction was analysed in duplicate.

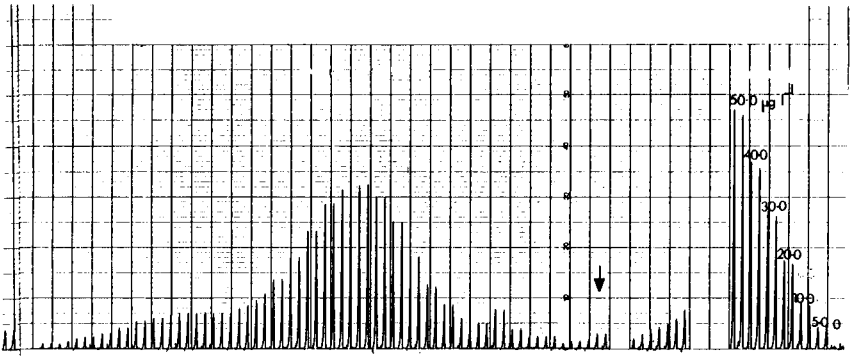

Fig. 4. Copper distribution in normal serum. Each fraction was analysed in duplicate. The arrow indicates the first fraction. The peaks to the right are for standards covering the range 0—50 $\mu g\ l^{-1}$.

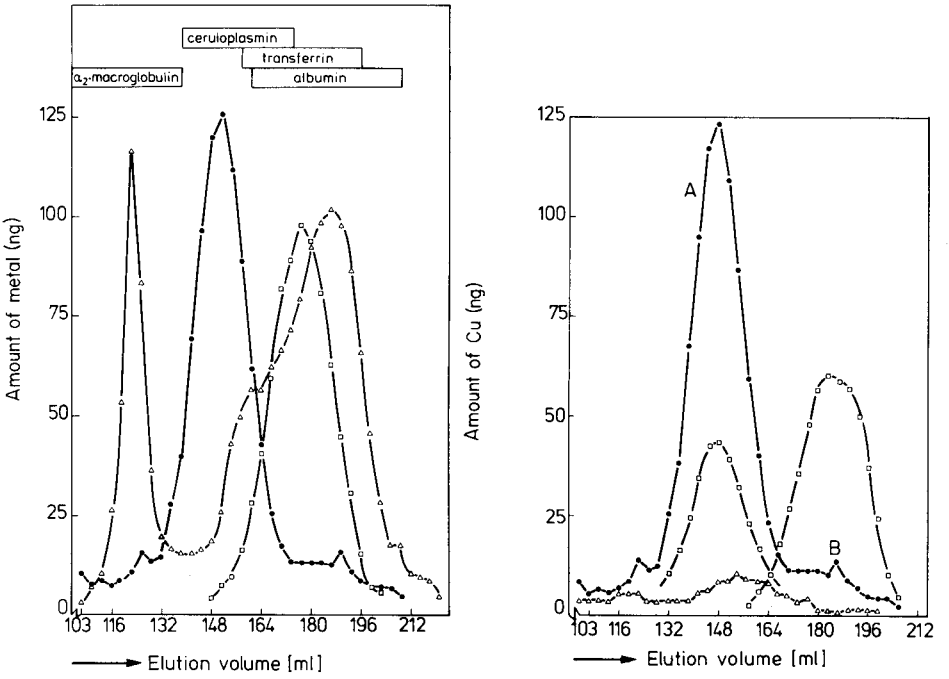

Fig. 5. Typical distributions of zinc (△), copper (●) and iron (□) after gel filtration of a serum sample from a healthy donor on a Sephadex G-100 column (2.6 × 100 cm) (1 ml of serum eluted with 0.05 M Tris-HCl buffer, pH 7.4, at 4°C and 20 ml h^{-1}; 3.2-ml fractions were collected after 100 ml of buffer had gone through the column).

Fig. 6. A comparison between the copper distribution in the serum of (△) a Wilson's disease patient and (●) a normal subject, compared with the distributions (□) of caeruloplasmin and albumin. The amount of caeruloplasmin was multiplied by 2 and the amount of albumin by 0.1 in order to plot the points.

without dilution of the sample, thus eliminating a potential source of contamination. The effect of altering the gas flow through the furnace on the response from zinc is illustrated in Fig. 2. The gas flow finally chosen was 100 ml min^{-1}, because the calibration graph was linear and thus the use of the calibration programme was feasible.

The concentration range required for the determination of zinc in the column fractions was 0—40 $\mu g\ l^{-1}$; 15 fractions collected contained below 5 $\mu g\ l^{-1}$. The peak concentration of zinc in most samples was 30 $\mu g\ l^{-1}$, corresponding to a dilution factor of 20—30 times the starting serum concentrations. In contrast, the concentration range used for the determination of copper was 0—80 $\mu g\ l^{-1}$. Copper is known to be associated principally with one protein, caeruloplasmin, whereas zinc is divided between two major fractions. Corresponding dilution factors for copper were 10—20 times the starting serum concentrations. Typical c.f.a.a.s. readouts of the zinc and copper distributions are presented in Figs. 3 and 4, respectively. Each sample was analysed in duplicate and the traces clearly show the good precision obtained by using the auto sampler.

The plots of the amount of analyte in each fraction vs. elution volume for copper, zinc and iron obtained from a single serum sample are shown in Fig. 5. Although iron was not one of the elements intended for study, it was determined in the fractions to demonstrate that the technique could be easily applied to examine its distribution. The sensitivities and detection limits obtained for the three elements are presented in Table 3. Both parameters measured were adequate for the determination of all three elements.

Fractionation of the copper-bound proteins

One of the well-known inborn errors of metabolism associated with copper is Wilson's disease. During this study three serum samples from patients with this disease were fractionated. A comparison between the copper distribution of a Wilson's disease patient and a healthy normal subject is shown in Fig. 6. Copper is known to be associated with caeruloplasmin and to a much lesser extent with albumin. Analysis of fractions for both proteins showed that the copper peak A coincided with the fractions containing caeruloplasmin and the shoulder B coincided with the fractions containing albumin.

TABLE 3

Detection limit, sensitivity and precision for Zn, Cu and Fe in Tris-HCl buffer

Element	Detection limit[a] ($\mu g\ l^{-1}$)	Sensitivity ($\mu g\ l^{-1}$)	Sample size (μl)	Coefficient of variation[b] (%)
Zn	0.31	0.47	10.0	3.15
Cu	1.29	1.08	20.0	6.47
Fe	0.56	0.66	20.0	2.78

[a]2s values from 20 measurements. [b]For concentrations of 5.0 μg Zn l^{-1}, 10.0 μg Cu l^{-1} and 10 μg Fe l^{-1}.

Copper associated with caeruloplasmin was found in the elution volume 132—167 ml and the copper associated probably with albumin was found in the elution volume 158—209 ml. Because of the overlap between the two fractionated proteins, the amounts of copper associated with the two fractions were calculated from elution volumes 132—164 ml and 167—207 ml, respectively. This approach was used in order to reduce the overlap to less than 5% of the total amount of caeruloplasmin. The percentage of copper found in the fractions containing caeruloplasmin in healthy normal subjects was 92.7 ± 7.3% (mean ±1 s.d.) and with albumin 7.3 ± 2.7% (n = 7). Delves [9], using electrophoresis and electrothermal atomisation, found that more than 95% of the total copper was present in the α_2-fraction but none was detectable in the other fractions. In Wilson's disease a greater proportion of the total serum copper (28.2 ± 6.8%) was found to be associated with albumin. This is to be expected since one of the characteristics of Wilson's disease is the decreased synthesis or the total absence of caeruloplasmin. However, the concentration of copper in this fraction in Wilson's disease is lower (44 ± 17 $\mu g\ l^{-1}$) than the 70 ± 17 $\mu g\ l^{-1}$ and 111 ± 45 $\mu g\ l^{-1}$ found in normal subjects and patients with non-hepatic diseases, respectively (Table 4).

Since copper is associated principally with caeruloplasmin, the serum samples fractionated on the column and additional samples were analysed for the protein by using the automated immunochemical nephelometric

TABLE 4

Distribution of copper in serum

Subject	Copper associated with caeruloplasmin ($\mu g\ l^{-1}$)	% of total recovered	Copper associated with albumin ($\mu g\ l^{-1}$)	% of total recovered	Recover (%)
D.F.[a]	840	95.5	40	4.5	102
P.G.[a]	616	88.0	84	12.0	106
F.K.[a]	1045	94.4	65	5.4	105
M.R.[a]	1020	93.6	70	6.4	116
J.H.[a]	1456	95.2	74	4.8	109
B.S.[a]	918	90.9	92	9.1	113
D.McL.[a]	717	91.9	63	8.1	100
(Mean ± 1 s.d.)	952 ± 277	92.7 ± 7.3	70 ± 17	7.3 ± 2.7	
A.R.[b]	805	84.7	145	15.3	104
J.C.[b]	832	91.4	88	9.6	115
H.McD.[b]	902	94.0	58	6.0	116
M.K.[b]	1319	89.8	151	10.2	116
(Mean ± 1 s.d.)	965 ± 240	89.9 ± 4.0	111 ± 45	10.3 ± 3.8	
S.L.[c]	120	70.6	50	29.4	106
P.M.[c]	102	65.6	58	34.4	89
T.F.[c]	95	79.2	25	20.8	75
(Mean ± 1 s.d.)	106 ± 13	71.8 ± 6.9	44 ± 17	28.2 ± 6.9	

[a]Normal subjects. [b]Patients with no obvious copper disease. [c]Wilson's disease patients.

TABLE 5

Concentration of serum copper and caeruloplasmin in patients and normal subjects

Subject	Category	Caerulo-plasmin ($g\ l^{-1}$)	Total serum copper ($\mu g\ l^{-1}$)	Subject	Category	Caerulo-plasmin ($g\ l^{-1}$)	Total serum copper ($\mu g\ l^{-1}$)
B.B.	Normal	0.30	1070	S.L.	Wilson's disease	<0.05	160
P.G.	Normal	0.27	660	P.M.	Wilson's disease	<0.05	180
G.S.	Normal	0.26	890	C.L.	Wilson's disease	<0.05	130
D.F.	Normal	0.25	860	T.F.	Wilson's disease	<0.05	160
D.McL.	Normal	0.23	780	J.C.[a]	Crohn's disease	0.29	810
F.K.	Normal	0.33	1100	W.K.[a]	Cardiac arrest	0.41	1280
Y.P.	Normal	0.43	1260	M.K.[a]	Colonic cancer	0.43	1270
P.D.	Normal	0.35	1410	H.McD.[a]	Therapeutic starvation	0.28	810
J.H.	Normal	0.34	1410				
M.C.	Normal	0.23	870	A.R.[a]	Malabsorption	0.30	910
M.R.	Normal	0.26	940				
(Mean ± 1 s.d.)		0.30 ± 0.06	1022 ± 251				

[a]Patients on total parenteral nutrition.

technique. Results obtained for the protein and the total serum copper levels are presented in Table 5. The sera of all four Wilson's disease patients had caeruloplasmin levels below 0.05 $g\ l^{-1}$ and the mean copper level was 158 ± 21 $\mu g\ l^{-1}$ against means of 0.30 ± 0.06 $g\ l^{-1}$ and 1022 ± 25 $\mu g\ l^{-1}$, respectively, in normal subjects. According to the literature [10], caeruloplasmin levels in normal subjects range from 0.20 to 0.38 $g\ l^{-1}$ and Cartwright et al. [11] found that caeruloplasmin levels in 28 Wilson's disease patients ranged from 0.02 to 0.22 $g\ l^{-1}$.

Fractionation of the zinc-bound proteins

In contrast to copper, the distribution of zinc is less clear. The distributions of zinc obtained from one normal subject and two patients are shown in Fig. 7; four areas of interest identified by A, B, C and D are shown. The peaks A and D coincide with the distribution of α_2-macroglobulin and albumin, respectively, as shown in Fig. 8. In fractions corresponding to shoulder B the major protein identified was immunoglobulin G (IgG). It has been suggested [12] that there is a possible interaction between zinc and IgG and that this interaction is electrostatic; this shoulder was not present in all the samples analysed here but it does suggest a possible zinc—protein interaction. Caeruloplasmin and transferrin were found in the fractions corresponding to the shoulder C. Transferrin is also one of the proteins that is thought to bind zinc although no conclusive evidence was found for this interaction. It has been suggested by Evans [13] that transferrin is responsible for the absorption and transportation of zinc in pertae blood. According to Linderman et al. [14] it is also possible that pre-albumin is involved in the binding of zinc. Evidence in support of this claim was obtained from the electrophoresis of a serum sample spiked with radio-zinc. Although the existence of a zinc—pre-albumin association is possible, conclusive evidence

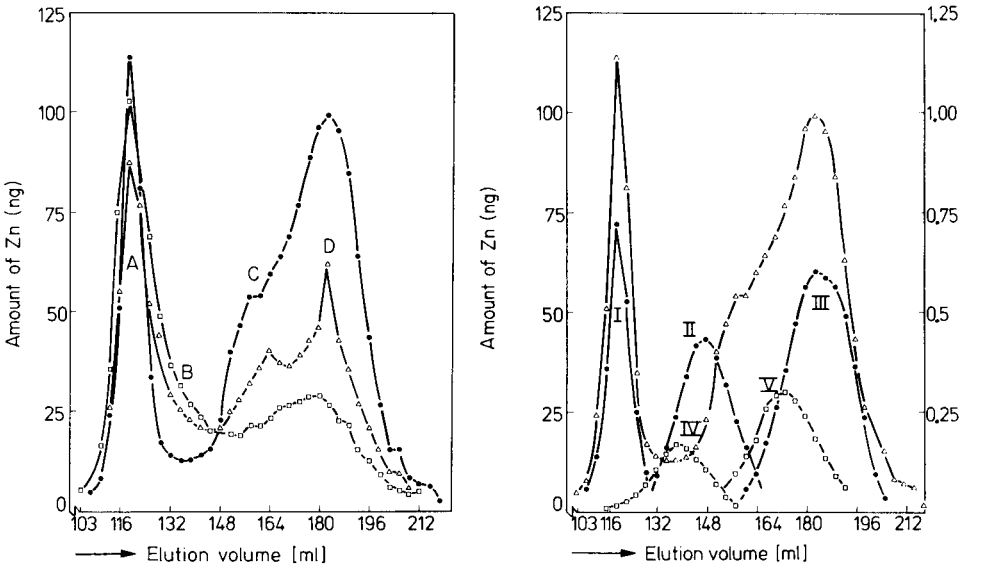

Fig. 7. Elution profile of zinc after gel filtration on a Sephadex G-100 column of sera from (•) a normal subject and (△, □) two patients on total parenteral nutrition. The letters A, B, C and D denote areas of suspected zinc binding to protein.

Fig. 8. Distribution of (△) zinc, (•, I) α_2-macroglobulin (× 1), (•, II) caeruloplasmin (× 2), (•, III) albumin (× 0.1), (□, IV) IgG (× 0.1) and (□, V) transferrin (× 1), after gel filtration on a Sephadex G-100 column of a serum sample from a healthy donor. The figures in parentheses are the factors by which the amount of protein in each fraction was multiplied before the points were plotted.

that the integrity of the zinc—protein complex is maintained during electrophoresis is not available. In the present study the protein pre-albumin was not identified but on the basis of its molecular weight it will probably coincide with the albumin fractions. However, because of the low pre-albumin concentration in serum, it is very unlikely to be a major zinc binder.

The concentrations of zinc found associated with Fraction I, corresponding to A and B, and Fraction II, corresponding to C and D, in both patients and healthy normal subjects are listed with the recoveries of the zinc applied to the column in Table 6. The mean concentrations of zinc in Fractions I and II obtained from the six normal sera examined were 346 ± 44 $\mu g\ l^{-1}$ and 662 ± 88 $\mu g\ l^{-1}$ (mean ± 1 s.d.) respectively. These values compare with 376 ± 88 $\mu g\ l^{-1}$ and 760 ± 100 $\mu g\ l^{-1}$ obtained by Falchuk [4] in a similar fractionation of ten normal sera. Falchuk obtained higher total serum zinc levels in normal subjects (960 ± 100 $\mu g\ l^{-1}$) than those obtained from 29 normal subjects in this study (809 ± 82 $\mu g\ l^{-1}$). There has been no general concensus of opinion on the total serum zinc levels in the literature but mean values between 800 and 1200 $\mu g\ l^{-1}$ have been quoted [15, 16]. In the present study it was found that two-thirds of the zinc is associated with

TABLE 6

Distribution of zinc in serum

Subject	Category	Zinc associated with fraction I ($\mu g\ l^{-1}$)	% of total recovered	Zinc associated with fraction II ($\mu g\ l^{-1}$)	% of total recovered	Total[a] zinc ($\mu g\ l^{-1}$)	Recovery (%)
P.G.	Normal	275	24.0	869	76.0	1040	110
B.B.	Normal	396	38.4	635	61.6	1780	103
P.D.	Normal	390	43.3	510	56.7	940	96
Y.P.	Normal	330	46.0	387	54.0	820	87
B.S.	Normal	345	30.3	795	69.7	880	130
J.H.	Normal	339	30.3	778	69.7	800	140
(Mean ± 1 s.d.)		346 ± 44	35.4 ± 8.6	662 ± 186	64.7 ± 8.6		
H.McD.[b]	Therapeutic starvation	410	44.2	517	55.8	1210	77
J.C.	Crohn's disease	494	64.5	272	35.5	550	139
M.H.	Pancreatic cancer	430	63.2	250	36.8	600	113
W.K.	Cardiac arrest	192	22.0	679	78.0	1370	64
A.R.	Malabsorption	276	48.8	311	51.2	690	88
M.K.	Colonic cancer	350	42.5	473	57.2	920	89
T.F.	Wilson's disease	357	33.1	710	66.9	1280	115

[a]Measured by flame atomic absorption spectrometry. [b]All patients were on total parenteral nutrition.

albumin and this agrees with previous studies using other techniques [7, 17]. In addition, the albumin fraction was found to be the more dynamic of the fractions examined.

The recovery of zinc in serum applied to the column was 104 ± 23% (Table 6). The high recoveries may be attributable to incidental contamination, in view of the ubiquitous nature of zinc. The low recovery values obtained for two patients suggest, however, the existence of weak zinc—protein interactions that have to be carefully studied.

Evans et al. [18] have highlighted two problems associated with gel filtration of labile metal—ligand complexes: the binding by the gel matrix of the metal, and dissociation of the complexes on the column during the fractionation process. Studies carried out by Johnson and Evans [19] have shown that the highly crossed-linked Sephadex G-10 binds more zinc and copper than the less cross-linked G-75 gel. Furthermore, Evans et al. [18] found that the amount of metal bound to gel decreased with increase in ionic strength of the buffer used for elution. However, the recoveries of copper and zinc in the present study were adequate, indicating that under the experimental conditions used, binding of the metals by the gel matrix was negligible.

More important, however, is the problem of dissociation of the labile complexes on the column during fractionation. From the study of the distribution of both elements, over 80% of the zinc and 90% of the copper present in serum could be specifically assigned to particular proteins. The evidence presented for zinc clearly indicates its association with α_2-macroglobulin and albumin, and the association of copper with caeruloplasmin is

demonstrated. Although dissociation of metal—protein complexes can occur on the column, a useful check would be to determine the metal and protein simultaneously when a possible association is suspected; if the gaussian distribution of both coincide, it could be concluded that a possible association exists. Evans et al. [18] and Yoza [20] suggested that a constant level of the metal of interest should be added to the buffer in order to maintain equilibrium. However, in a separate study [21] using ultrafiltration with a filter of 10000 daltons molecular weight cut-off, the amount of zinc and copper associated with the low molecular weight fractions was less than 1% of the serum levels. Since both zinc and copper form fairly stable complexes with amino acids, the amount of ionic zinc and copper in serum would be much less than 1%. Therefore, in the fractionation of serum proteins, the addition of zinc and copper to the buffer is not so critical.

This study has demonstrated that fractionation on a Sephadex G-100 column, coupled with c.f.a.a.s., offers a method that can be used to study the changes of zinc and copper binding to serum proteins both in healthy and diseased subjects. The combination offers a number of advantages. A small sample volume is required. The measurements of the metals and proteins are semi-automated. No sample pretreatment is required, thus eliminating a potential source of contamination and the technique could be extended to study other metal—protein interactions.

REFERENCES

1 S. R. Himmelhoch, H. A. Sober, B. L. Vallee, E. A. Peterson and K. Fuwa, Biochemistry, 5 (1966) 2523.
2 K. Fritze and R. Robertson, J. Radioanal. Chem., 1 (1968) 463.
3 D. Behne, P. Bratter, D. Gawlik, U. Rosick and W. Schmelzer, Nuclear Activation Techniques in the Life Sciences, IAEA-Sm-227/36, (1978) p. 117.
4 K. H. Falchuk, N. Engl. J. Med., 296 (1977) 1129.
5 R. T. Peaston, Med. Lab. Technol., 30 (1973) 249.
6 L. W. Killingsworth, G. F. Buffone, M. Sonawane and C. Lunsford, Clin. Chem., 20 (1974) 1548.
7 I. Vikbladh, Scand. J. Clin. Lab., Invest., 3 (1951) (Suppl. 2) 1.
8 D. J. R. Evans and K. Fritze, Anal. Chim. Acta, 44 (1969) 1.
9 H. T. Delves, Clin. Chim. Acta, 71 (1976) 495.
10 A. Sass-Kortsak, in H. Sobotka and C. P. Stewart (eds.) Advances in Clinical Chemistry, Vol. 8, Academic Press, New York, 1965, p. 1.
11 G. E. Cartwright, H. Markowitz, G. S. Shields and M. M. Wintrobe, Am. J. Med., 28 (1960) 555.
12 J. D. Boyett and J. F. Sullivan, Metabolism, 19 (1970) 148.
13 G. W. Evans, Proc. Soc. Exp. Biol. Med., 151 (1976) 775.
14 R. D. Linderman, D. J. Baxter, A. A. Yunice and S. Kraikitpanitch, Am. J. Med. Sci., 275 (1978) 17.
15 J. A. Halstead, J. C. Smith, Jr. and M. I. Irwin, J. Nutr., 104 (1974) 345.
16 D. J. Kosman and R. I. Henkin, Lancet, i (1979) 1410.
17 H. P. Wolff, Klin. Worchschr., 34 (1956) 409.
18 G. W. Evans, P. E. Johnson, J. G. Brushmiller and R. W. Ames, Anal. Chem., 51 (1978) 839.
19 P. E. Johnson and G. W. Evans, J. Chromatogr., 188 (1980) 405.
20 N. Yoza, J. Chem. Educ., 54 (1977) 284.
21 P. H. E. Gardiner, Ph.D. Thesis, The University of Strathclyde, 1979.

Analytica Chimica Acta, 124 (1981) 295—301

STUDIES OF REACTION SEQUENCES AND QUANTITATIVE CHANGES DURING TITRATIONS BASED ON THE RELEASING EFFECT IN ATOMIC ABSORPTION SPECTROMETRY†

D. Dj. STOJANOVIC[a] and J. D. WINEFORDNER*

Department of Chemistry, University of Florida, Gainesville, FL 32611 (U.S.A.)

(Received 5th May 1980)

SUMMARY

Atomic absorption inhibition release titrations are applied for studying reactions and quantitative changes that take place during evaporation and vaporization processes in flame photometric studies of solutions containing several metal ions and an anion, X, with which the metal ions form refractory compounds. A standard solution containing one metal ion, M, and anion, X, is added continuously to a solution containing two different metal ions, E_1 and E_2, and M in the resulting solution is monitored continuously by atomic absorption spectrometry. Information about reaction processes is deduced from characteristic changes that occur in response curves when the amounts of M and X added are equivalent to amounts E_1 and E_2 present. The characteristic changes occur when E_1 and E_2 have released equivalent amounts of M from MX. The order in which different releasing agents react as well as quantitative changes in equilibria were determined from mole ratios of the different species used in different experiments. In the titration of the chlorides of lanthanum as E_1 and of strontium or calcium as E_2 with magnesium as M and phosphate as X, it was shown that lanthanum reacts before either strontium or calcium to release magnesium from phosphate.

The releasing effect is a term used [1] to identify the process by which a high concentration of one metal ion enhances the flame photometric signal of a low concentration of another metal ion in the presence of an anion with which both cations form refractory compounds in flames. It has been postulated that the releasing effect is based on displacement of the equilibrium in droplets of solution which are aspirated into the flame [1].

The releasing effect can be described by means of the following process

$$MX + EY \leftrightarrows EX + MY \leftrightarrows M + Y \qquad (1)$$

where M is the metal of low concentration being determined, E is the releasing agent of high concentration, X is the anion that forms the refractory

†Part of the paper was presented at the XXIst CSI and 8th ICAS meeting in Cambridge, Gt. Britain, July, 1979.

[a]Present address: University of Belgrade, Institute for the Application of Nuclear Energy in Agriculture, Veterinary Medicine and Forestry, 11080 Zemun, Yugoslavia.

compound, and Y is an anion that forms a readily dissociated compound. The action of a releasing agent is to force the equilibrium to the right so that the ion of interest (M) is associated with the more labile anion (Y).

The method of atomic absorption inhibition release titration [2, 3] involves titration of a solution of the releasing element with a standard solution of metal (M) and an inhibitor anion (X) and monitoring M in the solution continuously by atomic absorption spectrometry. The absorption signal increases initially because the releasing element reacts with the anion as follows

$$E + (M + X) \leftrightharpoons EX + M \tag{2}$$

Further addition of titrant leads predominantly to reaction between metal M and anion X during droplet evaporation: $M + X \leftrightharpoons MX$. The thermostable compound, MX, is formed causing an abrupt change (usually a decrease) in the slope of the response curve, which is detected as the titration end-point.

This method has, up to now, been used for examining the possibility of determining rare earths [4], as well as for studying the mechanism of formation of alkaline earth phosphate compounds [5]. In the recent studies, only one releasing element was in the solution titrated. However, with regard to further application of this method, it was of interest to establish: (i) if this titration method can be used to study equilibrium processes when two or more metal ions are present; (ii) how the equilibrium in eqn. (2) is displaced if there are two releasing elements, E_1 and E_2, in the solution titrated; (iii) which of the species will react first with anion X; and (iv) how the change in concentration of one species will reflect the displacement of the equilibrium during droplet evaporation. The initial hypothesis was that for situations in which solubility products (K_{so}) were very different, i.e. $K_{so}(E_1X) \ll K_{so}(E_2X)$, the two releasing elements would react sequentially as follows

$$E_1 + E_2 + (M + X) \leftrightharpoons E_1X + E_2 + M \tag{3}$$

and

$$E_2 + (M + X) \leftrightharpoons E_2X + M \tag{4}$$

and that the reaction $M + X \leftrightharpoons MX$ would predominate only after all E_1 and E_2 had reacted.

In order to evaluate these considerations, solutions of lanthanum chloride with either calcium chloride or strontium chloride were titrated with a standard solution of magnesium chloride and phosphoric acid. The changes in magnesium absorption during the titrations were recorded.

EXPERIMENTAL

Equipment and reagents

An atomic absorption spectrometer (Unicam SP-90A) with a Sargent-Welch recorder was used with air—hydrogen flame and a hollow-cathode lamp for magnesium (285 nm) operated at 4 mA. Titrant was added at a constant flow rate with a peristaltic pump.

Standard lanthanum chloride solution was prepared by dissolving La_2O_3 (Johnson-Matthey) in 6 M HCl. Standard solutions of calcium chloride and strontium chloride were obtained by dissolving the corresponding carbonates in minimum volumes of 6 M HCl. A standard solution of magnesium chloride and phosphoric acid was prepared by mixing the required volumes of solutions of known concentration of each substance. A fixed concentration of magnesium ions (50 ppm) in the titrant was used in all studies; variable concentrations of phosphate (200 or 350 ppm), La (4—10 ppm), Ca (4 or 6 ppm), and Sr (4—8 ppm) were used.

Procedure

The same titration procedure was used as described previously [3]. Measured volumes of solutions to be titrated were placed in a 100-ml beaker, diluted to 50 ml with distilled water, and stirred with a magnetic stirrer during titration. The recorder was adjusted to zero signal with distilled water aspirated into the flame. The aspiration tube was then transferred to the beaker containing the solution to be titrated and the addition of the titrant was commenced simultaneously by switching on the peristaltic pump. Titrant was added at a constant rate which was approximately equal to the rate of aspiration of solution into the flame (2—3 ml min^{-1}). Changes in magnesium absorption were recorded for about 2 min. Manual titrations were performed initially to prove that mixing was complete.

RESULTS AND DISCUSSION

Titration curves and processes

Relative titration signal amplitudes combined with inflection points, peaks, valleys, and comparison of titration curve shapes along with thermochemical stability information of compounds of calcium(II), magnesium(II) and lanthanum(III) with phosphate were used to identify the order of reaction of species and the possible thermal species present at various points during the titration curves. For example, the signal amplitude at the inflection point (point a) in Fig. 1(B) shows clearly that lanthanum(III) (E_1) reacts before strontium(II) (E_2); similarly in Fig. 2, a comparison of the shapes of curves A and B implies the reaction of La(III) before Ca(II).

Titration curves similar to those in Figs. 1 and 2 were used to evaluate molar reaction ratios and obtain other useful information. The maxima marked correspond to points at which all releasing element(s) (E_1, E_2, or

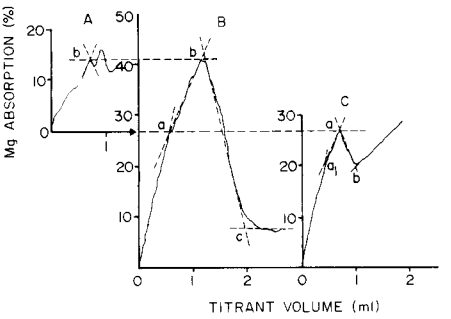

Fig. 1. Atomic absorption inhibition release titration curves for La(III), Sr(II), and mixtures of La(III) and Sr(II) titrated with a solution containing 50 ppm Mg(II) and 200 ppm phosphate. (A) 10 ppm Sr; (B) 6 ppm La + 10 ppm Sr; (C) 6 ppm La. Flow rates: air, 3 l min^{-1}; H_2, 11.5 l min^{-1}.

$E_1 + E_2$) has (have) reacted. The inflection points, when observable (point a on Fig. 1B) or determinable by comparison of the shapes of the curves (point a on Fig. 2B) represent the points at which all of E_1 has reacted. Point b (Fig. 1, curves A and B, and Fig. 2, curves A and B), represents the formation of a stable calcium (strontium) phosphate ($4CaO \cdot P_2O_5$ or $4SrO \cdot P_2O_5$). The second maximum in Figs. 1A and 2A represents the formation of another stable calcium (strontium) phosphate compound ($3CaO \cdot P_2O_5$ or $3SrO \cdot P_2O_5$ [2, 3]). The decrease in magnesium absorption between the two peaks in Fig. 1, curves A and B, is assumed to be a result of the formation of a thermostable compound between magnesium and phosphate. The subsequent increase in magnesium absorption to produce the second peaks in Fig. 1A and B is assumed to be a result of the releasing effect of calcium(II) or strontium(II) on the thermostable magnesium species. The final decrease in magnesium absorption and plateauing, or the decrease to a minimum and increase, Fig. 1A and C, is assumed to be a result of the formation of thermo-

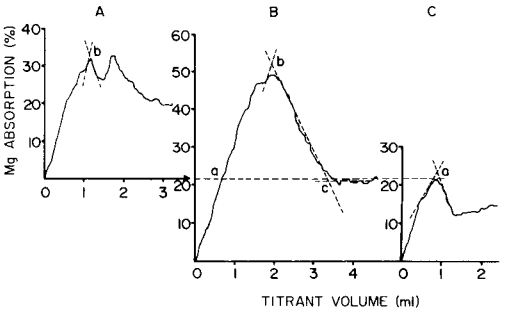

Fig. 2. Atomic absorption inhibition release titration curves for La(III), Ca(II) and mixtures of La(III) and Ca(II) titrated with a solution containing 50 ppm Mg(II) and 200 ppm phosphate. (A) 4 ppm Ca; (B) 4 ppm la + 4 ppm Ca; (C) 4 ppm La. Flow rates: air, 3.1 l min^{-1}; H_2, 9.31 l min^{-1}.

stable magnesium phosphate compounds and the continual addition of magnesium during the titration. In the case of Figs. 1C and 2C, where only lanthanum(III) is titrated, the first inflection point, a_1, represents the thermostable compound $3La_2O_3 \cdot 2P_2O_5$, whereas peak a represents the thermostable compound $La_2O_3 \cdot P_2O_5$.

Quantitative results

Numerical data are presented in Tables 1 and 2 for a variety of conditions. The three critical points (a, b, c) in Figs. 1 and 2 were used to evaluate the mole ratios of PO_4^{3-}/La^{3+}. PO_4^{3+}/Ca^{2+} or PO_4^{3-}/Sr^{2+}, and PO_4^{3-}/Mg^{2+} as functions of phosphate Ca(II) or Sr(II), and La(III).

The mole ratios of phosphate to lanthanum were in general near unity; however, as is evident from Fig. 1C or Fig. 2C, the ratio increased when Sr(II) or Ca(II), respectively, was not present. The concentration of phosphate (see Tables 1 and 2) had no significant effect on the mole ratio of phosphate to lanthanum. Therefore, the decrease in the phosphate/lanthanum ratio in the presence of Ca(II) or Sr(II) seems to be due to the releasing effect of Ca(II) or Sr(II) on La(III) (near the titration end-point for lanthanum).

The PO_4^{3-}/Ca(II) or PO_4^{3-}/Sr(II) ratios (with La(III) present) were near 0.5 for low concentrations of calcium (for 4 ppm, not for 6 ppm) or strontium (for 4—8 ppm, not for 10 ppm) but were significantly smaller than 0.5 for the higher Ca(II) or Sr(II) concentrations and seemed to decrease with increasing La(III) concentration. In addition, there was a less significant decrease in the PO_4^{3-}/La(III) ratios for both the strontium(II) and calcium(II) cases as the La(III) concentration increased. In the absence of lanthanum(III), the ratios PO_4^{3-}/Ca^{2+} or PO_4^{3-}/Sr^{2+} also were nearly 0.5. Therefore, it seems that an increase in calcium(II) or strontium(II) has relatively little effect on the displacement of eqn. (3). However, increasing the calcium(II) or strontium(II) concentration does appear to displace the equilibrium given in eqn. (4). The reduced PO_4^{3-}/Ca^{2+} or PO_4^{3-}/Sr^{2+} ratio from the expected

TABLE 1

Mole ratios for reactions of La(III) and Ca(II) with phosphate

La[a] (ppm)	50 ppm Mg + 200 ppm PO_4^{3-}						50 ppm Mg + 350 ppm PO_4^{3-}					
	Ca (ppm)	PO_4^{3-}/Ca	Ca (ppm)	PO_4^{3-c}/Ca	Ca (ppm)	PO_4^{3-}/La	Ca (ppm)	PO_4^{3-b}/Ca	Ca (ppm)	PO_4^{3-c}/Ca	Ca (ppm)	PO_4^{3-}/La
4	4	0.52[h]	2	0.55	4	1.07[f] (1.10)[d]	6	0.51[e]	4	0.49	6	0.94[g] (—)[d]
6	4	0.54[h]	3	0.52	4	0.96(1.05)	6	0.41[j]	6	0.50	6	0.99(1.10)
8	4	0.47	4	0.50[i]	4	0.90(1.05)	6	0.38	8	0.50	6	0.92(1.03)
10	4	0.47	5	0.51	4	0.81[e] (—)	6	0.36	—	—	6	0.92(1.07)
Mean		0.50		0.52		0.98(1.06)		0.38		0.50		0.94(1.06)

[a]For all data except calcium results without La(III). [b]With La(III). [c]Without La(III). [d]Values in parentheses are without Ca(II). [e]Not used in mean. [f—j]Relative standard deviations for five titrations were 5.3, 5.0, 4.6, 3.1 and 4.1%, respectively.

TABLE 2

Mole ratios for reactions of La(III) and Sr(II) with phosphate

La[a] (ppm)	50 ppm Mg + 200 ppm PO_4^{3-}						50 ppm Mg + 350 ppm PO_4^{3-}					
	Sr (ppm)	PO_4^{3-b} / Sr	Sr (ppm)	PO_4^{3-c} / Sr	Sr (ppm)	PO_4^{3-} / La	Sr (ppm)	PO_4^{3-b} / Sr	Sr (ppm)	PO_4^{3-c} / Sr	Sr (ppm)	PO_4^{3-} / La
6	10	0.45	4	0.48	10	0.99[h]	10	0.46	4	0.48	10	1.03[g]
8	10	0.44[f]	6	0.49	10	0.96	10	0.44[d]	6	0.49	10	0.98
10	10	0.40	8	0.46	10	0.94	10	0.40	8	0.50[e]	10	0.96
Mean		0.43		0.48		0.96		0.43		0.49		0.99

[a]For all data except strontium results without lanthanum. [b]With La(III). [c]Without La(III). [d–h]Relative standard deviations for five titrations were 4.8, 2.9, 5.1, 3.6 and 3.9% respectively.

value of 0.5 is most likely a competition between calcium(II) or strontium (II) and magnesium(II) for phosphate.

On the basis of the PO_4^{3-}/La^{3+} ratios at point a (Figs. 1B and 2B) and PO_4^{3-}/Ca^{2+} or PO_4^{3-}/Sr^{2+} at point b (Figs. 1B and 2B), it can be concluded that lanthanum(III) reacts with phosphate before Ca(II) or Sr(II) does, i.e., between 0 and point a. Between point a and point b, Ca(II) or Sr(II) reacts with phosphate, and between points b and c, Mg(II) reacts with phosphate; the PO_4^{3-}/Mg^{2-} compounds (ratio of 0.5 or 0.7 for 200 ppm phosphate or 350 ppm phosphate) produced here were consistent with those found in previous work [3].

Formation of the magnesium phosphate compound also occurs through a chain of intermediate compounds which, as was previously shown [6], can be represented in the general form x $MgO \cdot P_2O_5$. For these reasons, on the part of the curve (Figs. 1B and 2B) between points b and c there appears a number of inflection points. For these points, the ratio of PO_4^{3-}/Mg^{2+} is constant, which indicated that magnesium(II), similarly to calcium(II) or strontium(II) forms a compound of constant composition. The mechanism of formation of these compounds will be discussed in a subsequent paper.

Although the results of atomic absorption inhibition release titration curves are difficult to interpret, it seems possible to estimate stabilities of various compounds and to obtain supporting information for many of the thermal techniques such as differential thermal methods and thermogravimetry.

This work was supported in part by AF-AFOSR-F49620-8-C-005.

REFERENCES

1 J. I. Dinnin, Anal. Chem., 32 (1960) 1475.
2 D. Stojanović, V. Vajgand and M. Djurdjevic, Abstracts, 6th Yugoslav Conference on General and Applied Spectroscopy, Bled, October 1976, No. AA2, Proceedings Vol. I (1977) 174.

3 D. Stojanović, J. Bradshaw and J. D. Winefordner, Anal. Chim. Acta, 96 (1978) 45.
4 V. Vajgand and D. Stojanović, Chem. Anal. (Warsaw), 20 (1975) 973.
5 D. Stojanović, J. D. Winefordner, J. Bradshaw and V. Vajgand, Abstracts, 422 p., Euroanalysis III, Dublin, August 1978.
6 D. Dj. Stojanović, J. D. Winefordner and V. J. Vajgand, Abstracts, No. 125 XX CSI and 7th ICAS, Prague 1977.
7 J. Yofe, R. Avni and M. Stiller, Anal. Chim. Acta, 28 (1963) 331.

Analytica Chimica Acta, 124 (1981) 303—314

THE AMPEROMETRIC RESPONSE OF TUBULAR ELECTRODES APPLIED TO FLOW-INJECTION DETERMINATIONS

P. LAWRENCE MESCHI[a] and DENNIS C. JOHNSON*

Department of Chemistry, Iowa State University, Ames, IA 50011 (U.S.A.)

(Received 17th September 1980)

SUMMARY

The classical treatment by Taylor for the dispersion of mass injected into a fluid stream in a linear, tubular channel is applied for amperometric detection in flow-injection systems with a tubular, flowthrough electrode. Peak current is predicted to be dependent upon the 1/3rd root of flow rate for low dispersion and the −1/6th root of flow rate for high dispersion. Agreement between experimental results and theory is excellent for flow rates of 0.5 ml min^{-1} or less in a linear, tubular channel with an inner radius of 0.0483 cm. As examples, experimental and predicted currents agree to better than 0.1 μA throughout a peak with a maximum value near 2 μA, and effects of retention volume, sample volume, and flow rate on the ratio of peak current to steady-state current are predicted with errors of 9% or less.

A natural application of tubular electrodes is for amperometric detection of an electroactive species in a stream of supporting electrolyte. In numerous published examples, solutions are continuously passed through the tubular electrode at a constant flow rate so that steady-state currents are observed [1—7]. The relationship of the limiting steady-state current, I_{ss}, in a tubular electrode and the analytical concentration (C_o) is given [8, 9] by

$$I_{ss} = 5.43\, nFL^{2/3}\, v_f^{1/3}\, D^{2/3}\, C_o \qquad (1)$$

where D is the diffusion coefficient ($cm^2\ s^{-1}$), v_f is the flow rate ($cm^3\ s^{-1}$), L is the length of the tubular electrode (cm), n and F have their usual electrochemical significance, and C_o is the concentration (mol cm^{-3}) of the electroactive species in the sample solution.

In some recent work tubular electrodes have been applied for amperometric detection in liquid chromatography [10—15] and in flow-injection systems [15—17]. In flow-injection systems, a small volume of the sample, V_s, is introduced into a continuous stream in a system with a total retention volume, V_R. During transport of the sample from the point of injection to the detector, the sample is dispersed within the fluid stream because of diffusion and the non-uniform velocity profile in the fluid channel. For a small volume of sample, a peak-shaped response is normally obtained when

[a]Present address: EXXON Research and Engineering Co., Linden, NJ 07036, U.S.A.

the detector signal is recorded as a function of time. For amperometric detection, the peak value of the current, I_p, as well as the area of the peak, Q_p, have been found empirically to be linear functions of the concentration of electroactive species in the sample [10—14]. Because of dispersion, the concentration corresponding to the peak current may be significantly less than the concentration of the solution injected. Yet, in several publications describing applications of tubular electrodes under conditions of high dispersion, discussions of results have been prefaced by general statements regarding steady-state applications of tubular electrodes [10, 11, 16] that included the tacit implication that I_p is analogous to I_{ss} with a similar dependence on all experimental parameters, including flow rate.

Extensive research has been conducted on the dispersion of matter injected into a fluid stream, and Růžička and Hansen [18] have discussed the effect of dispersion in flow-injection systems. Růžička and Hansen introduced the term flow-injection analysis, but the term flow-injection system or determination is preferred here, because analysis implies a more extensive operation than the application of a sample-processing system with a monitoring transducer. Experimental verification of mathematical derivations, when provided, have generally utilized detection systems which sample the cross-section of the stream, e.g., by spectrophotometric detection. A tubular electrode detects only the electroactive species near the wall of the tubular channel. In this work, Taylor's treatment of dispersion [19, 20] is reviewed and applied to flow-injection systems with amperometric detection by tubular electrodes.

THEORY

Dispersion

The radial profile of the axial fluid velocity in a linear tubular channel, under the restriction of laminar flow, is described by the Poiseuille equation, $U(r) = U_o[1 - r^2/a^2]$, where U_o is the velocity at the axis of the channel ($r = 0$) and $U(r) = 0$ at the wall ($r = a$). For laminar flow, all fluid motion is parallel to the axis of the channel and radial velocity is zero at all points. The volume flow rate, v_f, in the channel is related to U_o [9] by $v_f = 0.5\,\pi a^2\,U_o$. (For convenience, all symbols are listed in Table 1.) A sample injected as a plug into the fluid stream is dispersed by convection as depicted in Fig. 1. Dispersion by diffusion in the axial direction is assumed to be negligible for all values of U_o used in practice; dispersion in the radial direction occurs solely by diffusion and arrows are shown in Fig. 1 to depict the direction of this diffusional transport. At the leading edge of the sample, diffusion is toward the wall of the channel; at the trailing edge of the sample, diffusion is toward the axis of the channel.

In the dispersion of mass injected into a fluid stream, the concentration, C, at any point in the stream will be a function of the radial and axial coordinates and time, $C = C(x,r,t)$. Taylor [19, 20] assumed that the problem

TABLE 1

List of symbols

a	Inner radius of tubular channel (cm)
C	Concentration of analyte (mol cm^{-3})
C_m	Mean value of C at a specified axial position in a tubular channel (mol cm^{-3})
C_o	Analytical concentration of analyte in sample (mol cm^{-3})
δ	Thickness of the diffusion layer at the electrode surface (cm)
d	Normalized distance of the outer boundary of the diffusion layer measured from the axis of the tubular electrode (cm)
D	Diffusion coefficient of analyte (cm^2 s^{-1})
F	Faraday constant (96,487 C $equ.^{-1}$)
I	Limiting electrode current (A)
I_p	Peak value of the limiting current (A)
I_{ss}	Steady-state value of the limiting current (A)
K	Dispersion coefficient (cm^2 s^{-1})
L	Length of the tubular electrode (cm)
n	Number of electrons in electrode reaction (equ. mol^{-1})
Q_p	Time integral of current—time peak (C)
r	Radial coordinate (cm)
t	Time variable (s)
τ	Value of t when C_m is a maximum in the detector (s)
U	Fluid velocity in axial direction (cm s^{-1})
U_m	Mean value of U at a specified axial position in a tubular channel (cm s^{-1})
U_o	Value of U at $r = 0$ (cm s^{-1})
v_f	Volume flow rate (ml s^{-1})
V_R	Retention volume (ml)
V_s	Sample volume (ml)
x	Axial coordinate of moving frame of reference (cm)
X	Axial coordinate of stationary frame of reference (cm)
X_D	Axial position of the detector (cm)
z	Normalized radial coordinate (r/a)
ζ	Arbitrary variable

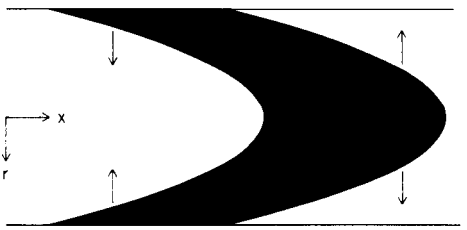

Fig. 1. Axial dispersion by convection illustrated for analyte injected into a fluid stream in a tubular channel flowing under laminar conditions. Arrows indicate direction of diffusional transport.

of dispersion in a narrow tubular channel can be modeled after the case of linear diffusion

$$\partial C_m(x,t)/\partial t = K\,\partial^2 C_m(x,t)/\partial x^2 \tag{2}$$

where $C_m(x,t)$ is the mean concentration and K is the dispersion coefficient. The mean concentration averaged over the cross-section of the channel at any point x measured along the axis is given by

$$C_m(x,t) = (2/a^2) \int_o^a r\, C(x,r,t)\, dr \tag{3}$$

The dispersion coefficient, K, in eqn. (2) is related to the diffusion coefficient, D, of the electroactive species and the mean velocity of the fluid, U_m, by

$$K = a^2 U_m^2/48D \tag{4}$$

where $U_m = (2/a^2) \int_o^a r\, U(r)\, dr$. The distance variable, x, is the axial coordinate in a frame of reference that is moving downstream at the velocity U_m. The relationship between x and axial coordinate of the stationary frame of reference, X, is given by $x = X - U_m t$. At $t = 0$, the center of the sample plug is positioned such that $x = X = 0$.

Equation (2) can be solved by standard procedures [21]. The solution, assuming that the detector volume is negligible, is given by

$$C_m(X_D,t) = (C_o/2)\,\{\text{erf}\,[(V_s + V_R - v_f t)/(2\pi a^2 (Kt)^{1/2})] + \text{erf}\,[(v_f t - V_R)/(2\pi a^2 (Kt)^{1/2})]\} \tag{5}$$

where $C_m(X_D,t)$ is the mean concentration at the position of the detector ($X = X_D$). In eqn. (5), erf is the error function defined as $\text{erf}\,(t) = (2/\pi^{1/2}) \int_o^t \exp(-y^2)\, dy$.

The results of experimental work [22, 23] and numerical calculations [24, 25] for narrow and straight channels are in good agreement with eqn. (5) for sufficiently large v_f and t, for which the assumption is met that axial diffusion can be ignored. Subsequent work has removed the restrictions of large v_f, and small a, and has extended Taylor's solution to include the effects of axial diffusion [26], the time dependency of K [25], and the effect of curvature of the tubular channel [27, 28]. The extended solutions, however, are generally not in a form convenient for use in quantitative work.

Amperometric response

The limiting amperometric response of a tubular electrode to dispersed electroactive species in the fluid stream depends on the concentration at the outer boundary of the diffusion layer at the electrode—solution interface rather than the mean concentration in the stream. Knowledge of the radial distribution of the concentration is necessary, therefore, to describe fully the amperometric response of a tubular electrode. The radial distribution of concentration for the normalized radial coordinate, $z = r/a$ [20], is given by

$$C(X_D,z,t) = C_m(X_D,t) + (a^2U_m/4D)\,[-1/3 + z^2 - 1/2\,z^4]\,dC_m(X_D,t)/dX \quad (6)$$

The derivative $dC_m(X_D,t)/dX$ can be evaluated by differentiating eqn. (5) with respect to V_R. Substitution for $C_m(X_D,t)$ and $dC_m(X_D,t)/dX$ into eqn. (6), for the radial distribution of the concentration at the position of the detector, yields

$$C(X_D,z,t) = C_o\left\{0.5\ \mathrm{erf}\left[\frac{V_s + V_R - v_f t}{2\pi a^2(Kt)^{1/2}}\right] + 0.5\ \mathrm{erf}\left[\frac{v_f t - V_R}{2\pi a^2(Kt)^{1/2}}\right]\right.$$
$$+ \frac{v_f}{8\pi^{3/2}D(Kt)^{1/2}}\left[-\frac{1}{3} + z^2 - \frac{z^4}{2}\right]\cdot\left\{\exp\left[-\left(\frac{V_s + V_R - v_f t}{2\pi a^2(Kt)^{1/2}}\right)^2\right]\right.$$
$$\left.\left. - \exp\left[-\left(\frac{v_f t - V_R}{2\pi a^2(Kt)^{1/2}}\right)^2\right]\right\}\right\} \quad (7)$$

The thickness of the diffusion layer at the surface of the tubular electrode, δ, is written as a normalized function of the radius of the tubular channel: $\delta = (aLD/U_o)^{1/3}$. Hence the normalized radial distance corresponding to the outer boundary of the diffusion layer is $z = d = 1 - \delta/a$. The value of $C(X_D,d,t)$ is expected to lag slightly behind the values of $C_m(X_D,t)$ for most practical flow-injection systems because radial diffusion is not sufficiently rapid to maintain radial homogeneity of the electroactive species in the flow stream, i.e. $dC/dr \neq 0$. The existence of the lag would cause a slight difference in the response of a spectrophotometric detector, which responds to $C_m(X_D,t)$, from that of the amperometric detector, which responds to $C(X_D,d,t)$.

For a very short tubular electrode, the net consumption of analyte is small and the presence of amperometric detection produces negligible error in eqn. (7). Furthermore the time-dependent response of the tubular electrode can be predicted with good accuracy by the equation

$$I(t) = I_{ss}\,C(X_D,d,t)/C_o \quad (8)$$

where I_{ss} is given by eqn. (1) and $C(X_D,d;t)$ is given by eqn. (7) solved for $z = d$. In effect, eqn. (8) is presumed valid when the rate of change of $C_m(X_D,t)$ is small relative to the transient response of the diffusion layer of the tubular electrode. Equation (8) is actually of general usefulness for flow-through amperometric detectors of any design where I_{ss} corresponds to the steady-state limiting current for that electrode.

Peak current

The value of the peak current, I_p, is observed approximately at the time when the origin of the moving frame of reference reaches the position of the detector, $t = \tau$, where τ is defined by

$$\tau = (0.5V_s + V_R)/v_f \quad (9)$$

At $t = \tau$, the derivatives $dC_m(X_D,\tau)/dX$ and $dC(X_D,z,\tau)/dz$ are zero (see eqns. 5 and 6). Hence, eqn. (6) becomes

$$C(X_D,d,\tau) = C_m(X_D,\tau) \tag{10}$$

and eqn. (5) becomes

$$C_m(X_D,\tau) = C_o \{\text{erf}\,[V_s/4\pi a^2(Kt)^{1/2}]\} \tag{11}$$

On the basis of eqn. (8), I_p is then given by

$$I_p = I_{ss} \{\text{erf}\,[V_s/4\pi a^2(K\tau)^{1/2}]\} \tag{12}$$

After substituting for τ based on eqn. (8), and using the definition of $K = a^2U_m^2/48D$, eqn. (4), eqn. (12) becomes

$$I_p = I_{ss} \{\text{erf}\,[V_s v_f^{1/2}/4\pi a^2 K^{1/2}(0.5V_s + V_R)^{1/2}]\} \tag{13}$$

It quickly becomes apparent upon examination of eqn. (13) that plots of log I_p vs. log v_f can have slopes which are equal to or less than the theoretical value of 1/3 for I_{ss} (see eqn. 1) depending on the values of v_f, V_s and V_R.

Equation (13) can be simplified for peaks observed under conditions of high dispersion, i.e. low v_f and $V_s \ll V_R$. Tabulated values of erf$\{\zeta\}$ are given in Table 2 for $0 \leqslant \zeta \leqslant 1.0$. The value of erf$\{\zeta\}$ is given approximately by $2\zeta/\pi^{1/2}$ for small ζ as shown in Table 2. The error in this approximation is only 1.3% for $\zeta = 0.2$. Hence, for low v_f and $V_s \ll V_R$, eqn. (13) approaches

$$I_p = I_{ss}\,[V_s/2\pi^{3/2}a^2]\,[v_f/K(0.5V_s + V_R)]^{1/2} \tag{14}$$

Since I_{ss} is proportional to $v_f^{1/3}$, and K is proportional to v_f^2, a plot of log I_p vs. log v_f is predicted to have a slope of $-1/6$ under the conditions of high dispersion. The log–log plot of I_p/I_{ss} vs. v_f is predicted to have a slope of $-1/2$ under these conditions.

EXPERIMENTAL

The platinum tubular electrode was the same as described earlier [29]. The inner radius was drilled to 0.0397 cm and the length of the electrode was 0.159 cm. The inlet channel of the detector was 5.4 cm long and was also drilled to an inner radius of 0.0397 cm. Procedures for polishing and

TABLE 2

Numerical evaluation of error function

ζ	erf$\{\zeta\}$	$2\zeta/\pi^{1/2}$	Error (%)
0.0	0.000	0.000	0.0
0.1	0.112	0.113	0.9
0.2	0.223	0.226	1.3
0.4	0.428	0.451	5.3
0.6	0.604	0.677	12.1
1.0	0.843	1.128	33.8

pretreatment of the electrode were those described earlier [29]. No attempt was made to determine the extent to which the polishing procedure may have enlarged the inner radius of the electrode. The reference electrode was a saturated calomel electrode (SCE) and the counter electrode was a spiral of Pt wire. The tubular electrode produced steady-state data for which the slope of plots of log I_{ss} vs. log v_f had an average value of 0.29 in acceptable agreement with eqn. (1). A brief discussion of some consequences of the deviation from theory observed for the sensitivity of a tubular electrode has been presented [29]. The benefit of comparing experimental and theoretical values of the ratio I_p/I_{ss} is that slight deviations in the sensitivity should have little effect on the validity of the comparisons.

The flow-injection system was constructed according to conventional designs [30] with pumping provided by a Minipuls 2-HP4 peristaltic pump (Gilson Medical Electronics, Inc., Middleton, WI); a dual piston pump, (Pine Instrument Co., Grove City, PA); or a Milton Roy MiniPump with the model 709 Pulse Dampener (Laboratory Data Control, Riviera Beach, FL). The flow rates were calibrated by measurement of the volume of supporting electrolyte delivered through the flow analyzer, during a known time period, under each set of experimental conditions. The Cheminert sample-injection valve and teflon tubing (nominally 0.031 in i.d.) are also available from Laboratory Data Control. The internal volumes of several segments of teflon tubing were determined titrimetrically. Each segment was installed as a "sample loop" on the injection valve and several aliquots of a standard solution of sulfuric acid were injected into a stream of triply-distilled water, collected in a flask and titrated with a standard solution of sodium hydroxide to the phenolphthalein endpoint. The inner radius of the teflon tubing was calculated to be 0.0483 ± 0.0002 cm from values of the internal volume and the lengths of the various segments.

The value of V_R for each configuration of the flow system was taken to be the sum of the internal volume of the connecting tubing and the internal volume calculated for the inlet channel of the detector. Values of I_p were observed to be very sensitive to the conformation of the tubing which connected the injection valve and the tubular electrode. All data presented here were obtained with the tubing maintained in a linear conformation.

Other details of experimental procedure are identical to those described earlier [29].

RESULTS AND DISCUSSION

Current—time peaks

A typical current—time peak for the anodic detection of iodide is shown in Fig. 2. Also shown are several theoretical values of $I(t)$ calculated for the identical experimental parameters on the basis of the predicted concentration at the outer boundary of the diffusion layer, $C(X_D,d,t)$, according to eqn. (8). For comparison, values of $I(t)$ are also given which were calculated in a

manner similar to eqn. (8) but using the mean concentration of analyte, $C_m(X_d,t)$, instead of $C(X_d,d,t)$. The value of I_{ss} used in these calculations was measured experimentally on the same apparatus operated under steady-state conditions to normalize the data for any slight change in the sensitivity of the detector; deviations of the observed values of I_{ss} from theory have been discussed [29]. As a consequence of the use of the observed value of I_{ss} for predicting $I(t)$, the curves in Fig. 2 are more significant as they pertain to the prediction of peak shape than to a prediction of absolute values of current. All experimental parameters affecting dispersion were measured in independent experiments. Values of V_s, V_R and v_f were obtained by the procedures described above; and a, the radius of the tubing, was calculated from the measured values of volume and the length of the segments of tubing. D, the diffusion coefficient for iodide, was obtained from the linear plots of the limiting anodic current for iodide at a rotating disc electrode as a function of the square root of the rotational velocity. Values of K were calculated from $K = a^2U_m^2/48D$; values of d were calculated from $d = 1 - \delta/a$. Since all the parameters affecting dispersion were obtained by procedures independent of the flow-injection method, the comparison of experimental and theoretical current—time peaks in Fig. 2 is a valid test of the theoretical model.

An examination of Fig. 2 shows the excellent agreement between theory and experiment. As predicted, the experimental peak correlates best with calculations based on the predicted concentration at the outer boundary of the diffusion layer in the detector, $C(X_D,d,t)$. The lower portion of the trailing edge of the experimental peak does deviate slightly from the theoretical values calculated from $C(X_D,d,t)$, and follows more closely the values calculated from the mean concentration, $C_m(X_D,t)$. This may indicate better radial mixing at the trailing edge of the sample zone than predicted

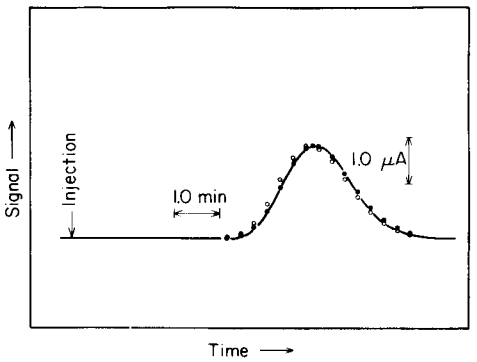

Fig. 2. Experimental and calculated I—t peaks for flow injection with the tubular electrode: (○) calculated for $C_m(X_D,t)$; (•) calculated for $C(X_D,d,t)$; (——) observed. Parameters: V_R = 2.25 ml, V_s = 0.145 ml, v_f = 0.50 ml min^{-1}, K = 220 cm^2 min^{-1}, C_o = 5.00 × 10^{-4} M, I_{ss} = 10.34 μA.

by the model. Nevertheless, the deviation is not significant and does not indicate a serious flaw in the theory.

Variation of V_R and V_s

The changes in current–time peaks obtained by the flow-injection method with the tubular electrode as a function of variations in V_R and V_s are shown in Figs. 3 and 4, respectively. An I–t peak is included in Fig. 3, which was calculated for the hypothetical case of no dispersion with V_R = 0 ml. The height of this peak is the experimental value of I_{ss} and the width is assumed equal to V_s/v_f.

A test of the theory is illustrated by data in Tables 3 and 4, where experimental values of I_p/I_{ss} are compared to the theoretical values predicted by eqn. (13) as a function of V_R and V_s. The agreement is excellent with no error in excess of 3%.

Variation of v_f

Experimental values of I_p/I_{ss} as a function of v_f are compared with the theoretical values in Table 5. Agreement is excellent at low v_f; however, error in excess of 10% is observed for large v_f. The deviation of experiment from theory is concluded to result from approximation in Taylor's solution. The Taylor solution represents a limiting case which is applicable to large values of retention time, i.e. large V_R and small v_f. The process of the dispersion of mass, as depicted by the Taylor solution, is established after a finite time following addition of the sample. In the interim, dispersion is

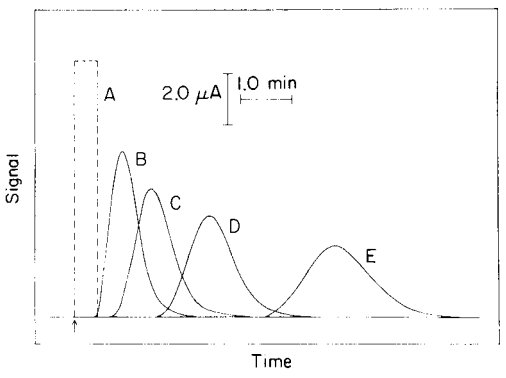

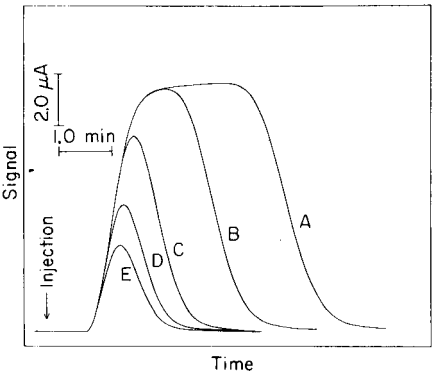

Fig. 3. Current vs. time peaks obtained for flow injection with the tubular electrode as a function of V_R. The V_R values are: (A) 0.00 ml (calculated); (B) 0.259 ml; (C) 0.569 ml; (D) 1.149 ml, and (E) 2.363 ml. Other parameters: V_s = 0.226 ml, v_f = 0.50 ml min^{-1} and C_o = 5.00 × 10^{-4} M.

Fig. 4. Current vs. time peaks obtained for flow injection with the tubular electrode as a function of V_s. The V_s values are: (A) 1.663 ml; (B) 0.955 ml; (C) 0.419 ml; (D) 0.226 ml; (E) 0.147 ml. Other parameters: V_R = 0.569 ml, v_f = 0.50 ml min^{-1} and C_o = 5.00 × 10^{-4} M.

TABLE 3

Peak current as a function of retention volume[a]

V_R (ml)	I_p observed (μA)	I_p/I_{ss}[b]		
		Observed	Eqn. (13)	Error (%)
0.286	4.50	0.435	0.424	2.5
0.594	3.37	0.326	0.319	2.1
0.821	2.95	0.285	0.277	2.8
1.168	2.46	0.238	0.236	0.8
2.254	1.79	0.173	0.174	−0.6

[a]Conditions: V_s = 0.145 ml, C_o = 5.0 × 10^{-4} M NaI in 0.10 M H_2SO_4, I_{ss} = 10.34 μA (observed), D = 1.74 × 10^{-5} cm^2 s^{-1}, a = 0.0483 cm, v_f = 0.503 ml min^{-1}, K = 2.20 × 10^{-2} cm^2 min^{-1} (calculated). [b]y = (0.954 ± 0.01)x + 0.008 ± 0.003; s_{yx} = 0.002; r = 0.9998.

TABLE 4

Peak current as a function of sample volume[a]

V_s (ml)	I_p observed (μA)	I_p/I_{ss}[b]		
		Observed	Eqn. (13)	Error (%)
0.060	0.74	0.072	0.073	−1.4
0.145	1.86	0.179	0.174	2.7
0.214	2.67	0.257	0.252	1.9
0.419	4.94	0.475	0.462	2.6

[a]Conditions: V_R = 2.254 ml, v_f = 0.503 ml min^{-1}, I_{ss} = 10.40 μA (observed); other parameters as specified in Table 3. [b]y = (0.967 ± 0.005)x + 0.0026 ± 0.0014; s_{yx} = 0.0015; r = 0.99997.

TABLE 5

Peak current as a function of volume flow rate[a]

V_f (ml min^{-1})	I_p observed (μA)	I_{ss} observed (μA)	I_p/I_{ss}[b]		
			Observed	Eqn. (13)	Error (%)
0.50	3.58	9.88	0.362	0.356	1.7
1.00	3.36	12.33	0.273	0.256	6.6
1.50	3.10	13.84	0.224	0.210	6.7
2.00	3.16	15.39	0.205	0.182	12.6

[a]Conditions: V_s = 0.226 ml, V_R = 1.168 ml; other parameters as specified in Table 3. [b]y = (1.0 ± 0.035)x − 0.04 ± 0.01; s_{yx} = 0.04; r = 0.999.

still diffusive in nature but corresponds to a coefficient of dispersion which is smaller than that predicted by eqn. (4). In this time period, K steadily increases from the initial value to the value given by eqn. (4). The theory summarized here, then, overestimates the extent of dispersion for small values of retention time. Gill and Sankarasubramanian [25] state in their analysis that K becomes essentially constant and approximately equal to Taylor's value at $t = 0.5\ a^2/D$. When their criterion is applied to this study, Taylor's solution (eqn. 4) becomes applicable for $\tau > 1.12$ min. This corresponds to $v_f <$ 1.14 ml min^{-1} in Table 5. The data in Tables 3 and 4, showing excellent agreement between experiment and theory, were obtained for $v_f = 0.5$ ml min^{-1}.

For the case of very high dispersion, i.e. $V_R \gg V_s$ and low v_f, I_p is predicted by eqn. (14) to be proportional to the $-1/6$th root of v_f, and a plot of log I_p/I_{ss} vs. log v_f will have a slope of $-1/2$. This prediction is tested in Fig. 5 for $V_R = 1.168$ ml, $V_s = 0.226$ ml and $0.5 \leqslant v_f \leqslant 2.0$ ml min^{-1}. These conditions are typical of those conveniently chosen for flow-injection systems. The best linear fit of the log–log plot of I_p/I_{ss} vs. v_f (dashed line) has a slope of -0.43. The experimental value of I_p/I_{ss} is in good agreement with the values predicted by eqn. (14) (solid line) only for the lowest value of v_f used in this study. The numerical value of the argument of the error function in eqn. (13) is 0.33 for $v_f = 0.5$ ml min^{-1} and it is clear, from an examination of Table 2, that dispersion under these conditions is just sufficiently large to conform to the limiting case predicted by eqn. (14).

Conclusions

Taylor's theory is reviewed for the dispersion of an analyte injected into a fluid stream under conditions of laminar flow in a linear, tubular channel, and the theory is applied to the use of a tubular electrode for amperometric flow-injection detection. It is demonstrated that the concentration profile of analyte sensed by the detector lags slightly behind the profile of the mean

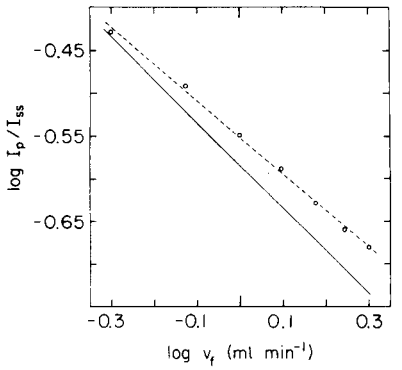

Fig. 5. Dependence of I_p/I_{ss} on v_f for case of high dispersion. (---) Linear fit of data; (—) theoretical from eqn. (14). $V_R = 1.168$ ml, $V_s = 0.226$ ml and $C_o = 5.00 \times 10^{-4}$ M.

concentration in the channel. The peak current is predicted to be proportional to the 1/3rd root of flow rate for low dispersion when the sample volume is large and the peak current approaches the steady-state current. Peak current is predicted to be proportional to the −1/6th root of the flow rate for cases of high dispersion when the sample volume is very small relative to the retention volume. It should be relatively simple to determine the combination of values for the operating parameters such that the peak current would have a minimal dependence upon flow rate.

The agreement of experimental results with theory is excellent for moderately low values of flow rate. Deviation of experimental results from theory at high values of flow rate is concluded to result from the limiting value used for the dispersion coefficient being inadequate for small values of the retention time. The effect of curvature in the tubing which connects the sample-injection valve and the detector will be considered in a subsequent publication.

Support for this work was from the National Science Foundation (CHE-7617826).

REFERENCES

1 T. O. Oesterling and C. L. Olson, Anal. Chem., 39 (1967) 1543.
2 W. J. Blaedel and C. L. Olson, Anal. Chem., 36 (1964) 343.
3 D. B. Easty, W. J. Blaedel and L. Anderson, Anal. Chem., 43 (1971) 509.
4 J. Bomstein, J. M. Shepp, S. T. Dawson and W. J. Blaedel, J. Pharm. Sci., 55 (1966) 94.
5 W. R. Seitz, R. M. Jones, L. N. Klatt and W. D. Mason, Anal. Chem., 45 (1973) 840.
6 W. J. Blaedel and S. L. Boyer, Anal. Chem., 43 (1971) 1538.
7 W. D. Mason and C. L. Olson, Anal. Chem., 42 (1970) 488.
8 V. G. Levich, Physicochemical Hydrodynamics, Prentice-Hall, Englewood Cliffs, NJ, 1962, pp. 112—116.
9 W. J. Blaedel, C. L. Olson and L. R. Sharma, Anal. Chem., 35 (1963) 2100.
10 R. W. Andrews and D. C. Johnson, Anal. Chem., 48 (1976) 1056.
11 R. J. Davenport and D. C. Johnson, Anal. Chem., 46 (1974) 1971.
12 E. C. Lewis and D. C. Johnson, Clin. Chem., 24 (1978) 1711.
13 A. MacDonald and P. D. Duke, J. Chromatogr., 83 (1973) 331.
14 D. N. Armentrout, J. D. McLean and M. W. Long, Anal. Chem., 51 (1979) 1039.
15 V. L. Morris, M.S. Thesis, Iowa State University, Ames, IA, 1976.
16 K. Stulik and V. Hora, J. Electroanal. Chem., 70 (1976) 253.
17 B. G. Snider and D. C. Johnson, Anal. Chim. Acta., 105 (1979) 25.
18 J. Růžička and E. H. Hansen, Anal. Chim. Acta, 99 (1978) 37.
19 G. Taylor, Proc. R. Soc. London, Ser. A, 219 (1953) 186.
20 G. Taylor, Proc. R. Soc. London, Ser. A, 225 (1954) 473.
21 J. Crank, Mathematics of Diffusion, Clarendon, Oxford, 1957, p. 13.
22 A. Bournia, J. Coull and G. Houghton, Proc. R. Soc. London, Ser. A 261 (1961) 227.
23 E. V. Evans and C. N. Kenney, Proc. R. Soc. London, Ser. A, 284 (1965) 540.
24 W. N. Gill and V. Ananthakrishnan, AlChE J., 13, (1967) 801.
25 W. N. Gill and R. Sankarasubramanian, Proc. R. Soc. London, Ser. A, 316 (1970) 341.
26 R. Aris, Proc. R. Soc. London, Ser. A, 235 (1956) 67.
27 M. Emin Erdogan and P. C. Chatwin, J. Fluid Mech., 29 (1967) 465.
28 R. J. Nunge, T.-S. Lin and W. N. Gill, J. Fluid Mech., 34 (1972) 363.
29 P. L. Meschi and D. C. Johnson, Anal. Chem., 52 (1980) 1304.
30 J. A. Lown, R. Koile and D. C. Johnson, Anal. Chim. Acta, 116 (1980) 33.

Analytica Chimica Acta, 124 (1981) 315—320

THE COULOMETRIC RESPONSE OF TUBULAR ELECTRODES APPLIED TO FLOW-INJECTION DETERMINATIONS

P. LAWRENCE MESCHI[a] and DENNIS C. JOHNSON*

Department of Chemistry, Iowa State University, Ames, IA 50011 (U.S.A.)

GLENN R. LUECKE

Department of Mathematics, Iowa State University, Ames, IA 50011 (U.S.A.)

(Received 17th September 1980)

SUMMARY

The equation derived in the preceding paper for the amperometric response of a tubular electrode for applications to flow-injection determinations is integrated to predict the relationship of peak area to the experimental parameters. The peak area is shown to be independent of the extent of dispersion of the sample. Ratios of the observed and predicted peak areas had an average value of 0.992 with a relative standard deviation of 2%.

The effect of dispersion upon amperometric detection in a fluid stream was considered in a previous paper and the response of a tubular electrode was derived for flow-injection determinations [1]. An equation was given for the peak current, I_p, and the dependence of I_p upon flow rate, v_f, under conditions of high dispersion was shown to be substantially different than observed under steady-state operation. The peak area, Q_p, has been observed empirically to be a useful measure of analytical concentration [2—4]. This paper describes the theoretical prediction of Q_p for a tubular electrode in flow-injection systems. The result is predicted to be generally applicable to liquid chromatography using a single internal standard because Q_p is indepndent of the dispersion, i.e., retention volume (V_R) and retention time (τ).

THEORY

The area of any current—time peak can be evaluated according to $Q_p = \int_0^\infty I(t)dt$. If $I(t)$ is written as $I(t) = I_{ss}C(X_D,d,t)/C_o$ (eqn. 8 [1]) in terms of the steady-state current, I_{ss}, for an analytical concentration, C_o then

$$Q_p = (I_{ss}/C_o) \int_0^\infty C(X_D,d,t)dt \qquad (1)$$

where $C(X_D,d,t)$ is given by eqn. (7) of ref. [1] evaluated at the outer boundary of the diffusion layer, $z = d$. Equation (1) can now be rewritten as

---

[a]Present address: EXXON Research and Engineering Co., Linden, NJ 07036, U.S.A.

$$Q_p = I_{ss} \int_0^\infty \left\{0.5 \operatorname{erf}\left[\frac{V_s + V_R - v_f t}{2\pi a^2 (Kt)^{1/2}}\right] + 0.5 \operatorname{erf}\left[\frac{v_f t - V_R}{2\pi a^2 (Kt)^{1/2}}\right]\right.$$

$$+ \frac{v_f}{8\pi^{3/2} D (Kt)^{1/2}} \left[-\frac{1}{3} + d^2 - \frac{d^4}{2}\right] \cdot \left\{\exp\left[-\left(\frac{V_s + V_R - v_f t}{2\pi a^2 (Kt)^{1/2}}\right)^2\right]\right.$$

$$\left.\left. - \exp\left[-\left(\frac{v_f t - V_R}{2\pi a^2 (Kt)^{1/2}}\right)^2\right]\right\}\right\} dt \qquad (2)$$

(where erf designates the error-function). (Symbols as defined in Table 1 of [1].)

For convenience, the integral of eqn. (2) is separated into two integrals, symbolized by A and B, such that Q_p is calculated by

$$Q_p = I_{ss} \{0.5\, A + (v_f / 8\pi^{3/2} D)[-1/3 + d^2 - (d/2)^4]\, B\} \qquad (3)$$

$$\text{where } A = \int_0^\infty \left\{\operatorname{erf}\left[\frac{V_s + V_R - v_f t}{2\pi a^2 (Kt)^{1/2}}\right] + \operatorname{erf}\left[\frac{v_f t - V_R}{2\pi a^2 (Kt)^{1/2}}\right]\right\} dt \qquad (4)$$

$$\text{and } B = \int_0^\infty \frac{1}{(Kt)^{1/2}} \left\{\exp\left[-\left(\frac{V_s + V_R - v_f t}{2\pi a^2 (Kt)^{1/2}}\right)^2\right] - \exp\left[-\left(\frac{v_f t - V_R}{2\pi a^2 (Kt)^{1/2}}\right)^2\right]\right\} dt \qquad (5)$$

For the evaluation of Integral A, the following substitutions are made for convenience: $b = V_R$; $c = V_s + V_R$; $f = 2\pi a^2 K^{1/2}$; $g = v_f$; $\alpha(t) = (gt - b)/t^{1/2} f$; $\beta(t) = (gt - c)/t^{1/2} f$.

Thus, eqn. (4) becomes

$$A = \int_0^\infty \{\operatorname{erf}[-\beta(t)] + \operatorname{erf}[\alpha(t)]\} dt \qquad (6)$$

The error function is an odd function, i.e. $\operatorname{erf}[-\zeta] = -\operatorname{erf}[\zeta]$, and eqn. (6) can be written as

$$A = \int_0^\infty \{\operatorname{erf}[\alpha(t)] - \operatorname{erf}[\beta(t)]\} dt \qquad (7)$$

Because $\alpha(t) > \beta(t)$ and $\operatorname{erf}[t] = (2/\pi^{1/2}) \int_0^t \exp[-y^2]\, dy$, eqn. (7) can be rewritten as the double integral

$$A = (2/\pi^{1/2}) \int_0^\infty \int_{\beta(t)}^{\alpha(t)} \exp[-y^2]\, dy\, dt = (2/\pi^{1/2}) \iint_R \exp[-y^2]\, dy\, dt \qquad (8)$$

The symbol R in eqn. (8) is the space between the two curves $y = \beta(t)$ and $y = \alpha(t)$. Equation (8) is solved by reversing the order of integration and integrating between new limits obtained by solving the equation $y = \alpha(t)$ and $y = \beta(t)$ for t. These limits are designated $\alpha^{-1}(y)$ and $\beta^{-1}(y)$, respectively. As t goes from 0 to ∞, y ranges from $-\infty$ to ∞. Hence

$$A = (2/\pi^{1/2}) \int_{-\infty}^{\infty} \int_{\alpha^{-1}(y)}^{\beta^{-1}(y)} \exp[-y^2]\, dt\, dy = (2/\pi^{1/2}) \int_{-\infty}^{\infty} \exp[-y^2]\, [\beta^{-1}(y) - \alpha^{-1}(y)]\, dy \qquad (9)$$

From the definition for $y = \alpha(t)$

$$\alpha^{-1}(y) = \{[y + (y^2 + 4gb/f^2)^{1/2}]/(2g/f)\}^2$$

From the definition for $y = \beta(t)$

$$\beta^{-1}(y) = \{[y + (y^2 + 4gc/f^2)^{1/2}]/(2g/f)\}^2$$

Hence

$$\beta^{-1}(y) - \alpha^{-1}(y) = (f^2/4g^2)\{2y[(y^2 + 4gc/f^2)^{1/2} - (y^2 + 4gb/f^2)^{1/2}] + (4g/f^2)\cdot (c - b)\} \quad (10)$$

Substitution of eqn. (10) into eqn. (9) gives

$$A = (f^2/2\pi^{1/2}g^2)\int_{-\infty}^{\infty} \exp[-y^2][2y(y^2 + 4gc/f^2)^{1/2} - (y^2 + 4gb/f^2)^{1/2}]\,dy + (f^2/2\pi^{1/2}g^2)\int_{-\infty}^{\infty} \exp[-y^2][4g(c - b)/f^2]\,dy \quad (11)$$

The numerical value of the first integral in eqn. (11) is zero because the integral is an odd function. Hence, Integral A is evaluated [5] according to

$$A = [2(c - b)/\pi^{1/2}g]\int_{-\infty}^{\infty} \exp[-y^2]\,dy = 2(c - b)/g = 2V_s/v_f \quad (12)$$

To aid in the evaluation of Integral B, the following substitutions are made: $b = V_s/2\pi a^2K^{1/2}$; $c = v_f/2\pi a^2K^{1/2}$; $f = V_R/2\pi a^2K^{1/2}$; $g = K^{-1/2}$; $x = t^{1/2}$; $dt/dx = 2x$.

Integral B is now written as

$$B = 2f\int_0^{\infty} \{\exp[-(b/x - cx)^2] - \exp[-(cx - f/x)^2]\}\,dx \quad (13)$$

After expansion of the quadratic terms, the change of variable is made $y = cx$. Then, $dx = dy/c$, $b/x = bc/y$, and $f/x = fc/y$. Because $c > 0$, Integral B becomes

$$B = (2g/c)\exp[2bc]\int_0^{\infty} \exp[-y^2 - (bc/y)^2]\,dy + (2g/c)\exp[2cf]\int_0^{\infty} \exp[-y^2 - (fc/y)^2]\,dy \quad (14)$$

Because [5] $\int_0^{\infty}\exp[-x^2 - (a/x)^2]\,dx = \pi^{1/2}/2\,\exp[-2a]$, Integral B can be solved by

$$B = (2g/c)\exp[2bc]\{(\pi^{1/2}/2)\exp[-2bc]\} - (2g/c)\exp[2fc]\{(\pi^{1/2}/2)\cdot \exp[-2cf]\} = 0 \quad (15)$$

Once the Integrals A and B have been evaluated, eqn. (3) is solved with the result

$$Q_p = I_{ss}V_s/v_f \quad (16)$$

Because I_{ss} is proportional to $v_f^{1/3}$ (see eqn. (1) [1]), Q_p is predicted to be proportional to $v_f^{-2/3}$. The peak area, Q_p is predicted to be independent of V_R. For the hypothetical injection of a homogeneous plug of electroactive species into a flow system for which V_R = 0 ml and where there is no effect of dispersion, the I—t plot will be a square wave for which the area is easily

calculated as the amplitude, I_{ss}, multiplied by the width, V_s/v_f. This of course, is identical to eqn. (16). The prediction that the area under the I—t peak is independent of V_R and K leads to the conclusion that Q_p will be independent of other factors which tend to affect dispersion including curvature, i.e. non-linearity, of the tubing which connects the detector to the sample-injection valve. This is substantially different than the case of I_p which is found to be very sensitive to the configuration of the connecting tubing.

EXPERIMENTAL

All instrumentation and procedures were identical to those described earlier [1, 6]. Many current—time peaks recorded by a strip chart recorder were integrated with a Kueffel and Esser planimeter. Peak areas were also integrated with an analog device, which was constructed in this laboratory according to a standard design, and connected directly to the output of the current to voltage converter of the potentiostat. Agreement between the two techniques for integration was generally better than 4—5%. Determination of the internal volumes of various segments of tubing was made titrimetrically as described earlier [1], and the inner radius of the tubing was calculated from the volume and length to be 0.0483 cm. The value of V_R for the use of each piece of connecting tubing is the sum of the internal volumes of the tubing and the inlet of the detector. In some experiments, the connecting tubing was maintained in a straight condition. This instrument with the straight tubing is referred to as the linear system. In many more experiments, the connecting tubing was allowed to form a coil. No effort was made to reproduce the dimensions of the coil but the average diameter was approximately 12 cm. The instrument with the coiled tubing is referred to as the non-linear system. The electroactive species was iodide (as potassium iodide) at a concentration of 5.0×10^{-4} M in 0.10 M H_2SO_4. All injections were made into a stream of 0.10 M H_2SO_4. The electrode potential was 0.80 V vs. SCE which corresponds to the limiting plateau for oxidation of iodide ($n = 1$). Values of I_{ss} were determined in conjunction with all measurements in the flow-injection systems.

RESULTS AND DISCUSSION

Typical data are given in Table 1 for the linear and non-linear flow systems for $V_s = 0.145$ ml and $v_f = 0.503$ ml min^{-1}. Experimental values of Q_p were normalized with division by $I_{ss}V_s v_f^{-1}$. The normalized value is, then, the fraction of the theoretical value for Q_p, as predicted by eqn. (16), which is achieved experimentally. Agreement between the results for the linear and non-linear systems is excellent and within the standard deviations of the results for each system. The fact that the results are slightly less than the theoretical value of unity results from the systematic tendency during the

study prematurely to terminate integrations of each current–time peak when the net signal was very close to the background signal.

The theoretical dependence of Q_p on V_s and v_f, according to eqn. (16), is verified by data given in Table 2 for the non-linear system. Peak areas for each pair of values of V_s and v_f were determined for five values of V_R. The average Q_p was normalized by division with the value of I_{ss} determined for the steady-state operation at the specified value of v_f. The slopes of the log–log plots of Q_p/I_{ss} vs. V_s and v_f are also given in Table 2: these results are in excellent agreement with theory.

A total of approximately ninety current–time peaks were obtained over a period of several months as a function of V_s, V_R and v_f. The average value of $Q_p/I_{ss}V_s v_f^{-1}$ was 0.992 with a relative standard deviation of 2%. The single greatest cause for the uncertainty was the integration, whether manual or electronic, of the current–time peaks. This difficulty was particularly evident under conditions of high dispersion when the peaks were very broad, and the leading and trailing edges were difficult to discern from the background signal.

The presentation here of data which have been normalized to the observed value of the steady-state current has the effect of eliminating from this consideration anomalous results produced by a decrease in the sensitivity of the electrode. A non-trivial loss in sensitivity is commonly known to occur when the effective area of the electrode is decreased as a result of the adsorption of numerous chemical compounds. The prescribed procedure of electrode pretreatment decreases, but does not eliminate, the frequency of such occurrences. When a loss of sensitivity occurs, the observed value of Q_p will, of course, be less than expected for a fully active electrode. All theoretical derivations presented here and in [1] assumed that the electrode current corresponds to the mass transport-limited value. Equation (15) is generally applicable for relating the observed values of Q_p and I_{ss} for any amperometric electrode regardless of sensitivity or configuration. However, the absolute application of eqn. (15) above, and of eqn. (1) of ref. [1] for

TABLE 1

Comparison of coulometric results for linear and non-linear flow systems

Linear system		Non-linear system	
V_R (ml)	Q_p $(I_{ss}V_s v_f^{-1})^a$	V_R (ml)	Q_p $(I_{ss}V_s v_f^{-1})^a$
0.286	0.982	0.286	0.984
0.594	0.966	0.596	0.963
0.820	0.989	—	—
1.168	0.970	1.176	0.965
2.254	0.959	2.390	0.980
Average	0.973 ± 0.012		0.973 ± 0.011

[a] V_s = 0.145 ml; v_f = 0.503 ml min^{-1}.

TABLE 2

Values of Q_p/I_{ss} as functions of V_s and v_f[a]

V_s (ml)	Q_p/I_{ss} values at v_f (ml min^{-1})				$\left(\frac{\partial \log Q_p/I_{ss}}{\partial \log v_f}\right)_{V_s}$
	0.50	1.00	1.50	2.00	
0.145	16.93	8.52	5.73	4.19	−1.00
0.226	26.19	13.15	8.78	6.52	−1.00
0.419	49.02	24.84	16.51	12.27	−1.00
0.955	115.6	56.95	37.54	28.15	−1.02
1.663	199.7	99.24	64.99	49.08	−1.01
$\left(\frac{\partial \log Q_p/I_{ss}}{\partial \log V_s}\right)_{v_f}$	1.02	1.01	1.00	1.01	

[a]Q_p measured in μC; I_{ss} measured in μA. Values tabulated are averages for V_R = 0.286, 0.596, 1.176 and 2.390 ml.

the calculation of C_o, based on an experimental value of Q_p for a tubular electrode, can only be accurate if all variables in these two equations are accurately known. This includes the effective length, L, of the tubular electrode. The use of calibration with appropriate standards under the experimental conditions corresponding to the unknown solution is prescribed instead of the use of equations with separately specified parameters.

Conclusions

The applicability of eqn. (16) has been demonstrated for predicting the area of current—time peaks obtained by coulometric detection with a tubular electrode in flow-injection determinations. The peak area is a linear function of I_{ss} and, therefore, a linear function of the analytical concentration of electroactive species in the sample injected. Consequently, addition of a single internal standard to the sample should suffice for obtaining a calibration constant for the detector which will be applicable for all peaks regardless of the band width or retention time.

Support for this research came, in part, from the National Science Foundation (CHE-7617826).

REFERENCES

1 P. L. Meschi and D. C. Johnson, Anal. Chim. Acta, 124 (1981) 303.
2 A. MacDonald and P. D. Duke, J. Chromatogr, 83 (1973) 331.
3 R. J. Davenport and D. C. Johnson, Anal. Chem., 46 (1974) 1971.
4 R. W. Andrews and D. C. Johnson, Anal. Chem., 48 (1976) 1056.
5 H. B. Dwight, Tables of Integrals and Other Mathematical Data, 4th edn. MacMillan, Toronto, 1969, Nos. 860.11, and 860.25.
6 P. L. Meschi and D. C. Johnson, Anal. Chem., 52 (1980) 1304.

Analytica Chimica Acta, 124 (1981) 321—331

EVALUATION OF KEL-F—GRAPHITE ELECTRODES AS DETECTORS FOR CONTINUOUS FLOW SYSTEMS

DAVID J. CHESNEY[a], JAMES L. ANDERSON[b]*, DUANE E. WEISSHAAR and DENNIS E. TALLMAN

Department of Chemistry, North Dakota State University, Fargo, ND 58105 (U.S.A.)

(Received 14th July 1980)

SUMMARY

A new electrode material, fabricated from Kel-F powder and graphite powder by pressing at 250°C and 1000 p.s.i., is applied as a detector in a thin-layer, flow-through cell, for applications to continuous flow streams. The detector is useful in a wide range of solvents for a wide range of species. Applications are described for 1,1'-bis(hydroxymethyl) ferrocene (BHMF), ascorbic acid, ferrocene, phenol, and hydroquinone, using various aqueous and methanolic solvent/electrolyte compositions. Detection limits range from 800 pg for BHMF to less than 20 pg for phenol. Background current fluctuations are used to estimate flow rate stability, which is the dominant factor in setting detection limits.

Recently much attention has been given to methods for rapid, repetitive determination of components in samples injected into flowing streams [1—4] and electrochemical detectors have been applied for determinations in an ever increasing range of samples processed in this manner [5—17]. For many species, electrochemical detectors can surpass refractive index, ultraviolet absorption, or fluorescence detectors in selectivity, detection limits, simplicity, and cost.

Numerous flow-through electrochemical detectors are based on carbon or graphite particles in packed beds [18], or mixed with Nujol or other liquids (carbon paste) [19], ceresin wax [20], silicone rubber [5, 21, 22], polypropylene [23], polyethylene [24], teflon [25], and Kel-F [26—29]. Numerous other detectors use various forms of solid carbon or graphite, including glassy carbon [30—32], low-temperature isotropic carbon [33], highly orientated pyrolytic graphite [34], reticulated vitreous carbon [9, 10, 35], and carbon cloth [36, 37]. Earlier literature on carbon electrodes has been summarized by several authors [21, 26, 38].

Carbon-based electrodes have typically served as working electrodes of choice for amperometric detection in the oxidative mode. One of the more popular detectors has been the thin-layer carbon paste electrode detector

[a]Present address: General Nutrition Company, Fargo, ND 58102, U.S.A.
[b]Present address: Department of Chemistry, University of Georgia, Athens, GA 30602, U.S.A.

developed originally by Kissinger et al. [19]. The most severe limitation of the carbon paste electrode is the tendency for the organic binder (commonly Nujol) to dissolve in solutions containing an appreciable fraction of organic modifier. Many of the other carbon electrode materials have been developed to overcome this problem of solvent stability.

Reported here is the application of a graphite/Kel F ("Kelgraf") electrode previously developed in this laboratory [26—29, 39], in a thin-layer detector suitable for use in flowing streams. This electrode overcomes many of the shortcomings of carbon paste, while providing an inexpensive and readily fabricated and machinable alternative to materials such as glassy carbon or pyrolytic graphite, which are expensive and difficult to fabricate. The Kelgraf electrode appears to be suitable for use in practically any organic solvent or modifier useful in electrochemical measurements.

The thin-layer detector described here is suitable for applications including continuous flow of sample streams [23, 35, 40—42], sample injection into flowing streams [5—17], and high-performance liquid chromatography [8, 11, 12, 19, 24, 27—30, 32, 34, 36, 37, 43]. Chromatographic applications of the Kelgraf electrode are described elsewhere [28, 29]. Discussion here will emphasize applications to single compounds. It was found advantageous in this work to inject samples onto a short reverse-phase C_{18} chromatographic column placed in the eluent stream before the detector. This approach minimized interference of the solvent injection blank with sample peaks at low concentration, and improved sample peak shapes and detection limits. Applications are reported for determination of 1,1′-bis(hydroxymethyl)ferrocene (BHMF), ascorbic acid and phenol in aqueous media, and for determination of ferrocene in aqueous acetonitrile and methanol, and phenol in aqueous methanol media. Sample detection limits were controlled primarily by current oscillations owing to insufficient pump flow dampening. A wide linear range was obtained for all species investigated.

EXPERIMENTAL

Chemicals and equipment

All chemicals used were reagent grade unless otherwise specified. Distilled, deionized water was used throughout. Methanol was Burdick and Jackson h.p.l.c. grade. Preparation of BHMF was by reduction of 1,1′-ferrocene dicarboxylic acid dimethyl ester (Strem Chemical) with lithium aluminum hydride.

A potentiostat of standard configuration was constructed using National Semiconductor Model LF356H operational amplifiers powered by a Boston Tech (Coral Gables, FL) ±15V power supply. Applied potentials were monitored by a Data Precision Model 245 digital voltmeter. A Houston Instruments Omniscribe B-5000 dual-pen strip chart recorder was used to monitor the detector output. The flow system was constructed using a Milton-Roy minipump (Model 396-31), an injection valve (Rheodyne Model

70-10) with a 20-μl sample loop for sample introduction and a glass column (25 cm length, 2 mm i.d.). The column was packed with Bondapak C_{18} Corasil (37—50 μm diameter; Waters Associates) by the tap-fill method, as suggested by Snyder and Kirkland [44]. All eluent connections were made with 1.6 mm o.d. teflon tubing (Altex). A 1000 p.s.i. (6.8 MPa) pressure gauge (Matheson) and a glass bourdon tube (2 mm i.d., 35 cm length) in a tee-configuration were used to dampen flow fluctuation.

Electrode. The fabrication of the Kelgraf electrode was reported previously [26, 39]. Electrodes were 25% graphite by weight. Kelgraf pellets (0.64 cm diameter) encased in a Kel-F sheath (1.9 cm diameter, 0.32 cm thick) were formed in a locally constructed die. After manual sanding with progressively finer grit sandpaper, the electrodes were polished to a smooth, shiny finish with 1 μm alumina (Buehler Micropolish) on kitten-ear polishing cloth (Buehler) mounted on locally constructed lapping wheels.

Cell. The thin-layer detector cell (Fig. 1) was of a demountable stage type [27, 28], in which the electrode could be easily removed and replaced. The center stage was vertically movable by means of the positioning screw. A

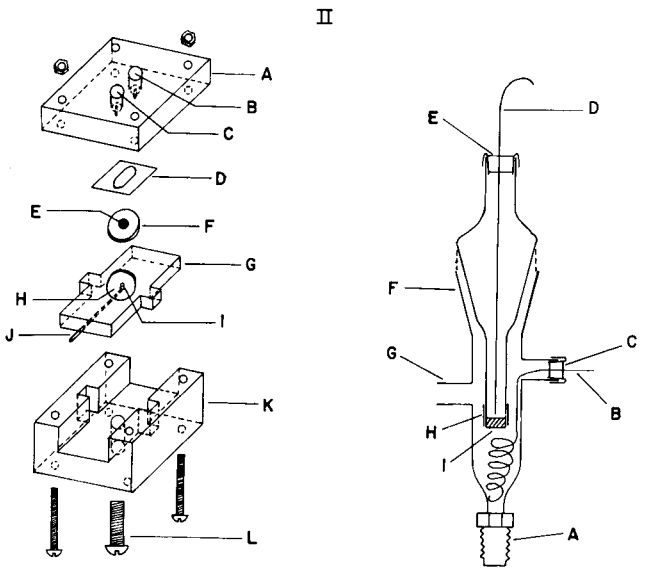

Fig. 1. Electrochemical detector. (I) Exploded diagram of detector cell: (A) Kel-F cell top; (B) inlet, 1/4-28 threaded to fit standard LC connectors; (C) outlet, 1/4-28 threaded to fit standard LC connectors; (D) teflon spacer; (E) Kelgraf electrode; (F) Kel-F electrode sheath, 3/4-in. diameter; (G) movable stage, plexiglas; (H) milled depression in stage, 3/4-in. diameter (to fit electrode sheath, F); (I) mercury contact to Kelgraf electrode; (J) outside copper electrode contact; (K) lower cell body plexiglas; (L) elevating screw for movable stage. (II) Reference and auxiliary electrode chamber: (A) standard nylon LC connector; (B) Pt auxiliary electrode; (C) rubber septum cap; (D) Ag/AgCl reference electrode (in 3.5 M KCl); (E) rubber septum cap; (F) standard taper joint (inner and outer); (G) effluent exit; (H) shrinkable teflon tubing attaching porous Vycor frit to glass tube; (I) porous Vycor isolation frit.

1.9-cm circular depression milled out in the center, ensured proper positioning of the Kelgraf electrode relative to the eluent inlet and outlet. A 125-μm thick teflon gasket (Bioanalytical Systems, West Lafayette, IN) was used as a spacer to form the thin-layer channel. No problems were encountered with eluent leakage caused by non-planar electrode surfaces. The center position of the adjusting screw assured equal pressure all around the electrode, enabling a tight gasket seal. A well drilled in the center of the depression provided mercury contact between the electrode and the copper external contact. The Kel-F cell top insured that only chemically inert materials contacted the flowing solution. All other cell parts were polymethyl methacrylate. The reference and counter electrodes (Ag/AgCl/3.5 M KCl, and Pt spiral, respectively) were positioned downstream in a locally fabricated glass chamber [27, 28]. The chamber was heated in a flame and press-fitted into a drilled-out nylon 1/4-28 threaded LC connector, which screwed into the cell. Epoxy cement applied to the outside surface of the press-fit junction helped to prevent leakage. All potentials are reported relative to Ag/AgCl.

RESULTS

Response linearity is evaluated from least-squares slopes of log i vs. log C data, where the slope should be unity (1.000 for perfect linearity) and the intercept is the logarithm of the sensitivity (nA μM^{-1}).

BHMF

Response for BHMF was measured in aqueous 0.1 M potassium nitrate at a potential of +800 mV vs. Ag/AgCl, at a flow rate of 0.90 ± 0.04 ml min^{-1}. The electrode response was linear for concentrations ranging from 0.25 to 750 μM (Fig. 2), obeying the equation: $\log i = (4.5 \pm 9.5) \times 10^{-3} + (1.028 \pm 0.005) \log C$, where units of current, i, and concentration, C, are nA and μM, respectively. The detection limit at a ratio of signal to peak-to-peak noise (S/N ratio) of 2:1 is 800 pg, for 50 pA peak-to-peak background noise. No concentrations higher than 750 μM were investigated.

Ferrocene

The response of ferrocene was evaluated in a solution prepared from a 1:1 acetonitrile/water mixture containing 0.05 M sodium dihydrogenphosphate, to assess the suitability of Kelgraf electrodes for use with high levels of non-aqueous solvents. Under these conditions, carbon paste tends to disintegrate. Response of a log—log plot at an applied potential of +0.90 V was linear over the investigated range of 0.1—100 μM (Fig. 2), according to the expression: $\log i = 0.45 \pm 0.01 + (1.00 \pm 0.01) \log C$. The signal-to-noise ratio of 0.1 μM was approximately 10 to 1, corresponding to a detection limit of 0.02 μM, or 400 femtomoles (74 pg) absolute, for a 20-μl injection (signal/noise ratio 2:1 at a background noise level of 30 pA peak-to-peak).

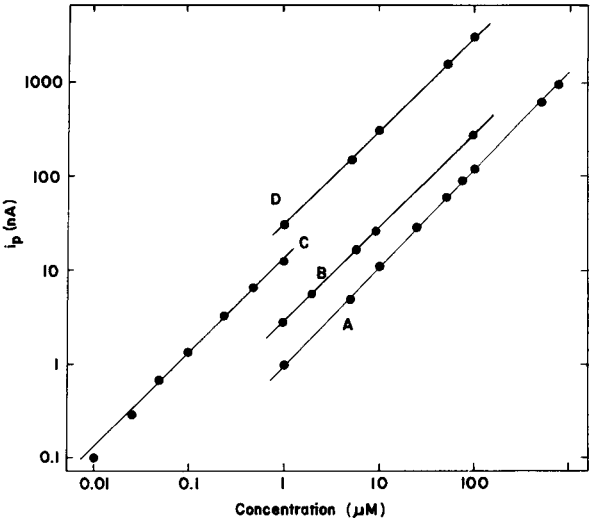

Fig. 2. Calibration curves for BHMF, ascorbic acid, ferrocene, and phenol. (A) BHMF with aqueous 0.1 M KNO_3 eluent at E_{app} = +0.8 V; (B) ferrocene with 1:1 acetonitrile/water eluent containing 0.05 M NaH_2PO_4 at E_{app} = +0.9 V; (C) phenol with 5:95 methanol pH 5 aqueous acetate buffer, eluent at E_{app} = +1.25 V; (D) ascorbic acid with aqueous acetate buffer, pH 4.7 eluent at E_{app} = +0.8 V. Flow rate = 0.90 ml min^{-1}, except for ferrocene and phenol (0.98 ml min^{-1}).

A hydrodynamic voltammogram (Fig. 3A) was obtained by injecting ferrocene samples at a series of increasingly positive detector potentials until a maximum current response was obtained. This procedure enables the operator to adjust the applied potential to ensure maximum selectivity and sensitivity, and also provides a measure of the rate of heterogeneous electron transfer.

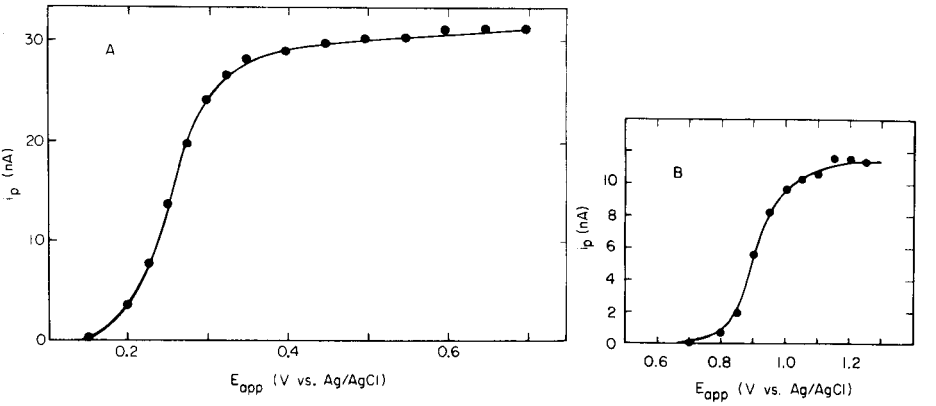

Fig. 3. Hydrodynamic voltammograms of ferrocene and phenol. (A) Ferrocene, 20μl, 10 μM, with 1:1 methanol pH 6 aqueous phosphate buffer eluent at 0.9 ml min^{-1}; (B) phenol, 20 μl, 10 μM, with 1:3 methanol pH 5 aqueous acetate buffer eluent at 0.97 ml min^{-1}.

Phenol

A phenol dilution series was examined at an applied potential of +1.25 V in a 5:95 mixture of methanol with aqueous acetate buffer (pH 5, ionic strength 0.1) at a flow rate of 0.98 ml min^{-1}, as shown in Fig. 2. The log–log plot obeyed the expression: $\log i = 1.13 \pm 0.03 + (1.04 \pm 0.02) \log C$. Response was linear over the 0.01—1 μM range examined, although the two lowest concentrations tend to fall below the linear range of the curve. This deviation is probably due to air oxidation of phenol, which is most evident at low concentrations. Higher phenol concentrations were avoided, to prevent possible electrode fouling by polymerization. The hydrodynamic voltammogram for phenol (Fig. 3B) was obtained for a 1-μM, buffered solution of phenol in water, injected into a solution prepared from a 3:1 mixture of aqueous acetate (ionic strength 0.1, pH 5) and methanol at a flow rate of 0.97 ml min^{-1}. Phenol elutes with the solvent front. The detection limit is less than 20 pg.

Ascorbic acid

As a further check on electrode linearity, the response for a series of ascorbic acid solutions was determined in pH 4.7 aqueous acetate buffer, at a flow rate of 0.90 ± 0.04 ml min^{-1}. The applied potential was +800 mV. Response was linear over the range 1—100 μM (Fig. 2), according to the expression: $\log i = 1.50 \pm 0.01 + (0.985 \pm 0.008) \log C$. Response for concentrations greater or less than these was not determined. The S/N ratio of 1 μM (>100) suggests a detection limit near 0.02 μM (70 pg).

Relative sensitivity

The responses of the Kelgraf and carbon paste electrodes were compared by injecting a series of BHMF and ascorbic acid samples with both electrode materials alternating as detector under identical conditions. The normalized current responses (nA μM^{-1} cm^{-2}) for BHMF and ascorbic acid on Kelgraf vs. carbon paste were 12 vs. 15 for BHMF, and 83 vs. 100 for ascorbic acid. Thus, the Kelgraf response was approximately 80% that of the carbon paste, per unit geometrical area, for both samples. The higher response of the carbon paste was expected, since the carbon paste was ca. 60% graphite by weight, vs. 25% for the Kelgraf electrode, and thus had a higher ratio of active to geometric area.

DISCUSSION

As can be seen from Fig. 3, the Kelgraf electrode exhibits acceptable electron-transfer behavior. The $E_{1/4}$—$E_{3/4}$ difference is ca. 67 mV for ferrocene (Fig. 3A) and ca. 90 mV for phenol (Fig. 3B), compared to the polarographic expectation of 57 mV for a fully-reversible one-electron transfer reaction, while the break in the current—voltage curve between baseline and the limiting current plateau is spread out over approximately 300 mV (Fig.

3A). Thus, electron transfer is quasireversible. While not exemplifying ideal behavior, the electrode compares favorably with many other carbon formulations, and is fully capable of providing selectivity for a given electroactive species by adjustment of the applied potential. The sharper the rise in the current—voltage plot for a given species, the better this selectivity becomes.

The major limitation in detection limit is periodic baseline fluctuation synchronized with the pump stroke. This pump noise, measured peak-to-peak, is caused by flow variations across the electrode, and appears to be electrochemical in nature, as it varies with applied potentials and with different eluents. With aqueous phosphate buffer/acetonitrile systems, pump noise is typically 20—25 pA peak-to-peak at potentials near +1 V. In various other solutions, pump noise ranges from 5 to 100 pA. Other investigators have seen similar phenomena, which were also attributed to the pumping system [34, 45]. Pump noise is most evident for solutions with high aqueous composition. Much of the pump noise is undoubtedly attributable to variations in the current arising from oxidation of water to oxygen, as flow rate fluctuates with pump strokes.

The correlation between pump noise and steady-state background oxidation current is illustrated in Fig. 4. The pump noise is constant below 0.8 V, indicating the inherent noise level of the measurement. Increases in pump noise amplitude above this constant level can be used to estimate flow rate fluctuations. At steady-state, current i, from solvent oxidation, should be of

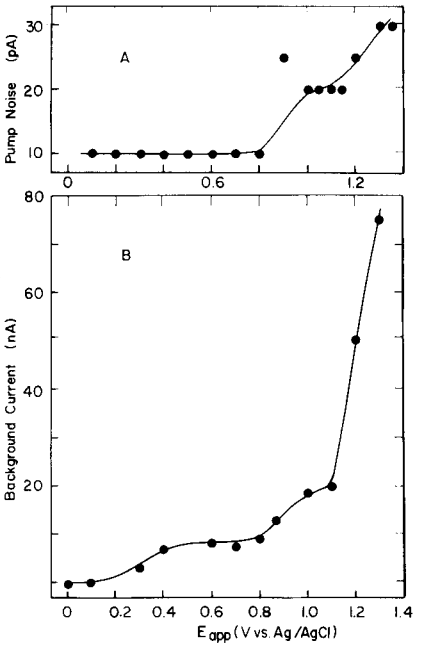

Fig. 4. Pump noise and steady-state solvent oxidation current: (A) pump noise; (B) background steady-state current. Eluent, 2.5:97.5 methanol pH 5 aqueous acetate buffer at 0.39 ml min^{-1}.

form, $i = kv^x$, where k is a constant, v is flow rate, and x is a constant ranging from 1/2 [22] to 1/3 [23] and the latter value is more likely for channel flow. The ratio of pump noise current amplitude to total solvent oxidation current can be obtained by differentiating the expression and taking a ratio. Rearrangement yields an expression relating relative flow rate fluctuation dv/v to current: $dv/v = x^{-1}di/i$. At potentials of 1.0—1.1 V, the ratio di/i of peak-to-peak pump noise current (after subtracting the potential—independent contribution) to background steady-state current is ca. 5×10^{-4}, while at 1.2—1.3 V the ratio is ca. 3×10^{-4}, corresponding, respectively to approximate flow rate fluctuations of 0.15% and 0.09% between the pump forward stroke and refill stroke if $x = 1/3$. Because of uncertainties in measurements at these levels, 0.1% fluctuation is a reasonable estimate of flow rate fluctuations. Independence of pump noise from the background wave with $E_{1/2}$ near 0.3 V suggests that the latter arises from oxidation of functional groups on the graphite electrode surface, since surface-bound processes are independent of flow rate. A pH-dependent oxidation of hydroquinone-like surface groups has been reported for pyrolytic graphite in this potential range [46]. Addition of a low-pass filter (R = 553 ohm, C = 1000 μF) between the potentiostat and the chart recorder reduces the amplitude of the pump noise by about 50%, but also restricts the response time of the system.

Electronic noise (1—5 pA) of the potentiostat and recorder was substantially less than the pump noise. Environmental noise in the laboratory necessitated the use of extensive shielding in the form of a faraday cage and coaxially shielded leads. This procedure has been recommended and used by some investigators [47—49], but has not substantially reduced environmental noise for others [50].

The cell design employed precluded study of extremely high concentrations, because of the large uncompensated resistance (typically 50—60 kohm) between the reference/auxiliary electrode chamber and the working electrode. While this would not be a severe restriction at the concentrations used here, the voltage iR drop from current flow across this resistance could cause a loss of sensitivity for species with oxidation potentials near the anodic limit of the system, as defined by electrode performance and the oxidation potential of the eluent. At the trace levels which are of most interest, the very low analytical currents yield negligible iR losses. It is expected that a cell design with auxiliary and reference electrodes positioned opposite the Kelgraf working electrode in the flow stream would exhibit linearity to still higher concentrations because of minimal interelectrode resistance.

The Kelgraf electrode shows adequate reproducibility. For a series of seven 20-μl injections of 100 μM ascorbic acid, the peak heights had a relative standard deviation (r.s.d.) of 2.3%. For a series of six 20-μl injections of 10 μM ferrocene, the r.s.d. was 1.7%. For a series of six 20-μl injections of 1 μM hydroquinone, the r.s.d. was 0.7%, as illustrated in Fig. 5. Detection limits obtained here are competitive or superior to results for compounds

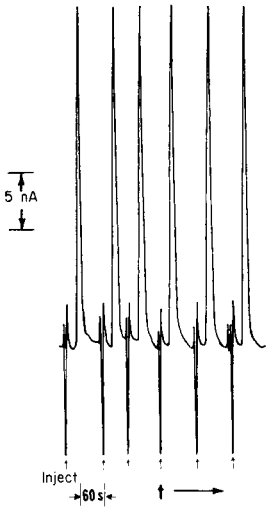

Fig. 5. Repetitive injections of hydroquinone (20 μl, 1 μM) with methanol/0.05 M acetic acid/0.1 M sodium acetate buffer eluent at 0.96 ml min^{-1}; applied potential +0.900 V vs. Ag/AgCl.

previously studied by other workers, e.g., phenol [7, 24] and ascorbic acid [9].

A problem with any electrode is passivation. In the oxidative mode, this is frequently caused by adsorption or polymerization of oxidation products on the electrode surface. While not immune to the problem of electrode fouling, the present cell design allows extremely easy electrode removal, resurfacing, and replacement. Electrodes can be resurfaced and the cell re-assembled in a few minutes; freshly polished electrodes, however, may require 10—15 min, or sometimes as long as 1—4 h of pre-equilibration before the background current becomes stable, enabling the use of the highest sensitivities. Lower graphite content (e.g., 15% by weight) reduces pre-equilibration time. The lowest background currents are obtained when the polished electrode has a minimum of visible pitting. Excessive polishing on a lapping wheel leads to degradation of the electrode surface because of the removal of large graphite particles by the nap of the lapping wheel. This phenomenon is variable from electrode to electrode, perhaps reflecting variations in the homogeneity of the Kel-F—graphite mixture in the electrode, as well as variations in polishing conditions (e.g., pressure, time, etc.).

The Kelgraf electrode appears to have wide applicability as a detector for flowing streams of sample. The electrode is similar to carbon paste in terms of response, linearity and selectivity, but is essentially impervious to organic solvents, vastly expanding the range of usefulness. Kelgraf is also easily fabricated and machined, making it easier to use than glassy carbon or pyrolytic graphite.

The authors thank John Kiely for assistance in the preparation of BHMF.

This work was supported by Grant Nos. A-049-NDAK, B-043-NDAK (J.L.A.), and A-062-NDAK (J.L.A. and D.E.T.) of the U.S. Department of the Interior, Office of Water Research and Technology. It was presented in part at the American Chemical Society National Meeting, Honolulu, Hawaii, April, 1979.

REFERENCES

1 D. Betteridge, Anal. Chem., 50 (1978) 832A.
2 J. Růžička and E. H. Hansen, Anal. Chim. Acta, 99 (1978) 37; 114 (1980) 19.
3 J. Růžička, E. H. Hansen, H. Mosbaek and F. J. Krug, Anal. Chem., 49 (1977) 1858.
4 M. Margoshes, Anal. Chem., 49 (1977) 1861.
5 G. Nagy, Zs. Fehér and E. Pungor, Anal. Chim. Acta, 52 (1970) 47.
6 B. Fleet, A. Y. H. Ho and J. Tenygl, Anal. Chem., 44 (1972) 2156.
7 Zs. Fehér and E. Pungor, Anal. Chim. Acta, 71 (1974) 425.
8 J. H. Larochelle and D. C. Johnson, Anal. Chem., 50 (1978) 240.
9 A. N. Strohl and D. J. Curran, Anal. Chem., 51 (1979) 1045.
10 A. N. Strohl and D. J. Curran, Anal. Chem. 51 (1979) 1050.
11 P. T. Kissinger, Anal. Chem., 49 (1977) 447A.
12 Bibliography of Recent Reports on Electrochemical Detection, Bioanalytical Systems, W. Lafayette, IN, 1979.
13 E. Pungor, Zs. Fehér, G. Nagy, K. Toth, G. Horvai and M. Gratzl, Anal. Chim. Acta, 109 (1979) 1.
14 H. K. Chan and A. G. Fogg, Anal. Chim. Acta, 111 (1979) 281.
15 B. Pihlar, L. Kosta and B. Hristovski, Talanta, 26 (1979) 805.
16 P. W. Alexander and M. H. Shah, Talanta, 26 (1979) 97.
17 J. Wang, E. Ouziel, Ch. Yarnitzky and M. Ariel, Anal. Chim. Acta, 102 (1978) 99.
18 W. J. Blaedel and J. H. Strohl, Anal. Chem., 36 (1964) 1245.
19 P. T. Kissinger, C. Refshauge, R. Dreiling and R. N. Adams, Anal. Lett., 6 (1973) 465.
20 R. J. Fenn, S. Siggia and D. J. Curran, Anal. Chem., 50 (1978) 1067.
21 E. Pungor and É. Szepesváry, Anal. Chim. Acta, 43 (1968) 289.
22 E. Pungor, Zs. Fehér and G. Nagy, Zs. Fehér and E. Pungor, Anal. Chim. Acta, 52 (1970) 47.
23 S. G. Weber and W. C. Purdy, Anal. Chim. Acta, 100 (1978) 531.
24 D. N. Armentrout, J. D. McLean and M. W. Long, Anal. Chem., 51 (1979) 1039.
25 L. N. Klatt, D. R. Connell, R. E. Adams, I. L. Honigberg and J. C. Price, Anal. Chem., 47 (1975) 2470.
26 J. E. Anderson, D. E. Tallman, D. J. Chesney and J. L. Anderson, Anal. Chem., 50 (1978) 1051.
27 D. J. Chesney, M.S. Thesis, North Dakota State University, 1979.
28 J. L. Anderson and D. J. Chesney, Anal. Chem., 52 (1980) 2156.
29 D. E. Weisshaar, D. E. Tallman and J. L. Anderson, submitted.
30 J. Lankelma and H. Popper, J. Chromatogr., 125 (1976) 375.
31 W. J. Blaedel and G. W. Schieffer, J. Electroanal. Chem. 80 (1977) 259.
32 C. Bollet, P. Oliva and M. Caude, J. Chromatrogr., 149 (1977) 625.
33 B. R. Hepler, S. G. Weber and W. C. Purdy, Anal. Chim. Acta, 102 (1978) 41.
34 R. M. Wightman, E. C. Paik, S. Borman and M. A. Dayton, Anal. Chem., 50 (1978) 1410.
35 W. J. Blaedel and J. Wang, Anal. Chem., 51 (1979) 799.
36 Y. Takata and G. Muto, Anal. Chem., 45 (1973) 1864.
37 J. E. Girad, Anal. Chem., 51 (1979) 836.
38 J.-P. Randin, in A. J. Bard (Ed.), Encyclopedia of Electrochemistry of the Elements, Vol. VII, M. Dekker, New York, 1976, pp. 1—291.

39 J. E. Anderson, Ph.D. Dissertation, North Dakota State University, 1979.
40 E. Pungor, Zs. Fehér and G. Nagy, Anal. Chim. Acta, 51 (1970) 417.
41 W. J. Blaedel, S. L. Boyer, Anal. Chem., 43 (1971) 1538.
42 D. J. Curran and A. N. Strohl, Anal. Chem., 51 (1979) 353.
43 B. Fleet and C. J. Little, J. Chromatogr. Sci., 12 (1974) 747.
44 L. R. Snyder and J. J. Kirkland, Introduction to Modern Liquid Chromatography, 2nd ed., Wiley—Interscience, New York, 1979. p. 207.
45 W. Lund, M. Hannisdal and T. Greibrokk, J. Chromatogr., 173 (1979) 249.
46 J. F. Evans and T. Kuwana, Anal. Chem., 51 (1979) 358.
47 R. Keller, A. Oke, I. Mefford and R. N. Adams, Life Sci., 19 (1976) 995.
48 W. A. MacCrehan, R. A. Durst and J. M. Bellama, Anal. Lett., 10 (1977) 1175.
49 C. L. Blank, J. Chromatogr., 117 (1976) 35.
50 F. Vandemark and T. H. Ryan, Chromatography Newsletter, Perkin Elmer Corp., Norwalk, CT, 1978, p. 20.

Analytica Chimica Acta, 124 (1981) 333—339

CATHODIC STRIPPING VOLTAMMETRY OF SELENOCYSTINE, CYSTINE, AND CYSTEINE IN DILUTE AQUEOUS ACID

RAYMOND ALAN GRIER and RICHARD W. ANDREWS*

Department of Chemistry, University of Alabama in Birmingham, Birmingham, AL 35294 (U.S.A.)

(Received 8th September 1980)

SUMMARY

Selenocystine, cystine, and cysteine can be determined by cathodic stripping voltammetry (c.s.v.) in 0.1 M $HClO_4$ or 0.1 M H_2SO_4. The amino acids are accumulated at potentials more positive than −0.35 V, −0.20 V, and −0.10 V vs. s.c.e., respectively, and the stripping peak potentials are −0.45 V, −0.38 V and −0.15 V, respectively. Limiting coverage of the mercury electrode surface is observed for cysteine and selenocystine, but not for cystine. The detection limit for selenocystine is 5×10^{-10} M in the presence of 100-fold amounts of cystine and cysteine. The detection limits for cystine and cysteine are 1×10^{-8} M and 1×10^{-9} M, respectively.

The selenium analogs of the naturally-occurring sulfur-containing amino acids are found in plants grown in seleniferous soil [1]. The selenium analog of cystine, selenocystine, is one of the principal organoselenium compounds found in aqueous extracts of grains and cereals [2]. Thiols and disulfides have been determined by cathodic stripping voltammetry by utilizing the formation of surface films of insoluble mercury—sulfur compounds [3—5]. This report describes the determination of sub-part per billion concentrations of selenocystine in the absence and presence of cystine and cysteine.

The polarographic behavior of cysteine and cystine has been studied extensively [6, 7]; and recently Bard and Stankovich [8] described the electrochemistry of cysteine and cystine in phosphate buffer. Nygard [9] described the electrochemistry of selenocystine, and Criddle and Huber [10] compared the $E_{1/2}$ values of cystine and selenocystine. Calusaru and Voicu [11] utilized the catalytic hydrogen prewave of nickel(II) observed in the presence of cystine and selenocystine to determine 5×10^{-7} M selenocystine. Recently Florence [12] reported the determination of cystine and cysteine at a micro mercury pool by cathodic stripping voltammetry (c.s.v.) and compared thin mercury film and hanging mercury drop electrodes (h.m.d.e.'s) for the determination of cysteine [13].

EXPERIMENTAL

Apparatus and reagents

Current—potential curves were obtained with a PAR Model 174 Polarographic Analyzer or a PAR Model 364 Polarographic Analyzer and a PAR

model 175 Universal Programmer (Princeton Applied Research Corporation, Princeton, NJ). A Hewlett-Packard Model 7015 X-Y recorder was used to record the current—potential curves. A Metrohm E410 Micrometer Hanging Mercury Drop Electrode (h.m.d.e.; Brinkman Instruments, Westbury, NY) and a PAR Model 303 Static Mercury Electrode served as working electrodes. The electrolysis vessel was a Metrohm titration cell fitted with salt bridges containing fine glass frits separating the reference and auxiliary electrodes from the main chamber. The cell bottom, salt bridges and purge tubes were soaked in 50% nitric acid for >3 h and rinsed with deionized, distilled water prior to use. All voltages were measured with a Keithley Model 163 digital multimeter.

All solutions were prepared from Fisher Analyzed Reagents unless otherwise noted. Selenocystine, L-cystine and L-cysteine were obtained from the Sigma Chemical Co., St. Louis, MO. Triply-distilled mercury was passed through a pinhole in Whatman No. 42 filter paper prior to filling the mercury electrodes. The water used in the preparation of solutions was deionized, distilled from alkaline permanganate, and redistilled under nitrogen.

Procedures

The capillaries used to form the h.m.d.e.'s were siliconized by treatment with dichlorodimethylsilane [14]. Solutions were thoroughly deaerated prior to dispensing mercury drops and a fresh mercury drop was dispensed for each experiment. Magnetic stirring was used during depositions, and the solutions were left unstirred for 15 s immediately prior to recording a stripping voltammogram.

RESULTS AND DISCUSSION

Studies with hanging mercury drop electrodes

Cyclic voltammograms recorded at a hanging mercury drop electrode from solutions of cystine, selenocystine and cysteine (Fig. 1) display some noteworthy differences. Cystine (RSSR) has a single cathodic peak at −0.25 V on the first negative-going scan, which subsequently disappears on the second scan wherein it is replaced by a somewhat larger peak at −0.10 V similar to that of cysteine (RSH). Apparently, cysteine is formed on the first scan. Selenocystine (RSeSeR) displays only one cathodic peak at −0.45 V and holding the potential more negative than −0.50 V for several minutes does not result in the formation of a second cathodic peak. It is concluded that RSeSeR and cystine are reduced by different mechanisms.

Stripping voltammetry also displays notable differences (Fig. 2). The quantity of charge consumed in the reduction of the accumulated RSH and RSeSeR reached a limiting value within 30 to 120 s of accumulation while the reduction peaks for RSSR are still growing after 10 min of accumulation (Fig. 3). The rather substantial differences in peak potentials and the rates of accumulation provide an opportunity to resolve mixtures of these amino

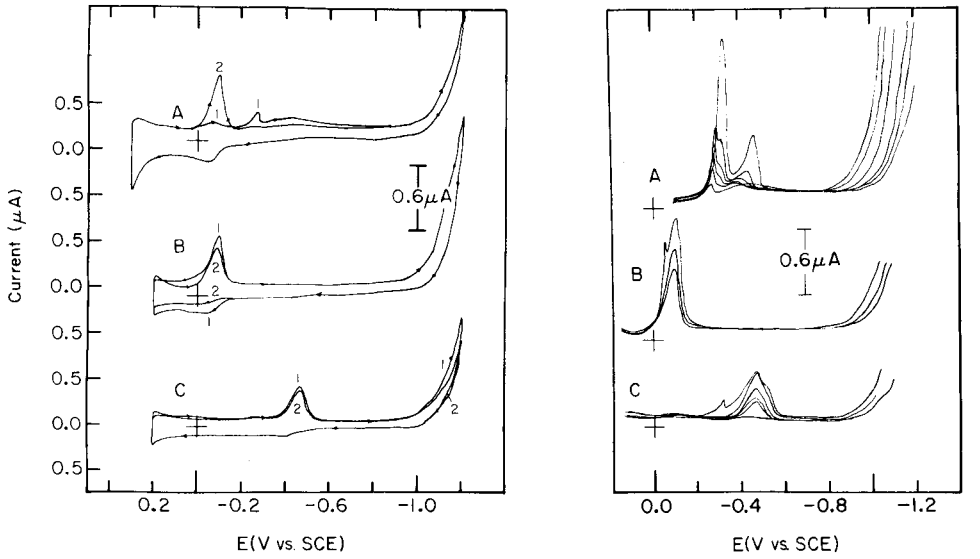

Fig. 1. Current—potential curves for selenocystine, cysteine and cystine at the h.m.d.e. in 0.1 M H_2SO_4 (100 mV s^{-1}). (A) 4 × 10^{-5} M cystine; (B) 1 × 10^{-5} M cysteine; (C) 1 × 10^{-5} M selenocystine. Curve 1 is the first sweep and curve 2 the second sweep, for each solution.

Fig. 2. Cathodic stripping voltammetry of selenocystine, cystine, and cysteine at the h.m.d.e. (50 mV s^{-1}, E_{dep} = +0.20 V, 0.1 M H_2SO_4). (A) 4 × 10^{-5} M cystine; (B) 1 × 10^{-5} M cysteine; (C) 1 × 10^{-6} M selenocystine. Stripping voltammograms are shown following accumulation for 0, 10, 20, 30, 60, 120, and 300 s for cystine; 0, 10, 20, 30 s for cysteine; and 0, 10, 20, 30, 60, and 120 s for selenocystine.

acids by c.s.v. This is particularly useful insofar as the sulfur-containing amino acids are considerably more abundant than their selenium analogs; and the acid dissociation constants are quite similar [10].

The influence of accumulation potential, accumulation time, sweep rate, and concentration on the c.s.v. of the amino acids was studied. Figure 4 is a plot of charge consumed vs. accumulation potential for each of the three amino acids. Cystine is present at a 10-fold greater concentration because of the poor sensitivity of c.s.v. for cystine. Figure 5 is a plot of peak current vs. sweep rate. The linear increase of peak current with sweep rate is expected for cathodic stripping of a slightly soluble surface film [15]. The isotherms shown in Fig. 3 were obtained from solutions sufficiently dilute that a single stripping peak was observed in all cases. When the concentration of amino acid exceeded 5 × 10^{-6} M either split peaks or multiple stripping peaks were recorded. A clear implication of Figs. 3 and 4 is that the formation of the surface film of mercuro-selenocystinate is energetically and kinetically more favorable than the corresponding mercuro-cystinate. Figure 4 also indicates that selenocystine can be accumulated at quite negative potentials and that resolution of mixtures of the amino acids might be affected by selection of electrolysis potential. The accumulation efficiency remained essentially

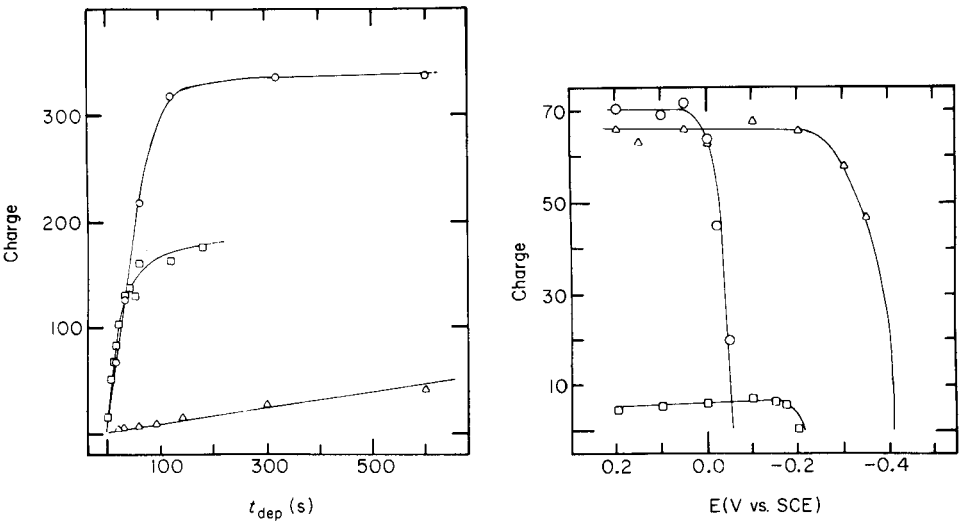

Fig. 3. Charge vs. deposition time at the h.m.d.e. Charge is given in units of mCl mol^{-1}. 50 mV s^{-1}; 0.1 M $HClO_4$; 1 × 10^{-6} M cysteine; 5 × 10^{-7} M selenocystine; 5 × 10^{-6} M cystine; E_{dep} = +0.20 V vs. SCE. (○) Selenocystine; (□) cysteine; (△) cystine.

Fig. 4. Charge vs. accumulation potential. Charge is given in units of mC mol^{-1}. Scan rate, acidity and concentrations as in Fig. 3; T_{dep} = 60 s. (△) Selenocystine; (□) cystine; (○) cysteine.

constant when the electrolysis potential exceeded the peak potential by 100 mV. This, coupled with the similarities of both peak shape and peak potential, indicates that the formation of the surface film precedes the reduction of the amino acids.

The sensitivity of stripping voltammetry can generally be improved by substituting pulse [16], staircase [17], or alternating current [18] voltammetric techniques for linear sweep voltammetry in the stripping step. Differential pulse cathodic stripping voltammetry (d.p.c.s.v.) was evaluated for the determination of these amino acids. Typical d.p.c.s.v. traces for RSeSeR are shown in Fig. 6; and plots of peak current normalized (by accumulation time) vs. concentration are linear. (The regression equation is i_p/t_{dep} (μA min^{-1}) = 9.22 × 10^9 C_{RSeSeR} (M) + 0.228. The standard deviation about the regression is 460; the standard deviation of the slope is 4.65 × 10^8; the standard deviation of the intercept is 3.72; and the square of the correlation coefficient is 0.999). The detection limits based on the concentration which yielded a stripping peak three times greater than the noise level of the blank within a 10-min accumulation period are 1 × 10^{-8}, 1 × 10^{-9} and 5 × 10^{-10} M for RSSR, RSH and RSeSeR, respectively.

The ability to resolve mixtures of these amino acids would be very helpful in their determination in plant extracts. Consequently, the determination of RSeSeR in the presence of RSH and RSSR was investigated. In those studies

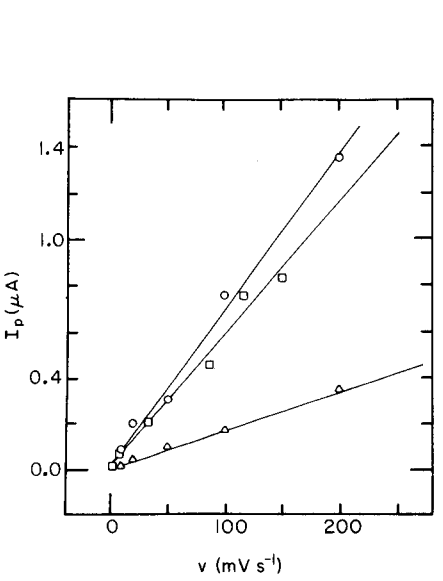

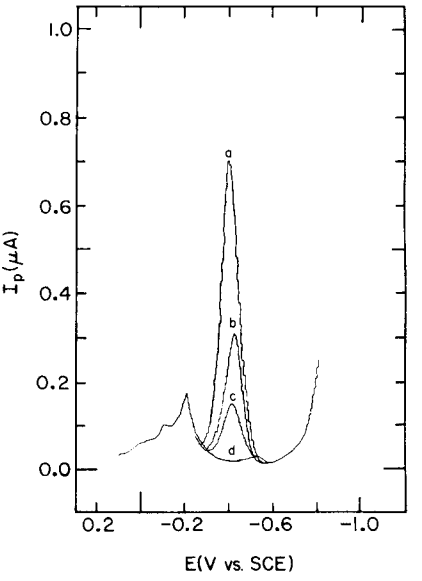

Fig. 5. Peak current vs. sweep rate at the h.m.d.e. in 0.1 M $HClO_4$. (□) 1×10^{-6} M cysteine; (○) 5×10^{-7} M selenocystine; (△) 5×10^{-6} M cystine. $E_{dep} = +0.20$ V; $T_{dep} = 60$ s.

Fig. 6. Differential pulse cathodic stripping voltammetry of selenocystine at the h.m.d.e. in 0.1 M H_2SO_4. (a) 5×10^{-9} M selenocystine; (b) 2×10^{-9} M selenocystine; (c) 1×10^{-9} M selenocystine; (d) blank. Scan rate 50 mV s^{-1}; pulse amplitude 25 mV; $T_{rep} = 0.5$ s; $E_{dep} = +0.20$ V; $T_{dep} = 10$ min.

the concentration of RSeSeR was varied from 1×10^{-9} M to 1×10^{-7} M, and the ratio of RSeSeR to RSH or RSSR was varied from 1:1 to 1:1000. The accumulation potential was held at +0.10 V in one series of experiments and at −0.40 V in a second series. Interference was measured by comparing the peak currents obtained for RSeSeR in the presence and absence of RSH or RSSR. Peak currents were typically reproducible within 5% (95% confidence limits, Student's t), and Table 1 summarizes the results of the interference study. The concentration of RSH or RSSR which resulted in a recovery less than 95% is identified as C_{max}. Plots of % recovery vs. concentration of RSH or RSSR generally showed a gradual decrease in recovery when the concentration exceeded C_{max}. When the recovery decreased to 70%, standard additions of RSeSeR were made, and the initial RSeSeR concentration was calculated. The initial concentration was estimated with an average error of ±4.7%. Consequently, the method of standard additions is concluded to be an appropriate method of quantifying RSeSeR when no prior separation of RSH and RSSR is performed. Table 1 indicates that the interference of RSH is quite serious when the accumulation potential is +0.10 V, but is minor at −0.40 V. This observation is consistent with the data summarized in Fig. 4. The interference of RSSR was less serious than that of RSH, but was not as profoundly influenced by the choice of accumulation potential.

TABLE 1

Interference study

Selenocystine concentration (mol l^{-1})	Accumulation potential (V vs. Ag/AgCl)	C_{max} cystine[a] (mol l^{-1})	C_{max} cysteine (mol l^{-1})
1×10^{-9}	−0.40	5×10^{-7}	1×10^{-5}
1×10^{-9}	+0.10	1×10^{-7}	1×10^{-8}
1×10^{-8}	−0.40	8×10^{-6}	3×10^{-5}
1×10^{-8}	+0.10	5×10^{-6}	2×10^{-8}
1×10^{-7}	−0.40	5×10^{-5}	2×10^{-5}
1×10^{-7}	+0.10	1×10^{-4}	2×10^{-7}

[a] C_{max} is defined as the concentration of RSH or RSSR that resulted in a recovery of less than 95% of added selenocystine.

The suitability of a variety of aqueous buffers in the pH range 3—10 was investigated for the determination of RSeSeR, RSSR, and RSH. The magnitude of the RSeSeR c.s.v. peak decreased with increasing pH and no c.s.v. peak was observed for a 1×10^{-4} M solution of RSeSeR at pH 10 in either ammonia or borate buffers. However, pH 10 ammonia buffers were suitable for the determination of 1×10^{-9} M RSSR and RSH by differential pulse c.s.v.

Studies with mercury pool electrodes

Florence [12] recently discussed the interference of dissolved oxygen and extraneous mercury in electrolysis cells in the determination of organosulfur compounds by c.s.v. and recommended the use of a mercury pool electrode for such determinations. A cell similar to that of Florence [12] and Delahay and Mattax [19] was constructed. Cyclic voltammograms and stripping voltammograms were obtained for solutions of RSeSeR, and the recommendations of Florence with respect to purging, electrode pretreatment and rendering the cell surfaces hydrophobic were followed. The cyclic and stripping voltammograms obtained with the mercury pool electrode and h.m.d.e. were virtually identical. Plots of peak current vs. sweep rate and charge vs. deposition time are linear. A plot of charge vs. accumulation potential gave an $E_{1/2}$ of −0.35 V which is similar to that shown in Fig. 4. The least concentrated solution yielding a c.s.v. peak three times the noise level of the blank was 5×10^{-10} M. This experiment suggests that in the determination of RSeSeR by c.s.v. no significant advantage was obtained with the mercury pool electrode except that the capillary noise characteristic of the h.m.d.e. was eliminated. It does strongly suggest that flow-through mercury cells similar to that recently used by Eggli and Asper [20] for the determination of cysteine and cystine might be helpful in the application of c.s.v. to organosulfur and organoselenium compounds.

The generous support of the Faculty Research Council of the University of Alabama in Birmingham and the American Cancer Society (Grant No. IN66R) is gratefully acknowledged.

REFERENCES

1 T. C. Stadtman, Science, 183 (1974) 915.
2 J. L. Martin, in D. T. Klayman and W. H. H. Gunther (Eds.), Organic and Biological Chemistry of Selenium Compounds, Wiley—Interscience, New York, 1973.
3 E. Davidson and G. Smyth, Anal. Chem., 49 (1977) 1195.
4 W. M. Moore and V. F. Gaylor, Anal. Chem., 49 (1977) 1386.
5 M. J. D. Brand and B. Fleet, Analyst, 93 (1968) 498.
6 I. M. Kolthoff and C. Barnum, J. Am. Chem. Soc., 62 (1940) 3061.
7 I. T. Miller and J. Teva, J. Electroanal. Chem., 36 (1972) 157.
8 M. T. Stankovich and A. J. Bard, J. Electroanal. Chem., 75 (1977) 487.
9 B. Nygard, Ark. Kemi., 27 (1967) 342.
10 R. E. Huber and R. S. Criddle, Arch. Biochem. Biophys., 122 (1967) 164.
11 A. Calusaru and V. Voicu, J. Electroanal. Chem., 32 (1971) 427.
12 T. M. Florence, J. Electroanal. Chem., 97 (1979) 219.
13 T. M. Florence, J. Electroanal. Chem., 72 (1976) 121.
14 F. Vydra, K. Stulik and E. Julakova, in J. Tyson (translation Ed.), Electrochemical Stripping Analysis, Halsted—Wiley, New York, 1976, p. 138.
15 Kh. Z. Branina, Electrokhimiya, 2 (1966) 901.
16 T. R. Copeland, J. H. Christie, R. A. Osteryoung and R. K. Skogerboe, Anal. Chem., 45 (1973) 2171.
17 U. Eisner, J. A. Turner and R. A. Osteryoung, Anal. Chem., 48 (1976) 1608.
18 W. L. Underkofler and I. Shain, Anal. Chem., 37 (1965) 221.
19 P. Delahay and C. C. Mattax, J. Am. Chem. Soc., 76 (1954) 874.
20 R. Eggli and R. Asper, Anal. Chim. Acta, 101 (1978) 253.

Analytica Chimica Acta, 124 (1981) 341—350

THE APPLICABILITY OF THE ARRHENIUS MODEL IN THERMAL ANALYSIS†

M. ARNOLD, G. E. VERESS, J. PAULIK and F. PAULIK*

Institute for General and Analytical Chemistry, Technical University, Budapest (Hungary)

(Received 14th September 1980)

SUMMARY

It is shown experimentally that dynamic thermoanalytical curves provide insufficient information for the purpose of reaction kinetic calculations. Mathematical considerations prove also that the parameters of the Arrhenius model cannot be calculated correctly from the thermoanalytical curves by curve-fitting and that there is no unique correlation between the estimated parameters and the measured curves.

For the past hundred years, the Arrhenius equation has been applied to the study of the kinetics of homogeneous reactions. From the magnitude of the activation energy calculated with the help of this model, investigators have assessed the extent of the reaction-hindering potential barrier; from the calculated value of the reaction order, they have deduced the mechanism of the elementary processes of the reaction. The question arises whether or not the validity of the Arrhenius equation may be extended to heterogeneous systems also, i.e., in a narrow sense, to those reactions of inorganic compounds which lead to equilibrium and which take place under the conditions of dynamic thermoanalytical studies. Many arguments can be used against the applicability of the Arrhenius model in the case of such reactions. Yet the first attempt, made some two decades ago, found many followers despite the difficulties in calculations and the uncertain results which were often rather contradictory [1].

The kinetics of homogeneous and heterogeneous reactions are fundamentally different. With homogeneous reactions, within a given time, the reaction will take place at a uniform rate in every space unit of the single phase; with heterogeneous reactions, the reaction takes place only on the phase boundaries of the contacting phases and at a rate permitted by the prevailing mass and heat transport processes. For realization of the reaction, the reacting species must reach the phase boundary or the reaction products must depart from there. Furthermore, in the case of endothermic reactions, even the heat required to ensure the progress of the transformation must

†Presented at the 6th ICTA Conference, Bayreuth, 1980.

reach this phase boundary; in the case of exothermic reactions, the heat evolved must leave the boundary.

Consequently, under conventional thermoanalytical conditions, even the simplest types of reactions $AB_{(s)} \rightleftharpoons A_{(s)} + B_{(g)}$ are composed of many elementary processes, as is shown schematically in Table 1.

The progress of a conversion is, of course, defined by the rate of the slowest process. It was proved experimentally some years ago [2, 3] that the elementary chemical reaction taking place on the surface of the phase boundary, is generally faster than the other elementary processes and that the course of transformations is usually defined by slow heat- and gas-transport processes (Table 1) which are greatly influenced by the experimental conditions. Therefore, the course of conventional thermoanalytical curves is more characteristic of the experimental conditions, or of the above-mentioned transport processes, than of the reaction itself. From this it

TABLE 1

Partial processes in thermal decomposition reaction of type: $AB_{(s)} \rightleftharpoons A_{(s)} + B_{(g)}$

Evolution of gaseous products			Relationship betw the rate of the par processes and the l ing program applie Fast, therefore not rate-determining
Release ⇌ return of gas molecules from or to the lattice			
Chemisorption ⇌ desorption of gas molecules at interface			
Departure of gaseous products by diffusion	*Formation of new solid phase*	*Heat transfer*	Similar, therefore may be rate-deter-mining
through the capillaries of the grain, interface ⇌ grain boundary	Nucleus formation	surface ⇌ centre of a single grain	
	Growth of nucleus		
	Recrystallization		
through the space unfilled with grain, grain boundary ⇌ sample surface		surface ⇌ centre of the sample	Slow, therefore in most cases rate-determining
in the sample holder, sample surface ⇌ surroundings		furnace ⇌ sample surface	

follows that "the correctness of reaction kinetic calculations on the basis of curves obtained by dynamic thermoanalytical methods is rather questionable", as stated previously [4].

THERMOANALYTICAL CURVES FOR CALCIUM CARBONATE AND AMMONIUM CHLORIDE

This problem will be studied for the example demonstrated in Fig. 1; all three curves illustrate the decomposition of calcium carbonate. Complementary explanations are given in the bottom part of Fig. 1. The curves are depicted with the intention of illustrating a schematic relationship between the changes in gas transport and heat transport that occur during the transformations and the rate of the conversion. The curves illustrate the variation of the partial pressure (Δp) of the gaseous decomposition products, of the temperature drop (ΔT) between the sample centre and the crucible, and of the rate of the weight change (dm/dt). These curves are traced in scales corresponding only to orders of magnitude.

Curves 1 and 2 in Fig. 1 were traced by using a labyrinth crucible [3], i.e. the reaction occurred in a self-generated, pure carbon dioxide atmosphere at atmospheric pressure. In this way, the course of both curves was made independent of the changes occurring in the partial pressures of the gaseous decomposition products liberated during the reaction (Fig. 1). Curve 1 was traced under dynamic conditions, and curve 2 under quasi-isothermal heating conditions [3, 4]. In the latter case, the sample decomposed exceedingly slowly (0.5 mg min^{-1}) and at a uniform rate; in the former case, because of the rapid temperature rise (10°C min^{-1}), the transformation was forced to take place at an ever-increasing rate which was finally two orders of magnitude higher than in the previous case (Fig. 1).

Because of these different conditions the courses of the two curves were different, which can be explained as follows. The specific heat of the materials

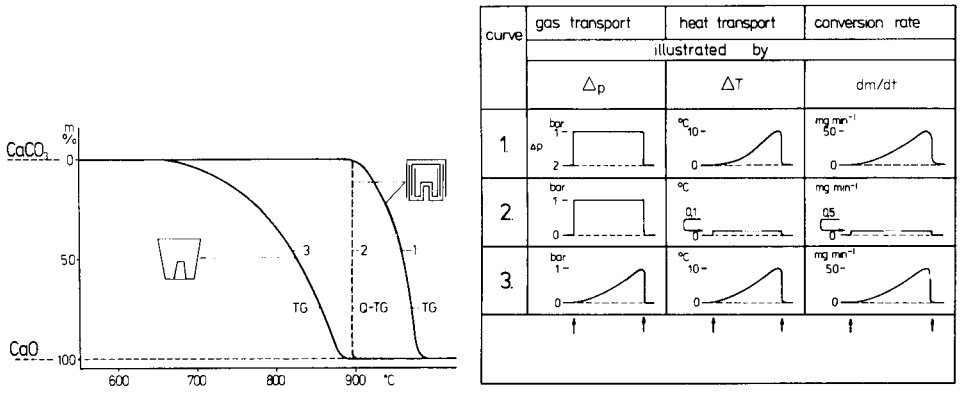

Fig. 1. Thermoanalytical curves for calcium carbonate with explanation of the processes.

is relatively small, and so the sample temperature can follow the temperature changes of the furnace with a negligible delay, until a transformation starts in the sample. However, the amount of heat necessary for the conversion is generally larger by orders of magnitude than the specific heat (in the case of calcium carbonate, $\overline{C}_p$ (800°) = 1.1 kJ K^{-1} mol^{-1}, and $\Delta H°_{diss}$ = 192.6 kJ mol^{-1}) and the sample cannot absorb this heat instantaneously from its surroundings. Therefore, there is transitionally a temperature drop between the outer layer and the centre of the sample [2]. Consequently, the transformation proceeds gradually from layer to layer towards the centre. With the progress of the transformation, the difference between the temperature of the sample and the temperature of the furnace continuously increases, causing the acceleration of the transformation.

By comparing curve 2 in Fig. 1 with curve 1, it can be seen that the significant temperature drop caused the course of curve 1 to shift in the direction of higher temperatures. Accordingly, the shape of this curve is characteristic primarily of the heat-transport effect.

From the differences existing between curves 1 and 3 in Fig. 1 conclusions can be drawn regarding the influence of the transport of the gaseous decomposition products (Table 1) upon the course of the transformation. Both curves were obtained with the same dynamic heating program, and the only difference being that curve 1 was traced for a labyrinth crucible, and curve 3 for an open crucible. Accordingly, for curve 1, the partial pressure of carbon dioxide during the whole experiment was 1 bar, while for curve 3, it changed continuously.

It is well known that the equilibrium of the decomposition reactions of inorganic compounds is defined by the relationship between decomposition pressure and temperature in a closed system, under isothermal and equilibrium conditions. However, in conventional thermoanalytical studies, heating is done in open sample holders and in the presence of air or another gas. Therefore, during the decomposition, gaseous decomposition products stream continuously away from the inside of the sample, while the ambient gas diffuses towards the sample centre. The extent of diffusion is greatly influenced by the experimental conditions, e.g., amount of sample, layer thickness, size and shape of the sample holder, etc. When the partial pressure of the gaseous decomposition products in the interior of the sample between the grains drops slightly below the actual value of the decomposition pressure, decomposition will start. However, when it reaches this value, decomposition will stop again. But meanwhile the temperature also increases, creating newer and newer equilibrium conditions by continuously increasing the actual equilibrium limit value of the partial pressure of the gaseous decomposition products. Summing up, the course of the transformation is regulated by the complications arising from the various elementary processes of gas transport and heat transport (Table 1) in such a way that the equilibrium of the system will correspond at any moment to the conditions of the decomposition pressure—temperature relationship.

From the above-mentioned argument, it follows that the difference between curves 1 and 3 is due solely to the gas transport under the given conditions, while the course of curve 3 illustrates the combined effects of gas transport and heat transport. However, the objection may be made that the course of the curves in Fig. 1 could have been due to some other elementary processes, as even in Table 1 many processes are listed. In order to resolve such doubts, the TG curves of ammonium chloride are shown in Fig. 2. The decomposition of ammonium chloride $NH_4Cl_{(s)} \rightleftharpoons NH_{3(g)} + HCl_{(g)}$ is very simple, comprising only three elementary processes, i.e. simple heat absorption, sublimation, and dissociation which takes place simultaneously with the sublimation. The TG curves of Fig. 2 were traced under the same experimental conditions as the TG curves of calcium carbonate (curves 1–3, Fig. 1). The results are also similar, serving as proof of the above suppositions.

In summary, it can be stated that the Arrhenius equation cannot be regarded as a theoretical model for reactions examined under dynamic thermoanalytical conditions. At best, the Arrhenius equation can be used only as an empirical model, whose parameters do not offer any realistic physicochemical content.

MATHEMATICAL TREATMENT OF THE ARRHENIUS MODEL

Recently, it was indicated [1, 5] that the applicability of the Arrhenius model can also be disputed on a mathematical basis. In the course of these studies, it became necessary to establish whether or not the parameters of the Arrhenius model can be estimated with confidence from the mathematical point of view, and to establish whether or not there is a mutual unambiguous connection between the obtained curve and the three estimated parameters (here called the parameter triplet [A, E, n]) which will describe such a curve unequivocally.

In this paper, thermal processes are defined as heterogeneous reactions proceeding to equilibrium and which are connected with mass changes and are examined under dynamic heating conditions and conventional experi-

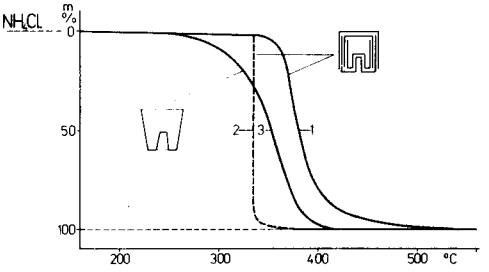

Fig. 2. Thermoanalytical curves for ammonium chloride.

mental conditions. These processes are interpreted on the basis of the TG curves.

In the present work, the Arrhenius model of reaction kinetics is used in the following form

$$d\alpha(t)/dt = A \exp [-E/RT(t)] [1 - \alpha(t)]^n \quad (1)$$

or in the case of a linear heating program

$$d\alpha(T)/dT = (A/G) \exp [-E/RT] [1 - \alpha(T)]^n \quad (2)$$

where A is the pre-exponential factor (s^{-1}), t is the time, n is the reaction order (dimensionless number), E is the activation energy (kJ mol^{-1}), T is the absolute temperature (K), α is the reaction coordinate (dimensionless number), G is the heating rate (K min^{-1}), and $\alpha = (m_o - m)/(m_o - m_v)$ where m_o is the initial, m the actual and m_v the final mass.

Assessment of the reliability of parameter estimates in the Arrhenius model

It is well known that, by applying various mathematical procedures to the evaluation of a given single curve, one can obtain rather different parameter triplets [1]. At the same time, it is clear that the different estimated parameters may define the measured curves equally well if their substitution into the model enables the calculated curves to fit the measured curves sufficiently well. Accordingly, the Arrhenius equation is a good empirical model for describing the examined process, but the parameter estimation is rather problematic.

In order to exclude the disturbing effect of errors of measurement, parameter estimation was also done on TG curves obtained numerically, where the values of A, E, n and heating rate were fixed.

When various mathematical methods were used to estimate the parameters of curves free from measuring errors, very differing values were obtained, as mentioned earlier [1]. From this, it can be concluded that the estimated parameter values are characteristic of the mathematical methods applied rather than of the curve itself. This proves that the application of the Arrhenius model leads to labile and poor parameter estimation.

The accuracy of the parameter estimates can be characterized by the so-called condition number [6]. The greater is this number, the worse is the reliability of the estimated values. The actual meaning of this concept can be demonstrated by a simple example originating from Ralston [7]. The parameters to be determined are x and y, while the coefficients are the measured values

$$1x + 3y = 4$$
$$2x + 6.00001y = 8.00001$$

The solution is $x = 1$, and $y = 1$. In the next measurement, the coefficients are changed by 0.0002%, giving the system of equations

$$1x + 3y = 4$$
$$2x + 5.99999y = 8.00002$$

The solution in this case is $x = 10$ and $y = -2$. Thus the slightest change in the coefficients causes a decisive change in the parameters. The condition number of the parameter estimate is 10^5, and so is very great in this example.

In this paper, a parameter estimate is called badly conditioned when $d[\delta(\epsilon)]/d\epsilon > \sigma(\delta)$, i.e. a small change of ϵ brings about a large change in δ. The parameter estimate is called well conditioned if this change of ϵ causes only a small change in δ (see Appendix).

The linearized Arrhenius model was examined in this way and was found to be badly conditioned, the condition number being about 10^5. From this, it can be concluded that, although the Arrhenius model is a well-fitting empirical model, the estimation of its parameters is unreliable. This statement leads to the second problem.

Correlation of a single parameter triplet with a unique TG curve

First, the differences caused in the curves [1] on application of the various parameter values of the model expressed by eqn. (2) will be examined. In order to be able to characterize the difference between two curves, a possible means of measuring the distance between two curves (Fig. 3) is introduced. If $f_j(T_i)$ is defined as the value of the jth curve belonging to temperature T_i (T_i, $T\epsilon\tau$, $f_j(T)\epsilon[0.1]$ where τ is the examined temperature interval), then the distance between curves $f_j(T)$ and $f_k(T)$ in the domain $T\epsilon\tau$ is by definition

$$\left(\sum_{i=1}^{N} [f_j(T_i) - f_k(T_i)]^2\right)^{1/2} \cdot 1/N = \Delta_{TG}(\tau) \qquad (3)$$

where $T_{i+1} - T_i = \tau/N$ (i = 1.....N) and $0 \leqslant \Delta_{TG}(\tau) \leqslant 1$. This measure of distance can be utilized for calculating the distances when the values of the parameters are changed.

For the sake of simplicity, the values of n and G are assumed to be known; these are treated as constants during the calculations. Only the effect of changes in the values of A and E will be examined. Further, it is assumed that the kinetic parameters of the examined TG curve obtained numerically

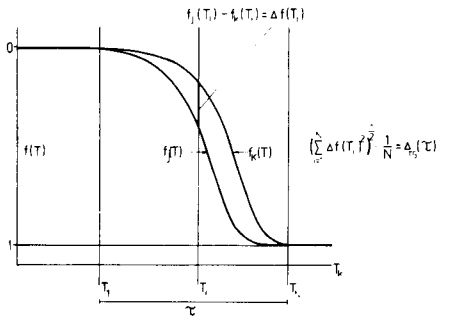

Fig. 3. Proposed measure of distance between two curves.

with the help of eqn. (2) are known. These known parameter values are regarded as set points in the parameter space ($A \times E$) and are marked in the Figs. by asterisks. Thereafter, a computer program is used to select those points in the parameter space, for which the curve belonging to these parameter values does not deviate from the original curve belonging to the set point by more than a preset distance. These parameter pairs are indicated in parameter space A, E and so the confidence domain shown in Fig. 4 is obtained. As can be seen, deviating parameter couples which fall into the domain, i.e. which are equally "good", can be selected over a broad interval: the curves calculated with their help would not deviate from the original curve by more than the preset distance limit. The protracted long and narrow domain in Fig. 4 illustrates how badly conditioned is the estimation. The dimensions of the ΔA and ΔE domains belonging to the given distance limit can be seen in Fig. 4. If the parameter estimates were well-conditioned, then this confidence domain would be nearly circular, indicating significantly smaller $\Delta A'$ and $\Delta E'$ domains. For the sake of comparison, the confidence domain of a well-conditioned parameter estimation is indicated in Fig. 4.

A natural consequence of the above considerations is that many deviating parameter couples, estimated from a single measured curve, could equally well describe the given curve within the permitted distance limits (Fig. 5). It can therefore be concluded that there is no unique correlation between the curve and the parameters estimated on the basis of the measured curve.

Further considerations

As has been shown, the parameter estimation can be performed only with uncertainty. However, it may not be clear why a certain kinetic calculation method should yield accurate and reproducible results, whereas another

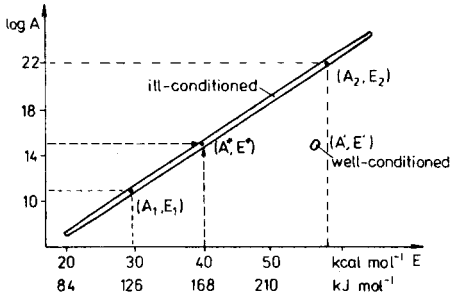

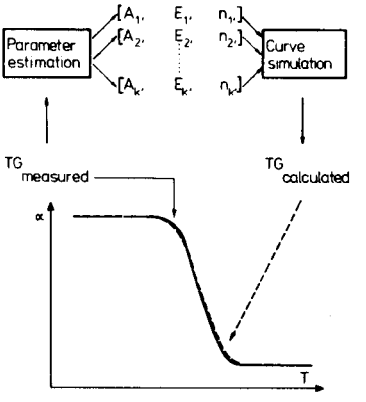

Fig. 4. Calculated confidence domains. Set points: $A = 10^{15}$; $E = 168$ kJ mol^{-1}.

Fig. 5. Comparison of measured and calculated TG curves.

method, although reproducible in itself, can yield strongly deviating results. The following general examination of the various methods of calculation clarifies this point.

One type of method is the so-called trial and error method. The iteration process, as indicated in Fig. 6A, starts from a certain initial value (A_o, E_o) and proceeds until the calculated curve does not fit sufficiently well, i.e. until the selected method does not reach the confidence value of the parameters. As can be seen in Fig. 6A, starting with another initial value or moving the search in another direction will yield differing parameter values, which will be equally good in the sense that the curve computed with their help would fit the measured data well. Another possible method first estimates E (E^* in Fig. 6A), then from this it seeks to establish the A value.

Methods based on linearization treat the parameter A as a constant. As can be seen in Fig. 6B, these methods reduce the dimensions of the parameter space and, depending on the applied mathematical operation, this constant attains various values. Accordingly, the estimated E values will also differ for the same measured curve. It is easy to see that methods based on difference—differentiation, second derivative or various heating rates could similarly yield an erroneous estimation.

Accordingly, it is evident that the calculated parameter values are characteristic of the applied mathematical procedure and not of the thermal reaction itself.

The correlation between the pre-exponential factor and activation energy is described by many authors as a compensation effect. However, nature may not actually produce such a compensation effect. What is actually observed is certainly a mathematical compensation effect, which is a trivial consequence of the badly conditioned parameter estimation.

Attempts were made to improve the reliability of the parameter estimation with the help of various transformations. The methods of moments, of orthogonal polynomials, and also the Karhunen—Loewe transformation, were examined. But even with the application of these transformations, the badly conditioned parameter estimation could not be improved.

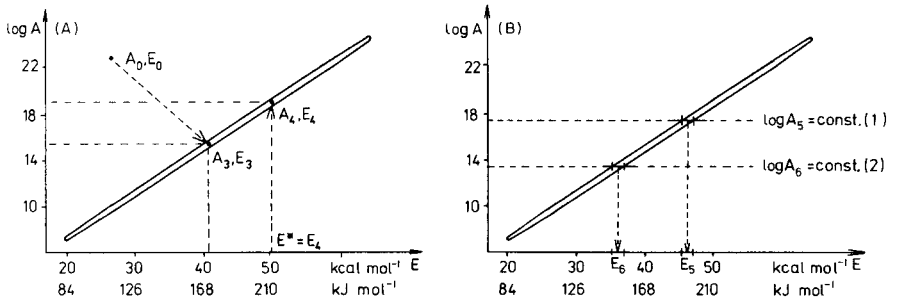

Fig. 6. Confidence domains calculated by an iteration method (A) and by a linearization method (B).

Conclusions

For the case of heterogeneous reactions leading to an equilibrium and examined under dynamic heating conditions, the Arrhenius equation cannot be regarded as an adequate theoretical model of the process.

The estimation of the parameters of the Arrhenius model is badly conditioned and unreliable. There is no unique correlation between the TG curve and the parameter values estimated from the curve: many and strongly divergent parameter triplets can be correlated with a single TG curve.

Finally, since the application of the Arrhenius equation leads to contradiction, it definitely should not be used for the interpretation of heterogeneous reactions examined under dynamic heating conditions.

The authors thank Prof. E. Pungor for valuable discussions.

APPENDIX

Consider the differential equation $\dot{\alpha} = f(\alpha, t, p)$, and assume that it has at least one $\alpha(t, p)$ solution which is continuous according to parameter p.

The problem is to estimate the parameter vector p based on the measured values $\alpha^*(t)$, where $\alpha^*(t)$ is one of the approximations of the solution curves of the differential equation. By substituting the estimated parameter vector (p^*) into the Arrhenius model, an approximation $\alpha'(t, p^*)$ of the solution $\alpha(t, p^*)$ can be made. The reliability of estimating parameter vector p by approximation $\alpha^*(t)$ is indicated by ϵ in the space α, if the difference between the calculated solution $\alpha(t, p^*)$ of the above differential equation and the approximate measured solution $\alpha^*(t)$ does not exceed a given limit. Thus the inequality $|\alpha'(t, p^*) - \alpha^*(t)| < \epsilon$ holds [where p^* is the parameter vector estimated on the basis of $\alpha^*(t)$, ϵ is the previously stated limit and $|\cdots|$ is a certain standard of functions $\alpha(t)$]. In the space α, the reliability of estimating p is indicated by δ, depending on ϵ and assuming any p^i and p^j values satisfying the conditions: $p^i, p^j \epsilon P$ and $|p^i - p^j| \leqslant \delta(\epsilon)$, for which the relation $|\alpha(t, p^i) - \alpha(t, p^j)| \leqslant \epsilon$ is valid.

REFERENCES

1 M. Arnold, G. E. Veress, J. Paulik and F. Paulik, J. Thermal Anal., 17 (1979) 507.
2 F. Paulik and J. Paulik, J. Thermal Anal., 5 (1973) 253.
3 F. Paulik and J. Paulik, Thermochim. Acta, 4 (1972) 189.
4 J. Paulik and F. Paulik, Anal. Chim. Acta, 56 (1971) 328.
5 M. Arnold, G. E. Veress, J. Paulik and F. Paulik, 6th ICTA Proceeding 1, (1980) 69.
6 G. E. Forsyte and C. B. Moler, Computer Solution of Linear Algebraic Systems, Prentice-Hall, Englewood Cliffs, NJ, 1973.
7 A. Ralston, A First Course in Numerical Analysis, McGraw-Hill, New York, 1965.

Analytica Chimica Acta, 124 (1981) 351—356

THE DETERMINATION OF DISSOLVED CHROMIUM(III) AND CHROMIUM(VI) AND PARTICULATE CHROMIUM IN WATERS AT $\mu g\ l^{-1}$ LEVELS BY THIN-FILM X-RAY FLUORESCENCE SPECTROMETRY

A. J. PIK, J. M. ECKERT* and K. L. WILLIAMS

Department of Inorganic Chemistry, University of Sydney, Sydney, N.S.W. 2006 (Australia)

(Received 8th September 1980)

SUMMARY

A method is described for the determination of particulate chromium and dissolved chromium(III) and (VI) in water at $\mu g\ l^{-1}$ levels. Particulate material is collected by filtration of the water sample through a membrane filter (0.4-μm pore-size). Chromium(III) and chromium(VI) are then coprecipitated, separately and in that order, with iron(III) hydroxide (at pH 8.5) and a cobalt—pyrrolidinedithiocarbamate carrier complex (at pH 4.0). Both precipitates are collected as thin films on membrane filters and, with the particulate material, analysed directly for chromium by x-ray fluorescence spectrometry. Detection limits, for a 100-ml water sample and counting times of 100 s, are 0.1 $\mu g\ Cr\ l^{-1}$. The method is unaffected by sea salt and is applicable, without modifications, to river and estuarine waters.

In an earlier paper [1], a method was described for the determination of dissolved Fe, Co, Ni, Cu, Zn, Cd and Pb in water at $\mu g\ l^{-1}$ levels, based on coprecipitation of the required metal ions with a carrier metal complex and measurement of the precipitate, as a thin film, by x-ray fluorescence spectrometry (x.r.f.). The technique is extended in this paper to a method for the separate coprecipitation of chromium(III) and chromium(VI) from filtered water at $\mu g\ l^{-1}$ levels and thin-film x.r.f. measurement of the precipitates, and particulate material from the initial filtration.

The combination of selective coprecipitation and thin-film x.r.f. does not appear to have been used previously for the speciation of chromium, yet it is an attractive one for several reasons. Many of the published methods for the determination of dissolved Cr(III) and Cr(VI) involve measuring the concentration of either Cr(III) or Cr(VI) in one sample and of total chromium, after oxidation or reduction, in another sample. The concentration of the other species is obtained by difference. The inherent inaccuracy of such methods, particularly when they are used for trace analysis, is avoided by selective coprecipitation.

The separation of reactive species as stable solids on easily stored membrane filters is convenient, and thin-film x.r.f. provides a simple, rapid means

of determining chromium in the precipitates. Acid digestion, a requirement of methods combining coprecipitation with a.a.s. or a.s.v., is unnecessary. Moreover, particulate material from filtered water samples, collected as a thin film on membrane filters, is well suited to direct measurement by x.r.f.

EXPERIMENTAL

Reagents and filtration equipment

Distilled-deionized water was used for all solution preparations and dilutions.

Iron solution (100 mg Fe(III) l^{-1}). Dissolve 0.432 g of iron(III) ammonium sulphate dodecahydrate in 0.01 M sulphuric acid and dilute to 500 ml with the sulphuric acid.

Cobalt solution (100 mg Co(II) l^{-1}). Dissolve 0.247 g of cobalt(II) nitrate hexahydrate in water and dilute to 500 ml.

Buffer pH 8.5. Dissolve 9.8 g of ammonium chloride in water, add 8 ml of 2 M ammonia and dilute to 500 ml with water. Remove trace metal impurities from this solution by addition of 5 ml of iron solution and filtration 1 h later through a membrane filter.

APDC solution. Dissolve 4 g of ammonium pyrrolidinedithiocarbamate (APDC) in water and dilute to 100 ml. Filter through a membrane filter and remove trace metal impurities from the filtrate by addition of 1 ml of cobalt solution and filtration after 1 h through a membrane filter. The resulting filtrate should be used within 24 h, but it may be kept for up to a week if stored at 4°C.

Buffer pH 4.0. Dissolve 20.4 g of potassium hydrogenphthalate in water and dilute to 500 ml. Purify the solution by addition of 1-ml quantities of cobalt and APDC solutions and filtration after 1 h through a membrane filter.

Membrane filters and filtration apparatus. All precipitates were collected on Nuclepore polycarbonate membrane filters (0.4-μm pore-size, 37 mm in diameter) with a Sartorius vacuum filtration unit (3.1-cm^2 filtration area).

Separation procedures

Separation of particulate material. Filter a measured volume of the water for analysis (at least 100 ml) through a membrane filter. Retain the loaded filter for the determination of particulate chromium and proceed immediately with the coprecipitation of dissolved chromium(III) from the filtrate.

Coprecipitation of chromium(III). To 100 ml of the filtrate, in a 250-ml polythene bottle fitted with a screw cap, add 1 ml of iron solution followed by 5 ml of buffer pH 8.5. The pH should now be 8.5 (±0.5). Cap the bottle, swirl the mixture for 15 s and allow it to stand for 1 h. Filter the suspension through a membrane filter and retain the loaded filter for the determination of chromium(III).

Coprecipitation of chromium(VI). To the filtrate from the previous step, in a 250-ml polythene bottle, add 5 ml of buffer pH 4.0 and 0.1 M nitric acid to give a pH of 4.0 (±0.5) (2 to 2.5 ml of the nitric acid is usually required). Add 1 ml of cobalt solution and 5 ml of APDC solution, cap the bottle, swirl for 15 s and allow to stand for 1 h. Filter through a membrane filter and retain the loaded filter for the determination of chromium(VI). Discard the filtrate.

Treatment of loaded membrane filters. Place the loaded filters in plastic boxes and allow to dry, first in an air oven at 50°C for 12 h and then in a vacuum desiccator for 2 h.

Preparation of thin-film standards

Prepare two sets of thin-film standards, including blanks, one set by the coprecipitation of Cr(III) from standard Cr(III) solutions, the other by coprecipitation of Cr(VI) from standard Cr(VI) solutions, in each case using the recommended procedure. It is necessary to prepare two sets of thin-film standards because chromium has different coprecipitation efficiencies in its two oxidation states. The Cr(III) standards, however, serve both for the dissolved Cr(III) and for the particulate chromium determinations. The standard chromium solutions were prepared from potassium dichromate and chromium potassium sulphate dodecahydrate.

The precipitates are stable and standards prepared on polycarbonate filters can be used repeatedly, unlike those on cellulose filters which deteriorate rapidly under an x-ray beam.

X.r.f. analysis

Mount the loaded filters with the sample side towards the x-ray beam and measure the net (i.e., peak minus background) fluorescent intensities. Calculate the amount of chromium present in each sample precipitate by comparison with the appropriate set of standards.

In this work, the precipitates were analysed with a Philips PW1450 automatic sequential x-ray spectrometer. The filters were mounted in standard sample holders (Philips type PW1527), fitted with adaptor rings to suit the PW1450 sample changer and with 2-mm thick teflon sleeves inside the holders to reduce the scattered background intensity. The following working conditions were used: gold anode tube operated at 60 kV and 45 mA, coarse collimator, LiF_{200} crystal, 2θ values of 69.36° and 71.00° for peak and background, respectively, automatic pulse-height selection, flow and scintillation detectors in tandem, and counting times of 100 s and 20 s for peak and background, respectively.

RESULTS AND DISCUSSION

The coprecipitation of chromium(III) with iron(III) hydroxide is a well-established procedure [2]. In the present application, this step was shown,

by atomic absorption spectrometry (a.a.s.) of the acid-dissolved precipitate, to proceed quantitatively at the 100 $\mu g\ l^{-1}$ level. That coprecipitation was quantitative over the whole concentration range (0—100 $\mu g\ l^{-1}$), was demonstrated by the linearity of the calibration graph; this indicated also that matrix effects of the precipitates, as thin films, were insignificant. The set of Cr(III) standards was therefore used, in the proposed method, for the determination of particulate chromium as well as dissolved chromium(III). As a check on this procedure, particulate material from a spiked natural water sample was analysed for chromium directly by thin-film x.r.f. and by a.a.s. after acid digestion. Results by the two methods were within 5% of each other.

In a previous use of cobalt(II) and APDC to coprecipitate chromium(VI) from water [3], the authors reported quantitative coprecipitation of Cr(VI) at concentrations of 10 and 100 $\mu g\ l^{-1}$ in 1-l samples. When an attempt was made in the present study to scale down this method for 100-ml samples, a coprecipitation efficiency of 50% was obtained. That of the method now reported, which used a different buffer system and an increased concentration of APDC, was found to be 83% for 100 μg Cr(VI) l^{-1}. The linearity of the calibration graph indicated that the coprecipitation efficiency was unchanged, within experimental error (see Table 2), over the whole concentration range (0—100 $\mu g\ l^{-1}$) and that matrix effects were not significant.

The selectivity of the coprecipitation step for chromium(III) was assessed by determining chromium(III) in the presence of different concentrations of chromium(VI). The results are given in Table 1. The presence of up to 100 μg Cr(VI) l^{-1} increases the apparent concentration of chromium(III) by a maximum of 2 $\mu g\ l^{-1}$. Similar results were obtained for the coprecipitation of Cr(VI) in the presence of Cr(III), but this source of interference was eliminated in the proposed method by the quantitative removal of chromium(III) in the first coprecipitation, leaving only the possible loss of chromium(VI) in the first coprecipitation to be considered.

In the pH range of most natural waters (7 ± 1), dissolved chromium(III) is rapidly lost from solution by adsorption on to the surfaces of containers [4]. Yet, if filtered natural waters are acidified, chromium(III) is stabilised but

TABLE 1

Recovery of Cr(III) from water in the presence of Cr(VI)

Cr(III) added ($\mu g\ l^{-1}$)	Cr(III) found ($\mu g\ l^{-1}$)	Cr(III) added ($\mu g\ l^{-1}$)	Cr(III) found ($\mu g\ l^{-1}$)	Cr(III) added ($\mu g\ l^{-1}$)	Cr(III) found ($\mu g\ l^{-1}$)
100 μg Cr(VI) l^{-1} added		*10 μg Cr(VI) l^{-1} added*		*1 μg Cr(VI) l^{-1} added*	
0.0	1.8	0.0	0.6	0.0	<0.1
1.0	2.9	1.0	1.5	1.0	1.1
10.0	12.0	10.0	10.7	10.0	10.0
100.0	101.1	100.0	100.0	100.0	101.0

TABLE 2

Sensitivity, background, precision and limits of detection

Oxidation state	Cr(III)	Cr(VI)
Sensitivity and background[a]		
m (c s^{-1} μg^{-1})	711	590
b (c s^{-1})	236	225
Precision[b]		
s_r (%) for 1 μg l^{-1}	6	7
s_r (%) for 10 μg l^{-1}	2	3
s_r (%) for 100 μg l^{-1}	1	1
Limits of detection (μg l^{-1})	0.1	0.1

[a]Slope and intercept of regression line in a typical calibration run; 8 standards in the range 0—100 μg l^{-1} were determined. [b]5 precipitates were determined at each concentration.

chromium(VI) is slowly reduced to chromium(III) [5]. Water samples should therefore be filtered as soon as possible after collection and the filtrates analysed for dissolved chromium within 2 or 3 h of the initial filtration.

Calibration, precision and limits of detection

Calibration graphs obtained with standard solutions of chromium(III) and chromium(VI) were linear in the concentration range 0—100 μg l^{-1}. Values obtained in typical calibration runs for m (sensitivity) and b (background) are presented in Table 2; m and b are parameters of the equation for the linear regression line $y = mx + b$, fitted to the standard x-ray intensity data, in which y is the net x-ray intensity and x is the mass, in μg, of chromium in the precipitate. Also given in Table 2 are estimates of precision at the 1, 10 and 100 μg l^{-1} levels and limits of detection, calculated as $(3/m)(b/T)^{1/2}$, where T is the counting time (100 s). The difference in m for the Cr(III) and Cr(VI) calibration evident in Table 2, is due to the difference in coprecipitation efficiencies and not to any effect of oxidation state on the x.r.f. measurements.

Interferences

No metal ions were found to interfere seriously at concentrations likely to be encountered in unpolluted river and estuarine waters; Mn, Fe, Cu and Zn, for example, can all be tolerated at concentrations of 1000 μg l^{-1}. Phosphate also does not interfere at this level.

The effect of salinity on the proposed method was tested by adding Cr(III) and Cr(VI) to filtered estuarine water samples varying in salinity from 0 to 31 parts per thousand (collected from the Hawkesbury River, N.S.W.). Comparison with standards prepared from solutions in distilled-deionized water gave recoveries in the range 80—105% at each concentration and over

TABLE 3

Recovery of chromium from estuarine water (salinity = 31°/$_{oo}$)[a]

Cr added[b] ($\mu g\ l^{-1}$)	Recovery (%)[c]	
	Cr(III)	Cr(VI)
5	100	100
20	105	98
100	101	99

[a]Concentrations in the water, before additions, were below detection limits for both species. [b]Cr(III) and Cr(VI) were added to separate aliquots. [c]The quoted values had standard deviations of 1—5%.

the whole salinity range. The results for a water sample of high salinity are shown in Table 3. The method appears to be well suited to estuarine water analysis.

This work was supported by a grant from the Australian Research Grants Committee; the x.r.f. equipment was made available by the Department of Geology and Geophysics at the University of Sydney.

REFERENCES

1 A. J. Pik, A. J. Cameron, J. M. Eckert, E. R. Sholkovitz and K. L. Williams, Anal. Chim. Acta, 110 (1979) 61.
2 See, e.g., J. P. Riley, Analytical Chemistry of Sea Water, Ch. 19, in J. P. Riley and G. Skirrow (Eds.), Chemical Oceanography, Vol. 3, 2nd edn., Academic Press, London, 1975, p. 280.
3 K. V. Krishnamurty and M. M. Reddy, Anal. Chem., 49 (1977) 222.
4 T. R. Gilbert and A. M. Clay, Anal. Chim. Acta, 67 (1973) 289.
5 G. J. de Jong and U. A. Th. Brinkman, Anal. Chim. Acta, 98 (1978) 243.

Analytica Chimica Acta, 124 (1981) 357—364

THE IDENTIFICATION OF CHLOROPHENOXYPHENOLS IN SOIL AND WATER SAMPLES BY SOLVENT EXTRACTION AND FIELD DESORPTION MASS SPECTROMETRY

JAMES F. PANKOW*, LORNE M. ISABELLE and DOUGLAS F. BAROFSKY

Department of Environmental Science, Oregon Graduate Center, Beaverton, OR 97006 (U.S.A.)

(Received 24th September 1980)

SUMMARY

The identification of microgram amounts of chlorophenoxyphenols is shown to be possible by solvent extraction and subsequent field desorption mass spectrometry (f.d.m.s.). Although the extraction step is performed under acidic conditions, the presence of humic and fulvic materials did not interfere in the interpretation of the f.d.m.s. spectra of soil and water samples contaminated with chlorophenoxyphenols. The pattern of oligomeric series and chlorine isotope clusters characteristic of the chlorophenoxyphenols as well as the soft-ionization properties (minimal fragmentation) of f.d.m.s. make this procedure well-suited for use in the rapid screening of liquid samples for the chlorophenoxyphenols.

While gas chromatographic separations of relatively volatile organic compounds have been developed to a fairly sophisticated degree, this is not the case for compounds of low volatility. Because ion production in field desorption mass spectrometry (f.d.m.s.) occurs on a highly charged wire surface and not in the gas phase, sample vaporization is not a prerequisite for ionization, and many relatively involatile compounds can be studied successfully by this technique. The recent determination of high-molecular-weight poly(oxyethylene) (POE) alkylphenyl ethers ($R—C_6H_4—O—(C_2H_4O)_n—H$) in water by Otsuki and Shiraishi [1] is a good example of the considerable utility of f.d.m.s. These researchers used nonpolar stationary phase liquid chromatography (l.c.) to concentrate mg l^{-1} levels of POE alkylphenyl ethers from spiked water samples, then monitored the l.c. fractions by f.d.m.s. The characteristic mass spectral patterns exhibited by the molecular ions of the various POE oligomers provided a distinct fingerprint for these mixtures.

In this study, f.d.m.s. was applied in a preliminary identification of compounds in another series, the chlorophenoxyphenols, in soil and water samples. The oligomeric phenoxyphenols can be described by the formula, $H—(C_6H_4O)_n—H$. The chlorophenoxyphenols are similar, but exhibit varying degrees of chlorination on each of the n rings. The lighter chlorophenoxyphenols are manufactured for use as bactericides and fungicides (e.g., 5-

chloro-2-(2,4-dichlorophenoxy)-phenol, I), while those of longer chain length are known to form as by-products during the manufacture of these bactericides [2] as well as during the production of other pesticides such as 2,4-dichlorophenoxyacetic acid (2,4-D) and polychlorophenols [3—5]. The level of n = 2 chlorophenoxyphenols with 4—9 total chlorine atoms often ranges as high as 1—5% in technical grades of tri-, tetra, and pentachlorophenol [3]. The biological activity of the chlorophenoxyphenols is not limited to bactericidal and fungicidal properties. Indeed, the mutagenicities of 5-chloro-2-(2,4-dichlorophenoxy)-phenol (I) and 2,3,4-trichloro-6-(2,4-dichlorophenoxy)-phenol (II) have been found to be similar to those of acridine orange and dimethylnitrosamine, respectively [6].

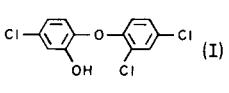

(I)

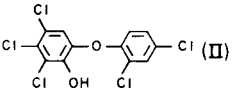

(II)

Such activity is not surprising since these two compounds are only one ring closure away from the polychlorinated dibenzodioxins (PCDD). (Indeed, as a result of this close similarity with the PCDD, these two chlorophenoxyphenols are known as "predioxins".) While higher chlorophenoxyphenols have not been studied in this regard, it is not unreasonable to suspect them of possessing similar toxicity.

In view of the large amounts of chlorophenoxyphenols currently residing in chemical dump sites and the continued production of chlorophenoxyphenols as products and by-products of pesticide manufacturing processes [7], a rapid analytical technique capable of screening for the presence of these materials is needed. Hites and Lopez-Avilla [2] recently described a liquid chromatographic electron impact mass spectrometric procedure for the identification of chlorophenoxyphenols in waste waters and verified the presence of chlorophenoxyphenols of chain length n up to 4 and molecular weight (m.w.) up to 666. Other work has demonstrated the presence of heavier homologues (m.w. > 1000) in technical grade pentachlorophenol [8]. The present paper describes a method based on solvent extraction and f.d.m.s. which is well-suited for the rapid screening of soil and water samples for the presence of both low and high m.w. chlorophenoxyphenols.

EXPERIMENTAL

Apparatus

Mass spectra were obtained with a Hitachi-Perkin Elmer RMU-6E, single-focussing mass spectrometer modified with a field ionization/field desorption ion source, a magnet capable of extending the practical f.d. mass range to 950 amu, and a PAR/SSR ion counting detection system consisting of a Model 1120 amplifier-discriminator and a Model 1105 data converter. Spectra were recorded on a Bell and Howell Datagraph S-134 oscillographic recorder. The activated emitters employed were prepared as described by Barofsky and Barofsky [9]. The emitter temperature was controlled manually

by varying the amount of heating current passing through the emitter. For each sample, f.d. mass spectra were obtained at a number of different heating currents. The spectra presented here were obtained by summing the peak intensities from each of these spectra.

Reagents

Sample pH adjustments were made using reagent-grade hydrochloric acid. Solvent extractions were done with dichloromethane (distilled-in-glass grade; Burdick and Jackson, Muskegon, MI). Diazomethane for sample methylations was prepared in ether using reagent-grade chemicals. Distillation residues from the commercial production of 2,4-dichlorophenol by chlorination of phenol were obtained from a commercial firm. A stock solution of 23.8 μg μl^{-1} of these tarry residues was prepared in methanol.

Procedure

The solvent extractions of natural and spiked water samples were performed by: (1) lowering the pH of the sample to 1 by adding 6 M HCl, (2) extracting with three 20-ml volumes of methylene chloride and combining these volumes, and (3) reducing the total volume with a gentle flow of ultra high-purity nitrogen. In the case of the tap water sample spiked at the 2.4 mg l^{-1} level with the dichlorophenol distillation residues, the volume extracted was 0.50 l, and the extract volume was reduced to 50 μl. Samples of ground water and soil samples which had become contaminated with chlorophenoxyphenol wastes were obtained on 9th October 1979 from a well 10 m from the boundary of the chemical disposal site at Alkali Lake, Oregon. The solvent extraction of ground water samples was performed using a 0.10-l sample and the procedure described above. A 20-g sample of soil and 300 ml of the solvent mixture (75:25 diethylether/ethanol) were placed in a brown screw cap (teflon insert) bottle, and the mixture was agitated on a shaker for 12 h. After filtration through a fast paper (No. 588, Schleicher and Schuell), 50 ml of distilled water was added to bring about a phase separation. The aqueous phase was discarded, and the organic phase was then reduced to 100 μl with a gentle flow of nitrogen. Approximately 0.5-μl aliquots of each extract described above as well as the chlorophenol residue stock solution were loaded on emitters using a microsyringe technique [10] and f.d.m.s. immediately followed the emitter loading.

RESULTS AND DISCUSSION

Table 1 presents a tabulation of the various possible chlorophenoxyphenols of n = 1—5. Each isotopic grouping or cluster is represented in Table 1 by its lowest molecular weight member; members within a cluster differ by two mass units. Many of these compounds are evidenced in the f.d. mass spectrum (Fig. 1) of the 2,4-dichlorophenol distillation residue. The m/z values representing the isotopic clusters evident in Fig. 1 have been enclosed in boxes in Table 1. The combination of the mass, proper chlorine

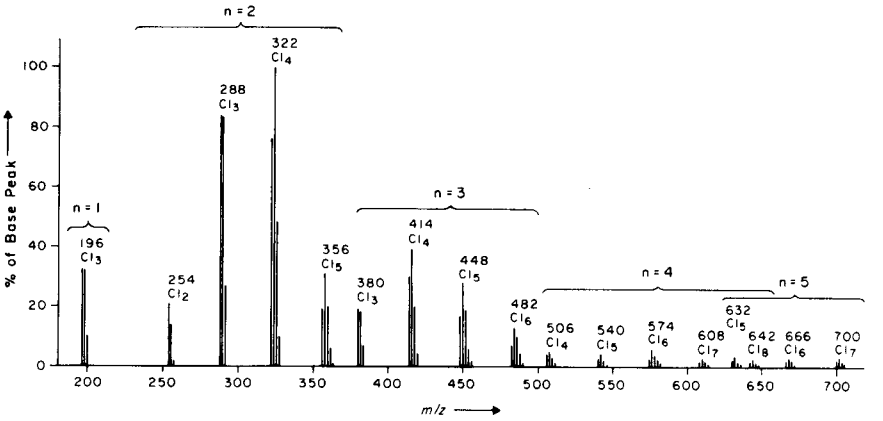

Fig. 1. Spectrum of distillation residues from the commercial manufacture of 2,4-dichlorophenol.

TABLE 1

Molecular weights for chlorophenoxyphenol oligomers with varying degrees of polymerization, n = 1—5, and varying degrees of chlorination, X. Boxed values refer to m/z values found (along with appropriate isotope cluster peaks) in the spectrum shown in Fig. 1.

n = 1		n = 2		n = 3		n = 4		n = 5	
X	m.w.	X	m.w.	X	m.w.	X	m.w.	X	m.w.
1	128								
2	162								
3	**196**								
4	230	1	220						
5	264	**2**	**254**						
		3	**288**	1	312				
		4	**322**	2	346				
		5	**356**	**3**	**380**	1	404		
		6	390	**4**	**414**	2	438		
		7	424	**5**	**448**	3	472		
		.		**6**	**482**	**4**	**506**	1	496
		.		7	516	**5**	**540**	2	530
		.		8	550	**6**	**574**	3	564
				.		**7**	**608**	4	598
				.		**8**	**642**	**5**	**632**
				.		9	676	**6**	**666**
						10	710	**7**	**700**
						.		8	734
						.		9	768
						.		.	
								.	
								.	

isotopic cluster proportions, and the presence of the other series members is a strong indication that the peaks in spectrum 1 may be interpreted in terms of Table 1. Some questions remain as to how the chlorine atoms of each member are distributed among its several rings. In view of the fact that no peaks appear in the spectrum corresponding to compounds for which the number of rings, n, exceeds the number of chlorine atoms present, the m.w. series 254, 380, 506, and 632 seems strongly indicative of the compound series III

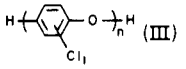
(III)

where n = 2—5, and there is one chlorine somewhere on each ring. These compounds did not appear in the spectra presented by Hites and Lopez-Avila [2]. Since the processes responsible for the wastes studied by Hites and Lopez-Avila were related to the manufacture of chlorophenoxyphenol antiseptics and not the synthesis of 2,4-dichlorophenol, this dissimilarity is not surprising.

The m.w. series 288, 414, 540, and 666, however, is evident in both spectrum 1 and the electron impact (e.i.) spectra of Hites and Lopez-Avila [2]. Based on the e.i. fragmentation patterns, and the knowledge that they were studying by-products from the manufacture of the antiseptic I, Hites and Lopez-Avila felt that the 288, 414, 540, and 666 m.w. series which they observed was due to the successive addition of 2,4-dichlorophenol units to this compound. This would lead to the compound series IV where n = 2—5. The m.w. series 288, 414, 540, and 666 evident in spectrum 1 is, however, likely due to a similar polymerization of 2,4-dichlorophenol leading to series V.

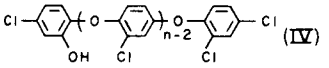
(IV)

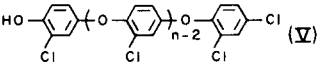
(V)

where again n = 2—5. Series V is isomeric with series IV.

Varying amounts of other isomers are no doubt also present as a result of the formation of small amounts of other chlorophenols during the synthesis of 2,4-dichlorophenol and their subsequent incorporation into these polymers. Indeed, the inclusion of phenols more highly chlorinated than dichlorophenol is evidenced by the two m.w. series, 322, 448, 574, and 700, and 356, 482, and 608, which possess one and two additional chlorines, respectively, over the n + 1 chlorines present in the series 288, 414, 540, and 666. Again, however, f.d.m.s. gives no information regarding the ring location of these additional chlorines. It is very likely that several isomers are contributing to the signal for each of these peaks.

The f.d.m.s. spectrum of the extract of the Alkali Lake chemical disposal site soil sample is presented in Fig. 2. The considerable intensity of some of the peaks required that the log of the intensities be plotted. The presence of

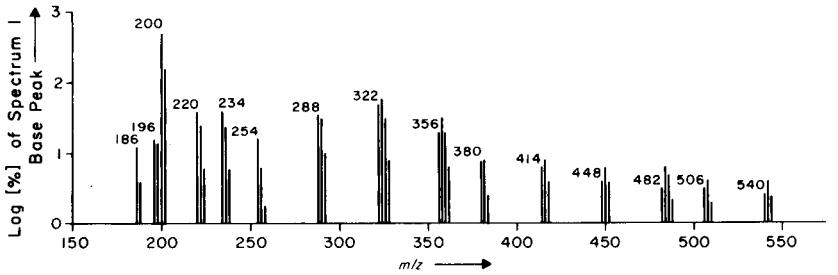

Fig. 2. Spectrum of soil extract from Alkali Lake, Oregon, chemical waste disposal site.

chlorophenoxyphenols of m.w. up to 540 is clearly indicated, and the relative proportions of the chlorine isotope clusters are in close agreement with the values expected based on the number of chlorines assigned to these peaks in Table 1. Though not apparent in this spectrum, low levels of higher homologues are no doubt also present.

The isotope clusters of the peaks at m.w. values of 186, 196, 200, 220, and 234 indicate the presence of one, three, one, two, and two chlorines, respectively. These data, together with the fact that chlorinated herbicides and chlorinated herbicide manufacturing residues are known to have been disposed of at the Alkali Lake site, support the assignments of chlorophenoxyacetic acid, trichlorophenol, methylchlorophenoxyacetic acid (MCPA), 2,4-dichlorophenoxyacetic acid (2,4-D), and 2,4-dichlorophenoxypropanoic acid (2,4-DP) for these peaks. Analysis by gas chromatography/mass spectrometry confirmed these assignments.

The spectrum of the extract of the well water obtained near the Alkali Lake site is presented in Fig. 3. The (n = 2) m.w. series 254, 288, 322, and 356 is clearly visible. The fact that chlorophenoxyphenols of m.w. greater than 356 did not appear in this spectrum may be due to either their absence in the well water, or low extraction recoveries or poor f.d. sensitivity caused by the presence of humic materials. Because the level of extractable organic matter in the soil sample was very likely greater than that in the well water

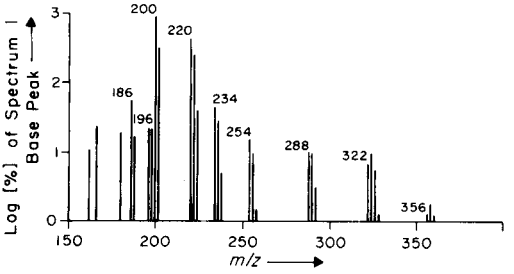

Fig. 3. Spectrum of extract of well water obtained 10 m from Alkali Lake, Oregon, chemical waste disposal site.

sample, and because the higher m.w. homologues would not be expected to leach as well as the shorter, more soluble chlorophenoxyphenols, the first explanation seems more probable.

All of the assignments made in Figs. 1—3 have in common the presence of a methylatable hydrogen (either carboxylic or phenolic). When each of the three extracts was treated with excess diazomethane, all of the peaks were shifted up by 14 amu, further confirming the above assignments.

The spectrum of the extract of the tap water sample which had been spiked at the 2.4 mg l^{-1} level with the 2,4-dichlorophenol distillation residue is presented in Fig. 4. Because the distillation residue (total chlorophenoxyphenols) was added at the mg l^{-1} level, the individual chlorophenoxyphenols were present at concentrations in the ng g^{-1} range. While f.d.m.s. is not well-suited for quantitative work, it was found that the peak intensities were reproducible to within ±40%. Thus, the intensities of the peaks in Fig. 3 imply that the Alkali Lake well water is contaminated with the $n = 2$ chlorophenoxyphenols in the ng g^{-1} to low μg g^{-1} range.

Although the acidic extraction conditions employed very likely resulted in the co-extraction of relatively large amounts of naturally-occurring organic compounds such as the so-called humic and fulvic acids, the spectra in Figs. 2—4 were virtually free of any peaks other than those attributable to the chlorophenoxyphenol series. This observation is consistent with our experience with f.d.m.s. in the structure elucidation of humic materials; despite a continuing effort in this area, it has been very difficult to obtain f.d. spectra of underivatized and undegraded humic materials. A second advantage of f.d.m.s. in qualitative works of this type results from its soft ionization characteristics. During the earlier study [2] of these compounds by direct probe e.i.m.s., liquid chromatographic fractionation was required to prevent spectral overlap of fragments of the larger oligomers with the molecular ions and fragments of the smaller chlorophenoxyphenols. Because

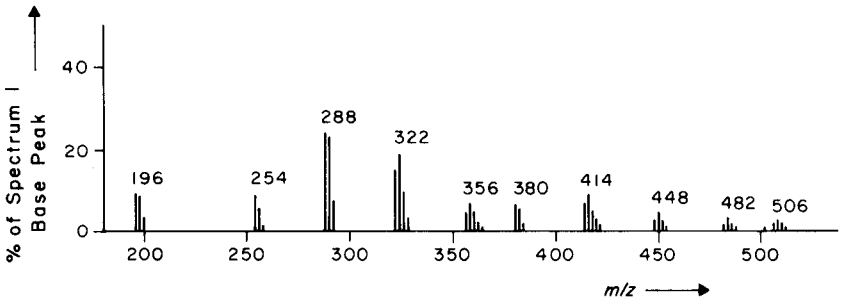

Fig. 4. Spectrum of extract of tap water spiked with chlorophenoxyphenol distillation residues at the 2.4 mg l^{-1} level.

little or no fragmentation occurs with f.d.m.s., this type of fractionation may be avoided and the screening for the presence of chlorophenoxyphenols can be completed in one run. These advantages are further enhanced by the regular mass distribution of the various oligomers as well as the distinctive nature of the accompanying chlorine isotope clusters.

The authors thank Elisabeth Barofsky for her very skillful preparation of the field desorption emitters used. We also thank Geo. Ward and Assoc., Inc., Portland, OR, for supplying the Alkali Lake samples.

REFERENCES

1 A. Otsuki and H. Shiraishi, Anal. Chem., 51 (1979) 2329.
2 R. A. Hites and V. Lopez-Avila, Anal. Chem., 51 (1979) 1452A.
3 C.-A. Nilsson and L. Renburg, J. Chromatogr., 89 (1974) 325.
4 M. Dienzer, J. Lamberton, D. Griffin and T. Miller, Biomed. Mass Spectrom., 5 (1978) 566.
5 M. Dienzer, D. Griffin, T. Miller, and R. Skinner, Biomed. Mass Spectrom., 6 (1979) 301.
6 R. Fahrig, C.-A. Nilsson and C. Rappe, in K. R. Rao (Ed.), Pentachlorophenol, Plenum, New York, 1977.
7 U.S. International Trade Commission, Synthetic Organic Chemicals, United States Production and Sales 1976, U.S.I.T.C. Publication No. 833, Washington, DC, 1979.
8 D. Griffin, Dept. Agricultural Chemistry, University of Oregon, Corvallis, 1980. personal communication.
9 D. F. Barofsky and E. Barofsky, Int. J. Mass Spectrom. Ion Phys., 14 (1974) 3.
10 H. D. Beckey, A. Heinrichs and H. U. Winkler, Int. J. Mass Spectrom. Ion Phys., 3 (1970) Appendices 9—11.

Analytica Chimica Acta, 124 (1981) 365—372

SELECTIVE SEPARATIONS BY REACTIVE ION EXCHANGE
Part 4. Preconcentration of Cadmium and Zinc by In Situ Precipitation as Hexacyanoferrate(II) Salts on Gel and Macroporous Ion-Exchange Resins

MICHELLE DELAYETTE-MILLS, LYA KARM, GILBERT E. JANAUER* and PING-KWAN CHAN

State University of New York at Binghamton, NY 13901 (U.S.A.)

WILLIAM E. BERNIER*

IBM Corporation, Endicott, NY 13760 (U.S.A.)

(Received 30th June 1980)

SUMMARY

The in situ precipitation of traces of cadmium(II) and zinc(II) ions as hexacyanoferrates from aqueous matrices was studied on conventional polystyrene gel and macroporous cation- and anion-exchange resins. Coprecipitation with each other or with copper(II) ions present in binary cation resins or in solution, and the influence of added non-precipitating ions of the same charge type such as magnesium(II) were investigated. Microporous (gel) cation exchangers gave reasonable recoveries and macroporous cation exchangers gave very good recoveries; but macroporous anion exchangers performed best, suggesting macroporous hexacyanoferrate(II) resin as an ideal phase for collection/preconcentration of traces of Cu^{2+}, Cd^{2+}, Zn^{2+}, and possibly Co^{2+}, Ni^{2+}, and Pb^{2+} from waters. As expected, very low yields were obtained with conventional anion exchange resin in the hexacyanoferrate form. Uniform distribution of Cu^{2+}, Zn^{2+}, and Cd^{2+} over macroporous anion-exchange resin phases were established by means of electron probe scans and taken as evidence for the formation of a uniform, well-developed precipitate layer covering the entire resin particle surface.

The thermodynamic basis and general principles underlying reactive ion exchange (r.i.e.) procedures were discussed in the first paper of this series [1]. Applications to preconcentration and subsequent quantification of trace elements have been described for chromate, vanadate, and permanganate [2, 3, 4], as well as selenium and tellurium species [5, 6] and hexacyanoferrate(II) and (III) [7].

Recently, the factors controlling in situ precipitation of copper hexacyanoferrate(II) were studied on small beds of binary Cu^{2+}—M^{n+}-loaded cation-exchanger resinates [8] of the conventional polystyrene sulfonate type over the mole fraction range of $\bar{X}_{Cu^{2+}} = 1.00$ to 0.002. The most important factor for the systems studied was the charge, n, of the non-precipitating counter ion M^{n+} accompanying Cu^{2+} in the binary resin phases. It was found that the virtual solubility product (v.s.p.) for $Cu_2[Fe(CN)_6]$, which permits meaningful comparison of different Cu^{2+}—M^{n+}-loaded systems,

decreases dramatically as n is changed from 1 to 3 to 2, in that order. Furthermore, the v.s.p. decreased for any given n as the formation constant, K_f, for the ion pairs $[MFe(CN)_6]^{(4-n)-}$ increased. The particle size of the exchange resin, although it does not significantly change the v.s.p., does decrease the yield of precipitate near the limiting resin mole fractions for precipitation. The percentage yield of precipitate passes through a maximum as a function of $Fe(CN)_6^{4-}$ solution flow rate, all other factors remaining the same. An increase in temperature decreases the overall yield of copper hexacyanoferrate(II) precipitate. At very low Cu^{2+} vs. Mg^{2+} loadings, this precipitate appears distributed throughout the entire minicolumn. These findings and the results of a study of the morphology of the precipitate on resin bead surfaces by scanning electron microscopy (s.e.m.) are consistent with the hypothesis that nucleation occurs primarily at the contact points of adjacent beads; "islands" of precipitate grow around nuclei first formed at bead contact points [6, 8].

The kinetics of the reaction at the surface of the resin beads, as well as the effective concentration of reactive and unreactive counter ions available, are most important is designing r.i.e. precipitation systems for practical applications. One practicable method for enhancing the rate is through the employment of macroporous ion-exchange resins. The large pores greatly increase the effective surface area of the resin. Therefore, a comparison of microporous vs. macroporous resins with hexacyanoferrate(II) r.i.e. precipitation systems was undertaken.

EXPERIMENTAL

BioRad ion-exchange resins AG 50W-X4 (100—200 mesh), AG 1-X4 (100—200 mesh), AG MP-50 (100-200 mesh) and AG MP-1 (100—200 mesh) were employed in column experiments. Analytical-grade reagents and deionized distilled water were used except as otherwise noted. Binary resinates were prepared and characterized as described earlier [8]. All experiments and determinations were performed in triplicate.

The standard column preconcentration and elution procedure for the anion-exchange resins consisted of preswelling multiple samples of 0.2 g each of resin in the chloride form in water for 24 h. The resin slurries were then poured into the standard 0.70-cm diameter minicolumns to form beds approximately 1 cm in height, and 25 ml of 0.1 M potassium hexacyanoferrate(II) equivalent to a four-fold excess with respect to total bed exchange capacity was added. Excess of hexacyanoferrate(II) was removed by subsequent washing with 100 ml of water. Varying trace amounts of copper and/or cadmium and/or zinc were added to 250 ml volumes of water, Binghamton tap water or Susquehanna River water, and the samples were passed through the minicolumns at a constant 2 ml min^{-1}, except when clogging slowed the flow rate. Precipitates formed were dissolved and eluted with 5 ml of aqueous 7.4 M ammonia, the eluate was collected, and metal

ions were quantified by atomic absorption spectrometry. This standard preconcentration and elution procedure was essentially the same as that reported earlier [7] for gel type (microporous) cation-exchange resins and was applied to macroporous and microporous exchange resins alike.

For the purpose of electron probe microdeterminations, individual AG MP-1 resin particles carrying surface deposits of the trace metal hexacyanoferrate(II) precipitates were mounted and embedded in an epoxy resin. The cross-sections of the resin particles were gradually polished starting with a grit of 240 and ending with a diamond polish. The samples were then carbon-coated, as is usual to provide a conductive path for current from the incident beam. The sample was placed on the specimen stage of the unit and a vacuum of 10^{-5} torr was applied overnight. The electron probe was set to scan across the diameter of the resin particle cross-sections to determine the spatial distribution of the three selected trace elements. The pure metal ion forms of the corresponding macroporous cation-exchange AG MP-50 were used for reference scans so that results could be normalized relative to absolute standards.

RESULTS AND DISCUSSION

Binary Cu^{2+}–Mg^{2+}-loaded cation-exchange resins can be used to collect hexacyanoferrate(II) traces quantitatively from distilled water. As shown in Table 1, both gel and macroporous resin structures are effective. Earlier work by Ramseyer and Janauer [7] demonstrated that the microporous Cu^{2+}-loaded resin is equally effective with tap water and river water samples for hexacyanoferrate(II). Similarly, the attempted coprecipitation of $Cd_2Fe(CN)_6$ with $Cu_2Fe(CN)_6$ on microporous Cu^{2+}—Mg^{2+}-loaded resin was nearly quantitative in distilled water but only partially successful in the case of river water as shown in Table 2. The reasons for this difference are not clear.

Macroporous and microporous anion-exchange resins gave significantly different results when hexacyanoferrate(II) was the resinate ion. Experiments showed that the microporous anion exchanger was unsuitable for concentrating Cu^{2+}, Cd^{2+}, or Zn^{2+} as the hexacyanoferrate(II) precipitate even when

TABLE 1

Concentration of hexacyanoferrate(II) (1 μg ml^{-1}) from deionized water

$\bar{X}_{Cu^{2+}}$[a]	Yield (% ± 7)	$\bar{X}_{Cu^{2+}}$[a]	Yield (% ± 7)
With MP-50 resin[b]	*With Dowex 50W-X4 resin*	*With MP-50 resin*[b]	*With Dowex 50W-X4 resin*
0.08	88	1.0	95
0.12	95	0.20	98
0.14	94	0.06	86

[a] Mg^{2+}—Cu^{2+} mixed resin mole fraction. [b] Particle size is 100—200 mesh.

TABLE 2

Concentration of Cd^{2+} traces from water samples on Dowex 50W-X4 Cu^{2+}—Mg^{2+} resinates

$\bar{X}_{Cu^{2+}}$	Matrix[a]	Particle size (mesh)	Yield (% ± 7)	Comments
0.5	River water[b]	100—200	50	Columns clogged
0.3	River water	100—200	60	Very slow flow rate
0.1	River water	50—100	60	Very slow flow rate
0.1	Distilled water	100—200	94	—

[a]Sample spiked with 0.1 ppm Cd^{2+} and 1.0 ppm $Fe(CN)_6^{4-}$. [b]Susquehanna River water.

excess of accompanying ion was added to the trace metal solutions. However, macroporous anion-exchange resin beds effected virtually quantitative precipitation and retention of traces of each of these metals (85—100%). When excess Mg^{2+} was added to the feed solution, even more Cu^{2+} and Zn^{2+} precipitated. Furthermore, the macroporous anion-exchange resin in the hexacyanoferrate(II) form achieved equally rapid and near quantitative formation/retention of hexacyanoferrate(II) precipitates with mixtures of trace metal ions (Table 3). In each case, there was a similar increase in yield with addition of 45 ppm of Mg^{2+} as the accompanying ion. Further experiments with aqueous matrices such as tap water and river water gave nearly quantitative yields for binary solution mixtures containing varying proportions of Cu^{2+}, Cd^{2+}, and Zn^{2+} traces (Table 4).

The observed superior performance of macroporous over microporous resins in these precipitation systems studied is not surprising, because macroporous resins have consistently shown faster ion-exchange rates than the con-

TABLE 3

Comparison of precipitation yields on MP50 (100—200 mesh) resin for varying concentrations of various binary metal ion systems in deionized distilled water

Trace ions			Initial concentration (mg l^{-1})		% Yield		
A	B	C	$[M^{n+}]$	$[Mg^{2+}]$	A	B	C
Cu^{2+}	Cu^{2+}	Zn^{2+}	0.9	0.0	89.6	93.7	92.3
Cd^{2+}	Zn^{2+}	Cd^{2+}	0.1		96.9	91.6	92.3
Cu^{2+}	Cu^{2+}	Zn^{2+}	0.9	45.0	93.2	93.4	93.0
Cd^{2+}	Zn^{2+}	Cd^{2+}	0.1		103.0	93.2	93.7
Cu^{2+}	Cu^{2+}	Zn^{2+}	0.5	0.0	92.5	91.2	90.4
Cd^{2+}	Zn^{2+}	Cd^{2+}	0.5		96.7	94.0	92.5
Cu^{2+}	Cu^{2+}	Zn^{2+}	0.5	45.0	93.1	93.7	91.6
Cd^{2+}	Zn^{2+}	Cd^{2+}	0.5		97.0	94.5	93.7
Cu^{2+}	Cu^{2+}	Zn^{2+}	0.1	0.0	92.1	90.1	90.0
Cd^{2+}	Zn^{2+}	Cd^{2+}	0.9		95.5	93.0	95.7
Cu^{2+}	Cu^{2+}	Zn^{2+}	0.1	45.0	95.5	91.5	91.6
Cd^{2+}	Zn^{2+}	Cd^{2+}	0.9		96.0	93.5	95.9

TABLE 4

Comparison of precipitation yields on MP50 (100—200 mesh) resin for binary metal ion systems in various matrices

Trace ions			$[M^{n+}]$ (mg l^{-1})	$[Mg^{2+}]$	Matrix[a]	Yield (%)		
A	B	C				A	B	C
Cu^{2+}	Cu^{2+}	Zn^{2+}	0.9	0.0	Deionized	86.9	91.2	92.3
Cd^{2+}	Zn^{2+}	Cd^{2+}	0.1			82.8	94.0	92.3
Cu^{2+}	Cu^{2+}	Zn^{2+}	0.9	45.0	Deionized	86.9	93.7	93.0
Cd^{2+}	Zn^{2+}	Cd^{2+}	0.1			90.5	94.5	93.7
Cu^{2+}	Cu^{2+}	Zn^{2+}	0.9	0.0	Tap	90.7	92.0	94.3
Cd^{2+}	Zn^{2+}	Cd^{2+}	0.1			96.8	93.6	94.7
Cu^{2+}	Cu^{2+}	Zn^{2+}	0.9	45.0	Tap	92.7	92.7	94.7
Cd^{2+}	Zn^{2+}	Cd^{2+}	0.1			98.8	94.2	95.3
Cu^{2+}	Cu^{2+}	Zn^{2+}	0.9	0.0	River	94.8	94.7	95.2
Cd^{2+}	Zn^{2+}	Cd^{2+}	0.1			98.7	95.5	95.6
Cu^{2+}	Cu^{2+}	Zn^{2+}	0.9	45.0	River	95.0	94.7	95.1
Cd^{2+}	Zn^{2+}	Cd^{2+}	0.1			98.9	95.7	95.5

[a]Deionized distilled water, Binghamton tap water, and Susquehanna River water.

ventional microporous (gel) type resins [9]. Intraparticle diffusion of highly charged species is, in general, restricted by their strong coulombic attraction to fixed sites attached to the resin backbone and, furthermore, the selectivity of aromatic matrix anion exchangers for hexacyanoferrate(II) is particularly high. These limitations of diffusion rate are in effect for both micro and macroporous resins. However, there is a tremendous disparity in effective surface areas. The macroporous resin has a much higher surface/volume ratio and intra-particle diffusion is a much less important factor here. The large pores allow the bulk solution to enter the pores of the resin particle even though the Donnan effect still excludes co-ions. Conventional, microporous resins exclude entry of significant amounts of bulk solution into the resin interior. Thus, intra-particle diffusion of counter ions is more likely to control exchange rate.

The effect of accompanying ions on the in situ precipitation of the target metal ions in the resin bed is important also. As the total counter-ion concentration of bulk solution increases, the precipitation and retention of target species on the resin becomes more quantitative. This is caused not only by mass action exchange of inert accompanying counter ions from solution against reactive ions from the resin but also by the ion-pairing tendency [8] of accompanying co-ions (here Mg^{2+}) with resinate hexacyanoferrate(II) ions. Both effects tend to draw more hexacyanoferrate(II) ions into solution where they can react with the target trace metal species (Cu^{2+}, Cd^{2+}, Zn^{2+}, etc.). Accompanying ions do not increase the yield for the microporous resins because of the overriding limitation of slow intra-bead diffusion of hexacyanoferrate(II) as mentioned above.

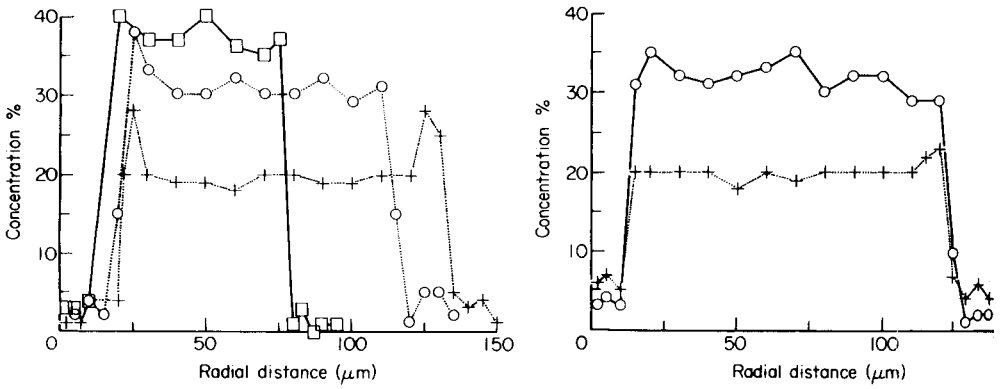

Fig. 1. Elemental distributions of metal traces precipitated in pores of resin particles as determined by electron probe microanalysis. Copper and zinc distributions over particle cross-section are measured as a function of radial distance. (○) Precipitation carried out with 1 ppm Cu^{2+}; particle boundaries occur at 15 μm and 120 μm. (○) Precipitation carried out with 1 ppm Cu^{2+} in the presence of 45 ppm Mg^{2+}; particle boundaries occur at 10 μm and 80 μm. (+) Precipitation carried out with 1 ppm Zn^{2+}; particle boundaries occurred at 20 μm and 135 μm.

In all cases the $[Fe(CN)_6]^{4-}$ form of AG MP-1 (100—200 mesh) was used. Metal concentrations are relative and given as percent of the concentrations found for similar scans over cross-sections of AG MP-50 (cation exchanger) particles in the pure Cu^{2+} or Zn^{2+} forms, respectively.

Fig. 2. Copper (○) and zinc (+) distributions over particle cross-section as a function of radial distance. Precipitation with solution containing 1 ppm each of Cu^{2+} and Zn^{2+}; particle boundaries occur at 10 μm and 130 μm. Metal concentrations are given relative as percent normalized with respect to pure AG MP-50 Cu^{2+} and Zn^{2+} forms.

Figures 1 and 2 depict electron microprobe scans across surfaces of macroporous anion-exchange particle cross-sections. They show that in each case the precipitate is formed uniformly throughout the interior pores of the particle. Comparison with analogous results seen in s.e.m. photomicrographs obtained earlier on microporous resin surfaces [8] suggests that precipitate is apparently forming over the entire surface of the large pores of the macroporous resin particles. Even in binary metal ion systems (Fig. 2) both ions are uniformly distributed throughout.

Macroporous cation-exchange resins behaved similarly to macroporous anion-exchange resins in coprecipitation experiments with all metal ions studied. This is noteworthy in view of the fact that only copper hexacyanoferrate(II) is precipitated at concentrations approaching its low intrinsic solubility limit when microporous resins are used. The ions Cd^{2+}, Zn^{2+}, Co^{2+}, and Ni^{2+} precipitate at much higher solution concentrations despite very similarly low solubility products [10]. With macroporous cation resin in the Cu^{2+} or Cd^{2+} form, it is possible to coprecipitate a number of sparingly soluble heavy metals as their hexacyanoferrate(II) salts at low concentrations. Table 5 reports results obtained with microporous and macroporous binary

TABLE 5

Precipitation of cadmium hexacyanoferrate(II) on Cd^{2+}—Mg^{2+}-loaded resins from deionized distilled water solutions

$\overline{X}_{Cd^{2+}}$	Yield (%)	$Fe(CN)_6^{4-}$ concentration (mg l^{-1})	Resin
0.07	95	1	Macroporous
0.11	97	1	Macroporous
0.01	<10	1	Microporous
0.10	<10	1	Microporous
0.01	<10	20	Microporous
0.10	76	20	Microporous

cation resins loaded with various mole fractions of Mg^{2+} and Cd^{2+}. Precipitation occurs quantitatively on low mole fraction Cd^{2+} macroporous resin with a typical feed solution 1 ppm in hexacyanoferrate(II). At similar mole fractions of Cd^{2+} loaded on microporous cation exchange resins, much higher concentrations of hexacyanoferrate(II) were necessary to effect in situ precipitation. As in the case of the anion exchangers, the better performance of macroporous resins can be explained by the much greater effective surface areas due to the larger pore volumes.

Conclusions

Traces of zinc(II) and cadmium(II) ions present in aqueous matrices can be collected/preconcentrated by in situ coprecipitation with copper(II) on cation exchangers in the Cu^{2+} and Cu^{2+}—Mg^{2+} forms. Even better results are obtained by in situ precipitation of $M_2^{II}Fe(CN)_6$ ($M^{II} = Cu^{2+}$, Zn^{2+}, Cd^{2+}, etc.) on small beds of macroporous anion-exchange resin in the hexacyanoferrate(II) form. Because Mg^{2+} forms a strong ion pair with hexacyanoferrate(II), addition of Mg^{2+} to samples further aids quantitative recovery. Thus, $\mu g\ l^{-1}$ concentrations of Zn^{2+}, Cd^{2+} (and according to preliminary studies, also Co^{2+}, Ni^{2+}, and Pb^{2+}) can be quantified following a convenient preconcentration step.

Slow intra-particle transport of hexacyanoferrate(II) apparently limits in situ ion-exchange precipitation of sparingly soluble hexacyanoferrates such as the magnesium salt on conventional, microporous anion-exchange resins. Very low precipitate yields are obtained. Film diffusion, otherwise known to prevail in ion-exchange processes under trace conditions, would be expected to afford rapid transport and high precipitate yields. The quantitative recoveries achieved and uniform $M_2Fe(CN)_6$ precipitate distribution on macroporous anion-exchange resins established by electron probe microdeterminations are, however, consistent with film diffusion control for the macroporous resins.

REFERENCES

1 G. E. Janauer, G. O. Ramseyer and J. W. Lin, Anal. Chim. Acta, 73 (1974) 311.
2 J. F. Pankow and G. E. Janauer, Anal. Chim. Acta, 69 (1974) 97.
3 J. F. Pankow, D. P. Leta, J. W. Lin, S. E. Ohl, W. P. Shum and G. E. Janauer, Sci. Tot. Environ., 7 (1977) 17.
4 J. W. Lin and G. E. Janauer, Anal. Chim. Acta, 79 (1975) 219.
5 W. E. Bernier and G. E. Janauer, in D. D. Hemphill (Ed.), Trace Substances in Environmental Health-X, University of Missouri, 1976, p. 323.
6 W. E. Bernier, Ph.D. Dissertation, S.U.NY, Binghamton, New York, 1979.
7 G. O. Ramseyer and G. E. Janauer, Anal. Chim. Acta, 77 (1975) 133.
8 W. E. Bernier and G. E. Janauer, J. Colloid Interface Sci., 70 (1979) 192.
9 Technical Bulletins giving specifications of Macroporous Resins, Rohm & Haas, Philadelphia, PA.
10 G. E. Janauer and W. E. Bernier, unpublished.
11 F. G. Helfferich, in J. A. Marinsky (Ed.), Ion Exchange, Vol. 1, M. Dekker, New York, Ch. 2, 1966.

Analytica Chimica Acta, 124 (1981) 373—380

CHOICE OF BORON SHIELD IN EPITHERMAL NEUTRON ACTIVATION DETERMINATIONS

HENRYK BEM[a] and DOUGLAS EARL RYAN*

Trace Analysis Research Centre, Chemistry Department, Dalhousie University, Halifax, Nova Scotia B3H 4J1 (Canada)

(Received 25th August 1980)

SUMMARY

Boron trioxide, boron nitride, boron carbide and elemental boron giving different boron surface densities have been used as neutron shields in epithermal neutron activation determinations. Boron ratios and advantage factors for 29 nuclides have been determined. A new expression of the advantage factor has been derived from statistics of radioactive decay viewpoint. A real improvement, in comparison with classical neutron activation methods, can be obtained for the determination of As, Br, Cd, I, Mo, Sb, Sn, Th, W and U by use of boron shields.

Neutron activation has frequently been applied to trace determinations in different materials. After activation with the whole reactor spectrum of neutrons, macro activities of ^{24}Na, ^{28}Al, ^{32}P or ^{38}Cl are produced, especially in biological materials, which may interfere with γ-activities of determined elements or increase their detection limits. The above mentioned nuclides and many others are produced from nuclides following the so-called $1/v$ law where their cross-section in (n, γ) reactions is inversely proportional to the neutron velocity. In contrast, a number of important nuclides (^{75}As, ^{197}Au, ^{111}Cd, ^{127}I, ^{100}Mo, ^{121}Sb, ^{123}Sb, ^{124}Sn, ^{238}U, etc.) strongly absorb neutrons of specific-resonance energies in the epithermal region (0.5 eV—1 MeV) having high values of ratio of the resonance integral, I_o to the thermal cross-section (2200 ms^{-1}), σ_o. Epithermal neutron activation (e.n.a.) with the use of a neutron filter to screen out the thermal portion of the neutron flux can in some cases enhance the desired activity relative to interfering nuclides. Both cadmium and boron (or boron compounds) are used as neutron shields. Cadmium is an effective shield for neutrons with kinetic energies less than 0.5 eV while the filter cutoff energy of neutrons for boron depends on the thickness of shield in the range up to 280 eV [1].

Boron or boron—cadmium shields with a different thickness of boron ranging up to 2.3 g cm^{-2} have been applied [2—10]. For multielement

---

[a]On leave from Institute of Applied Radiation Chemistry, Technical University, Lodz, Poland.

e.n.a., the choice of the shield with the proper surface density of boron is very important; several elements have strong resonance absorption peaks in the range to several eV [11, 12], and use of shields for which the cutoff energy is higher than resonance absorption energy of nuclides of interest can cause decrease of advantage factors.

Boron compounds giving shields of different surface densities were therefore studied to determine changes in advantage factors. A container was constructed which can be used in routine multielement determinations and the substances used to fill the container shield were boron oxide, boron nitride, boron carbide and boron.

EXPERIMENTAL

All elemental standards were prepared by evaporation of Alfa Atomic Absorption 1000 $\mu g\ ml^{-1}$ solutions or from analytical-grade reagents. The boron compounds used as shielding materials were obtained from Alfa Products-Ventron Corp. The containers for the boron shield were made by combining two different-sized polyethylene vials as shown in Fig. 1; the ring shown was cut from the stopper of the longer vial. These polyethylene vials are typical of the sizes used in irradiation facilities doing neutron activation. The cutoff energies were calculated for the boron shields on the basis of the plot given by Rossitto et al. [1].

The surface densities and corresponding cutoff energies were 65 mg cm^{-2} for B_2O_3 ($\approx$0.1 eV), 95 mg cm^{-2} for BN ($\approx$0.2 eV), 440 mg cm^{-2} for B_4C ($\approx$12 eV), and 650 mg cm^{-2} for B ($\approx$20 eV).

The shielding containers with sample vial were inserted into 7-dram polyethylene vials and irradiated in the outer site of the research reactor (SLOWPOKE) at a flux of 5×10^{11} n $cm^{-2}\ s^{-1}$. All samples except fluorine standards were irradiated for 10 min; fluorine standards were irradiated for 3 min. The outer polyethylene vials were opened after irradiation and sample vials were removed from shield containers. The decay period before measurement was 1 min (40 s for fluorine). Samples were counted for 10 min (3 min for fluorine) with a 60-cm^3 Canberra Ge(Li) detector (full width at half maximum

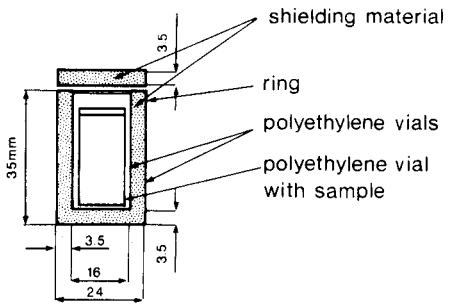

Fig. 1. Boron shield container.

of 1.88 keV at the 1.332 MeV photopeak of ^{60}Co, peak-to-Compton ratio 35:1, and an efficiency of 9.5%) in conjunction with a Tractor Northern TN-11 4096-channel pulse-height analyzer.

RESULTS AND DISCUSSION

The nuclear data and sensitivities of elements studied without boron shields are shown in Table 1. The sensitivities were determined under standard conditions for an outer site of the reactor. These values are 3—10 times

TABLE 1

Nuclear data and sensitivities of detected elements

Element	Nuclide measured	γ-ray used (keV)	Main resonance energies (eV)	$\frac{I_o}{\sigma}$	Sensitivity[a] (counts per μg)
Aluminium	^{28}Al	1779	2.7×10^4, 5×10^4, 10^5	1.05	1010
Antimony	^{122m}Sb	61	6.2, 16, 30	20.9	350
Antimony	^{122}Sb	564	6.2, 16, 30	20.9	105
Antimony	^{124}Sb	603	22, 50	54.9	23
Arsenic	^{76}As	559	47	9.5	217
Bromine	^{80}Br	617	35	18.5	1960
Bromine	^{82}Br	776	100	15	70
Cadmium	^{111m}Cd	245	90	19.7	68
Chlorine	^{38}Cl	2167	2.7×10^4	0.49	85
Cobalt	^{60m}Co	59	135		6640
Fluorine	^{20}F	1633	2.7×10^4	3.9	0.56[b]
Fluorine	^{19}O	197	F.n.r.[c]		0.36[b]
Gold	^{198}Au	412	5	15.7	1640
Indium	^{116m}In	417	1.5, 3.8, 9	13.6	133000
Iodine	^{128}I	443	38, 32, 45	23.7	4450
Iridium	^{194}Ir	329	1.3	12.6	1490
Manganese	^{56}Mn	847	340	1.04	13100
Mercury	^{199m}Hg	158	23	102	17.7
Molybdenum	^{101}Tc	307	370	21.2	134
Phosphorus	^{28}Al	1779	F.n.r.[c]		0.4
Samarium	^{153}Sm	103	8	15.1	27000
Samarium	^{155}Sm	104		4.2	175000
Silicon	^{28}Al	1779	F.n.r.[c]		1.34
Sodium	^{24}Na	1369	2800	0.66	125
Thorium	^{233}Th	86	22, 24	9.8	1215
Tin	^{125m}Sn	332	63	62	142
Tungsten	^{187}W	134	18	11.4	270
Uranium	^{239}U	74	6.8, 21, 36	97	25000
Vanadium	^{52}V	1434	4.2×10^3, 6.8×10^3	0.6	19100

[a]10 min irradiation, 1 min decay, and 10 min count. [b]3 min irradiation, 40 s decay, and 3 min count. [c]Fast neutrons reaction.

lower than values determined for inner site irradiation, because of differences in applied neutron flux and thermal-to-epithermal ratio in these sites [13]. The sensitivities for nuclides formed in fast neutron reactions are 12 times lower and correspond exactly to the ratio of fast neutron flux in inner and outer sites of the reactor. An outer reactor site was used in this study because it permits application of thick boron shields and larger sample sizes.

The vials with boron shields were slightly radioactive on return from the reactor because of impurities present. The concentrations of impurities forming γ-emitting isotopes in these compounds were determined and are given in Table 2. The radiation fields on the surfaces of the polyethylene vials are shown in Table 3. The elemental boron shield gives a somewhat higher radiation field which decreases slowly because of manganese and tungsten impurities. However, the radiation level allows safe handling of the samples after 10 min irradiations in a flux of 5×10^{11}n cm^{-2} s^{-1}. Results of determinations of boron ratios and advantage factors are summarized in Table 4.

The advantage factors [14] were calculated relative to sodium-24: $F = X_i/X$, where X_i denotes the boron ratio for sodium and X denotes the

TABLE 2

Concentrations (μg g^{-1}) of impurities in boron compounds used as boron shields

Impurities	B_2O_3	BN	B_4C	B_4C[a]	B
Na	6	6	14	216	<4
Cl	6.2	5.5	17	3.5	9.0
Al	<0.5	4.0	11	4.0	29.8
Mn	0.08	0.16	1.00	0.32	56.2
V	<0.01	0.10	0.21	1.0	0.5
W	<1.5	<1.5	<2.0	<2.0	85.8

[a]Ultra-pure.

TABLE 3

Radiation fields of γ-radiation on the surfaces of the polyethylene vials with boron shields

Time after irradiation	Dose rate (mR h^{-1})				
	B_2O_3	BN	B_4C	B_4C[a]	B
30 s	1.5	2.0	2.6	3.0	9.0
1 min	1.0	1.5	1.8	2.0	5.5
1 h	0.2	0.15	0.2	0.2	3.0
24 h	Background	Bkg.	Bkg.	Bkg.	0.2

[a]Ultra-pure.

boron ratio for the nuclide of interest. Boron ratios are calculated for individual nuclides by dividing the activity obtained without the shield by that observed with the shield.

It is evident from Table 4 that advantage factors reach high values for several nuclides, especially when boron carbide and boron are used as shields. The cutoff energies for boron oxide and boron nitride are low (≈0.1 eV and 0.2 eV, respectively) and advantage factors are low, except for nuclides such as $^{19}F(n,p)^{19}O$, $^{28}Si(n,p)$ ^{28}Al or $^{31}P(n,\alpha)$ ^{28}Al that are formed in fast neutron reactions. In such cases, the boron ratio is approximately equal to unity for all shields. It is noteworthy that advantage factors for nuclides with resonance energies of 1—20 eV (^{116m}In, ^{122}Sb, ^{122m}Sb, ^{153}Sm, ^{187}W, ^{198}Au) are higher for boron carbide than for boron (or at least equal within the limit of experimental error). This is particularly

TABLE 4

Boron ratios, X, and advantage factors, F, of detected elements

Element	Nuclide measured	B_2O_3		BN		B_4C		B	
		X	F	X	F	X	F	X	F
Aluminium	^{28}Al	11.6	1.2	16.1	1.5	143	1	162	1.1
Antimony	^{122m}Sb	2.6	5.4	2.9	8.6	5.7	25.5	7.6	23
Antimony	^{122}Sb	2.6	5.4	2.9	8.6	5.5	26	7.2	24
Antimony	^{124}Sb	2.5	5.6	2.7	9.3	4.5	32	5.5	32
Arsenic	^{76}As	3.9	3.6	4.7	5.3	6.7	22	7.4	23.5
Bromine	^{80}Br	4.6	3	5.4	4.6	8.8	16.5	9.2	19
Bromine	^{82}Br	3.3	4.2	5.0	5.0	5.3	27	5.7	30.5
Cadmium	^{111m}Cd	2.1	6.7	2.4	10.5	2.8	52	2.9	60
Chlorine	^{38}Cl	15	0.9	30.6	0.8	178	0.8	238	0.75
Cobalt	^{60m}Co	12.5	1.1	17.3	1.4	41.5	3.5	51.5	3.5
Fluorine	^{20}F	9.7	1.4	16.1	1.6	35.5	4.0	39	4.5
Fluorine	^{19}O	0.9	15.5	0.95	26	1.0	145	0.95	184
Gold	^{198}Au	4.6	3.0	5.0	5.0	14.5	10	20.5	8.5
Indium	^{116m}In	4.6	3.0	6.3	4.0	24.5	5.9	37.1	4.7
Iodine	^{128}I	3.1	4.5	3.6	6.9	5.1	29	6.1	29
Iridium	^{194}Ir	5.0	2.8	7.4	3.4	23	6.3	28	6.3
Manganese	^{56}Mn	12.5	1.1	21.7	1.2	77	1.9	89	2.0
Mercury	^{199m}Hg	1.55	9.0	1.8	14	1.9	76	2.05	85
Molybdenum	^{101}Tc	3.5	4.0	4.2	6.0	4.7	31	4.7	37
Phosphorus	^{28}Al	1.05	13.5	1.1	22.5	1.05	138	1.05	167
Samarium	^{153}Sm	4.0	3.5	5.7	4.4	13.0	11	17	10.3
Samarium	^{155}Sm	6.8	2.1	12	2.1	18.5	7.8	21	8.3
Silicon	^{28}Al	1.1	12.7	1.1	23	1.05	138	1.1	159
Sodium	^{24}Na	14	1	25	1	145	1	175	1
Thorium	^{233}Th	4.8	2.9	5.75	4.3	8.15	18	9.5	18.5
Tin	^{125m}Sn	1.85	7.6	2.0	12.5	2.7	53	3.25	54
Tungsten	^{187}W	4.7	3.0	5.9	4.2	9.4	15.5	14	12.5
Uranium	^{239}U	1.6	8.8	1.85	13.5	3.1	47	3.5	50
Vanadium	^{52}V	13.6	1.0	28	0.9	168	0.9	190	0.9

evident for tungsten which has a strong resonance peak at 18 eV. The elemental boron shield, with a cutoff energy of about 20 eV, absorbs most of the neutrons with energies in the resonance range in contrast to the boron carbide shield (cutoff energy $\approx$12 eV).

The defined advantage factor does not give a true picture of the potential of e.n.a. because it does not take into consideration the growth in error of radioactivity measurements when activities are depressed by factor X (i.e., when one may be working close to the detection limits). In usual radiometric practice, the activity, N, of the nuclide of interest is defined as the difference between total activity, N_s, and background, N_b

$$N = N_s - N_b \tag{1}$$

The variance of measurements equals $S_N^2 = S_{N_s}^2 + S_{N_b}^2$, where $S_{N_s}^2 = N_s$ and $S_{N_b}^2 = N_b$, so that the standard deviation is given by $S_N = (N_s + N_b)^{1/2}$. Substitution of N_s from eqn. (1) gives $S_N = (N + 2N_b)^{1/2}$. The relative standard deviation is then given by

$$\delta_N = S_N/N = [(1/N) + (2N_b/N^2)]^{1/2} \tag{2}$$

For e.n.a., an analogous expression for relative standard deviation, δ_{N_e}, is

$$\delta_{N_e} = [(1/N_e) + (2N_{be}/N_e^2)]^{1/2} \tag{3}$$

where N_e and N_{be} denote the activities of the nuclide of interest and background, respectively, when the shield is used.

Defining the real advantage factor, F_s in another way, as $F_s = \delta_N/\delta_{N_e}$, and substituting from eqns. (2) and (3) into this expression gives

$$F_s = [(1/N) + (2N_b/N^2)]^{1/2}/[(1/N_e) + (2N_{be}/N_e^2)]^{1/2} \tag{4}$$

From the definition of shield ratio, $X = N/N_e$ and $X_i = N_i/N_{ie}$, where N_i and N_{ie} denote the activities of interfering nuclide without and with shield. Replacement of N_e by N/X thus gives

$$F_s = [(1/N) + (2N_b/N^2)]^{1/2}/[(X/N) + (2X^2N_{be}/N^2)]^{1/2} \tag{5}$$

This expression can be used to calculate the real advantage factors. If it is assumed that the background in the region of the nuclide of interest is caused mainly by the Compton part of the spectrum of interfering nuclide, then $N_b = N_i$ and $N_{be} = N_{ie}$, where the latter is strictly valid for a cadmium shield or thin boron shields, when natural background and detector noise are still low in comparison with the background caused by the interfering nuclide. Insertion of these parameters along with $N_{ie} = N_i/X_i$ into eqn. (5) gives

$$F_s = [(1/N) + (2N_i/N^2)]^{1/2}/[(X/N) + (2X^2N_i/X_iN^2)]^{1/2} \tag{6}$$

In practice, e.n.a. is used when the activities of interfering nuclides are much higher than the activity of determined nuclide. In such cases, without neutron shield, the statistical fluctuations of background in the region of

interest made exact measurements impossible. If $N_i \gg N$, then $1/N \ll 2N_i/N^2$, and $1/N \ll 2N_iX^2/N^2X_i$, and it follows that $F_s = X_i^{1/2}/X$.

This equation gives the maximum values of advantage factors for particular elements because, in practice, the background level is lowered by a factor less than $- X_i$, especially in the low energy region. However, it may be used as a simple criterion of the utility of e.n.a. for particular elements. Advantage factors, F_s, calculated on the basis of this equation are shown in Table 5. These values are lower than those calculated from the simple expression and listed in Table 4 but it gives a truer picture of the advantage of e.n.a.

It is evident from Table 5 that there is a real improvement of determination ($F_s > 1$) by means of e.n.a. with boron shields for antimony (^{122}Sb, ^{122m}Sb or ^{124}Sb), arsenic (^{76}As), bromine (^{80}Br and ^{82}Br), cadmium (^{111m}Cd), iodine (^{128}I), mercury (^{199m}Hg), molybdenum (^{101}Tc), thorium (^{233}Th), tin

TABLE 5

The real advantage factors, F_s, for measured nuclides

Element	Nuclide measured	Shield			
		B_2O_3	BN	B_4C	B
Aluminium	^{28}Al	0.3	0.3	0.1	0.08
Antimony	^{122m}Sb	1.4	1.7	2.1	1.7
Antimony	^{122}Sb	1.4	1.7	2.2	1.8
Antimony	^{124}Sb	1.5	1.85	2.7	2.4
Arsenic	^{76}As	1.0	1.1	1.8	1.8
Bromine	^{80}Br	0.8	0.9	1.4	1.4
Bromine	^{82}Br	1.1	1.0	2.3	2.3
Cadmium	^{111m}Cd	1.8	2.1	4.3	4.6
Chlorine	^{38}Cl	0.25	0.2	0.1	0.05
Cobalt	^{60m}Co	0.3	0.3	0.3	0.25
Fluorine	^{20}F	0.4	0.3	0.35	0.35
Fluorine	^{19}O	4.0	5.0	12	14
Gold	^{198}Au	0.8	1.0	0.85	0.65
Indium	^{116m}In	0.8	0.8	0.5	0.35
Iodine	^{128}I	1.2	1.4	2.4	2.2
Iridium	^{194}Ir	0.75	0.7	0.6	0.5
Manganese	^{56}Mn	0.3	0.25	0.2	0.15
Mercury	^{199m}Hg	2.4	2.8	6.3	6.5
Molybdenum	^{101}Tc	1.0	1.2	2.5	2.8
Phosphorus	^{28}Al	3.5	4.5	11.5	12.5
Samarium	^{153}Sm	0.9	0.9	0.9	0.8
Samarium	^{155}Sm	0.6	0.4	0.65	0.6
Silicon	^{28}Al	3.4	4.4	11.5	12
Thorium	^{233}Th	0.8	0.9	1.5	1.4
Tin	^{125m}Sn	2.0	2.5	4.5	4.1
Tungsten	^{187}W	0.8	0.85	1.3	0.95
Uranium	^{239}U	2.3	2.7	3.9	3.8
Vanadium	^{52}V	0.3	0.2	0.07	0.07

(^{125m}Sn), tungsten (^{187}W) and uranium (^{239}U). For most of these nuclides, the boron carbide shield gives higher values of the advantage factor — F_s. There is no improvement for all shields for nuclides with low resonance energies (below 10 eV) such as gold (^{198}Au), indium (^{116m}In), iridium (^{194}Ir) and samarium (^{153}Sm). In these cases, a cadmium shield gives better results [6, 15]. Although an advantage factor may not imply any advantage, overall activity is reduced with a shield (with the activity of the interfering nuclide being reduced more if it has a higher boron ratio) and it is possible to count the activity when it would be impossible without shield because of high dead times.

It is evident from Table 5 that boron shields even thicker than 600 mg cm^{-2} may be successfully applied in neutron activation determinations by fast neutron reactions.

This work was supported by a grant from the Natural Sciences and Engineering Research Council of Canada.

REFERENCES

1 F. Rossitto, M. Terrani and S. Terrani, Nucl. Instrum. Methods, 103 (1972) 77.
2 Z. Randa, Radiochem. Radioanal. Lett., 24 (1976) 157.
3 A. G. Hanna and H. Al-Shahristani, J. Radioanal. Chem., 37 (1977) 581.
4 L. E. Wangen and E. S. Gladney, Anal. Chim. Acta, 96 (1978) 271.
5 J. D. Jones, P. B. Kaufman and W. L. Rigot, J. Radioanal. Chem., 50 (1979) 261.
6 J. Kucera, Radiochem. Radioanal. Lett., 38 (1979) 229.
7 E. S. Gladney and D. R. Perrin, Anal. Chem., 51 (1979) 2015.
8 E. S. Gladney and D. R. Perrin, Anal. Chem., 51 (1979) 2299.
9 W. D. Ehmann, J. Bruckner and D. M. McKown, J. Radioanal. Chem., 57 (1980) 491.
10 D. C. Stuart and D. E. Ryan, Can. J. Chem., in press.
11 R. Van der Linden, F. De Corte, P. Van den Winkel and J. Hoste, J. Radioanal. Chem., 11 (1972) 133 (Part 1); R. Van der Linden, F. De Corte and J. Hoste, J. Radioanal. Chem., 20 (1974) 695 (Part 2).
12 D. J. Hughes and R. B. Schwartz, Neutron Cross-Sections, USAEC Report BNL-325, 1958.
13 D. E. Ryan, D. C. Stuart and A. Chattopadhyay, Anal. Chim. Acta, 100 (1978) 87.
14 D. Brune and K. Jirlow, Nukleonik, 6 (1964) 242.
15 E. Steinnes, Epithermal Neutron Activation Analysis of Geological Material, in A. O. Brunfelt and E. Steinnes (Eds.), Activation Analysis in Geochemistry and Cosmochemistry, Universitetsforlaget, Oslo, 1971, pp. 113—128.

Analytica Chimica Acta, 124 (1981) 381—389

THERMAL LENSING SPECTROPHOTOMETRIC ANALYSIS WITH ION-PAIR SOLVENT EXTRACTION

KAZUHIKO MIYAISHI, TOTARO IMASAKA and NOBUHIKO ISHIBASHI*

Faculty of Engineering, Kyushu University, Hakozaki, Fukuoka 812 (Japan)

(Received 18th August 1980)

SUMMARY

Thermal lensing spectrophotometry is applied to the determination of iron(II) with 4,7-diphenyl-1,10-phenanthroline disulfonic acid in aqueous solution, and in chloroform by ion-pair extraction with trioctylmethylammonium chloride. A phase-sensitive detection system with digital processing was used, the optimum modulation frequency being 5—10 Hz. A baseline drift of 0.03% was achieved. In water, the enhancement factor (sensitivity relative to conventional spectrophotometry) was 70 at an exciting power of 800 mW, and 2×10^{-9} M iron(II) was determined. In chloroform 2×10^{-10} M iron(II)—complex could be detected, the enhancement factor being 1200.

Recently ultra-sensitive fluorimetry and spectrophotometry have been achieved by using lasers. Whereas the sensitivity of fluorimetry is proportional to the intensity of the exciting source, the sensitivity of spectrophotometry is usually independent of the source intensity, and source stability and the precision of the signal processing equipment are crucial. Direct application of lasers to absorption spectrophotometry thus normally provides no advantages of sensitivity. For the advantageous use of lasers, non-linear absorption in the laser cavity [1], and heat induced by a radiationless transition following laser excitation can be used for measuring small absorbances. Photoacoustic spectrophotometry has been shown to be especially useful for the measurement of non-transparent materials [2, 3]. Alternatively, a thermal lens formed in the sample solution by the laser beam can be used to measure very small absorbances.

In 1965 Gordon et al. [4] found build-up and decay transients when a liquid cell was placed within the resonator of a He—Ne laser, and indicated that the basic phenomenon is a lens effect in the liquid cell produced by local heating along a beam, leading to a change of refractive index in the vicinity of the laser beam. Because of its high sensitivity, several spectroscopic studies based on this thermal lens effect have been carried out. Swofford et al. [5] used the technique to measure vibrational overtones of organic molecules [5—7]. Colson et al. investigated the electronic excited states of trans-butadiene by two photon excitation in the gas phase [8, 9]. Since the thermal lens originates in a radiationless transition, absolute fluorescence quantum yields, e.g. of fluorescein and cresyl violet, can be

determined [10, 11]. However, very few analytical applications of the thermal lens effect have been reported.

When an intense laser beam is focussed into the sample solution, it is partially absorbed. The absorbed electronic energy is transferred to vibrational and rotational energy, and finally to translational energy through radiationless transitions. The local temperature rise in the sample, causes a transverse gradient of the refractive index. When a laser with a Gaussian beam profile is used as an exciting source, the focal length (f) of the induced thermal lens can be expressed by

$$f = \pi k w^2(1 + t_c/2t)/P_{abs}(dn/dT) \quad (1)$$

where $P_{abs} \equiv P_0(1 - 10^{-A})$ is the power absorbed by the sample; P_0 is the exciting laser power; A is absorbance of the sample and k its heat conductivity; w is the beam radius; (dn/dT) is the variation in refractive index with temperature; and $t_c \equiv w^2\rho C/4k$, where ρ is density and C is specific heat [4, 12]. A probe laser beam passing through this thermal lens is defocussed, and the probe laser intensity at the beam center decreases. The intensity variation can be expressed by

$$(I_0 - I_\infty)/I_\infty = -\theta + \theta^2/2 \quad (2)$$

where $\theta \equiv P_{abs}(dn/dT)/\lambda k$; λ is the wavelength of the second laser; I_0 and I_∞ are the probe beam intensities at the beam center without and with irradiation of the heating laser, respectively [12]. When θ and A are small, this equation becomes

$$(I_0 - I_\infty)/I_\infty \simeq -2.303\,(P_0/\lambda k)(dn/dT)A \equiv 2.303\,EA \quad (3)$$

where $E \equiv -(P_0/\lambda k)(dn/dT)$.

In conventional spectrophotometry the Beer—Lambert law can be written $(I_0 - I)/I_0 = 1 - 10^{-A} \simeq 2.303\,A$ (for $A \ll 1$), where I_0 and I are the intensities of the incident and transmitted light, respectively. Comparing this equation with eqn. (3), it is apparent that E is an enhancement factor [13]. For sensitive thermal lensing spectrophotometry, two factors should be taken into account: the exciting laser beam intensity, and the optical and physical parameters of the solvent. Since the sensitivity is proportional to the exciting intensity, the use of a laser with a high average power is indicated. The value of $(dn/dT)/k$ depends strongly on the solvent; for an organic solvent it is generally higher than for water. Therefore, the combination of solvent extraction and thermal lensing spectrophotometry is attractive.

The first analytical application of thermal lensing spectrophotometry was described by Dovichi and Harris [13]. In the determination of copper(II) with EDTA in a single-beam system, the enhancement factor was 0.22 in water and 2.0 in a mixed water—acetone solvent. In a previous study [14] it was demonstrated that iron(II) could be determined with 4,7-diphenyl-1,10-phenanthroline (bathophenanthroline) disulfonic acid in water, and that an enhancement factor of 7.3 could be achieved with an intense argon

ion laser (100 mW) and a dual-beam system, which permits the precise reading of the probe beam intensity under non-heating conditions [5].

In the study described here, the previous dual-beam system was improved by using a digital lock-in amplifier for the sensitive detection of the thermal lens signals, and the direct determination of iron(II) with bathophenanthroline disulfonic acid in water was shown to be feasible. Considerable improvement of the enhancement factor by using solvent extraction is also reported.

EXPERIMENTAL

Apparatus

Figure 1 shows a block diagram of the dual-beam thermal lensing system. An argon ion laser (NEC GLG 3200), whose output power can be adjusted to 0—800 mW is modulated by a chopper driven by a controlled-speed motor (4—100 Hz). The beam is reflected by a mirror (M_1) split by a quartz wedge, and detected by a photodiode (1). The probe beam, a He—Ne laser, is coaxially aligned with a heating laser beam by adjusting the quartz wedge beam splitter (BS_2). The absorption cell is a conventional 1-cm square quartz cell, whose position is adjusted to give the maximum thermal lens signal. The exciting beam is subsequently completely absorbed by a solution of potassium dichromate (0.02 g l^{-1}). The center part of the He—Ne laser beam passes through the filter and is detected by a photodiode (2). The photocurrent signal is amplified by a picoammeter (Keithley 417) or a BB 3421K operational amplifier. This analog signal is transformed by a voltage-to-frequency (V—F) converter (2 MHz), and counted by a NF PC-545A counter synchronously with the reference signal. The signal is typically accumulated for about 20 s, and recorded by a digital printer.

The waveforms of the signals in the detection system are shown in Fig. 2. When the chopper opens the exciting laser beam, the diameter of the probe laser beam expands. The intensity at the beam center decreases gradually to a constant value. The signal detected by the photodiode (1) is shifted by

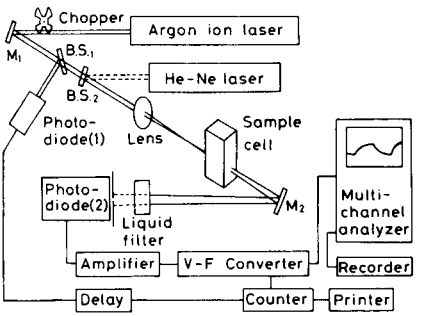

Fig. 1. Block diagram of the apparatus.

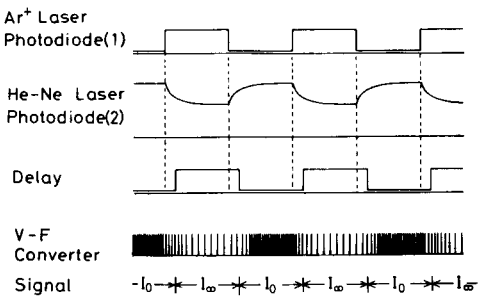

Fig. 2. Waveforms of signals in the detection system.

a delay circuit, and the delay time is adjusted so that the optimum thermal lens signal can be recorded. The measurement was carried out as follows. First, by using the DATA mode of the counter, the value of $(I_0—I_\infty)$ was counted ten times and recorded by the printer. Secondly, the intensity of I_∞ was measured by the NOISE mode ten times. The ratio $(I_0—I_\infty)/I_\infty$ and its standard deviation were then calculated.

For recording a transient thermal lens signal, a multichannel analyzer (IT 5300) was used instead of the counter. The time resolution of the present system (2.5 ms) was limited by the response time of the amplifier.

Reagents and procedures

The preparation of the samples in water has been reported in detail elsewhere [14]. Trioctylmethylammonium chloride (Capriquat; DOTITE) was dissolved (7×10^{-3} M) in chloroform and used as the extracting reagent. The sample solutions contained iron(II), bathophenanthroline disulfonic acid (disodium salt), acetate buffer, and hydroxylamine, and the iron(II)—bathophenanthroline disulfonate chelate formed was extracted into chloroform with Capriquat.

RESULTS

Spectrum

Bathophenanthroline disulfonic acid had no absorption band in the visible region, but on the addition of iron(II), the solution becomes dark red; the absorption maximum is at 533 nm. The molar absorptivity of the complex is 1.94×10^4 l mol^{-1} cm^{-1} at 514.5 nm, the wavelength of an intense line of the argon ion laser. When the complex was extracted into chloroform, very little variation was observed in the spectrum ($\epsilon_{514.5} = 1.7 \times 10^4$), indicating that the composition of the complex was not changed.

Signal processing apparatus

The limit of detection of thermal lensing spectrophotometry is controlled by the amplitude noise of the probe beam, as in the case of conventional spectrophotometry. Long-term drift was caused by temperature instability of the cavity resonator, and sufficient warm-up reduced this instability. Short-term fluctuations originated from discharge instability and beam ripple of the laser. From the specification of the He—Ne laser, long-term drift was ca. 5%, and short-term fluctuation ca. 3%. The exciting beam of the argon laser was blocked between the beam splitters BS_1 and BS_2, and the fluctuations of $(I_0—I_\infty)$ and I_∞ were measured. At 5 Hz, the values were 0.03% of the laser intensity, and were similar to the precision of a conventional spectrophotometer (ca. 0.1%). Thus, if an enhancement factor of 1000 could be achieved, an absorbance as low as 10^{-7} might be measurable. This result shows the value of the digital signal processing equipment.

Intensity of the exciting source and modulation frequency

The sensitivity of the thermal lens spectrophotometer depends on the power of the heating laser (eqn. 3). Excellent linear relationships were obtained when the output power of the argon laser was plotted against the enhancement factors for samples in water and in chloroform: maximum enhancement factors of 70 (at 700 mW) and 1200 (at 800 mW), were achieved (Fig. 3). Theoretical calculation predicts that enhancement factors of 166 and 6400 respectively can be achieved: the efficiency of the proposed system is 0.4 in water and 0.2 in chloroform. The observed enhancement factors depended critically on the alignment of the laser beams and on the position of the photodiode (2).

The signal response in thermal lensing spectrophotometry depends on the physical parameters of the solvent used. Therefore, to minimize flicker noise, the frequency of the heating beam should be adjustable. The frequency dependence of the signals is shown in Fig. 4. The signal intensity for aqueous solution increases as the frequency decreases and becomes almost constant at low frequency (5—10 Hz). The trends in water and chloroform are similar, but the thermal lens signal at 5 Hz in chloroform is much larger than that at 10 Hz. Background noise is almost independent of the solvent species and the modulation frequency at 200 mW, and seems to originate from the amplitude noise of the He—Ne laser. Fluctuations of $(I_0—I_\infty)$ and I_∞ were measured, and S/N ratios at various frequencies were calculated. As expected, the optimum frequency was ca. 5—10 Hz for aqueous solution, and ca. 5 Hz for chloroform. These frequencies are lower than the optimum frequencies (185 Hz) in photoacoustic spectrophotometry [15].

Figure 5 shows the transient signals of the thermal lens effect at the modulation frequency of 5 Hz in water and chloroform. In water, the signal is close to a square wave. The response of the samples in chloroform is slower than in water: this is consistent with the finding that an increase in the modulation frequency from 5 Hz to 10 Hz decreases the intensity of the signal in chloroform.

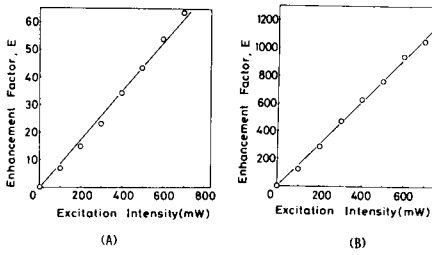

Fig. 3. Dependence of the enhancement factor on the output power of the argon laser: (A) in water; (B) in chloroform.

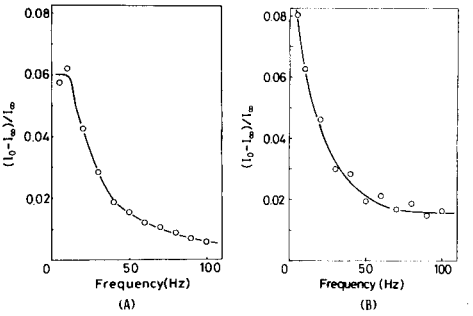

Fig. 4. Effect of the modulation frequency on the intensity of the thermal lens signal: (A) in water; (B) in chloroform.

Because of the slow response of the signal, the time constant of the measurement should be adjusted to ca. 20 s to improve the S/N ratio. As a result, the use of an analog lock-in amplifier may suffer from current leakage of the integrated circuit. The digital lock-in system used in this study has essentially no drift or current leakage and very suitable for the detection of the small thermal lens signal.

Detection limits

The dependence of the $(I_0—I_\infty)/I_\infty$ signal on the iron(II) concentration in water was found to be linear over the range 10^{-8}—10^{-7} M, the signal increasing from 0.02 to 0.115; the blank signal was 0.01. At higher concentrations the calibration graph deviated from linearity. However, the analytical curve with respect to $-\theta$ (eqn. 2) is proportional to the concentration, and this relation can be used even at high concentrations. A detection limit of 2×10^{-9} M iron(II) was achieved by using the exciting argon laser at 800 mW, the detection limit being defined as the concentration at which S/N = 2. The signal of the blank solution corresponds to that of a 1×10^{-8} M sample solution. However, the fluctuation of the blank is small, and the background can be subtracted from the sample signal. At the detection limit, the noise originated from the intensity fluctuation of the probe beam.

The solvent extraction system allowed iron(II) to be determined at even lower concentrations. A large background signal which seemed to arise from contaminating metals in the chloroform, made it difficult to detect iron(II) directly at low concentrations. Accordingly, to establish the detection limit and sensitivity, the iron(II)—bathophenanthroline disulfonate complex was formed at 10^{-3} M, extracted into chloroform, and then diluted stepwise with chloroform. The plot of $(I_0—I_\infty)/I_\infty$ signals against concentration was then straight down to 1×10^{-9} M because of the large enhancement effect of the thermal lens signal in the organic phase. In this case, the detection limit was 2×10^{-10} M. Ultra-trace determinations of iron(II) may thus be achieved by purification of the reagents and the solvent.

DISCUSSION

Analysis of transient signal

Irradiation with the heating argon laser beam induces expansion of the probe beam. This transient behavior of the thermal lens signal can be expressed by

$$I_t = I_0[1 - \theta(1 + t_c/2t)^{-1} + (1/2)\theta^2(1 + t_c/2t)^{-2}]^{-1} \quad (4)$$

where a characteristic time constant, $t_c = w^2\rho C/4k$ [12].
When $\theta \ll 1$, eqn. (4) becomes

$$I_t = I_0[1 - \theta(1 + t_c/2t)^{-1}]^{-1} \quad (5)$$

and rearrangement gives

$$I_t/(I_0—I_t) = (-t_c/2\theta)(1/t) - 1/\theta \quad (6)$$

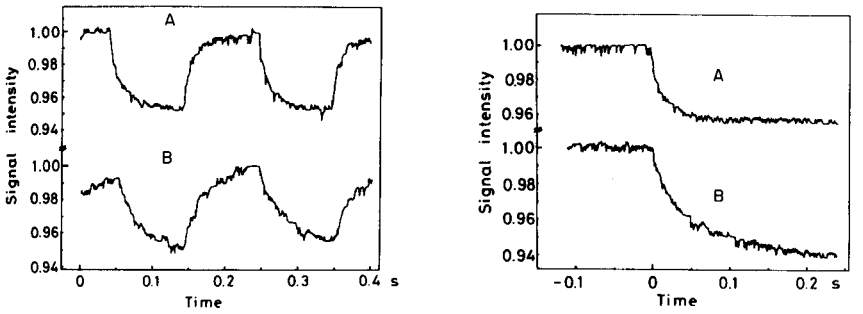

Fig. 5. Transient signals under irradiation by modulated (5 Hz) heating beam: (A) 1×10^{-7} M Fe(II) in water; (B) 2×10^{-8} M Fe(II) in chloroform.

Fig. 6. Signal transient of the thermal lens effect.

The observed transient signals of the samples in water and chloroform are shown in Fig. 6. The experimental values of $I_t(I_0 - I_t)$ plotted against $(1/t)$ gave straight lines in fair agreement with theoretical prediction though a slight deviation from the straight line was observed for the sample in water. This analysis gave values of t_c of 18 ms and 73 ms in water and chloroform, respectively. Values of t_c can also be calculated from the physical parameters of the solvents. The ratio of t_c in chloroform to t_c in water was calculated to be 1.2, which is much lower than the experimental value.

Solvent extraction system

A list of the enhancement factors calculated from variations in refractive index with temperature and heat conductivity [16] is shown in Table 1. Dielectric constants are also included. The Table shows that water is a very poor solvent for the thermal lens effect, and organic solvents generally have large enhancement factors. The use of solvent extraction in thermal lens spectrophotometry is therefore attractive. Non-polar solvents have substantial enhancement factors. A 1,10-phenanthroline derivative has been extracted into nitrobenzene as an ion pair with perchlorate [17, 18], but nitrobenzene provides a less favorable enhancement factor than other immiscible solvents. Extraction of the ion-pair of bathophenanthroline sulfonate with a high molecular weight quaternary ammonium ion was used in this study, so that chloroform could be used. Stability constants in an organic phase may be larger than those in water, thus facilitating determinations of ions at the ultra-trace level.

Application

Spectrophotometry based on the thermal lens effect with solvent extraction is more sensitive than conventional spectrophotometry by three orders of magnitude. The method thus has the potential to be used for determinations at ultra-trace levels. Furthermore, the transient signal of the thermal

TABLE 1

Calculated enhancement factors for an exciting power of 1 W[a]

Solvent	E	k ($\times 10^{-4}$ cal s^{-1} cm^{-1} K^{-1})	(dn/dT) ($\times 10^{-4}$)	ϵ
Pentane	7700	2.70	5.5	—
Hexane	6660	2.95	5.2	—
Heptane	6300	3.00	5.0	1.924
Cyclopentane	7060	3.05	5.7	—
Cyclohexane	6920	2.95	5.4	2.015
Methanol	3070	4.80	3.9	32.6
Ethanol	3680	4.00	3.9	24.30
Propanol	3930	3.75	3.9	20.1
Butanol	4070	3.62	3.9	17.8
Benzene	7010	3.45	6.4	2.284
Toluene	6650	3.18	5.6	2.4
Pyridine	5290	4.00	5.6	12.3
Nitrobenzene	4830	3.60	4.6	34.82
Aniline	4790	4.10	5.2	6.89
Tetralin	5240	3.10	4.3	—
Chloroform	8000	2.74	5.8	4.806
Carbon tetrachloride	8940	2.45	5.8	2.2
Dichloromethane	6070	3.3(?)	5.3	7.77
Xylene	5760	3.15	4.8	2.27
Carbon disulphide	8080	3.60	7.7	2.6
Acetone	4970	3.80	5.0	20.7
Diethyl ether	6820	3.10	5.6	—
Isooctane	7870	2.40	5.0	—
Water	207	14.6	0.8	78.54

[a] E, enhancement factor; k, heat conductivity; (dn/dT), variation in refractive index with temperature; ϵ, dielectric constant.

lens effect provides information on the physical parameters of the solvent. This sensitive method can also be applied to research in chemical physics, since it permits direct observation of radiationless transitions (cf. photoacoustic spectroscopy). The response time of the thermal lens signal can be made very fast by combining a pulsed laser heating beam with a photodetector having a fast rise time; the response of the photoacoustic effect is limited by the rise time of a microphone or a piezo-electric transducer. Radiationless transitions induced by molecular collisions, especially in the gas phase, interest many chemists [19, 20]: this method will make it possible to obtain information on such transitions.

This research was supported by a Grant-in-Aid for Scientific Research (Grant No. 547061) and for Environmental Science (Grant No. 503041) from the Ministry of Education.

REFERENCES

1 W. T. Hill III, R. A. Abreu, T. W. Hänsch and A. L. Schawlow, Opt. Commun., 32 (1980) 96.
2 A. C. Tam, C. K. N. Patel and R. J. Kerl, Opt. Lett., 4 (1979) 81.
3 S. Oda, T. Sawada, Y. Moriguchi and H. Kamada, Anal. Chem., 52 (1980) 650.
4 J. P. Gordon, R. C. C. Leite, R. S. Moore, S. P. S. Porto and J. R. Whinnery, J. Appl. Phys., 36 (1965) 3.
5 R. L. Swofford, M. E. Long and A. C. Albrecht, J. Chem. Phys., 65 (1976) 179.
6 R. L. Swofford, M. E. Long, M. S. Burberry and A. C. Albrecht, J. Chem. Phys., 66 (1977) 664.
7 M. S. Burberry, J. A. Morrell, A. C. Albrecht and R. L. Swofford, J. Chem. Phys., 70 (1979) 5522.
8 V. Vaida, R. E. Turner, J. L. Casey and S. D. Colson, Chem. Phys, Lett., 54 (1978) 25.
9 G. C. Nieman and S. D. Colson, J. Chem. Phys., 68 (1978) 2994.
10 J. H. Brannon and D. Magde, J. Phys. Chem., 82 (1978) 705.
11 J. H. Brannon and D. Magde, in A. H. Zewail (Ed.), Advances in Laser Chemistry, Springer-Verlag, New York, 1978.
12 C. Hu and J. R. Whinnery, Appl. Opt., 12 (1973) 72.
13 N. J. Dovichi and J. M. Harris, Anal. Chem., 51 (1979) 728.
14 T. Imasaka, K. Miyaishi and N. Ishibashi, Anal. Chim. Acta, 115 (1980) 407.
15 S. Oda, T. Sawada and H. Kamada, Anal. Chem., 50 (1978) 865.
16 D. Solimini, J. Appl. Phys., 37 (1966) 3314.
17 D. W. Margerum and C. V. Banks, Anal. Chem., 26 (1954) 200.
18 Y. Yamamoto, Jpn. Analyst, 21 (1972) 418.
19 T. Imasaka, T. Ogawa and N. Ishibashi, Chem. Phys., 45 (1980) 273.
20 V. M. Donnelly and F. Kaufman, J. Chem. Phys., 69 (1978) 1456.

Analytica Chimica Acta, 124 (1981) 391—401

IMPROVED SPECTROPHOTOMETRIC DETERMINATION OF CHROMIUM IN ANIMAL TISSUE DIGESTS WITH DIPHENYLCARBAZIDE

W. G. BRYSON and C. M. GOODALL*

Hugh Adam Cancer Biology Research Unit, Department of Surgery, University of Otago, P.O. Box 913, Dunedin (New Zealand)

(Received 10th August 1980)

SUMMARY

The usual spectrophotometric method for determination of chromium involves permanganate oxidation of chromium(III) to chromium(VI), followed by complex formation with diphenylcarbazide. When chromium-spiked liver tissue samples were mineralised by acid digestion, permanganate oxidation was not complete even on a boiling water-bath, but cerium(IV) oxidised chromium(III) completely at room temperature, the rate of oxidation being dependent on pH and matrix composition. Phosphate and iron(III) ions interfered. Precipitation of cerium(IV) by phosphate was avoided by addition of sulphuric acid. The coloured complex formed by iron(III) with diphenylcarbazide could be extracted with dichloromethane. High concentrations of some other metals and complexing agents interfered with the determination of chromium standards, but these substances did not occur in interfering concentrations in mouse liver digests. With the modified assay, standard chromium(III) and chromium(VI) solutions and mineralised liver samples containing standard additions of chromium(III) or chromium(VI) could be measured in the range 2.00×10^{-5}—4.00×10^{-3} g dm^{-3}. The four analytical curves were linear, and the superposition of standard and sample curves indicated that chromium was completely recovered from the tissue digestion step.

Chromium has widespread use in industry [1] and chronic exposure to chromium in the chromate-producing and chrome-pigment industries [2] has been associated with a high incidence of pulmonary carcinoma in employees. Short-term exposure to high levels of soluble chromates also causes ulcerations and other toxicity in man [3], whereas at much lower levels chromium is known to be an essential trace element in human nutrition [1]. An interest in understanding chromium metabolism in humans and animals, and the need to monitor chromium in the workplace and environment, has led to application of increasingly complex analytical techniques, including atomic absorption spectrometry (a.a.s.), polarography, stable isotope dilution g.c.—m.s. [4], electrothermal a.a.s. [5] and neutron activation [6]. Electron spin resonance spectroscopy serves to determine chromium(III) specifically in aqueous solutions but has inadequate sensitivity for environmental analyses [7]. The expensive and sophisticated apparatus needed for the most sensitive trace techniques is not widely available and not always necessary for study of chromium toxicity or carcinogenicity.

In this study the diphenylcarbazide spectrophotometric method was re-evaluated as an inexpensive and reasonably sensitive method for determinations of chromium, by application to aqueous chromium standards and to tissue digests. A simple wet acid digestion scheme was devised to give complete mineralisation of liver tissue samples containing standard chromium additions, without loss of chromium by the formation of volatile compounds. Chromium(III) in aqueous acid solution was oxidised to chromium(VI) with cerium(IV) at room temperature. Chromium(VI) then reacted quantitatively with diphenylcarbazide to form the well-known red-violet chromium—diphenylcarbazide complex (Cr—DPC) [8, 9], allowing sensitive spectrophotometric determination of chromium, at 546 nm.

Preliminary studies of reaction conditions involved measuring the oxidation rates using as oxidants either potassium permanganate as standardly recommended [10], or cerium(IV) as suggested by Blundy [11]. The effects of pH and of acid anions (nitrate and sulphate) on oxidation rates and Cr—DPC stability were also measured. Various ions or complexing agents that might interfere were studied, and simple procedures were found for removal of the principal interfering substances. Analytical parameters were determined in standard chromium(III) and chromium(VI) solutions and in digested mouse liver homogenates containing standard additions of chromium(III) or chromium(VI). The principal object was the development of an assay suitable for studying chromium levels in tissues of animals exposed to chromium doses during experimental treatment, rather than the measurement of the low naturally occurring levels.

EXPERIMENTAL

Apparatus and reagents

A Gilford 2400 spectrophotometer was used with 1-cm pathlength quartz (Suprasil) sample cells for absorbance measurements from 0.000 to 3.000. An instrumentation Laboratories Model 245 pH/mV electrometer with a glass combination pH electrode was used for pH measurements. Glassware was washed in 10% nitric acid and rinsed with distilled water.

Nitric acid (d = 1.42, BDH) was glass-distilled to remove chromium. Sulphuric acid (d = 1.84, May and Baker), chromium(III) chloride hexahydrate, ammonium hexanitratocerate, diphenylcarbazide (BDH), dichloromethane, potassium permanganate, potassium dichromate, and the reagents used in the interference studies were of analytical-reagent grade. Sodium azide was laboratory grade (BDH). Glass-distilled water was used for all dilutions.

The stock chromium(III) (0.1 g dm^{-3}) was prepared from $CrCl_3 \cdot 6H_2O$, and standardised by titration with disodium ethylenediamine tetraacetate [12]. Working standards were prepared by dilution of the stock solution, and adjusted to pH 2.0 with hydrochloric acid to prevent formation of precipitates due to hydrolysis, olation and related reactions [13]. A 0.05 mol dm^{-3}

cerium(IV) solution was prepared in 1.0 mol dm^{-3} nitric acid. A fresh diphenylcarbazide solution (0.5% w/v) was prepared weekly in acetone.

Procedures

Digestion of liver tissue. Mouse livers (NZC ♂) were freed of blood and homogenized (20% w/v) in distilled water. Seven Kjeldahl flasks, each containing 5 cm^3 of homogenate (representing 1 g of original liver), were spiked with chromium(III) standard solutions to give final concentrations (in the spectrophotometer) ranging from 2.00×10^{-5} to 4.00×10^{-3} g dm^{-3}. A duplicate set was prepared with chromium(VI) standards used in place of chromium(III). Additional flasks containing unspiked liver homogenate were used to correct for matrix effects and for trace levels of chromium naturally present. Flasks with reagents only were also taken through the digestion stage to ensure that reagents and glassware were freed of chromium contamination.

Samples were wet-ashed with concentrated nitric acid by simmering on microburners, to form clear yellow solutions. Progress was slowed by water formed during digestion, and this was removed by distillation, with loss of residual nitric acid. Before the first distillation step, concentrated sulphuric acid (0.05 cm^3) was added to prevent flasks from boiling dry; dry flasks overheated, with the risk of loss of volatile chromium compounds [14]. The distillation step was considered complete when residual organic matter was dehydrated (charred) by the re-concentrated sulphuric acid, forming a thick tarry suspension. Flasks were then cooled below 60°C, further concentrated nitric acid was added (1 cm^3 per cm^3 of residual material), and the above cycle was repeated. After several digestion cycles, the samples were completely mineralised; only a white ash remained suspended in a clear sulphuric acid solution. The digests were then transferred to 5-cm^3 volumetric flasks and diluted with distilled water.

Cerium(IV) oxidation and determination of standard chromium solutions. Standard chromium(III) aqueous solutions were oxidised by transferring 1 cm^3 of the appropriate standard to a test tube, adding 3.80 cm^3 of distilled water, 0.05 cm^3 of concentrated nitric acid, and 0.15 cm^3 of cerium(IV) solution, giving a final volume of 5 cm^3. Under these conditions, oxidation of chromium(III) to chromium(VI) was complete within 4 min. After oxidation, 0.01 cm^3 of sodium azide solution (5% w/v) was added to reduce excess of cerium(IV), the yellow colour of which would otherwise interfere. Diphenylcarbazide reagent (1 cm^3) was added and mixed in thoroughly. After 5 min to allow colour development, and within 45 min, the absorbance was measured at 546 nm. Although chromium(VI) standard solutions did not require oxidation they were treated in the same manner.

Oxidation and analysis of liver homogenate samples. Aliquots (1 cm^3) of digested liver homogenate samples were oxidised and analysed as for the standard aqueous chromium samples, except that nitric acid was replaced by concentrated sulphuric acid (0.10 cm^3) to prevent phosphate interference,

and after the addition of diphenylcarbazide, samples were extracted with 0.5 cm^3 of dichloromethane to remove iron(III) interference (see Results). To be effective, the sulphuric acid must be added before cerium(IV). Distilled water (3.75 cm^3) was added to give a final volume of 5.0 cm^3. Oxidation was slower when sulphuric acid was used, requiring one hour for completion. Complete mineralisation of liver samples was essential: undigested organic material can reduce cerium(IV). If solutions did fade significantly during the oxidation period, further cerium(IV) solution (0.15 cm^3) was added and the solutions were left for another hour.

Effects of other chemical species. The effects of some commonly encountered ions and complexing agents on the determination of an aqueous standard 1.00×10^{-3} g Cr(III) dm^{-3} solution were evaluated over the concentration range 10^{-5}—10^{-1} mol dm^{-3}.

Test samples were prepared by adding 1 cm^3 of chromium(III) solution, 1 cm^3 of the appropriate solution concentration of the substance being investigated, 2.80 cm^3 of distilled water, 0.05 cm^3 of concentrated nitric acid and 0.15 cm^3 of cerium(IV) solution to a stoppered test tube, giving a final volume of 5.0 cm^3. Samples were oxidised overnight (16 h). This was longer than necessary but was intended to show the effects of any slow reactions. Where a chemical species did interfere, its maximum tolerable concentration in the sample, defined as that concentration sufficient to cause a 5% change in absorbance, was determined.

RESULTS AND DISCUSSION

The usual procedure for oxidation of chromium(III) to chromium(VI) with potassium permanganate [10, 15—18] involves acidifying the aqueous sample, addition of permanganate and heating on a steam-bath for 20 min. If the permanganate colour fades, further permanganate is added, and oxidation is assumed complete when the pink colour persists, usually for 5 min. Sodium azide (5% w/v) is added dropwise to reduce permanganate, and then diphenylcarbazide is added.

Saltzman's [10] permanganate oxidation procedure was chosen for detailed study and optimisation, as it seemed the most easily adapted for the present purpose. When applied to mineralised liver samples containing standard chromium additions, results were low when compared with analyses of aqueous chromium(VI) standards. Another problem was that repeated sample analyses from the same tissue digest did not give reproducible results, even when 1-h oxidation periods were allowed. Longer oxidation times resulted in precipitation of manganese dioxide because permanganate is unstable in hot acidic solutions [19].

Blundy [11] reported that complete oxidation was not achieved with permanganate at low chromium(III) concentrations, and that oxidations with ammonium persulphate were unreliable, while cerium(IV) sulphate or ammonium hexanitratocerate in hot sulphuric acid solution did give complete

oxidation or good reproducibility. Fritz and Sickafooze [20], using a flow system with cerium(IV) in 0.75 mol dm^{-3} nitric acid, found chromium(III) oxidation to be complete in 2 min at room temperature. These two methods were adapted here for application to tissue digests.

Avoidance of azide side-reactions

Azide reduces chromium(VI) under certain conditions [18], causing low results for chromium. To establish if azide would reduce chromium(VI) under experimental conditions more extreme than those used in the present modified assay, a tenfold excess of azide (0.1 cm^3) was added to a chromium(VI) standard and placed in a steaming water bath for 30 min (instead of 5—10 s); no reduction in apparent chromium(VI) concentration was found. However, when this experiment was repeated in liver digests containing standard chromium(VI) additions, low chromium recoveries were obtained. Presumably azide reduces substances in the digest matrix which are re-oxidised by chromium(VI), so that less chromium—diphenylcarbazone complex is formed. Therefore, the diphenylcarbazide reagent must be added immediately when the azide has removed the cerium(IV) colour, to ensure that chromium(VI) does not react with chemicals that may have been reduced by azide. Also, the minimum quantity of azide required to reduce all cerium(IV) must be used, to minimise the excess of azide available to reduce other chemicals. A small excess of cerium(IV) would be preferable to excess of azide for general usage.

Development and stability of the chromium—diphenylcarbazide complex

Chromium(VI) reacts with diphenylcarbazide in acidic solution to form a characteristic red-violet complex [8—10]. Bose [8] reported an absorption maximum around 540—550 nm, and wavelengths in this range have been widely used. In the work reported here the wavelength calibration was checked with a holmium oxide filter and the broad peak with λ_{max} at 546 nm [21] was confirmed. The absorbance at 546 nm was 1% higher than at 540 nm.

The absorbance (at 546 nm) reached a maximum 2 min after diphenylcarbazide and chromium(VI) had been mixed. Because of the low pH conditions used here, the rate of colour fading with concentrated nitric acid or sulphuric acid was investigated. With concentrated nitric acid (0.05 cm^3), colour faded by 1% of the maximum value in 45 min, while with concentrated sulphuric acid (0.1 cm^3) colour faded by 1% at 30 min and 1.4% at 45 min. Keeping solutions in the dark did not slow down the rate of colour fading.

Determination of standard aqueous chromium(III) and chromium(VI) solutions

A plot of absorbance of standard chromium(III) solutions versus concentration (in the solution measured) was linear from 2.00×10^{-5} to 4.00×10^{-3} g dm^{-3}, with a coefficient of determination $r^2 = 0.9997$. The equation

of the line was: Absorbance = 0.003 + 844.2 (g Cr(III) dm^{-3}), obtained by a least-squares fit to the data. The upper limit of determination was 4.0×10^{-3} g Cr(III) dm^{-3} in 1-cm cells.

Analytical precision was determined at five different chromium(III) concentrations from standard solutions covering the linear range, being calculated as the percentage relative standard deviation from the mean absorbance of five determinations at each concentration. Chromium(III) concentrations of 2.00×10^{-3} g dm^{-3} and 8.00×10^{-4} g dm^{-3} gave precisions of ±0.5% and ±0.4%, respectively; at lower chromium(III) concentrations, the sample absorbances all agreed within the instrumental uncertainty of ±0.0005 absorbance units.

From the slope of the calibration plot for chromium(III), the spectrophotometric sensitivity [22] was 1.18×10^{-3} μg cm^{-2}, and the molar absorptivity for the chromium—diphenylcarbazide complex was calculated as 43500 dm^3 mol^{-1} cm^{-1}, in agreement with literature values when analytical-grade diphenylcarbazide was used [9, 10, 18, 21]. The purity of the diphenylcarbazide, concentration, and solvent used, as well as the pH, are all known to affect the apparent molar absorptivity values [8, 21].

Analysis of chromium(VI) standard solutions gave the least-squares equation: Absorbance = —0.005 + 835.8 (g Cr(VI) dm^{-3}), with $r^2 = 0.9992$. Comparison with the chromium(III) curve indicated complete oxidation to chromium(VI) at all concentrations tested.

Analysis of liver samples with added chromium

Curves of absorbance versus chromium concentrations were plotted after analysis of digested liver homogenate samples containing standard additions of chromium(III) or chromium(VI). Iron caused an interfering colour and was extracted with dichloromethane. Liver blanks, also extracted with dichloromethane, had low absorbances indicating natural liver chromium levels in these mice of about 0.5 μg Cr g^{-1} of liver, in accord with some literature estimates. Absorbances of liver blanks were always near the lower limit of detection, and to correct for natural trace chromium levels as well as any other minor contributions from unknown elements in the digestion matrix, the absorbances of spiked samples were corrected by subtraction of liver digest blanks treated in the same manner.

The calibration graph for chromium(III)-spiked liver samples was linear ($r^2 = 0.9980$) over the full concentration range 2.0×10^{-5}—4.0×10^{-3} g Cr(III) dm^{-3}, and was described by: Absorbance = —0.011 + 821.3 (g Cr(III) dm^{-3}). For liver spiked with chromium(VI), the graph was also linear ($r^2 = 0.9998$) and was described by: Absorbance = —0.012 + 835.2 (g Cr(VI) dm^{-3}). The slight negative intercepts were considered insignificant and are probably due to accumulation of very small losses during the digestions, and subsequent manipulations, particularly for tissue homogenates. The four analytical curves were so closely similar that for practical purposes they could be considered identical and collectively described by the equation: Absorbance = —0.004 + 836.6 (g Cr dm^{-3}).

This implied both chromium(III) and chromium(VI) in liver homogenate samples were fully recovered by the acid digestion procedure, that chromium(III) was completely oxidised, and that the chromium—diphenylcarbazide complex was retained in the aqueous phase during the extraction of iron.

Interferences

Compounds that did not interfere up to a concentration of 10^{-1} mol dm^{-3} in the sample are listed in Table 1. Nickel(II) interfered slightly at higher concentrations. Of the substances which interfered with the determination of a 1.0×10^{-3} g Cr(III) dm^{-3} sample (1 cm^3), only iron and phosphate are present in human liver in sufficient amounts to cause problems (Table 1).

Removal of phosphate interference. If sufficient phosphate was present in samples acidified with nitric acid, a colourless cerium(IV) phosphate precipitate formed during the oxidation stage and was not dissolved by sulphuric or nitric acid. Phosphate concentrations exceeding 2.0×10^{-3} mol dm^{-3} caused incomplete oxidation of chromium(III) by precipitating cerium(IV). This phosphate precipitate also interfered by dissolving and forming a stable pale yellow-orange complex when diphenylcarbazide was added; the colour was identical to that formed when diphenylcarbazide was added to cerium(IV)

TABLE 1

Effects of diverse ions

Substances tolerated at concentrations $\leq 10^{-1}$ mol dm^{-3}

NH_4NO_3	Na_2SO_4	$Mg(NO_3)_2 \cdot 6H_2O$	$CH_3COONa \cdot 3H_2O$
$NaClO_4$	KNO_3	$AlCl_3 \cdot 6H_2O$	$H_2NCH_2CH_2NH_2$
$NaNO_3$	KCl	$Ca(NO_3)_2 \cdot 4H_2O$	
NaCl		$Ni(NO_3)_2 \cdot 6H_2O$	
		$Zn(NO_3)_2 \cdot 3H_2O$	

Interfering substances

Compound	Maximum tolerable concentration (mol dm^{-3})	Element levels in human liver [23] (mol kg^{-1})	Compound	Maximum tolerable concentration (mol dm^{-3})
KI	4.0×10^{-5}	(I^-) 1.6×10^{-6}	Oxalate[a]	2.2×10^{-3}
$Na_3PO_4 \cdot 12H_2O$	2.0×10^{-3}	(PO_4^{3-}) 8×10^{-2}	Tartrate[a]	2.0×10^{-3}
			Citrate[a]	5.4×10^{-4}
$VO_2SO_4 \cdot 5H_2O$	1.4×10^{-4}	(V) $< 2.5 \times 10^{-7}$	Quinoline	
$MnSO_4 \cdot 4H_2O$	2.0×10^{-2}	(Mn) $2-3 \times 10^{-5}$	sulphate	6.0×10^{-3}
$Fe(NO_3)_3 \cdot 9H_2O$	7.8×10^{-4}	(Fe) 3.8×10^{-3}	EDTA[a]	7.8×10^{-4}
$Co(NO_3)_2 \cdot 6H_2O$	1.2×10^{-2}	(Co) $4-28 \times 10^{-7}$		
$Cu(NO_3)_2 \cdot 3H_2O$	6.0×10^{-2}	(Cu) $1-2 \times 10^{-4}$		

[a]Added as sodium salt.

alone in dilute nitric acid. Cerium(III) neither precipitated with phosphate nor reacted with diphenylcarbazide. Azide had no effect on the cerium(IV) phosphate.

The liver tissue digests regularly contained sufficient phosphate to give the above-mentioned interferences. However, addition of 0.10 cm^3 of concentrated sulphuric acid to samples before the cerium(IV) eliminated the interference; the sulphatocerate did not react with phosphate, and was reduced easily by azide, thus preventing reaction of cerium with diphenylcarbazide. Cerium—diphenylcarbazide complex could be completely extracted by dichloromethane.

A study with aqueous solutions showed that the amount of sulphuric acid required to prevent precipitate formation increased with the amount of phosphate. For example, in chromium(III) samples containing 10^{-1} mol dm^{-3} phosphate (or less), 0.2 cm^3 of concentrated sulphuric acid prevented precipitation but increased the time required for oxidation of chromium(III) to chromium(VI) to 8 h. Under the recommended experimental conditions, the times required for complete oxidation of chromium(III) when 0.05, 0.10, 0.15, 0.20 and 0.25 cm^3 of sulphuric acid was used, were 0.5, 1, 4, 8 and 16 h, respectively. Also the chromium—diphenylcarbazide complex was less stable at the lower pH values; absorbances decreased with time as shown in Table 2.

Iron interference. Digested liver samples, spiked with less than 4×10^{-4} g Cr dm^{-3}, became orange-pink after diphenylcarbazide addition, instead of the usual red-violet. Tests showed that this was due to formulation of the iron—diphenylcarbazide complex. Dichloromethane (0.5 cm^3, mixed vigorously for 60 s, and centrifuged for 1 min) extracted 99% of the iron complex, and varying amounts (0.05—0.2 cm^3) of sulphuric acid did not affect the extraction efficiency. Experiments with chromium(VI) solutions alone, showed that the chromium complex remained in the aqueous phase. The optimum time for extraction with dichloromethane was found to be 5 min

TABLE 2

Effect of sulphuric acid concentration on colour stability[a]
(Results are given as % of the absorbance measured at 2 min)

Time after mixing (min)	H_2SO_4 added (cm^3)				
	0.05	0.10	0.15	0.20	0.25
8	100	100	100	100	100
15	100	100	99.3	99.0	98.9
30	100	99.0	97.9	97.6	97.0
45	99.3	98.6	96.3	96.1	94.9
60	98.6	97.5	95.6	95.1	93.4

[a]A 1 cm^3 sample of 1.0×10^{-3} g Cr(III) dm^{-3} solution was treated as described in the procedure, except that the tabulated amount of concentrated H_2SO_4 was added before the oxidation step.

after addition of diphenylcarbazide. Chromium(VI) required 2 min to react completely, whereas the iron complex formed more slowly.

The maximum concentration of iron(III) that this extraction procedure corrected for was 1.0×10^{-2} mol Fe(III) dm^{-3} in a 1-cm^3 sample in the standard assay system. Doubling the amount of iron(III) or diphenylcarbazide resulted in the formation of a small amount of yellow precipitate. However, human liver contains 3.8×10^{-3} mol Fe(III) kg^{-1} [23], and because samples are usually diluted during preparation, the modified assay technique accommodates amounts of iron(III) 5—50 times the quantities likely to occur in animal tissue samples.

In nitric acid media, iron(III) reacted with azide, to form an orange-brown complex, which was not extracted by dichloromethane but was decomposed by sulphuric acid. Accordingly, under the modified assay conditions, there was no interference from this source.

In the analysis of samples (e.g., alloys) with high iron concentrations, it has been suggested [10, 15] that addition of phosphate prevents iron interference up to certain amounts. However, in the present experiments, addition of phosphate did not prevent the formation of the iron—diphenylcarbazide colour.

Experiments with chromium(VI) standard solutions containing iron(III) showed that the rate of fading of the chromium—diphenylcarbazide colour increased in the presence of the iron complex, even after the dichloromethane extraction and removal of the organic layer. The rate of fading also increased with increasing iron(III) concentration (Table 3).

TABLE 3

Effect of iron(III) on colour stability
(Tubes contained 1 cm^3 of 10^{-3} g Cr(VI) dm^{-3} solution with final concentrations of Fe(III) shown in 5 cm^3 of complete assay mixture as described in the procedure. All tubes were extracted with CH_2Cl_2 5 min after addition of diphenylcarbazide. Absorbances read at the times shown are expressed as percentage of original absorbance in control tubes at 17 min.)

Time (min)[a]	Control (0.0)	Fe(III) concentration (mol dm^{-3})		
		2.0×10^{-4}	1.0×10^{-3}	2.0×10^{-3}
17	100%(0.147)	97.3	94.6	94.6
22	100	95.2	91.8	91.8
31	99.3	93.9	88.4	87.1
45	98.6	91.2	86.4	82.3
60	94.5	88.4	80.3	77.6

[a]After addition of diphenylcarbazide.

Conclusions

Cerium(IV) oxidation of digested liver homogenate samples spiked with chromium(III) or chromium(VI), followed by complexation of chromium(VI) with diphenylcarbazide, allowed chromium to be determined over the concentration range 2.00×10^{-5}—4.00×10^{-3} g dm^{-3}. No losses of chromium occurred during the nitric acid digestion stage. Samples must be completely mineralised before oxidation. The fact that potassium permanganate incompletely oxidised chromium in digested tissue homogenate samples, and the formation of MnO_2 precipitates, made permanganate unsuitable as an oxidant in this type of assay. Cerium(IV) oxidised chromium(III) completely at room temperature in 1 h, provided that sulphuric acid was added first tc eliminate phosphate interference. Sufficient time must be allowed for complete chromium(III) oxidation, and absorbances must be determined before colour fading. Iron interference was removed by extraction of an iron—diphenylcarbazide complex with a small volume of dichloromethane. Interference studies showed that several other compounds could affect the final absorbance, but their concentrations were insignificant in liver tissue.

When unknown samples of variable chromium concentration have to be analysed, the modified assay allows the volume of sample taken to be selected within the range 0.05—4.75 cm^3. Separate dilution of the original sample is normally unnecessary.

We thank the Cancer Society of New Zealand, the Cancer Research Trust, and the University of Otago for financial support. We also thank Ms. Jacqui Smith and Mr. Len Wakefield for laboratory assistance.

REFERENCES

1 National Academy of Sciences, Chromium, Series on Medical and Biological Effect of Environmental Pollutants, Washington, DC, 1974, pp. 62 and 108.
2 F. W. Sunderman, Jr., Prev. Med., 5 (1976) 279.
3 M. Barborik, Ind. Med., 39 (1970) 45.
4 C. Veillon, W. R. Wolf and B. E. Guthrie, Anal. Chem., 51 (1979) 1022.
5 A. T. Zander, T. C. O'Haver and P. N. Keliher, Anal. Chem., 49 (1977) 838.
6 J. Versieck, J. Hoste, F. Barbier, H. Steyaert, J. Rudder and H. Michels, Clin. Chem., 24 (1978) 303.
7 W. G. Bryson, D. P. Hubbard, B. M. Peake and J. Simpson, Anal. Chim. Acta, 116 (1980) 353.
8 M. Bose, Anal. Chim. Acta, 10 (1954) 201, 209.
9 P. F. Urone, Anal. Chem., 27 (1955) 1354.
10 B. E. Saltzman, Anal. Chem., 24 (1952) 1016.
11 P. D. Blundy, Analyst, 83 (1958) 555.
12 A. I. Vogel, Quantitative Inorganic Analysis, 3rd edn., Longmans, London, 1962, p. 962.
13 C. L. Rollinson, in J. C. Bailar, H. J. Emeleus, R. S. Nyholm and A. D. Trotman—Dickenson (Eds.), Comprehensive Inorganic Chemistry, Vol. 3, 1st edn., Pergamon, Oxford, 1973, Ch. 36.
14 D. Shapcott, K. Knoury, P. Demers, J. Vobecky and J. Vobecky, Clin. Biochem., 10 (1977) 178.

15 C. Y. Gooderson and F. J. Salt, Lab. Pract. 17 (1968) 921.
16 F. J. Feldman, E. C. Knoblock and W. C. Purdy, Anal. Chim. Acta, 38 (1967) 489.
17 M. A. Schroeder, J. J. Balassa and W. H. Vinton, Jr., J. Nutr., 83 (1964) 239.
18 E. S. Pinkington and P. R. Smith, Anal. Chim. Acta, 39 (1967) 321.
19 F. A. Cotton and A. Wilkinson, Advanced Inorganic Chemistry, Wiley—Interscience, New York, 3rd edn., 1972, p. 845.
20 J. S. Fritz and J. P. Sickafooze, Talanta, 19 (1972) 1573.
21 T. L. Allen, Anal. Chem., 30 (1958) 447.
22 E. B. Sandell, Colorimetric Determination of Traces of Metals, Vol. 3, 3rd edn., Interscience, New York, 1959, p. 83.
23 G. V. Iyengar, W. E. Kollmer and H. J. M. Bowen, The Elemental Composition of Human Tissue and Body Fluids, Verlag Chemie, Weinheim, 1978.

Analytica Chimica Acta, 124 (1981) 403—408

A NOVEL METHOD FOR THE DIRECT DERIVATIZATION OF STRAIGHT-CHAIN ALIPHATIC CARBOXYLATES AFTER TRAPPING ON ANION-EXCHANGE RESIN

SHUGO MATSUNO, TAEKO MASAKI, MASATO TAZAKI, MAKOTO TAKAGI and KEIHEI UENO*

Department of Organic Synthesis, Faculty of Engineering, Kyushu University, Hakozaki, Higashi-ku, Fukuoka 812 (Japan)

(Received 1st September 1980)

SUMMARY

A novel procedure for the characterization of traces of lipophilic straight-chain aliphatic carboxylate ions in aqueous samples is described. The carboxylates are adsorbed on an Amberlyst A26 [Cl^-] resin column. The resin is then dried and suspended in methyl iodide at room temperature. A gas chromatographic analysis of the methyl iodide solution allows the determination of the carboxylates as their methyl esters. Full characterization of each carboxylate with an overall recovery over 84% from 1 ppm aqueous sample solutions is attained.

A novel procedure for the characterization and determination of traces of lipophilic anions such as alkylbenzenesulphonate ion or straight-chain aliphatic carboxylate ion in aqueous samples, has long been sought to attain more rapid analysis and more accurate results. Conventional procedures include lengthy steps for the concentration and derivatization of analytes for gas or liquid chromatographic determinations [1].

In this paper, a novel procedure is reported for the derivatization and gas chromatographic determination of traces of lipophilic straight-chain aliphatic carboxylate salts in aqueous samples. The principle of the method is based on concentration of the anions on a column of strongly basic anion-exchange resin, followed by the direct esterification of the trapped carboxylate ion with methyl iodide at room temperature on the resin matrix as illustrated in Fig. 1.

With this procedure, straight-chain aliphatic carboxylate salts (C_8—C_{16}) at ppm levels can be determined by gas chromatography in the form of their methyl esters.

EXPERIMENTAL

Reagents

Stock solutions of straight-chain carboxylate ions (1000 ppm). Weighed amounts of each carboxylic acid (C_8, C_{10}, C_{12}, C_{14} and C_{16}) were dissolved

in ethanol—water (2:1, v/v) to make 50-ml solutions. Aliquots of each solution were mixed and diluted with a slight excess of sodium hydroxide solution to the desired concentration before use.

Standard solution of methyl carboxylates for the gas chromatographic determination. Weighed amounts of each carboxylic acid (10 mg each) were dissolved in ether together with a weighed amount of undecanoic acid (C_{11} acid, 10 mg) which served as internal standard. The resulting solution was treated with an excess of ethereal solution of diazomethane. After esterification, ether was carefully evaporated and the residue was taken up in carbon tetrachloride to give 10 ml of solution. It was diluted to the desired concentration with methyl iodide before the gas chromatographic determination.

Strongly basic anion-exchange resin. The commercial grade Amberlyst A26 (chloride form, 40—60 mesh) was purified as follows: the resin was treated successively with methanol, acetone, methanolic 1 M hydrochloric acid, methanolic 1 M sodium hydroxide, 1 M sodium chloride solution and finally with deionized water until the effluent became free from chloride ion. The resulting resin was dried under vacuum (0.1 mmHg), and kept over silica gel.

The exchange capacity of the resin was calculated by determining chloride in the solution after exchange with sodium nitrate solution, or by determining the chlorine content after Schöniger combustion of the resin. The chloride ion was titrated potentiometrically with standard silver nitrate solution. The exchange capacity was 4.02 (mmol of anion per g of dry resin [Cl^-]) by nitrate exchange and 4.04 by Schöniger combustion. The water content of the resin as determined by the Karl Fischer method was 5.2% by weight.

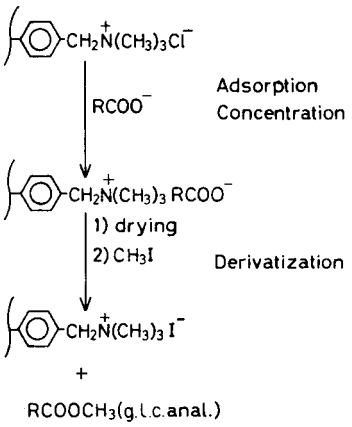

Fig. 1. Characterization of trace carboxylates in water.

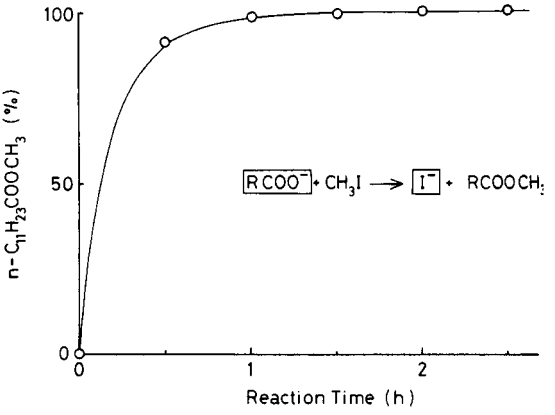

Fig. 2. Reaction of resin [n-$C_{11}H_{23}COO^-$] with methyl iodide. Resin, 60 mg (0.135 mmol n-$C_{11}H_{23}COO^-$); CH_3I, 1 ml (16 mmol); internal standard, n-$C_{18}H_{38}$.

Apparatus

Gas chromatograph. A Yanaco Model G-180 chromatograph equipped with f.i.d. was used. The column was a stainless steel tube (3 mm × 2 m) packed with Chromosorb W (AW-DMCS; 60—80 mesh) containing 5% silicone OV-3 (10% phenyl), which was treated with hexamethyldisilazane. The peak areas were calculated with the aid of a microprocessor (Shimadzu Chromatopack ElA). Conditions for chromatography were as follows: injection port temperature, 190°C; oven temperature, programmed at 7.5 K min^{-1} from 80 to 250°C.

Procedures

Derivatization after batchwise adsorption. A weighed amount of the dried resin (0.2 g) and 20 ml of the sample solution were placed in a 50-ml vial, and the mixture was shaken on a mechanical shaker at room temperature for a given period of time. The resin was then separated on a glass filter, successively washed with deionized water, methanol and acetone, and finally dried under vacuum (0.1 mmHg). An aliquot (ca. 30 mg) of the resin was placed in a 1-ml reaction vial with rubber septum (Reacti-vial, Pierce Chem. Co.), to which were added 60 μl of methyl iodide and 4—6 μl of a carbon tetrachloride solution of hexadecane as internal standard; the mixture was kept at room temperature for 2.5 h. An aliquot (1 μl) of the liquid phase was analysed for the methyl carboxylates on the temperature-programmed gas chromatograph.

Derivatization after column adsorption. A weighed amount of the dried resin (0.2 g) was packed in a glass tubing (4 mm i.d., 110 mm long) to make a resin column of about 1.3 ml, through which 100 ml of sample solution was passed at a space velocity of 11 h^{-1} with the aid of a constant flow microfeeding pump. After the adsorption, the resin column was washed successively with deionized water and methanol, and finally dried under vacuum (0.1 mmHg). The dried resin from the column was mixed thoroughly, and a weighed aliquot of the resin was treated with methyl iodide in a similar manner as above.

RESULTS AND DISCUSSION

Direct derivatization on the resin

It is well known that organic anions which exist as ion-pairs in aprotic medium behave as so-called "naked anions", and show high nucleophilic reactivity [2]. Similar reactivity can be expected for carboxylate ions trapped on anion-exchange sites of strongly basic anion-exchange resins, if the resin matrix is free of water. Thus, the carboxylate ion in the dry resin matrix would readily react with methyl iodide to form methyl carboxylate.

Figure 2 illustrates how easily the trapped carboxylate ion can be esterified with methyl iodide in the resin matrix. In this experiment, 60 mg of anion-exchange resin containing 26.9 mg (0.135 mmol) of dodecanoate (laurate)

was suspended in 1 ml (16 mmol) of methyl iodide at room temperature in a closed vessel. The reaction proceeded quantitatively in 1 h.

Various carboxylates were loaded on the anion-exchange resin, and treated with methyl iodide to give the methyl carboxylates, which were eventually analyzed by gas chromatography using hexadecane as internal standard. The reactions were 90—100% complete after 2.5 h at room temperature (Table 1). Thus, it was concluded that the carboxylate ion in the dried resin matrix reacts readily with methyl iodide to form methyl carboxylate almost quantitatively at ambient temperatures. In the recommended procedure, the duration of reaction with methyl iodide was set for 2.5 h to ensure complete conversion.

Gas chromatographic determination of carboxylic acids

Mixtures of carboxylate ions of various chain lengths were loaded on the anion-exchange resin and derivatized with methyl iodide. In this process, two internal standards were employed: undecanoate ion (C_{11} acid) was added to the aqueous mixture of carboxylate ions, and hexadecane was added to methyl iodide before derivatization. Undecanoic acid was chosen because it does not exist in nature; it was used to estimate the relative concentrations of the methyl carboxylates in the final reaction mixture. Hexadecane was used to estimate the absolute yield of each carboxylate ion after concentration and the reaction with methyl iodide.

In the case of batchwise adsorption, mixtures of carboxylate ions at 5 and 0.5 ppm levels were analyzed by temperature-programmed gas chromatography after conversion to their methyl esters. The results, summarized in Table 2, show that the recoveries of each carboxylate ion (C_{10}—C_{16} acids) are almost constant at 65—68% after 4 h shaking; thus, these anions can be determined at the 5 ppm level by batch adsorption with C_{11} acid as the internal standard. However, the recoveries were found to be so low (8%) at the 0.5 ppm level for the C_8—C_{16} acids that the batchwise process is of no practical value for the determination of their anions at this level.

TABLE 1

Reaction of adsorbed carboxylates with methyl iodide for 2.5 h at room temperature

$RCOO^-$		Exchange of resin by $RCOO^-$ (%)	Resin (mg)	$RCOOCH_3$ recovered (mg)	Reaction (%)
Dodecanoate	a)	100	63.5	28.9	100
	b)	42	56.7	16.8	103
	c)	10	105.9	7.7	91
Benzoate		100	60.7	19.2	92
Adipate		100	60.1	15.1	99
Oleate		100	62.5	33.3	87
Phenylacetate		100	60.9	24.9	89

TABLE 2

Recovery(%) of methyl carboxylates from aqueous solutions (5 ppm) of straight-chain saturated aliphatic carboxylate salts after batchwise adsorption

Chain length	Shaking time (h)			
	0.5	1	2	4
C_8	34	41	51	52
C_{10}	45	40	61	67
C_{12}	49	49	54	65
C_{14}	49	51	60	67
C_{16}	49	49	62	68

If advantage is taken of column adsorption with a large volume of sample solution, the recovery for carboxylate ions can be greatly improved. The results obtained in this way are summarized in Table 3. The recoveries of each acid at 5—0.1 ppm levels, based on the C_{11} acid, are around 100% with few exceptions. Thus, direct derivatization after column adsorption seems to be a very promising method for the determination of traces of straight-chain carboxylic acids.

The unusually low recovery of the C_8 acid at the 5 ppm level may be due to poor adsorption of this acid on the resin, because competition with the more lipophilic acids (C_{10} or higher homologues) would become severe during the column adsorption process. The use of finer resin ($\geq$ 60 mesh) removed this anomaly. There was some experimental indication that the highly lipophilic carboxylates are adsorbed preferentially at the periphery of the resin particle, thus interfering with the penetration of less lipophilic carboxylates into the vacant core of the resin.

The higher recovery of the C_8 acid at the 0.1 ppm level is a result of overlapping of its peak with an unknown impurity peak. At the 0.1 ppm level, even a trace of contaminant can give rise to a significant error. Accordingly, it is advisable to avoid organic materials in handling the resin when low concentrations of the carboxylates have to be determined. For example, washing the resin with acetone before drying may give rise to an unidentifiable peak from a condensation product of acetone. Therefore, the resin was washed with water followed by pure methanol after adsorption. The use of a glass column instead of a stainless steel column for gas chromatography is also advisable to improve reproducibility.

In the presently adopted column adsorption procedure, there is obviously an optimal concentration of carboxylate in a sample solution for effective trapping and derivatization. At the 1 ppm level, the recovered carboxylate amounts to 84% or more of the applied sample solution for all the carboxylic acids tested; if dodecanoic acid is taken as an internal standard, the recoveries of other carboxylic acids lie in the range 96—108% (Table 3). It is rather surprising that carboxylic acids at concentrations as low as 10^{-6} M can be effectively trapped and derivatized by such a simple procedure.

TABLE 3

Recovery of methyl carboxylates from aqueous solutions of straight-chain saturated aliphatic carboxylate salts after column adsorption

Chain length	Recovery (%) from 5 ppm solution		Recovery (%) from 1 ppm solution		Recovery (%) from 0.1 ppm solution	
	Based on $n\text{-}C_{16}H_{34}$	Based on C_{11} acid	Based on $n\text{-}C_{16}H_{34}$	Based on C_{11} acid	Based on $n\text{-}C_{16}H_{34}$	Based on C_{11} acid
C_8	30	40	87	100	89	157
C_{10}	71	96	94	108	65	115
C_{11}	74	100	87	100	56	100
C_{12}	75	100	84	97	57	101
C_{14}	78	105	88	101	61	108
C_{16}	81	109	84	96	55	97
Average	76 ± 7[a]		87 ± 8		64 ± 13	

[a] C_{10}–C_{16}.

Recently, the use of crown ethers for the activation of carboxylate anions in derivatization to their phenacyl esters has been reported [3, 4]. The method is most suitable for the derivatization of an isolated, free carboxylic acid or mixtures of free acids. The procedure developed here has a similar feature in the sense that the nucleophilic activation of the carboxylate anion is attained in an aprotic reaction medium, but has the advantage that selective concentration of lipophilic carboxylates from very dilute aqueous solutions is simultaneously achieved. Lipophilic neutral compounds which also become adsorbed on the resin along with the carboxylates are readily removed by washing with methanol. A quantitative study on the effects of such co-existing compounds, including inorganic anions present in high concentrations, is now in progress.

This work was partially supported by Grant-in-Aid for Environmental Science (1) 503028 from the Ministry of Education, Science and Culture.

REFERENCES

1 K. Blau and G. S. King (Eds.), Handbook of Derivatives for Chromatography, Heyden, London, 1978, Ch. 2 and 14.
2 C. M. Starks and C. Liotta, Phase Transfer Catalysis, Principles and Techniques, Academic Press, New York, 1978, Ch. 4.
3 H. D. Durst, M. Milano, E. J. Kihta, Jr., S. A. Connelly and E. Grushka, Anal. Chem., 47 (1975) 1797.
4 E. Grushka, H. D. Durst and E. J. Kihta, J. Chromatogr., 112 (1975) 673.

Analytica Chimica Acta, 124 (1981) 409—414

EVALUATION OF WASH SOLUTIONS AS A PRELIMINARY STEP FOR COPPER AND ZINC DETERMINATIONS IN HAIR

VINCENT D. MATTERA, Jr.,[a] VINCENT A. ARBIGE, Jr., STERLING A. TOMELLINI,[b] DAVID A. ERBE, MARK M. DOXTADER[c] and R. KEN FORCÉ*

Department of Chemistry, University of Rhode Island, Kingston, RI 02881 (U.S.A.)

(Received 11th August 1980)

SUMMARY

The ability of various washing agents to extract copper and zinc from human hair is evaluated. Nitric acid, sodium dodecyl sulfate (SDS), and SDS in combination with EDTA were evaluated for their metal-extracting capability as a function of time. It was found that a solution of 0.125% nitric acid removed 95% of the zinc in 30 h. Solutions of a mixture of 5% SDS and 1.25% EDTA exhibited increasing extraction capability with increasing pH. A solution of 5% SDS at pH 6.3 appears to extract very little zinc. An average of 78% of exogenously deposited copper was removed by a 30-min wash with a 5% SDS solution at pH 7.0.

Hair is known to be a depository for trace elements in the body [1—5]. Because hair is easy to collect and store, its utility as an indicator of the trace element status in the body has been the subject of recent investigations. Trace elements are thought to accumulate in hair at concentrations higher than in blood, serum, and urine [1]. Indeed, it has been suggested that trace element determinations in human hair samples have the potential of becoming an important diagnostic aid to complement routine trace element determinations in urine, blood, and serum.

A literature search reveals that the basic quantitative scheme is to collect about 0.3 g of hair from the scalp, wash it with a surfactant, rinse, dry the sample, and wet-ash using concentrated perchloric and nitric acids (1 + 1) prior to measurement by atomic absorption spectrometry.

The extent to which metal-to-hair binding can be explained in terms of metals which are of endogenous or exogenous origin is an unsettled question that is currently the subject of debate [1, 3, 6, 7]. Different investigators have reported successful attempts to remove surface-deposited, surface-bound, metals of exogenous origin [3]. Others [6, 7] have concluded that trace element determinations in human hair are too sensitive to preparative techniques to be a reliable source of clinically important information.

[a—c]Present addesses: (a) Brown University, Providence, RI 02912, U.S.A.; (b) Merck, Sharp & Dohme Research Laboratories, Rahway, NJ 07065, U.S.A., (c) University of Pennsylvania, Philadelphia, PA, U.S.A.

Both arguments implicate the wash treatment as the major contributor to the apparent uncertainty of results. The focal point of this investigation was to evaluate the effects of various washing agents on the concentrations of copper and zinc in human hair. The different washing agents employed in this study were ethylenediaminetetraacetic acid (EDTA), sodium dodecyl sulfate (SDS), nitric acid, and various combinations of EDTA and SDS.

EXPERIMENTAL

Reagents

Working standards for each element were prepared from 1000 μg ml^{-1} stock solutions according to the Perkin-Elmer Analytical Methods and Materials Manual. Standards with concentrations less than 20 μg ml^{-1} were prepared daily. Dilutions were made with distilled deionized water.

Reagent-grade nitric acid, perchloric acid, potassium dihydrogenphthalate buffers, disodium EDTA, sodium dodecyl sulfate (SDS) (J. T. Baker), and borax buffers (Mallinckrodt) showed no absorbance within the present detection limits for copper and zinc.

Apparatus

All wash experiments were prepared and monitored in a class 100 laminar-flow hood (EACI Model CME-100 Plus) to reduce the possibility of contamination from external sources. In addition, all digested samples were prepared in the same hood. All washes were carried out in 250-ml Nalgene beakers. Two Gordon-Keeble 0—5-ml variable pipets with disposable plastic tips were used for all wash solution extractions.

All acid digestions were performed in glass 30-ml flasks (cleaned as described below) in a custom-designed digestion chamber, designed to maintain a suitably clean atmosphere.

In addition to the 250-ml Nalgene beakers, specially designed polyethylene screens and a variety of polyethylene volumetric flasks (50—250 ml capacity) were also used. Ordinary laboratory glassware was used only where necessary, primarily in the digestion procedure. To alleviate problems of contamination, all glassware and plastics underwent a rigorous leaching procedure for not less than four days (usually a week) in 8 M nitric acid. All pipet tips were also leached in 8 M nitric acid.

Precautions taken in handling the hair included the use of plastic forceps and metal forceps wrapped with a 0.6 cm layer of parafilm.

Elements were quantified using Perkin-Elmer Model 303 and 403 atomic absorption spectrometers. A single slot burner was used for atomization. Hollow-cathode lamps, copper (Markson) and zinc (Perkin-Elmer), were adjusted to the currents suggested by the manufacturer. Slit settings and gas flow rates were also set as suggested by the manufacturer.

Procedures

A random sampling procedure was used to select samples. Approximately

30 g of human hair was obtained from a local barber shop and was cut into segments of 0.1—1 cm in length with stainless steel surgical scissors. The hair was then immersed in 3 l of deionized-distilled water and mixed for 30 min. A polyethylene screen was used to collect the hair from the mixing vat. Finally, it was dried for two days in an oven at 100°C under filtered nitrogen. Copper and zinc determinations on twenty-two accurately weighed hair samples of 0.35 g each yielded metal concentrations of 36 ± 4 and 208 ± 12 $\mu g\ g^{-1}$, respectively.

The digestion was a two-step procedure with HNO_3—$HClO_4$ performed in the sealed digestion chamber. Because of the necessity to maintain a tightly sealed environment from the beginning to end during digestion, the nitric and perchloric acids were added simultaneously. However, because nitric acid boils at a much lower temperature than perchloric acid (120.5°C as compared to 200°C [8]) and is depleted long before the perchloric acid, this procedure does parallel a two-step digestion. Tests on various ratios of $[HNO_3]/[HClO_4]$ indicated that 5 ml of a (1 + 1) composition yielded the best results on a 0.3-g hair sample.

The plan was to evaluate preparative wash procedures cited in the literature as to their effects on the exogenous and endogenous zinc and copper levels of hair. Of particular interest were the effects of dilute nitric acid solutions, dilute solutions of a common surfactant (SDS), dilute solutions of EDTA, and combined effects of SDS and EDTA. The procedure was the same for each wash experiment, with the wash solutions and exposure times being the only differences.

The basic experimental procedure was as follows. The wash solution (usually 2 l) in question was prepared, and a 200-ml aliquot was transferred to a 250-ml Nalgene beaker. The pH was adjusted to the desired level, and a 2-g hair sample was added. The wash was then stirred for the duration of the experiment. At predetermined intervals, 5-ml aliquots were withdrawn and transferred to appropriately labeled 10-ml polyethylene vials which were immediately sealed. Copper and zinc were then determined in these solutions.

After a wash experiment was completed, a portion of the washed hair was rinsed, dried, and digested, along with samples of untreated hair, and the copper and zinc in the digested samples were quantified.

In an attempt to evaluate the wash procedure further, its effectiveness in removing exogenously bound copper from hair samples was studied. For this experiment, twelve accurately weighed samples of 0.3 g each were used. Four were unexposed and eight were exposed to a 20 ppm copper(II) solution for 48 h. After this time, four of the eight exposed samples were rinsed with deionized-distilled water, dried and processed. The other four exposed samples were subjected to a 30-min wash treatment using a 5% (w/v) SDS solution before processing. The unexposed samples were not subjected to any treatment prior to digestion and quantification.

RESULTS AND DISCUSSION

Because nitric acid is a common reagent in the digestion of human hair, its utility as a washing agent would be suspect. It was known that at high concentration it would break down the hair protein structure, thereby releasing most or all bound metals. But at low concentrations it was postulated that nitric acid might remove only exogenous metals. From the results of the 0.0125% and 0.125% nitric acid wash experiments (Fig. 1) it is evident that this is not the case. At the higher concentration, a sharp and steady rise in the zinc concentration of the wash solution is observed over a period of the first 5 h. The concentration then begins to level off over the remainder of the 30-h period. At the lower concentration (0.0125%), the same trend is observed but with zinc concentration about one-third as high as that from the 0.125% nitric acid wash. The two most important trends observed were a sharp extraction curve over the first 5 h, followed by a steady, consistent extraction over the duration of the experiment. The only leveling-off that did occur was with 0.125% nitric acid, in the 25—30-h period when over 95% of the initial zinc had been removed.

Two conclusions that can be drawn from this experiment are that the initial leaching curve for both wash concentrations indicates no differentiation between endogenously and exogenously leached zinc and that the less concentrated nitric acid leaches metals at a slower rate.

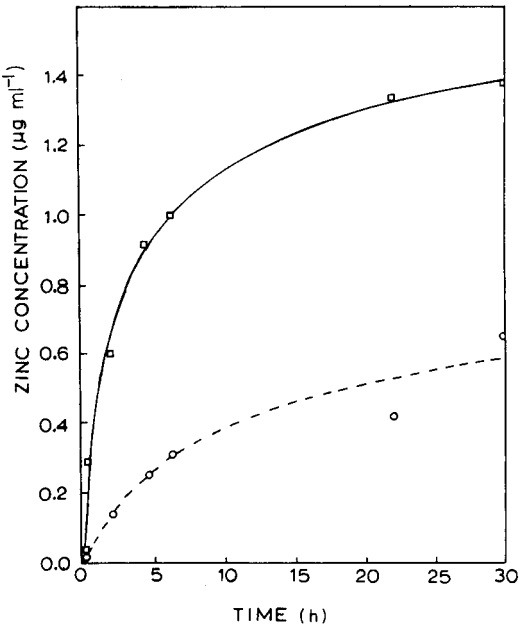

Fig. 1. Observed zinc concentration in nitric acid hair wash solutions as a function of time: (□) 0.125% HNO_3; (○) 0.0125% HNO_3.

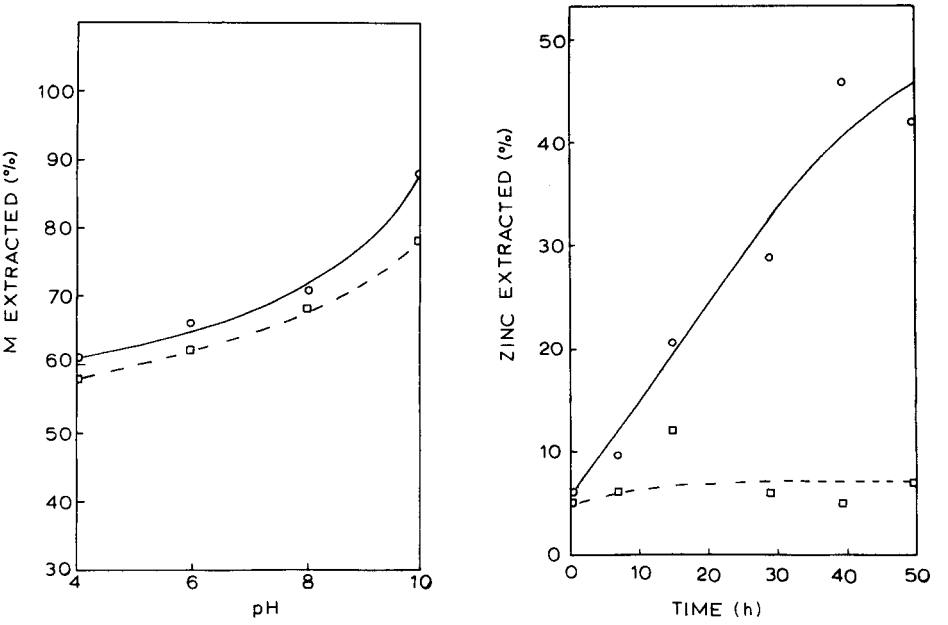

Fig. 2. Extraction capability of 5% SDS + 1.25% EDTA solutions for copper (□) and zinc (○) as a function of pH.

Fig. 3. Percentage of zinc extracted from hair at pH 6 as a function of time for different wash agents: (○) 5% SDS + 1.25% EDTA: (□) 5% SDS.

The results of the next series of experiments involving SDS and EDTA (Fig. 2) illustrate two interesting, though not unexpected, results. It is observed that a wash solution of 5% SDS and 1.25% EDTA varies in binding capacity with pH, with the greatest extracting ability occurring at the higher pH, as expected. But what is more important is that even at the lower pH values, over 60% of the available copper and zinc are leached from the hair samples.

Results obtained for SDS and EDTA used separately are shown in Fig. 3. The first observation that can be made is the initial leaching of about 5% of the total zinc in the first 30 min by both wash solutions. The SDS—EDTA solution then continues to extract zinc during the next 50 h, reaching 45% by the fiftieth hour. The extracting capacity of SDS becomes constant after the first initial rise. These results indicate that SDS is not capable of extracting significant amounts of endogenously bound zinc.

A summary of the zinc and copper concentration in hair from all experiments is given in Table 1, which illustrates the leaching potential of nitric acid. Even at a 0.0125% concentration, over 70% of the initial zinc is leached out. Similarly, a large percentage of both copper and zinc is leached out by the 5% SDS—1.25% EDTA wash. Even in the 5% SDS wash at pH 4, over 50% of the initial zinc is leached out. It is only in the 5% SDS wash at pH 6 that very little zinc was leached from the sample.

TABLE 1

Results for copper and zinc after exposure to various washing agents

Solution	Exposure time (h)	pH	Metal concentration ($\mu g\ g^{-1}$)			
			Copper[a]		Zinc[a]	
			Hair	Wash soln.[b]	Hair	Wash soln.[b]
0.125% HNO_3	30	1.7	14 ± 1[d]	≤0.1	6.7 ± 0.5[d]	1.5 ± 0.2[d]
0.0125% HNO_3	30	2.7	30 ± 4	<0.1	61 ± 7	0.7 ± 0.2
5% SDS	76	4.0	24 ± 1	<0.1	97 ± 10	0.73 ± 0.03
5% SDS	76	6.3	25 ± 4	0.1	208 ± 11	0.07 ± 0.03
5% SDS + 1.25% EDTA	76	4.0	15 ± 1	0.16 ± 0.08	81 ± 1	0.62 ± 0.03
5% SDS + 1.25% EDTA	76	6.0	14 ± 1	≤0.1[c]	72 ± 1	0.70 ± 0.03
5% SDS + 1.25% EDTA	76	8.0	12 ± 1	≤0.1[c]	61 ± 7	1.02 ± 0.03
5% SDS + 1.25% EDTA	76	10.0	8 ± 1	0.23 ± 0.03	26 ± 3	1.22 ± 0.03

[a]Mean values of metal content for untreated samples were copper = 36 ± 4 and zinc = 208 ± 12 $\mu g\ g^{-1}$. [b]Detection limits (S/N = 2) with the air—acetylene flame were found to be 0.1 $\mu g\ g^{-1}$ for copper and 0.05 $\mu g\ g^{-1}$ for zinc. [c]These low solution values may be due to copper adsorption onto the container walls. [d]The uncertainties quoted are all one standard deviation.

Four samples of hair that had been exposed to a 20 $\mu g\ ml^{-1}$ solution of copper(II) were washed with a 5% SDS solution at pH 7 to determine the effectiveness of SDS for removal of exogenously deposited copper. The four samples were found to contain 40 ± 6 μg Cu g^{-1} before exposure. After a 48-h exposure, the copper level was found to have increased to 62 ± 8 $\mu g\ g^{-1}$. After a 30-min wash with the 5% SDS at pH 7, the copper level was down to 45 ± 8 $\mu g\ g^{-1}$. This corresponds to a removal efficiency of 78% for surface-bound copper.

What is significant from all these experiments is that only a mild wash (5% SDS, for example) at or near physiological pH is acceptable for hair sample preparation.

This work was supported by the National Science Foundation (Grant #SPI-7905276). Part of this work was presented at the 1980 Pittsburgh Conference on Analytical Chemistry and Applied Spectroscopy, Atlantic City, NJ, March 1980.

REFERENCES

1 T. H. Maugh, Science, 202 (1978) 2171.
2 W. Harrison, J. P. Yurachek and C. A. Benson, Clin. Chim. Acta, 23 (1969) 83.
3 T. A. Hinners, W. J. Terill, J. L. Kent and A. V. Colucci, Environ. Health Persp., 8 (1974) 191.
4 L. Kopito and H. Shwachman, J. Lab. Clin. Med., 70 (1967) 326.
5 D. I. Hammer, J. F. Finklen, R. H. Hendricks, C. M. Shy and R. J. M. Horton, Am. J. Epidemiol., 93 (1971) 84.
6 D. C. Hilderbrand and D. H. White, Clin. Chem., 20 (1974) 148.
7 G. S. Assarian and D. Oberleas, Clin. Chem., 23 (1977) 1771.
8 Handbook of Chemistry and Physics, 49th edn., The Chemical Rubber Co., Cleveland, OH, 1968.

Analytica Chimica Acta, 124 (1981) 415—419

Short Communication

ACCURATE MEASUREMENT OF LONG CARBON-13 SPIN—SPIN RELAXATION TIMES BY THE SPIN-ECHO FOURIER TRANSFORM (SEFT) METHOD WITH CARBON DISULFIDE AS EXAMPLE

BERNARD TIFFON, BERNARD ANCIAN and JACQUES-EMILE DUBOIS*

Institut de Topologie et de Dynamique des Systèmes de l'Université Paris VII, associé au C.N.R.S., 1, rue Guy de la Brosse, 75005 Paris (France)

(Received 19th September 1980)

Summary. Experimental conditions for accurate measurement of long spin—spin relaxation times by the CPMG—SEFT method are described. The expected ^{13}C value, $T_2 = T_1 \simeq 44$ s for carbon disulfide, is reported for the first time and experimental diffusion behavior agrees with classical theory.

Ever since the work by Vold et al. [1], it has been widely recognized that the spin—spin relaxation time T_2 is the most difficult n.m.r. parameter to measure. However, knowledge of T_2 can yield information about the low frequency components in molecular motion [2]; hence T_2 measurements can be quite useful. Long T_2 measurements require multipulse refocussing sequences such as the Carr—Purcell—Meiboom—Gill (CPMG) sequence [3, 4]. Such methods can lead to serious instrumental difficulties [1, 5—7]. Since for non-viscous liquids in the absence of scalar relaxation or exchange processes, the rotating frame spin-lattice relaxation time $T_{1\rho}$ is equal to T_2 [2], the spin-locking experiment is a more convenient method for measuring T_2. However, in order to measure long $T_{1\rho}$ (i.e. lasting more than a few seconds), long spin-locking pulses are required, and high-resolution n.m.r. probes are not designed for this.

The purpose of this work is to determine the requirements for measuring long carbon-13 spin—spin relaxation times by the CPMG—SEFT method. Carbon disulfide has been chosen as an example, because the chemical shift anisotropy contribution to relaxation rates is negligible at room temperature and 25 MHz [8—10]. Although, in this case, the theory sets T_2 equal to T_1 in the extreme narrowing conditions [2], this has never been shown experimentally and the reported T_2 values are over 20% lower than those for T_1 [11, 12].

Experimental

Measurements were performed at 25.03 MHz and 25°C on a Jeol PFT-100 Fourier transform n.m.r. spectrometer fitted with a crossed-coil carbon-13

probe, an 8-kHz time-shared deuterium field-lock channel and a Jeol PG100 digital pulse programmer. The sample was contained in a 10 mm o.d. n.m.r. tube while the lock compound (DMSO-d_6) was located in a coaxial 4 mm o.d. n.m.r. tube held by a teflon plug, thereby avoiding gas—liquid CS_2 exchange. The sample was degassed by four freeze-pump-thaw cycles. T_2 measurements were run on a non-spinning sample tube [1] because rotation induces time-dependent field gradients whose dephasing effects are not, in any way, reversible by π pulses. Since, as pointed out by Allerhand [5], any kind of vibrations can also create such gradients, any gas flow temperature control must be avoided.

Nevertheless, as expected, rotation and vibration of the sample tube do not affect the T_1 values which can always be measured on a spinning as well as on a non-spinning sample. In order to minimize the cumulative effects of small pulse imperfections, particularly prejudicial to the CPMG experiment [1, 6, 7], the π pulse was always determined by the null method on the actual sample. A 500-Hz spectral width (single-phase detection) was always used, and the frequency offset ranged from 30 to 250 Hz, down- and up-field; 8K points were acquired and Fourier-transformed with a 1.2-Hz sensitivity enhancement exponential window. T_1 values were measured by the Inversion-Recovery method, and T_2 values by the CPMG sequence.

The time interval τ between the $\pi/2$ pulse and the first π pulse ranged from 25 to 500 ms; no sample heating was observed, even at the highest π pulse repetition rate $(2\tau)^{-1}$ used. The software package was modified to incorporate an automatic measurement routine where the number of π pulses of a CPMG sequence is automatically varied (up to 20 different values) and the last even half-echo is digitalized; 2—12 transients were averaged with a sequence repetition time equal to 250 s (ca. $5T_1$).

Three types of experiments (A, B and C) were run under the appropriate operating conditions (sample, π pulse width, field inhomogeneity T_2^*, field stability) for each series (Table 1).

TABLE 1

Operating conditions

	A	B	C
	Natural CS_2	20% ^{13}C-enriched CS_2	20% ^{13}C-enriched CS_2
π pulse (μs)	104 ± 2	104 ± 2	61 ± 1
T_2^*(ms)	80	115	160
Number of transients	10	2	2
Field stability	Unrevised	Unrevised	Revised
T_1 (s)	44.1 ± 1	43.5 ± 1	44.1 ± 1
T_2 (s)	See text	See text	43.6 ± 1

Results and discussion

Relaxation times T_1 and T_2 were computed on-line using both peak heights and peak areas with either a two- or a three-parameter exponential curve-fitting routine. In either case, there was fairly good agreement and reproducibility between calculated T_1 values (ca. ± 3%).

In contrast, cumulative effects of imperfect π pulses generate a CPMG baseline drift which grows exponentially to a value M_b with a time constant T_2 [1, 6, 7]; then the magnetization $M(2n\tau)$ to the n^{th} echo is given in the absence of diffusion [7] by

$$M(2n\tau) = M_s \exp(-2n\tau/T_2) + M_b [1 - \exp(-2n\tau/T_2)] \quad (1)$$

M_s, which is independent of the echo number, depends on the equilibrium longitudinal magnetization of the spin system, on relaxation times T_1 and T_2, on the interval time τ, and on the π pulse imperfections. Rearrangement of eqn. (1) to

$$M(2n\tau) = (M_s - M_b) \exp(-2n\tau/T_2) + M_b \quad (2)$$

shows that the magnetization of the n^{th} echo is an exponential function dependent on three parameters (M_b, $M_s - M_b$, T_2). Thus, to obtain T_2 values, a three-parameter exponential curve-fitting of experimental data is required, and values of $2n\tau$ must go up to ca. $5T_2$ to ensure the accuracy of the M_b parameter.

Moreover, as shown for the measurements under the C conditions (Fig. 1), T_2 values obtained from peak areas differ largely from those obtained from peak heights. Indeed, careful observation of the shape of echoes inside a CPMG sequence shows that the echo linewidth narrows when the echo number increases: for example, in the C series, the original linewidth is 2 Hz, whereas for τ = 25 ms, the line-widths of the echoes numbered 40, 700, and 4000 are, respectively, 1.9, 1.7 and 1.5 Hz. In addition, over a given time period, $2n\tau$, the echo linewidth decreases when τ increases: for example, in

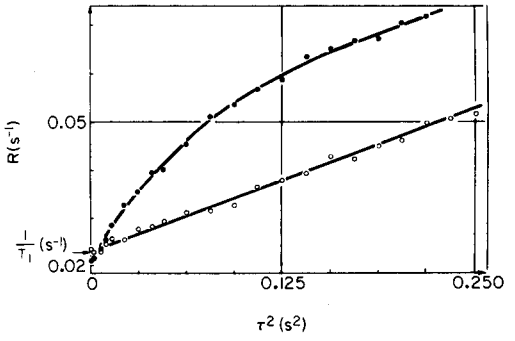

Fig. 1. Relation of the apparent relaxation rate R vs. the square of the π pulse repetition time τ^2. (○) peak heights; (●) peak areas.

the C series, for $\tau = 250$ ms, the linewidths of the echoes numbered 4, 70 and 400 are, respectively, 1.7, 1.3 and 1.1 Hz.

This observation can be qualitatively explained. It is likely that the field gradient G over the sample is not constant, so that the irreversible dephasing caused by diffusion is not the same for all the isochromats. The magnetization arising from spins moving in high field gradients would be destroyed faster than that from spins moving in low field gradients. Thus, the peak area would decay faster than the peak height and the former would lead to a greater apparent relaxation rate than the latter (Fig. 1). Indeed, it seems that the peak area decay should not be exponential.

Because of molecular diffusion, the rate of decay of spin echoes in a CPMG experiment on an ordinary liquid characterized by a single transverse relaxation time T_2 is given by

$$R = T_2^{-1} + 1/3D\gamma^2G^2\tau^2 \tag{3}$$

where D is the self-diffusion coefficient of the liquid, γ the ^{13}C magnetogyric ratio, and G the magnitude of the field gradient assumed to be constant over the sample [3, 13]. As noted above, G is certainly not constant in a high resolution experiment and G^2 must be replaced by an appropriate average $<G^2>$. The decay of the spin echo train is still given, with a very good approximation, by eqn. (2) in which the relaxation rate R is equal to $T_2^{-1} + 1/3D\gamma^2 <G^2>\tau^2$ instead of to T_2^{-1}. Thus, the plot of R vs. τ^2 should be a straight line whose intercept gives T_2^{-1}.

The first set of measurements, A, performed on a spectroscopic-grade carbon disulfide sample gives $T_1 = 44.1 \pm 1$ s, in close agreement with previous results [8, 11, 12]. However, there is no linear dependence of R vs. τ^2 within the entire τ scale when T_2 is measured. R would seem to be a linear function of τ for $\tau < T_2^*$ which extrapolates to approximately T_1 when $\tau = 0$, and a linear function of τ^2 when $\tau > T_2^*$. Similar results have been previously found by Haeberlen et al. [12] on carbon disulfide and by Vold et al. [1] on benzene.

It has been suggested that coherent radiation damping may be responsible for such behavior, particularly in the range $\tau < T_2^*$ [14]. In order to check this assertion, a second experiment, B, with a better field homogeneity ($T_2^* \simeq 115$ ms) was carried out on a 20% ^{13}C-enriched compound, thereby giving greater echo amplitude (Table 1). Here, T_1 is still 43.5 ± 1 s, and the CPMG study yields results similar to the previous ones, showing that radiation damping does not affect the spin echo train.

This indicates that it is instrumental artefacts which preclude the obtainment of reliable data. Therefore, the current stabilizer chopper of the magnetic field stabilization system was changed, and the amplifier of the pulse power unit stability was checked. Results obtained from the C series of experiments after this revision (Table 1) were completely different from those for A and B. T_1 is still 44.1 ± 1 s, but now the plot of the apparent transversal relaxation rate R vs. τ^2 is linear

$$R_2 = 0.1144\,\tau^2 + 0.0229 \qquad (4)$$

when R_2 is expressed in s^{-1} and τ in s (Fig. 1). The intercept of the plot gives T_2 = 43.6 s, which, with extremely good accuracy, is equal to T_1. Moreover, given $D = 4.1 \times 10^{-5}$ cm^2 s^{-1} [15] and $T_2^* = 160$ ms (Table 1), the slope of eqn. (4) yields a sample dimension, $d \approx 0.15$ cm, qualitatively in agreement with the actual annulus width (0.25 cm).

Conclusions

This work describes the stringent experimental conditions required to measure long spin—spin relaxation times by the CPMG—SEFT method with an accuracy as well as a reproducibility of ±3%. It is to be noted that even a good time field stability for chemical shift studies is insufficient for T_2 measurements: the best time field stability is needed to ensure the theoretical linear dependence of R vs. τ^2. On this ground, it can be inferred that previous results which fail to satisfy such a relation for $\tau < T_2^*$ [1, 12] arise from instrumental effects.

It is a pleasure to thank Dr. J. P. Lemaire and Jeol Europe S.A. for their help in software modifications.

REFERENCES

1 R. L. Vold, R. R. Vold and H. E. Simon, J. Magn. Reson., 11 (1973) 283.
2 T. C. Farrar and E. D. Becker, Pulse and Fourier Transform NMR, Academic Press, New York, 1971.
3 H. Y. Carr and E. M. Purcell, Phys. Rev., 94 (1954) 630.
4 S. Meiboom and D. Gill, Rev. Sci. Instrum., 29 (1958) 688.
5 A. Allerhand, Rev. Sci. Instrum., 41 (1970) 269.
6 D. G. Hughes and G. Lindblom, J. Magn. Reson., 13 (1974) 142; 26 (1976) 464.
7 D. G. Hughes, J. Magn. Reson., 26 (1977) 481.
8 J. R. Lyerla, D. M. Grant and R. D. Bertrand, J. Phys. Chem., 75 (1971) 3967.
9 H. Jaeckle, U. Haeberlen and D. Schweitzer, J. Magn. Reson., 4 (1971) 198.
10 H. W. Spiess. D. Schweitzer, U. Haeberlen and K. H. Hausser, J. Magn. Reson., 5 (1971) 101.
11 R. R. Shoup and D. L. van der Hart, J. Am. Chem. Soc., 93 (1971) 2053.
12 U. Haeberlen, H. W. Spiess and D. Schweitzer, J. Magn. Reson., 6 (1972) 39.
13 H. C. Torrey, Phys. Rev., 104 (1956) 563.
14 A. Abragam. Les Principes du Magnétisme Nucléaire, Presses Universitaires de France, Paris. 1961, Ch. III.
15 Landolt-Bornstein, Zahlenwerten und Fonktionen, Springer Verlag, Berlin, Vol. III/5. 1963, 6th edn.

Analytica Chimica Acta, 124 (1981) 421—425

Short Communication

SEPARATION OF YTTRIUM AND RARE EARTH ELEMENTS FROM GEOLOGICAL MATERIALS

J. A. C. BROEKAERT*

Institut für Spektrochemie und angewandte Spektroskopie, Postfach 778, 4600 Dortmund (W. Germany)

P. K. HÖRMANN

Mineralogisch-Petrographisches Institut der Universität Kiel, Olshausenstrasse 40/60,2300 Kiel (W. Germany)

(Received 1st September 1980)

Summary. The isolation of rare earth elements (REE) from geological materials by ion-exchange chromatography with Dowex 50W-X8 is described. Elution curves for Y, La, Ce, Nd, Sm, Eu, Gd and Yb are determined by inductively-coupled plasma emission spectrometry. Separation from the main constituents including aluminium is accomplished by elution with 0.8 M, 4 M and 6 M hydrochloric acid. Recoveries of the individual REE are 90—100%. The method was confirmed by tests on synthetic basalt, andesite and dacite.

The rare earth element (REE) contents of abundant rock types are mostly in the range 0.1—10 ppm. Consequently, the determination of these elements requires the use of sensitive methods, e.g., neutron activation or mass spectrometry. X-ray fluorescence and optical emission spectrometry suffer from spectral interferences and matrix effects: the limited sensitivities of these methods may not allow direct determination of the REE.

Many attempts have been made to isolate the REE prior to spectrometric determination. For example, Edge and Ahrens [1] successfully separated Sc, Y, La, Ce and Nd from granitic and basaltic rocks by cation-exchange chromatography. Herrmann and Wedepohl [2] isolated REE by coprecipitation with iron hydroxide and calcium oxalate from 25-g samples, prior to determination. For example, Edge and Ahrens [1] successfully separated Sc, metry; this procedure is time-consuming for routine application. Other methods have been based on carbonate-type anion-exchange resins [3], anion-exchange separations in malonic and ascorbic acid media [4], and anion-exchange isolation from mixtures of acids and organic solvents, e.g. ethanol or methanol [5, 6]. In these methods, the REE are concentrated in relatively small volumes of eluate, but the organic matter makes their subsequent determination troublesome.

In this work, isolation of the REE by a cation-exchange method with hydrochloric acid as the eluent was preferred. As the aim was to develop a method applicable to all geological materials, the influence of elemental

composition on the elution process was tested. The constitution of elution curves requires an accurate and sensitive determination of the REE. Inductively-coupled plasma emission spectroscopy (i.c.p.—a.e.s.) proved suitable because of its high analytical precision and accuracy and its low detection limits for the REE [7].

Experimental

Instrumentation. Ion-exchange columns of Dowex 50W-X8, 100—200 mesh, were used; the columns were 1050 mm in length and 16.3 mm in diameter. Liquids were passed through the columns at a flow rate of 1.3 ml min^{-1}. Fractions (25 ml) were collected with an automatic sampler. The concentrations of the REE (and aluminium and yttrium) in the fractions were measured by i.c.p.—a.e.s. The i.c.p. instrumentation working conditions and detection limits are listed in Table 1. Alkali and alkaline earth elements were determined by conventional atomic absorption spectrometry in air—acetylene flames.

Procedure. Samples (5 g) covering the major element compositions of the most abundant rock types (Table 2) were prepared from Spec-pure substances (Johnson and Matthey) and doped with 400 μg of different REE. The substances (elements, chlorides, nitrates) were dissolved in hydrochloric acid and converted to chlorides by evaporation. The salt residue was re-

TABLE 1

Instrumentation, working conditions and detection limits for the determination of REE

Inductively-coupled plasma equipment	
R.f. generator	FS 10 (Linn, Kontron) frequency 27.12 MHz, free-running, operation power 4 kW, stability ±0.5%.
Burner	As described by Greenfield et al. [8].
Nebulization	Concentric glass nebulizer (Meinhard), uptake rate 1 ml min^{-1}, controlled with a peristaltic pump (Gilson).
Gas flows	Carrier gas 0.5 l Ar min^{-1} at 3 bar, outer gas flow 20 l N_2 min^{-1}, intermediate gas flow 8 l Ar min^{-1}.
Observation zone	4 mm × 4 mm, 4—8 mm above the coil.
Spectral equipment	
Monochromator	0.9 m Czerny—Turner.
Grating	90 mm × 90 mm, grating constant a = 1/2400 mm.
Slit width	Entrance slit 15 μm, exit slit 25 μm.
Background measurement	With a quartz refractor plate in front of the exit slit [9].
Microprocessor	80/20 Intel.
Integration time	5 s.
Detection limits[a] (μg ml^{-1})	Y 371.0 nm, 0.005; La 408.7 nm, 0.02; Ce 401.2 nm, 0.15; Nd 430.4 nm, 0.05; Sm 392.8 nm, 0.15; Eu 413.0 nm, 0.03; Gd 364.6 nm, 0.06; Yb 369.4 nm, 0.005.

[a]Detection limits are defined as the concentrations giving an analytical signal $x = \bar{I}_U + 3 \cdot 2^{1/2} s(I_U)$, where $\bar{I}_U$ is the mean and $s(I_U)$ the standard deviation calculated from 10 background measurements [10].

TABLE 2

Composition of synthetic test samples in weight percent
(Samples (5 g) contained 400 μg of the individual REE. Data represent the average composition of tholeiite, andesite and dacite according to Taylor [11].)

Component	Tholeiite	Andesite	Dacite	Component	Tholeiite	Andesite	Dacite
$(SiO_2)^a$	(51.7)	(59.5)	(65.1)	CaO	11.0	7.0	4.8
Al_2O_3	16.9	17.2	16.5	Na_2O	3.1	3.7	4.6
FeO	10.4	6.1	3.9	K_2O	0.4	1.6	2.1
MgO	6.5	3.4	1.5				

[a] SiO_2 was not used in the test samples. The data are used here for the geochemical characterization of the samples.

dissolved in 50 ml of 6 M HCl. The test samples did not contain silicon because in the analysis of silicate rocks this constituent is usually removed as hexafluorosilicic acid prior to the determination of other elements [1].

Iron was removed by passing the solution through a column of Dowex 1-X8 (100—200 mesh) anion-exchange resin in the chloride form. The eluate was evaporated nearly to dryness and the residue taken up in 50 ml of 0.8 M HCl. This solution was applied to the Dowex 50W-X8 cation-exchange column. The elements were eluted with hydrochloric acid at different concentrations (0.8—6 M).

Results and discussion

The results for Li, Na, K, Rb, Mg, Ca, and Y and the REE are represented in Figs. 1 and 2. The volumes necessary for complete elution of the elements Li—Ca (Fig. 1) vary from 4600 ml of 0.8 M HCl for dacite to 5000 ml of 0.8 M HCl for basalt. The end of the calcium elution can be determined by a.a.s. It is possible to standardize the separation of the matrix elements Li—Ca with a volume of 5000 ml; only traces of aluminium are eluted with 0.8 M HCl. A complete separation of Al from Y and the REE is achieved by subsequent elution with 270 ml of 4 M HCl (Fig. 2). The end of the Al elution can be determined exactly by i.c.p.—a.e.s., or semi-quantitatively by Al-test-strips, e.g., Merckoquant 10016. When the elution process is continued with 6 M HCl, yttrium and the REE are removed from the columns in sequence (Fig. 2.) Yttrium and the heavy REE (e.g., Yb) appear at the beginning of the elution followed by the light REE. Elution of the REE is complete when 730 ml of 6 M HCl, i.e. 1000 ml of 4 M + 6 M HCl, have passed through the column. The sequence of the individual REE in Fig. 2 was found to differ when six columns with different flow rates were used. Recoveries (Table 3) indicate that quantitative separation of the REE from a complex matrix is possible.

In natural materials, yttrium and the REE are accompanied by barium and scandium [1]. Additional tests with natural rock samples showed that about 80% of the barium and 25% of the scandium, but no other elements, were present in the REE fractions.

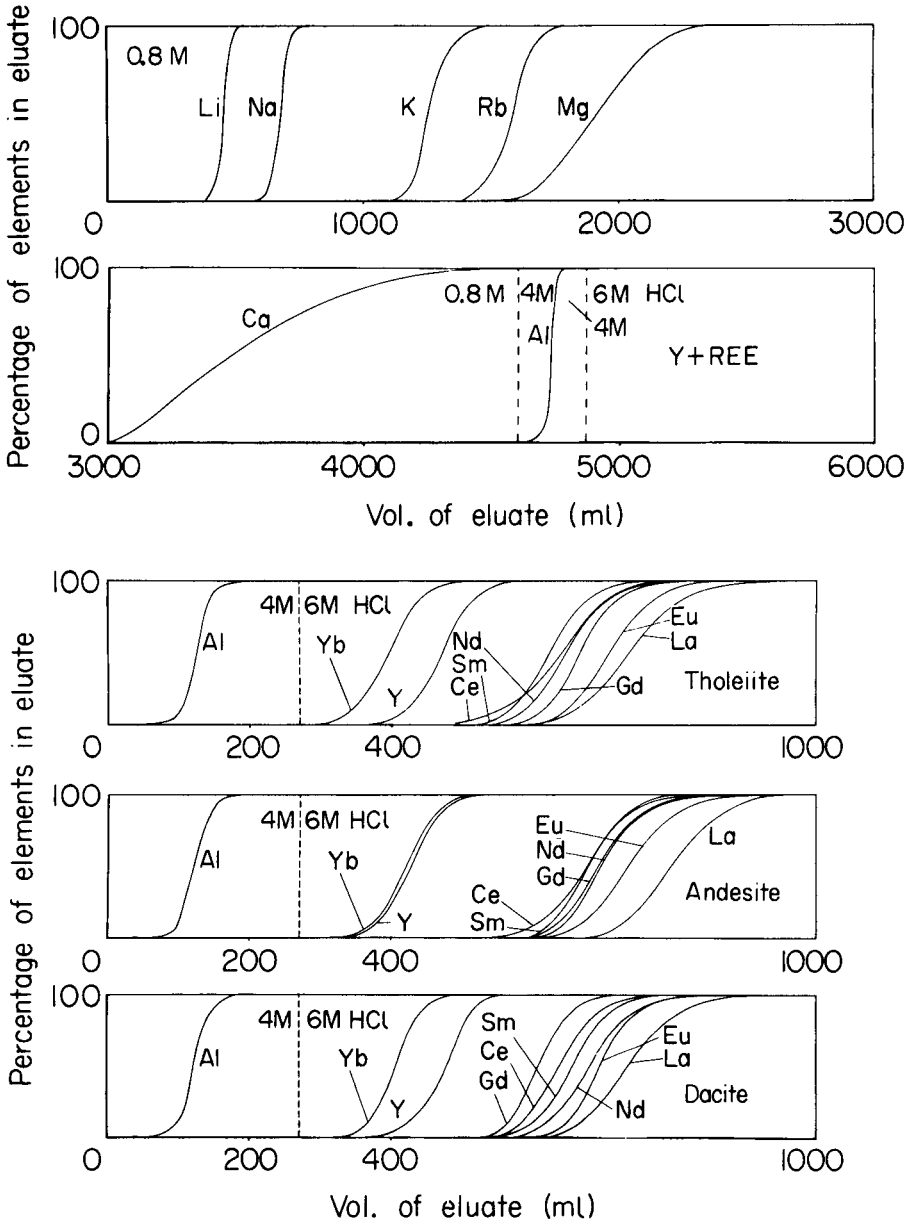

Fig. 1. Separation of the main constituents from Y and the REE. Elution curves for Li, Na, K, Rb, Mg and Ca (dacite sample) determined by a.a.s., Al by i.c.p.—a.e.s.

Fig. 2. Elution curves for Y and the REE in tholeiite, andesite and dacite samples as determined by i.c.p.—a.e.s.

TABLE 3

Recoveries of REE by the proposed method from the doped synthetic samples of tholeiite, andesite and dacite

Element	Recovery (%)[a]			Element	Recovery (%)[a]		
	Tholeiite	Andesite	Dacite		Tholeiite	Andesite	Dacite
Y	97.1	94.2	n.d.	Sm	102.0	98.1	n.d.
La	92.9	n.d.	100.5	Eu	93.5	100.6	105.8
Ce	n.d.	98.2	100.8	Gd	n.d.	89.9	93.1
Nd	n.d.	100.5	98.5	Yb	95.7	97.4	n.d.

[a]n.d. = not determined.

The results show that the ion-exchange procedure described here is effective for the quantitative isolation of the REE from a complex silicate matrix. The method provides a preconcentration of the REE and minimizes matrix effects in the subsequent spectrometric determination. The procedure is applicable to geological samples of very different chemical composition. It is a simple and powerful method of determining REE in geological materials with low REE contents.

This work was supported by the Deutsche Forschungsgemeinschaft and the Ministerium für Wissenschaft und Forschung des Landes Nordrhein-Westfalen.

REFERENCES

1 R. Edge and L. H. Ahrens, Anal. Chim. Acta, 26 (1962) 355.
2 A. G. Herrmann and K. H. Wedepohl, Fresenius Z. Anal. Chem., 225 (1967) 1.
3 V. D. Eristavi and L. L. Kashakashvili, Izv. Akad. Nauk Gruz. SSR Ser. Khim., 3 (1977) 38.
4 M. Chakravorty and S. M. Khopkar, Chromatographia, 10 (1977) 100.
5 H. Kakihana and K. Kurokawa, Bunseki Kagaku, 23 (1974) 1321.
6 J. Roelandts, G. Duyckaerts and A. O. Brunfelt, Anal. Chim. Acta, 73 (1974) 141.
7 J. A. C. Broekaert, F. Leis and K. Laqua, Spectrochim. Acta, 34B (1979) 73.
8 S. Greenfield, I. L. Jones and C. T. Berry, Analyst, 89 (1964) 713.
9 N. Nordmeyer, Fresenius Z. Anal. Chem., 225 (1967) 247.
10 H. Kaiser and H. Specker, Fresenius Z. Anal. Chem., 149 (1956) 46.
11 S. R. Taylor, Proc. Andesite Conf., Oregon State Dept. Geol. Min. Ind. Bull., 65 (1969) 43.

Analytica Chimica Acta, 124 (1981) 427—430

Short Communication

SURFACE TREATMENT OF BOROSILICATE GLASS BEAKERS FOR PREVENTION OF SODIUM CONTAMINATION

ATSUSHI MIZUIKE* and AKIRA IINO

Faculty of Engineering, Nagoya University, Chikusa-ku, Nagoya 464 (Japan)

(Received 14th October 1980)

Summary. Pyrex glass beakers are treated with molten $Ca(NO_3)_2$—KNO_3 (20:80 mol %) mixture at 500°C for 3 h. Treated beakers can be used successfully in wet oxidation of SRM-1571 Orchard Leaves for sodium determination; at least 10 oxidations can be done without sodium contamination. Mass spectrometry is used to investigate the depth profiles of glass components within 60 nm of the glass surfaces and to clarify the mechanism of the sodium contamination.

Platinum, silica, borosilicate glass, and polyfluorocarbons are common materials for vessels used in wet oxidation of organic samples. Borosilicate glasses are cheapest, but they cannot be applied in wet oxidations for sodium determination, because the sodium constituent of the glass contaminates the solution. De-alkalization of the glass surfaces with mineral acids or reactive gases such as sulfur dioxide does not seem promising for prevention of this contamination.

A new method of surface treatment is described in this communication: borosilicate glass beakers are immersed in a molten $Ca(NO_3)_2$—KNO_3 (20:80 mol %) mixture at 500°C for 3 h, so that sodium in the near surface layer is replaced by calcium and potassium. Treated beakers were successfully applied in the determination of sodium in the standard reference material Orchard Leaves. Depth profiles of sodium, potassium, and calcium near the glass surfaces were measured by mass spectrometry using neutral oxygen molecule bombardment and secondary ion mass spectrometry to clarify the mechanism of the sodium contamination.

Experimental

Surface treatment of borosilicate glass beakers. The 50-ml Pyrex glass beaker (Iwaki Code 7740; 80.9 SiO_2-12.7 B_2O_3-2.3 Al_2O_3-4.0 Na_2O-0.04 K_2O, wt. %) was washed with 1 M nitric acid at 90°C for 2 h and then with distilled water and dried in a desiccator. The beaker was completely immersed in a molten $Ca(NO_3)_2$—KNO_3 (20:80 mol %) mixture at 500°C for 3 h, withdrawn, cooled, washed with water, and dried in a desiccator.

Wet oxidation. In a 50-ml beaker covered with a polyfluorocarbon disk, 0.25 g of botanical sample and 4 ml each of nitric acid (62%) and sulfuric acid (97%) were heated for 15 min on a sand bath at 300°C. After addition

of 2 ml of hydrogen peroxide solution (30%), the heating was continued for another 15 min.

Flame photometric determination. A Nippon Jarrell-Ash AA-1 Mark II atomic absorption/flame emission spectrometer was used with a Yanaco Model YR 101 recorder, a 10-cm slit burner SA-61 [air (7 l min^{-1}), acetylene (2 l min^{-1}) for sodium and potassium], and a 5-cm slit burner SN-63 [nitrous oxide (6 l min^{-1}), acetylene (5 l min^{-1}) for calcium]. Wavelengths (nm) used were: Na 589.3, K 767.0, and Ca 422.7.

Mass spectrometric depth profiling. In a Hitachi IMA-2 ion microanalyzer with an attachment for neutral particle bombardment, glass surfaces were bombarded with neutral oxygen molecules (O_2^0, 4 and 7 keV) or ion (O_2^+, 12 keV) beams, and sputtered ions were mass-analyzed. Experimental procedures have been reported elsewhere [1, 2].

Results and discussion

Surface treatment. The original intention in this work was to treat Pyrex glass surfaces with molten calcium nitrate (m.p. 561°C) at 565°C for 3 h, so as to replace sodium in the near surface layer by calcium and block the movement of sodium from the interior of the glass. The treated surfaces, however, were etched extensively, becoming frosted. Surface treatment with a molten $Ca(NO_3)_2$—KNO_3 (20:80 mol %) mixture (m.p. 240°C) at 500°C for 3 h gave smooth surfaces, when observed under an optical microscope (400×, with a Nomarski interference contrast attachment) and a scanning electron microscope (10000×).

Contamination with sodium, potassium, and calcium from beakers during wet oxidation. Blank runs for wet oxidation were carried out to evaluate the degree of contamination with sodium, potassium, and calcium from 50-ml beakers made of silica, and treated and untreated Pyrex glass. The results shown in Table 1 were corrected for impurities in the reagents used, which

TABLE 1

Contamination from beakers (All results are given as μg)

Beaker material	Element tested	Blank run			
		1st	2nd	3rd	10th
Silica	Na	1.0	<0.15	<0.15	<0.15
	K	0.1	<0.1	<0.1	<0.1
	Ca	<0.5	<0.5	<0.5	<0.5
Pyrex glass, treated	Na	1.4	<0.15	<0.15	<0.15
	K	14	2.0	0.45	0.3
	Ca	1.6	<0.5	<0.5	<0.5
Pyrex glass, untreated	Na	15	7.2	2.8	0.35
	K	0.2	0.2	0.2	0.2
	Ca	<0.5	<0.5	<0.5	<0.5

were measured separately. The surface treatment is very effective in reducing the sodium contamination. A treated beaker can be used for at least 10 successive wet oxidations without sodium contamination.

The U.S. National Bureau of Standards SRM-1571 Orchard Leaves was decomposed by wet oxidation for the determination of sodium. All the beakers were used for the wet oxidation after a blank run had been done, because there was significant contamination with sodium in the first run (see Table 1). A small amount of insoluble siliceous residue (probably from external sand or soil contamination of the Orchard Leaves [3]) was disregarded. Analytical results (Table 2) show again that the proposed surface treatment is very effective in reducing the sodium contamination originating from Pyrex glass.

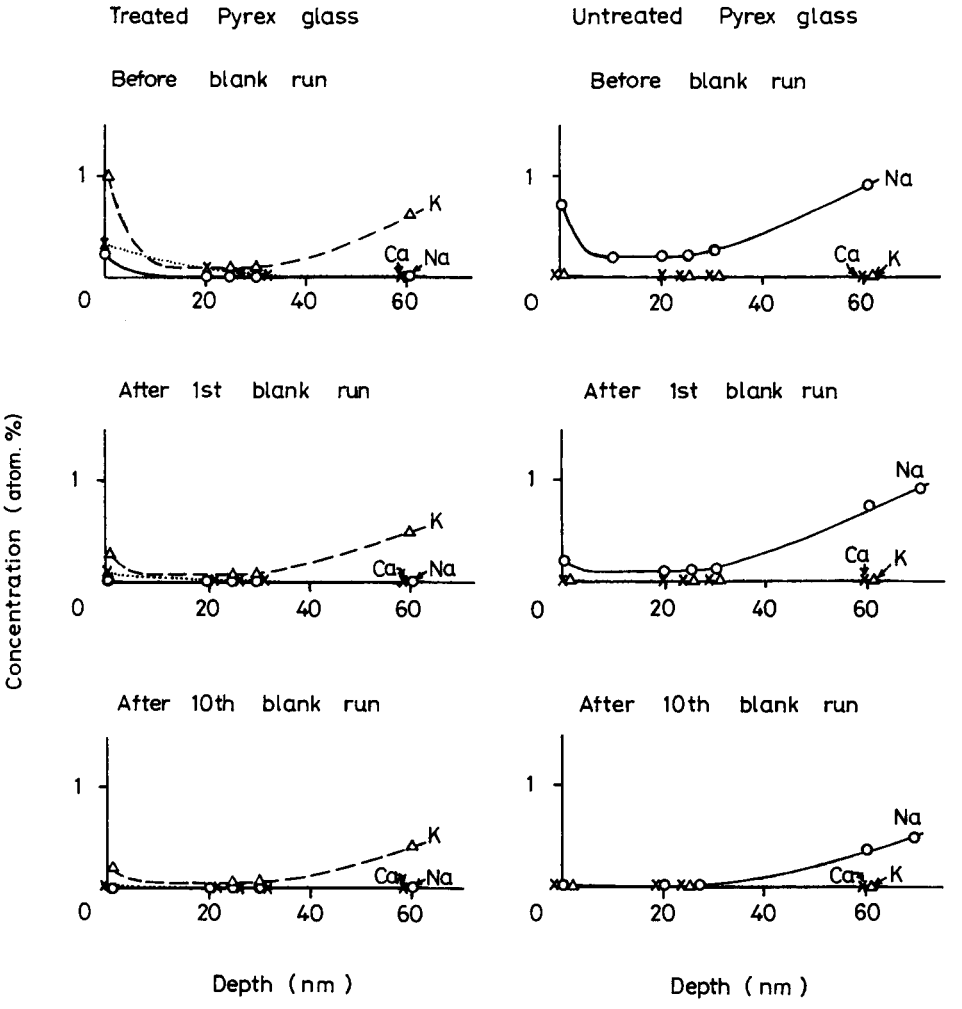

Fig. 1. Depth—concentration profiles (○) Na; (△) K; (×) Ca.

TABLE 2

Analysis of SRM-1571 Orchard Leaves[a] for sodium

Beaker material	Sodium found ($\mu g\ g^{-1}$)[b]	
Silica	77, 80, 80, 82	(av. 80)
Pyrex glass, treated	80, 81, 80	(av. 80)
Pyrex glass, untreated	88, 88, 90	(av. 89)

[a]Certified value for sodium: 82 ± 6 $\mu g\ g^{-1}$. [b]Corrected for contamination from reagents measured separately.

Depth profiles of glass surfaces. Figure 1 shows depth—concentration profiles of the surfaces of the treated and untreated Pyrex glass beakers, before and after blank runs of the wet oxidation. It is clear that diffusion of sodium from the interior of the glass causes the sodium contamination during wet oxidation.

The authors thank Mr. Y. Nishimura for his help in the experimental work.

REFERENCES

1 A. Iino and A. Mizuike, Bull. Chem. Soc. Jpn., submitted.
2 A. Iino, H. Nakamura and A. Mizuike, Nippon Kagaku Kaishi (J. Chem. Soc. Jpn.), (1977) 1324.
3 E. J. Maienthal, J. Assoc. Off. Anal. Chem., 55 (1972) 1109.

Analytica Chimica Acta, 124 (1981) 431—436

Short Communication

DETERMINATION OF RESIDUAL CHLORINE BY DERIVATISATION WITH 2,6-DIMETHYLPHENOL AND GAS CHROMATOGRAPHIC SEPARATION

J. ELLIS* and P. L. BROWN

Chemistry Department, University of Wollongong, P.O. Box 1144, Wollongong, N.S.W. 2500 (Australia)

(Received 14th August 1980)

Summary. Residual chlorine in aqueous solution is converted to 4-chloro-2,6-dimethylphenol, which is extracted into hexane and determined by gas chromatography. Relative standard deviations (n = 5) are 0.36—1.1% for chlorine concentrations of 8.6—0.01 mg l^{-1} and chlorine recoveries are 99.2—101%. In the presence of dichromate (30 mg l^{-1}), relative standard deviations (n = 5) are 1.19—2.71% for chlorine concentrations of 9.3—0.1 mg l^{-1}. Oxidants and coloured solutes do not interfere.

The widespread use of chlorine as a disinfectant of drinking water and as an additive to cooling waters to inhibit algal growth has prompted the development of a variety of techniques for its determination [1—4]. The techniques most commonly employed are iodimetric and amperometric titrations and the *o*-toluidine colorimetric method [2]. If the amperometric titration is carried out within specified pH ranges, it can discriminate between free available chlorine and combined chlorine. More recently, a computerised determination of trace residual chlorine (3—100 ppb) with a chlorine electrode has been reported [5]. This electrode develops a potential based on the relative levels of iodine and iodide ion in solution after in situ stoichiometric conversion of iodide to iodine by oxidising chlorine species. In the case of chlorinated sea water, Wong [6] has pointed out precautions which must be taken during the amperometric titration to avoid serious errors arising from the presence of other oxidising species, notably iodate. However, industrial cooling waters are often treated with chromate as well as chlorine to inhibit corrosion and the resultant colour interferes with colorimetric determinations of residual chlorine. Moreover, dichromate is itself an oxidising agent and may therefore interfere with many analytical methods based on the oxidising character of chlorine.

Most determinations of "residual chlorine" are in fact measurements of total oxidising capacity: there is no discrimination between the various chlorine-containing species present which may include chloramines plus species produced by reaction of chlorine with water.

$$Cl_2 + H_2O \rightleftharpoons HOCl + HCl \overset{H_2O}{\rightleftharpoons} H_3O^+ + ClO^-$$

The relative proportions of chlorine, hypochlorous acid and hypochlorite ion vary markedly with pH and have been calculated by Wong [6] over the pH range 0—14 for chlorine (1 mg l^{-1}) in 0.55 M sodium chloride, using the thermodynamic data given by Garrels and Christ [7]. The concentration of hypochlorous acid is at a maximum at pH 5; at low pH, chlorine is dominant and at high pH, hypochlorite ion is dominant. Hypochlorous acid solutions slowly disproportionate irreversibly into oxygen and hydrochloric acid, with a consequent fall in residual chlorine.

The advances which have been made in recent years in the isolation and identification of chlorinated phenols as trace pollutants in surface waters [8—10] suggested the determination of chlorine by reaction with a suitable phenol followed by gas chromatographic determination of the chlorinated phenol. Phenols react rapidly with chlorine or bromine in aqueous or non-aqueous media via an electrophilic substitution mechanism. If the *ortho* and *para* positions are not already substituted and if sufficient halogen is available, the 2,4,6-trihalophenol is almost the sole organic product.

The phenol selected for the present purpose was 2,6-dimethylphenol. It is readily available commercially at low cost and has the following desirable properties: it is moderately soluble in water and readily extracted into hexane; only the *para* position is available for electrophilic substitution (no polychlorinated products formed unless chlorine is present in large excess); the methyl groups are weakly electron-donating, which enhances electrophilic substitution; the hydroxyl group is not too sterically hindered and is readily derivatised by BSTFA [bis-(trimethylsilyl)-trifluoroacetamide].

The compound selected as an internal standard was 4-bromo-2,6-dimethylphenol. It has similar solubility and extraction characteristics to 4-chloro-2,6-dimethylphenol, is resistant to chlorination (all active sites are blocked) and its trimethylsilyl derivative is readily separated by gas chromatography from the trimethylsilyl derivatives of 4-chloro-2,6-dimethylphenol and 2,6-dimethylphenol (Fig. 1).

The 2,6-dimethylphenol can be chlorinated by chlorine and by hypochlorous acid, to give 4-chloro-2,6-dimethylphenol. In either case, one mole of the chlorine species is equivalent to one mole of the monochlorinated phenol.

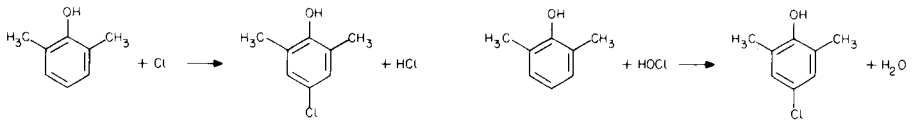

Experimental

Materials. 2,6-Dimethylphenol (Fluka) was used. Water was distilled and redistilled twice from quartz. Chlorine water was prepared by bubbling chlorine (Matheson) through distilled water and was stabilised by making it 10^{-3} M in sodium hydroxide. This solution was standardised by the iodimetric method [2] immediately before dilution for use in the derivatisation method.

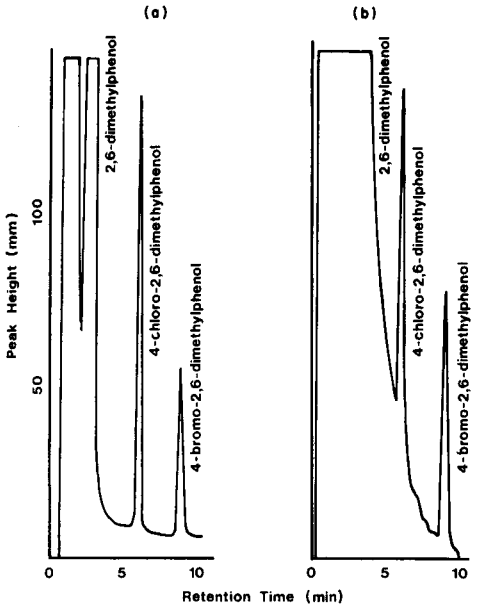

Fig. 1. Gas chromatogram of silylated hexane extract of aqueous chlorine solution treated with 2,6-dimethylphenol and 4-bromo-2,6-dimethylphenol. Injection temperature, 250°C; column temperature, 135°C. (a) $[Cl_2]$ = 8.6 mg l^{-1}. Aqueous concentrations: 2,6-dimethylphenol, 2.5 × 10^{-3} M; 4-chloro-2,6-dimethylphenol, 1.2 × 10^{-4} M; 4-bromo-2,6-dimethylphenol, 9.4 × 10^{-5} M. Injection volume, 1 μl; attenuation, 10 × 32. (b) $[Cl_2]$ = 0.07 mg l^{-1}. Aqueous concentrations: 2,6-dimethylphenol, 2.5 × 10^{-3} M; 4-chloro-2,6-dimethylphenol, 9.9 × 10^{-7} M; 4-bromo-2,6-dimethylphenol, 9.4 × 10^{-7} M. Injection volume, 2 μl; attenuation, 10 × 4.

4-Chloro-2,6-dimethylphenol and 4-bromo-2,6-dimethylphenol were prepared from 2,6-dimethylphenol as described in the literature; their uncorrected melting points were respectively 80°C (lit. 81—82°C [11]) and 78—79°C (lit. 79.5°C [12]). Bis-(trimethylsilyl)-trifluoroacetamide (BSTFA) was Regis. Molecular sieves were Line 3 Å. All other chemicals were analytical-reagent grade.

A Packard Becker Model 409 gas chromatograph with flame ionization detection (f.i.d.) was used. A glass column (2m × 2mm i.d.) packed with 80—100 mesh Gas-Chrom Q coated with 3% GC-GE-SE-30 (Applied Science Laboratories Inc.) was used for the separation of the trimethylsilyl derivatives of the phenols. Column temperature was 135°C isothermal; injector and detector temperatures were 250°C. Nitrogen carrier gas was used at 25 ml min^{-1}. A 5-μl microsyringe (SGE-5A-RN-GP) was used.

Procedure. Adjust the water sample to pH 10 by addition of 10^{-3} M sodium hydroxide. To 50.0 ml of the sample, add 2,6-dimethylphenol solution (50 ml; 300 mg l^{-1}) and 0.1—25 ml of 4-bromo-2,6-dimethylphenol solution (190 mg l^{-1}). Acidify to pH 1—3 with 0.05 M sulphuric acid, allow to react for 5 min and then extract once with 5 ml of n-hexane. Dry the

extract over molecular sieves, withdraw 2 ml of the hexane solution and blow down under nitrogen. Add 100—200 μl of BSTFA and warm the solution to 100°C for 30 min. Inject 1—2 μl into the gas chromatograph and measure the relative areas of the 4-chromo-2,6-dimethylphenol and the 4-bromo-2,6-dimethylphenol standard.

Results and discussion

When a solution of chlorine water with a residual chlorine concentration of 40 mg l^{-1} was treated with 200 mg l^{-1} of 2,6-dimethylphenol, the chlorine recovery was only 55%. However, when the chlorine water was first raised to pH 10 by addition of sodium hydroxide and the pH then lowered to 1—3 by addition of dilute sulphuric acid prior to the addition of the phenol, the chlorine recovery rose to 100 ± 1%. This requires a more rapid chlorination of the phenol by hypochlorous acid than by chlorine and further requires that the reversible reaction of hypochlorous acid to give chlorine and water is relatively slow. A large excess of phenol over the stoichiometric amount was used to ensure complete reaction within a short reaction time and to minimise the possibility of side reactions. The optimum reaction time was established by allowing a solution of 2,6-dimethylphenol (300 mg l^{-1}) and chlorine (13.5 mg l^{-1}) to react at 25°C for varying times in the range 5—30 min. At this concentration level of chlorine and even at the 0.01 mg l^{-1} level a reaction time of 5 min was sufficient.

The accuracy and precision of the method were explored by making five replicate runs at four different chlorine concentrations (Table 1). Residual chlorine in the stock solution of chlorine was determined by the iodimetric method [2] immediately before dilution for application of the phenol derivatisation method. Chlorine recoveries over this concentration range were 99.2—101.4% with relative standard deviations of 0.36—1.1%. When the f.i.d. detector is used, the limiting lower concentration of chlorine which can be measured is determined by the gas chromatographic peak for the 4-chloro-2,6-dimethylphenol being superimposed on the much larger peak of the 2,6-dimethylphenol. Use of an electron capture detector would eliminate this difficulty and might extend the working concentration range well below 0.01 mg l^{-1}.

TABLE 1

Determination of residual chlorine by phenol derivatisation and gas chromatography

Pure solutions				
Residual chlorine (mg l^{-1})	8.6	1.2	0.1	0.01
Recovery (%)	99.8	99.6	101.4	99.2
R.s.d. (%; n = 5)	0.36	1.11	0.48	0.56
In presence of dichromate (30 mg l^{-1})				
Residual chlorine (mg l^{-1})	9.29	2.22	0.103	
Recovery (%)	100.5	100.2	99.3	
R.s.d. (%; n = 5)	1.19	1.92	2.71	

Interferences. When these determinations were repeated with solutions containing dichromate (30 mg l^{-1}) in addition to the chlorine, the recovery of chlorine was reduced to 70%. Some of the 2,6-dimethylphenol was oxidised by the dichromate to the corresponding *p*-quinone and diphenoquinone (which precipitated from the solution on standing) and the effective concentration of 2,6-dimethylphenol was thereby lowered. When the 2,6-dimethylphenol concentration was increased to 5 g l^{-1}, the chlorine recovery increased to >99% (Table 1), with relative standard deviations of 1.19—2.71%.

The presence of manganese dioxide, copper(II) ion, iodate or nitrite (30 mg l^{-1}) did not alter the chlorine recovery. However, when nitrite was present, an additional peak (t_r = 6 min 50 s) appeared in the gas chromatogram. The peak was due to 4-nitroso-2,6-dimethylphenol and did not interfere with the peak area measurements of the 4-chloro and 4-bromo derivatives. Unlike colorimetric methods, this method is unaffected by the presence of coloured impurities in the aqueous chlorine solution.

Conclusion

The phenol derivatisation followed by gas chromatography affords a simple, rapid and sensitive method for determining residual chlorine in water. With a flame ionisation detector, concentrations as low as 0.01 mg l^{-1} can be determined with chlorine recovery >99% and a precision of around 0.6%. Because the chlorine or hypochlorous acid are behaving as chlorinating rather than oxidising agents, the method has a high inherent selectivity and freedom from interference by other oxidising agents.

Organic impurities which co-extract into hexane and which have the same retention time as the silylated phenols would interfere. Such interfering substances can be detected readily by hexane extraction of the original water sample, without addition of 2,6-dimethylphenol. By use of a different internal standard, the method should be suitable for simultaneous determination of both chlorine and bromine as present, for example, in chlorinated sea water [13]. When a simulated seawater ([NaCl] = 0.55 M, [NaBr] = 1.67 × 10^{-5} M) was chlorinated ([Cl_2] = 12.4 mg l^{-1}) and analysed by using 2,4,6-trichlorophenol as internal standard, the following recoveries and standard deviations (n = 3) were obtained: chlorine (11.8 mg l^{-1}), 11.6 ± 0.14 mg l^{-1}; bromine (1.34 mg l^{-1}); 1.33 ± 0.04 mg l^{-1}.

REFERENCES

1 N. J. Nicolson, Analyst, 90 (1965) 187.
2 M. C. Rand, A. E. Greenberg and M. J. Taras (Eds.), Standard Methods for the Examination of Water and Waste Water, 14th edn., American Public Health Association, Washington, DC, 1976.
3 Annual Book of ASTM Standards, Standard D-1253-76, American Society for Testing and Materials, Philadelphia, PA, 1976, Vol. 31, p. 276.
4 Annual Book of ASTM Standards, Standard D-1427-68, American Society for Testing and Materials, Philadelphia, PA, 1976, Vol. 31, p. 283.
5 L. P. Rigdon, G. J. Moody and J. W. Frazer, Anal. Chem., 50 (1978) 465.

6 G. T. F. Wong, Water Res., 14 (1980) 51.
7 R. M. Garrels and C. L. Christ, Solutions, Minerals and Equilibria, Harper Row, New York, 1965.
8 C. O. Chriswell, R. C. Chang and J. S. Fritz, Anal. Chem., 47 (1975) 1325.
9 W. Krijgsman and C. G. van de Kamp, J. Chromatogr., 131 (1977) 412.
10 R. C. C. Wegman and A. W. M. Hofstee, Water Res., 13 (1979) 651.
11 A. S. Kende and P. MacGregor, J. Am. Chem. Soc., 83 (1961) 4197.
12 K. Auwers and T. Markovitz, Ber. Dtsch. Chem. Ges., 41 (1908) 2332.
13 J. A. Sweetman and M. S. Simmons, Water Res., 14 (1980) 287.

Analytica Chimica Acta, 124 (1981) 437—441

Short Communication

UTILIZATION OF FLOW INJECTION WITH HYDRAZINE REDUCTION AND PHOTOMETRIC DETECTION FOR THE DETERMINATION OF NITRATE IN RAIN-WATER

B. C. MADSEN

Department of Chemistry, University of Central Florida, Orlando, FL 32816 (U.S.A.)

(Received 23rd July 1980)

Summary. The hydrazine reduction method for determination of nitrate at the parts per million level is adapted to flow injection sample processing of rain-water. Reagent composition and physical variables were evaluated and optimized. Forty samples per hour can be processed. A precision of better than 3% is possible in the range of 1.0—10.0 ppm nitrate. Results for nitrate obtained from 9 rain-water samples agreed favorably with those determined by ion chromatography.

The flow injection (f.i.) sample processing approach is proving to be a versatile tool for both routine chemical determinations and research applications [1]. Although several f.i. methods have been developed for the determination of nitrate, these methods utilize a heterogeneous phase reduction of nitrate to nitrite prior to spectrophotometric measurement of a highly colored product formed by diazotization—coupling reactions [2, 3]. An exception is the determination based on ultraviolet absorption of nitrate [4].

Segmented flow methods for determination of nitrate based on homogeneous-phase hydrazine reduction of nitrate to nitrite have been described [5, 6]. This communication describes the adaptation of this hydrazine reduction to a flow injection procedure for the determination of nitrate at the parts per million (ppm) level without any sample pretreatment. Time, temperature, and reagent dependence [5, 6] of the method are considered. Selected operating conditions permit up to 40 samples/h of rain-water to be processed.

EXPERIMENTAL

Flow injection systems. Several systems were evaluated with basic construction features shown in Fig. 1. A Buchler 2-6100 polystatic pump which provides maximum flow rates as shown in Fig. 1 was used. Pump pulse-damping coils (3 m) were utilized in all reagent streams. Tygon tubing (0.79 mm i.d.) was used for all reagent streams. The water stream into which the sample was injected and the reaction coils were 1.59 mm i.d. Samples were injected using an Altex 202-00 rotary injection valve and 1.0-ml sample loop.

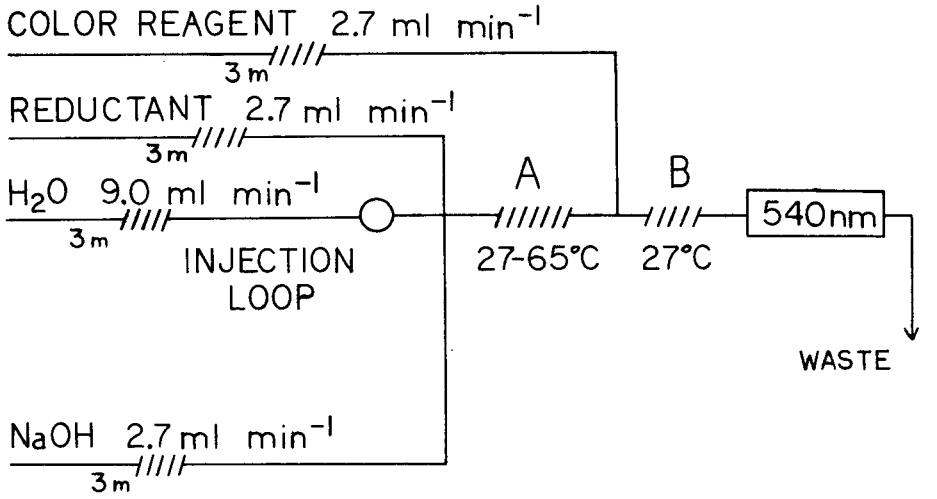

Fig. 1. Components of flow injection sample processing system.

Connectors were prepared from drilled plexiglas blocks as previously described [7]. The lengths of reduction coil (A) and color development coil (B) were varied to determine optimum residence times within the system. The reduction coil was placed in a constant-temperature water bath operated at various temperatures. The color development coil was placed in a water bath operated near ambient temperature. Detection was performed at 540 nm by a Perkin-Elmer 552 spectrophotometer. Absorbance outputs were recorded on a Perkin-Elmer Hitachi model 57 *X-Y* recorder. Quantification was based on peak height. The 2.0-cm flow cell was constructed from a plexiglas block with a 3.2-mm bore which yielded a 160-μl internal volume.

Reagents and f.i. system characteristics. Reagent-grade chemicals were used exclusively. Standard stock solutions were prepared to contain 1.613×10^{-2} mol l^{-1} sodium nitrate and sodium nitrite, respectively. Working standards were prepared daily by dilution of the stock solutions. The reductant contained 1.0 g of hydrazine sulfate, 0.4 g of $ZnSO_4 \cdot 7H_2O$, and 0.09 g of $CuSO_4 \cdot 5H_2O$ per liter. The color reagent contained 3.5 g of sulfanilamide (SAA), 0.6 g of N-1-naphthylenediamine dihydrochloride (NED) and 100 ml of hydrochloric acid per liter. These two solutions were prepared fresh daily. Sodium hydroxide was 0.54 M. Nitrate in rain-water samples was determined using f.i. system III as specified in Fig. 2. Reduction conditions were 60-s residence time at 45°C, 190 mg l^{-1} hydrazine sulfate, 17 mg l^{-1} Zn(II), 4 mg l^{-1} Cu(II) and 0.10 M NaOH. Color development conditions were 30-s residence time at 27°C, 550 mg l^{-1} SAA, 95 s mg l^{-1} NED, and 0.18 M HCl. Signal characteristics in f.i. system III include 95 for peak arrival at the detector, 120 s for the peak maximum, and 160 s to return to baseline.

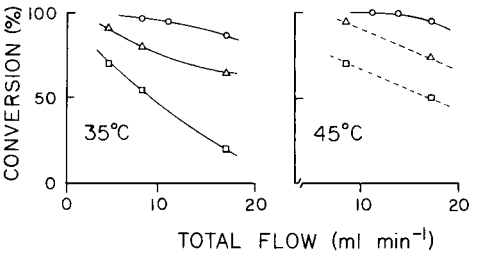

Fig. 2. Effect of temperature and flow rate on conversion of nitrate to nitrite (□) System I: (A) 2 m; (B) 2 m. (△) System II: (A) 4 m; (B) 4 m. (○) System III: (A) 8 m; (B) 4 m.

Results and discussion

System variables. Several combinations of reduction and color development coils (Fig. 1) were evaluated by comparing reduction efficiencies for equivalent amounts of nitrate and nitrite injected under identical conditions. Results presented in Fig. 2 show that system III provides reduction of nitrate approaching 100% completion even at maximum flow rate, and that system was selected for additional studies. Below 30°C, reduction efficiency is low, and above 50°C, formation of air bubbles in the reduction coil is a serious problem.

Because of the extended residence time (approximately 180 s) associated with system III, a maximum of 20 samples can be run per hour if one allows a sample to be removed from the system before the next sample is introduced. The 65-s period required for the absorbance peak to pass through the detector flow cell represents the smallest time interval between sample injections if baseline resolution is to be accomplished. Repeatability of results associated with injection of a 2.5-ppm nitrate standard at 90-s and 180-s intervals was evaluated to determine whether injection of a sample into the system before the previous sample is removed will significantly influence results. The *F*-test of the variance ratios and the paired *t*-test [9] applied to maximum absorbance values suggested no significant difference at the 95% confidence level.

Chemical variables. Those reagents which directly influence formation of the absorbing species were evaluated to determine optimum concentrations that will provide high absorbance without utilization of a large excess of reagents. The influences that changing concentrations of hydrazine sulfate, SAA, NED, and NaOH have on absorbance are presented in Fig. 3. Increasing hydrazine sulfate concentration exhibits a negative influence on absorbance, which is apparently due to reduction of nitrite to a lower oxidation state [6]. As the concentrations of other reagents increase, the absorbance increases and levels off. This indicates that the large excess of SAA previously reported [5, 6] is not necessary when the flow injection technique is utilized. The Cu(II) catalyst and Zn(II) concentrations were not evaluated. The presence of Zn(II) is reported to minimize interference in nitrate determinations in fresh water [6].

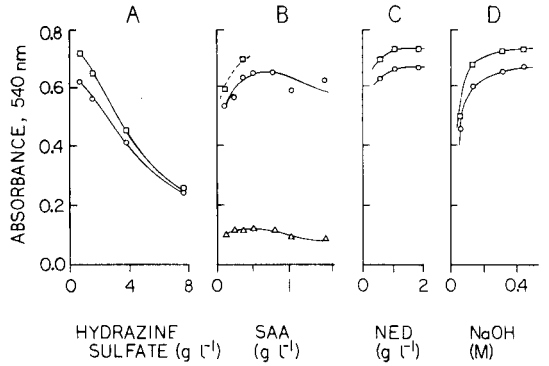

Fig. 3. Effect of reagent concentrations on the absorbance from nitrate and nitrite solutions. (○) 5.00 ppm nitrate; (△) 1.00 ppm nitrate; (□) 3.60 ppm nitrite. Individual reagents were evaluated under the following conditions: hydrazine sulfate was 600 mg l^{-1} except in (A). SAA was 14.7 g l^{-1} in (A) and 3.5 g l^{-1} in (C) and (D). NED was 600 mg l^{-1} in (A) and (B) and 1.90 g l^{-1} in (D). NaOH was 0.54 M except in (D).

Maximum absorbance from the system also depends on system design because moderate or large diffusion reduces the absorbance maximum. Dispersion [1] was determined to be approximately 0.3 by comparing the absorbance maximum from a 1.00-ppm nitrate standard injected into the system with the steady-state absorbance obtained when the water carrier stream was replaced with 1.00-ppm nitrate standard.

Rain-water determinations. The described method was evaluated for suitability in determination of nitrate in rain-water. The determinations were performed with 90-s injection intervals by injecting sequentially three different standards followed by six different samples. This approach was repeated using 10.00, 8.00, 6.00, 4.00, 3.00, 2.00 and 1.00-ppm nitrate standards and nine rain-water samples and spikes until triplicate measurements were made. The calibration curve is linear over the range considered and is described by: Absorbance = (0.118 ± 0.001)(ppm NO_3^-) + (0.002 ± 0.005), with standard error of estimate of 0.008. Triplicate results obtained for 9 rain-water samples having 0.5—4.0 ppm nitrate had standard deviations of less than 3%. Recoveries for 0.80 ppm and 0.20 ppm nitrate added to each of two different rain-water samples were 107% and 90%, respectively. Comparison of flow injection results ($C_{f.i.}$) with those determined by ion chromatography $C_{i.c.}$ [8] yielded the correlation: $C_{f.i.} = (0.948 \pm 0.011)\, C_{i.c.} + (0.048 \pm 0.023)$ ppm, with standard error of estimate 0.028 ppm. Comparison of f.i. and i.c. results using the *t*-test with multiple samples [9] suggests no significant difference in results obtained by the two methods at the 99% confidence level. The f.i. method has been found to be reasonably rapid, accurate, and precise for routine determination of nitrate in rain-water.

Partial support for this project was provided under NASA contract NAS10-8986.

REFERENCES

1 J. Růžička and E. H. Hansen, Anal. Chim. Acta, 114 (1980) 19.
2 M. F. Giné, H. Bergamin F°, E. A. G. Zagatto and B. F. Reis, Anal. Chim. Acta, 114 (1980) 191.
3 L. Anderson, Anal. Chim. Acta, 110 (1979) 123.
4 J. Slanina, F. Bakker, A. Bruijn-Hes and J. S. Mols, Anal. Chim. Acta, 113 (1980) 331.
5 M. T. Downes, Water Res., 12 (1978) 673.
6 L. J. Kamphake, S. A. Hannah and J. M. Cohen, Water Res., 1 (1967) 205.
7 J. Růžička and E. H. Hansen, Anal. Chim. Acta, 78 (1975) 145.
8 P. J. Galvin and J. A. Cline, Atmos. Environ., 12 (1978) 1163.
9 G. D. Christian, Analytical Chemistry, 3rd edn., J. Wiley, New York, 1980, pp. 72—76.

Analytica Chimica Acta, 124 (1981) 443—448

Short Communication

DOSAGE SPECTROPHOTOMETRIQUE DU NEPTUNIUM

P. CAUCHETIER

DCAEA/SEACC, Centre d'Etudes Nucléaires, BP 6, F-92260, Fontenay-aux-Roses (France)

(Reçu le 1 septembre 1980)

Summary. (Spectrophotometric determination of neptunium.) Use of the absorption peak of the NpO_2^+ ion at 981 nm is discussed. Quantitative conversion to Np(V) requires oxidation of Np(IV) by Ce(IV), reduction of Np(VI) and excess of Ce(IV) with hydrazinium nitrate, and destruction of excess of hydrazine by nitrite. The measurable concentration range in the cuvette is 2—1000 mg l^{-1} and the precision is ±1% in the higher range. Uranium and plutonium at ratios Me/Np ⩽ 10^{-3} do not interfere.

Résumé. L'utilisation du pic d'absorption de l'ion NpO_2^+ à 981 nm est intéressante. L'obtention quantitative du neptunium(V) nécessite l'oxydation de Np(IV) par Ce(IV), la réduction de l'excès de Ce(IV) et de Np(VI) par le nitrate d'hydrazinium et la destruction de l'excès de celui-ci par le nitrite. La gamme de concentrations accessibles dans la cuve est 2—1000 mg l^{-1} et la précision est voisine de ±1% en haut de gamme. Le dosage est possible sans séparation en présence d'uranium et de plutonium dans des rapports Me/Np ⩽ 10^{-3}.

Les ions du neptunium présentent, en solution aqueuse, la propriété d'absorber les photons: leurs spectres d'absorption permettent de les caractériser. Parmi ces ions, deux sont suffisamment stables et faciles à obtenir pour être utilisés aux fins de dosage quantitatif du neptunium. Les caractéristiques respectives de leur principale bande d'absorption sont les suivantes en milieu peu ou pas complexant: NpO_2^{2+} (λ_{max} = 1223 nm, $\epsilon \approx 45$ l mol^{-1} cm^{-1}, largeur à mi-hauteur ≈ 50 nm), et NpO_2^+ (λ_{max} = 981 nm, $\epsilon \approx 400$ l mol^{-1} cm^{-1}, largeur à mi-hauteur ≈ 6,5 nm). Au vu de ces caractéristiques. l'utilisation de l'ion NpO_2^+ est plus favorable. Sa sensibilité est près de 10 fois supérieure à celle de NpO_2^{2+}. L'étroitesse du pic le rend en outre à la fois plus libre d'interférence par d'autres espèces absorbantes et plus facile à distinguer du "bruit de fond" et donc à détecter.

Dès 1971, nous avions proposé de doser le neptunium en utilisant la spectrophotométrie de Np(V) [1]. Nous décrivons ici les modifications que nous avons dû apporter au mode opératoire pour éliminer certaines sources de difficulés ou inhiber certaines interférences ainsi que les différentes observations faites au cours d'une dizaine d'années d'utilisation de cette méthode.

Obtention du neptunium(V)

Cas des solutions nitriques pures. En général, en l'absence de réducteur, le neptunium se trouve, en milieu nitrique, sous forme d'un mélange des degrés d'oxydation (V) et (VI). Pour plus de sécurité, nous proposions [1] de porter la prise d'essai à ébullition avant d'ajuster le milieu à la concentration molaire en acide nitrique. Dans de nombreux cas, cette précaution n'est pas nécessaire.

Le neptunium(VI) est réduit dans ce milieu très rapidement par le nitrate d'hydrazinium en neptunium(V) et celui-ci est stable. En effet, le temps nécessaire pour ajuster le volume de la fiole, remplir la cellule et faire la mesure est plus grand que celui qu'exige la réaction pour être complète dans nos conditions opératoires (1 ml de solution de nitrate d'hydrazinium molaire). Plus d'un mois après préparation, la hauteur du pic demeure inchangée dans les limites de précision de la lecture.

Cas des solutions renfermant du fer. Etant donné que cet élément est fréquemment présent dans les solutions d'usine (il provient des gaines et de la corrosion des cuves), nous avons étudié son influence sur le dosage. Ni Fe(II), ni Fe(III) n'absorbent dans cette zone de longueurs d'onde, mais le fer est réduit par l'hydrazinium et le fer(II) formé réduit Np(V) en Np(IV). La conséquence en est que le pic de NpO_2^+ décroît lentement au cours du temps, mais d'autant plus vite cependant qu'il y a davantage de fer. Il est possible de stopper cette réaction par ajout d'un excès de nitrite (200 mg de $NaNO_2$) par rapport à l'hydrazinium. L'acide nitreux réoxyde le fer(II) et très lentement Np(IV) en Np(V): on a donc intérêt à ajouter le nitrite de sodium assez rapidement après l'ajout du nitrate d'hydrazinium (0,5—1 min) pour éviter la formation de Np(IV). L'inconvénient de ce procédé réside dans la violence de la réaction du nitrite avec le nitrate d'hydrazinium: l'ajout doit être effectué avec précaution dans la solution placée dans un bécher et non dans une fiole pour éliminer les risques de débordement. Il faut attendre que le dégagement gazeux cesse, même sous agitation, ce qui demande quelques minutes, avant d'ajuster le volume, et faire attention à ce qu'il ne se forme pas de microbulles sur les parois de la cuve de mesure. Moyennant ces précautions, la méthode est tout à fait satisfaisante.

Cas de solutions renfermant du neptunium(IV). Outre la diminution de l'absorbance à 981 nm, la présence de Np(IV) se traduit par une déformation du pied du pic vers les courtes longueurs d'onde, son spectre d'absorption comportant 3 pics de faible sensibilité ($\epsilon \leqslant 40$ l mol^{-1} cm^{-1}) dans la zone 935—975 nm. On a vu précédemment qu'il suffisait d'ajouter du nitrite de sodium et d'attendre. Il est toutefois plus rapide d'ajouter du cérium(IV) en excès (1 ml à la concentration 0,1 M), puis, après avoir laissé réagir environ 5 min, le nitrate d'hydrazinium en quantité habituelle. Si des éléments suceptibles de provoquer la réduction du neptunium au degré d'oxydation(IV) sont présents, il faut ensuite ajouter du nitrite de sodium.

Nous proposons, dans le cas où la composition de la solution est mal connue, d'effectuer le cycle de valence complet (cérium(IV)—hydrazinium—

nitrite) qui, malgré les inconvénients signalés (formation de bulles), est rapide et sûr.

Cas de solutions contenant des ions sulfate. Lorsque la solution contient des ions sulfate, il n'est pas possible de les éliminer par évaporation. Dans ce cas, nous préférons ajuster leur concentration à 0,5 M. L'étalonnage effectué en milieu H_2SO_4 0,5 M montre que le coefficient d'absorption molaire n'est que peu affecté: 387 l mol^{-1} cm^{-1} au lieu de 403 l mol^{-1} cm^{-1} en milieu nitrique molaire. Dans ce milieu, cependant, l'influence d'éléments tiers susceptibles de réduire le neptunium(V) est renforcée par la complexation du neptunium(IV) et celui-ci est encore plus difficile à réoxyder par le nitrite: le cycle de valence complet sera plus souvent nécessaire. En outre, le sulfate d'hydrazinium est peu soluble: nous le remplaçons par le chlorure d'hydroxylammonium, aussi efficace dans ce milieu (les ions chlorure n'ont aucune influence à ce niveau de concentration).

Résultats

En utilisant une cuve de 1 cm de parcours optique, il est possible de doser le neptunium à des concentrations comprises entre 2 mg l^{-1} et 1 g l^{-1} dans la cuve avec une incertitude de ±2,5 mg l^{-1} pour une seule détermination en bas de gamme et de ±1% au niveau de 350 mg l^{-1} (avec un spectrophotomètre Cary 17).

Nous avons signalé plus haut l'influence du fer. Parmi les autres éléments susceptibles d'accompagner le neptunium, il nous faut mentionner spécialement l'uranium et le plutonium.

Influence de l'uranium. Des auteurs ont signalé l'existence de complexes intercationiques entre NpO_2^+ et certains cations [2—5] dont UO_2^{2+}. La concentration du neptunium au moment des mesures spectrophotométriques varie de 10^{-5} à quelques 10^{-3} M, celle de l'uranium ne dépasse jamais 10^{-1} M pour ne pas modifier trop la concentration des anions. Dans ces conditions, nous n'avons jamais pu mettre en évidence le complexe en question. En revanche, nous avons constaté que l'uranium catalysait la réduction du neptunium(V): le pic diminue et nous observons un accroissement de l'absorbance dans la zone 930—970 nm. Comme dans le cas du fer, l'addition de nitrite stoppe cette évolution et ramène quantitativement le neptunium au degré d'oxydation (V). Le mécanisme de cette réduction n'est pas éclairci: il pourrait s'agir d'une réduction photochimique de l'uranium en uranium(IV) qui, au lieu de se réoxyder par action de l'oxygène dissous ou de l'acide nitrique, réduirait le neptunium(V). Nous nous proposons de vérifier cette hypothèse. Moyennant l'ajout de nitrite, il est possible de doser le neptunium en présence d'uranium dans un rapport $U/Np \leqslant 10^3$.

Influence du plutonium. Le plutonium(VI) constitue l'une des rares véritables interférences de la méthode: son spectre (Fig. 1) présente un pic tout à fait similaire à celui du neptunium, centré à 981 nm. Son influence peut être déduite de la mesure de son pic d'absorbance situé à 831 nm [6] ou plus simplement de celui qui est centré à 950 nm et auquel correspond

un coefficient d'absorption molaire identique à celui que l'on observe à 981 nm: 32 l mol^{-1} cm^{-1} en milieu nitrique molaire. Le plutonium(VI) est réduit lentement par le nitrate d'hydrazinium jusqu'en plutonium(III) (Fig. 2) et il est possible d'avoir une proportion importante du plutonium à ce degré d'oxydation sans que le neptunium(V) soit réduit. Les plutonium(III) et (IV) absorbent également dans la zone de longueurs d'onde qui nous intéresse (Fig. 3): leur présence rend plus difficile la mesure précise de l'absorbance du neptunium mais ne constitue pas une interférence au sens strict du terme. Cependant, le plutonium(III) est susceptible de réduire lentement le neptunium(V) en (IV): cette réduction est plus rapide en milieu sulfurique. L'addition de nitrite stoppe cette réaction et réoxyde lentement Pu(III) et Np(IV). Il faut noter que si le plutonium(VI) n'est pas totalement réduit au moment de l'ajout de nitrite, celui-ci le réduit mais très lentement, il faut alors attendre que sa décroissance soit suffisante pour permettre le dosage du neptunium avec une précision suffisante. En présence de grandes quantités de ^{238}Pu, il devient impossible d'obtenir quantitativement Np(V) sans ajout de nitrite. La réduction rapide en Np(IV) est sans doute liée à l'action simultanée de l'hydrazinium et du peroxyde d'hydrogène formé par radiolyse: nous utilisons un tel mélange pour obtenir, par ailleurs, quantitativement Np(IV) en milieu nitrique. L'ajout de nitrite, en revanche, rend possible le dosage même en milieu sulfurique (Fig. 4) et nous avons pu doser (1000 ± 500) ppm de neptunium dans du plutonium-238, sans

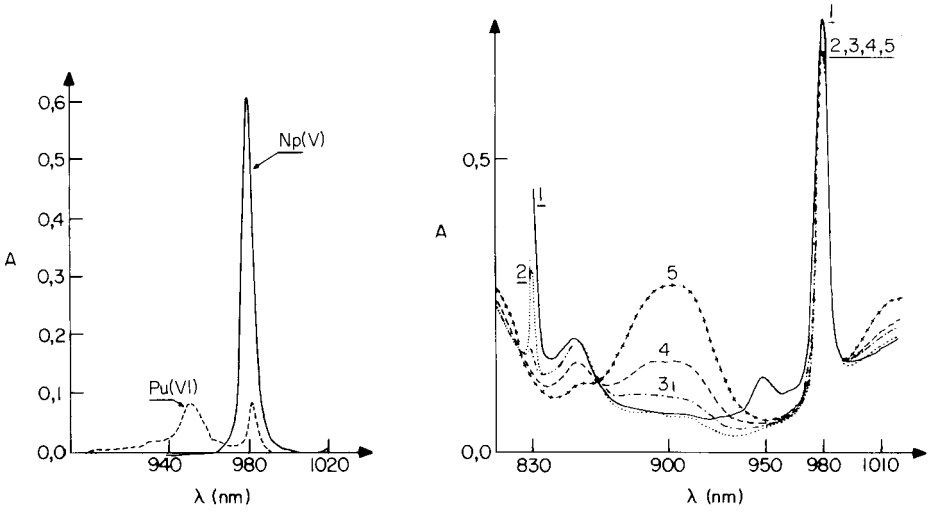

Fig. 1. Spectres d'absorption en milieu HNO_3 1 M de: (——) Np(V) 0,352 g l^{-1}; (----) Pu(VI) 0,65 g l^{-1}.

Fig. 2. Evolution en fonction du temps écoulé après ajout du nitrate d'hydrazinium d'une solution HNO_3 1 M de Np (0,352 g l^{-1}) et de Pu (4,19 g l^{-1}), en l'absence de nitrite. Temps écoulé: (1) 20 min; (2) 3 h; (3) 3.8 h; (4) 5.25 h; (5) 18 h.

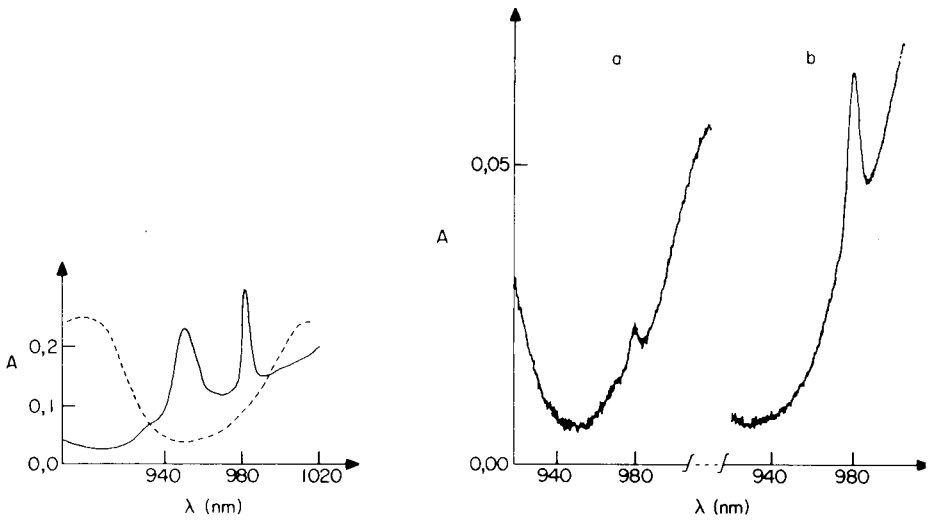

Fig. 3. Spectres d'absorption en milieu HNO_3 1 M de Pu (4,19 g l^{-1}): (—) Pu(VI) + (IV); (----) Pu(IV) + (III).

Fig. 4. Dosage de Np dans une solution de ^{238}Pu (Pu/Np = 150). (a) Milieu HNO_3 0,8 M—H_2SO_4 0,1 M; NO_2Na ajouté 15 h après le nitrate d'hydrazinium; Np = 7,5 mg l^{-1} (environ 60% en Np(IV)). (b) Milieu H_2SO_4 0,5 M; NO_2Na ajouté 1 min après l'hydrazinium; Np = 15 mg l^{-1}.

séparation. Des essais synthétiques nous ont montré que, en présence de plutonium à 1,45 g l^{-1}, on pouvait doser 13 mg l^{-1} de neptunium avec une incertitude voisine de 20% et évaluer à environ 1 mg l^{-1} la présence de neptunium réellement introduit à la concentration de 1,35 mg l^{-1}.

Lorsque le neptunium à doser est initialement en présence de plutonium(III), il est plus rapide et plus sûr de procéder à un cycle de valence complet, comprenant l'oxydation par le cérium(IV). Si des réducteurs tels que l'hydrazinium ou l'hydroxylammonium sont présents en quantité notable, il peut être utile de les détruire par ajout de nitrite et d'éliminer l'excès de celui-par ébullition avant de procéder au cycle de valence.

Conclusions

Peu soumise à interférence, cette méthode est applicable en présence de nombreux éléments sans séparation, moyennant un cycle de valence complet (cérium(IV)—hydrazinium—nitrite). En l'absence d'éléments susceptibles de favoriser la réduction en Np(IV), nous préconisons cependant de ne pas ajouter le nitrite qui peut provoquer la formation de bulles dans la cuve de spectrophotométrie. Nous avons appliqué également cette méthode au dosage du neptunium dans le mélange tributyl phosphate—dodécane: le neptunium est réextrait quantitativement en phase aqueuse par trois mises en équilibre successives, volume à volume, avec de l'acide sulfurique 0,5 M

et dosé directement dans ce milieu. Dans ce cas, l'oxydation par le cérium(IV) est indispensable. Relayée vers les faibles concentrations par la polarographie différentielle à impulsions [7], cette méthode permet à l'analyste d'effectuer le dosage du neptunium dans une large gamme de concentration et dans des matrices variées. Associé à une méthode de séparation qui fera l'objet d'une publication ultérieure, l'ensemble de ces deux méthodes permet de répondre à presque tous les besoins liés au retraitement des combustibles nucléaires.

Nous tenons à remercier ici Mme. Monette Hucleux qui avait commencé cette étude et M. Pierre Decambox qui a réalisé la plupart des mesures utilisées dans ce travail.

BIBLIOGRAPHIE

1 P. Cauchetier, C. Guichard et M. Hucleux, IAEA-SM-149/53, Vienne, 1972.
2 J. C. Sullivan, J. C. Hindman et A. J. Zielen, J. Am. Chem. Soc., 83 (1961) 3373.
3 J. C. Sullivan, J. Am. Chem. Soc., 84 (1962) 4256.
4 J. C. Sullivan, Inorg. Chem., 3 (3) (1964) 315.
5 C. Madic, B. Guillaume, J. C. Morisseau et J. P. Moulin, J. Inorg. Nucl. Chem., 41 (1979) 1027.
6 M. Hucleux et P. Cauchetier, Note CEA N-1551, 1972.
7 P. Cauchetier, J. Radioanal. Chem., 51 (1979) 225.

Analytica Chimica Acta, 124 (1981) 449—452

Short Communication

DOSAGE SPECTROPHOTOMETRIQUE DU PLUTONIUM APRES OXYDATION PAR LE CERIUM(IV)

P. CAUCHETIER

DCAEA/SEACC, Centre d'Etudes Nucléaires, BP 6, F-92260 Fontenay-aux-Roses (France)

(Reçu le 1 septembre 1980)

Summary. (Spectrophotometric determination of plutonium after oxidation with cerium (IV)). Plutonium is frequently determined by measuring the absorption peak of Pu(VI) at 831 nm. To facilitate automation, replacement of the usual silver(II) oxide by cerium(IV) is suggested. Oxidation is complete in less than 15 min at room temperature in 4 M nitric acid medium. Polymerized plutonium is quantitatively oxidized in 3.5 h.

Résumé. Le dosage basé sur la mesure du pic d'absorption de Pu(VI) à 831 nm est largement utilisé. Pour en faciliter l'automatisation, nous proposons de remplacer l'addition d'oxyde d'argent(II) par celle de cérium(IV). L'oxydation est complète à froid, en milieu nitrique 4 M en moins de 15 min. Le plutonium polymérisé est quantitativement oxydé en 3.5 h.

L'utilisation du pic d'absorption propre de l'ion PuO_2^{2+} à 831 nm pour doser le plutonium est très répandue, notamment dans les usines de traitement des combustibles irradiés. Cette méthode à la fois sensible et spécifique a l'advantage de générer peu d'effluents. Le mode opératoire et les caractéristiques de la méthode ont fait l'objet déjà de plusieurs publications [1—4].

Inconvénients de l'emploi d'oxyde d'argent(II)

L'oxydation du plutonium est effectuée par ajout d'un excès d'oxyde d'argent(II) qui est ensuite détruit par chauffage. Cette façon d'opérer complique l'automatisation de la méthode. En effet, l'oxyde d'argent(II) ne peut être introduit que sous forme solide car il est instable en solution. Il est cependant possible d'en préparer des pastilles compactées facilitant la séquence correspondante de l'automate. La destruction de l'excès d'oxydant par chauffage est d'autant plus délicate à automatiser qu'il faut prévoir un refroidissement reproductible de la solution par la suite, compte tenu de l'influence très importante de la température sur la valeur du coefficient d'absorption molaire [4]. Cette étape nécessite soit des délais très longs, soit une thermorégulation.

Plusieurs laboratoires ont proposé de remplacer cette destruction à chaud par l'ajout, à froid, d'une solution d'acide sulfamique. Il est en effet possible de détruire ainsi suffisamment quantitativement l'excès d'oxydant pour obtenir une solution limpide et permettre le dosage. Toutefois, les essais que

nous avons effectués montrent que si l'ajout d'acide sulfamique est trop important, la mesure est entachée d'une erreur négative (de l'ordre du pour-cent pour un ajout d'une millimole dans la fiole de 25 ml) et décroît lentement dans le temps. Il semblerait que l'acide sulfamique réduise lentement le plutonium(VI): en l'absence d'oxydant en excès (oxydation par l'acide perchlorique à fumées blanches) le phénomène est encore plus prononcé, alors qu'il est pratiquement inexistant en présence de cérium(IV).

Choix d'un autre oxydant

Ces constatations nous ont incité à rechercher un oxydant suffisamment stable en solution pour être introduit sous cette forme et dont l'excès ne soit pas gênant pour la spectrophotométrie du plutonium(VI). De ce point de vue, le cérium(IV) paraissait intéressant. Les solutions nitriques de cérium(III) et de cérium(IV) n'absorbent pas au-dessus de 450 nm. Il a été proposé par plusieurs auteurs pour oxyder quantitativement le plutonium à l'état hexavalent en milieu nitrique 1 M [5, 6]. Comme l'ont montré MacDonald et Savage [6], cette oxydation est d'autant plus lente et difficile que la concentration de l'acide nitrique est plus élevée en raison de la complexation de l'ion Pu^{4+}. La spectrophotométrie étant effectuée en milieu nitrique 4 M, nous avons choisi d'opérer avec la solution de cérium la plus concentrée possible, tout en maintenant l'apport des ions nitrate à 4 mmol ml^{-1} en raison de leur influence sur la valeur du coefficient d'absorption molaire du plutonium(VI) [4]. Pour éviter l'hydrolyse du cérium(IV) et celle du plutonium (IV) au moment de l'introduction de la solution oxydante, nous nous sommes imposé de maintenir l'acidité libre de celle-ci à la concentration 0,5 M, ce qui limite la concentration du cérium(IV) à 0,58 M, le sel utilisé étant l'hexanitrate de cérium(IV) et d'ammonium. Dans un rapport publié pendant que nous faisions cette étude, Savage et Cook [7] ont proposé une méthode similaire dans son principe, mais un peu différente en ce qui concerne les conditions opératoires.

Partie expérimentale

La solution oxydante est obtenue en dissolvant 31,98 g de $(NH_4)_2Ce(NO_3)_6$ (Merck pour analyse) dans 50 ml d'acide nitrique 1 M, puis en complétant à 100 ml avec de l'eau.

A la prise d'essai préalablement mise en milieu nitrique 4 M, on ajoute 2 ml de la solution oxydante et complète au volume désiré (25 ml par exemple) avec de l'acide nitrique 4 M.

La mesure spectrophotométrique est effectuée à l'aide d'un spectrophotomètre Cary 17, adapté à une boîte à gants et équipé d'un photomultiplicateur Hamamatsu R928S. Les mesures sont interprétées en utilisant l'étalonnage obtenu par oxydation à l'argent(II).

Résultats

Ce mode opératoire a été appliqué, parallèlement au mode opératoire utilisant l'oxyde d'argent(II), à des solutions pures et à des échantillons

réels, dont un provenant d'un combustible irradié de réacteur à eau séparé de la majeure partie des produits de fission par coextraction de U et Pu par le tributyl phosphate. Les essais ont porté sur des prises d'essai contenant jusqu'à environ 11 mg de plutonium (soit environ une absorbance de 0,8 pour une fiole de 25 ml et un parcours optique de 1 cm). Nous n'avons pas observé de différence significative entre les deux méthodes.

L'oxydation n'est pas instantanée. Par exemple, pour 6,6 mg de plutonium initialement totalement sous forme de Pu(IV), elle n'est complète que 10 min environ après l'ajout de cérium. Avec des rapports molaires Ce/Pu tels que ceux que nous avons utilisés (>20), l'oxydation est quantitative en moins de 15 min.

Nous avons appliqué également cette méthode à 2 ml d'une solution de plutonium à 3,46 g l^{-1} presque entièrement sous forme de polymère, en milieu nitrique 0,2 M: sa concentration est connue par titrage volumétrique de la solution mère qui a servi à préparer le polymère [8]. Cette solution parfaitement limpide, dont le spectre d'absorption tout à fait similaire à celui qui est attribué à cette espèce [9] est représenté sur la Fig. 1, se trouble lors de la mise en milieu nitrique 4 M. Après ajout du cérium(IV), elle ne redevient limpide qu'au bout de 30 min, alors qu'avec le mode opératoire habituel, elle redevient limpide dès la destruction de l'excès d'oxyde d'argent (II). La hauteur du pic de Pu(VI) croît avec le temps pour se stabiliser au bout de 3.5 h. La mesure correspond alors à une concentration de la solution analysée de 3,46 g l^{-1}. Par oxydation avec l'oxyde d'argent(II), la mesure effectuée après un temps de refroidissement à l'air de 4 h correspond à 3,40 g l^{-1}.

Conclusions

La modification proposée simplifie le mode opératoire qui se résume au mélange de la prise d'essai avec une autre solution et ajustage du volume. L'attente nécessaire (15 min en général) reste raisonnable et est en tout cas

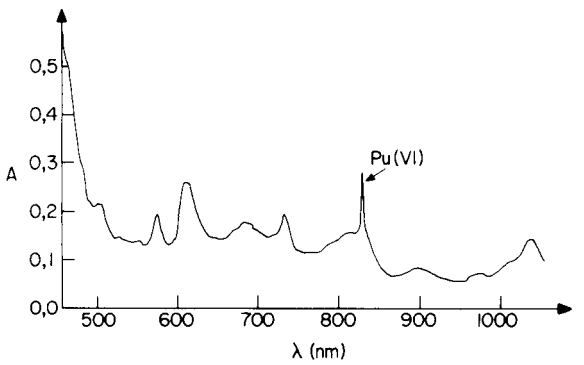

Fig. 1. Spectre d'absorption de la solution de plutonium polymérisé. [Pu] = 3,46 g l^{-1}; [Pu(VI)] = 50 mg l^{-1}.

plus courte que le temps nécessaire à la destruction à chaud de l'oxyde d'argent(II) et au refroidissement. En outre, elle est plus sûre compte tenu de l'influence de la température.

La méthode reste valable pour doser le plutonium polymérisé bien que le temps nécessaire à l'obtention d'une oxydation quantitative soit plus long. Elle n'est probablement pas utilisable cependant telle quelle dans des matrices aussi variées qu'avec l'utilisation de l'oxyde d'argent(II). La présence de réducteurs en forte concentration nécessitera d'augmenter l'ajout de cérium(IV). La présence d'anions complexants tels que sulfate interdira sans doute l'oxydation quantitative [5], alors qu'elle est possible par l'oxyde d'argent(II) [4].

Nous tenons à remercier ici M. Pierre Decambox qui a affectué les manipulations nécessaires à cette étude et M. Claude Guichard qui nous a fourni la solution de plutonium polymérisé.

BIBLIOGRAPHIE

1 M. Hucleux et R. Mollet, Note CEA N-969, 1968, p. 6.
2 K. Buijs, B. Chavane de Dalmassy et M. J. Maurice, Anal. Chim. Acta, 43 (1968) 409.
3 M. Hucleux et P. Cauchetier Note CEA N-1551, 1972.
4 P. Cauchetier, Analusis, 8 (1980) 336.
5 G. Phillips et D. Crossley, IAEA — SM 231/56, 1978.
6 A. MacDonald et D. J. Savage, IAEA — SM 231/52, 1978.
7 D. J. Savage et N. D. Cook, Rapport ND-R-309(D), 1979.
8 C. Guichard, communication privée, publication en préparation.
9 J. C. Hindman, dans G. T. Seaborg et J. J. Katz (Eds.), The Actinide Elements, NNES, Division IV — 14A, McGraw-Hill, New York, 1954.

ANALYTICA CHIMICA ACTA, Vol. 124 (1981)

AUTHOR INDEX

ACA announcements

BIOCHEMICAL ANALYSIS 1982 PRIZE

The German Society for Clinical Chemistry awards the prize BIOCHEMICAL ANALYSIS every two years at the conference "Biochemische Analytik" in Munich.

The prize of DM 10.000,– is donated by BOEHRINGER Mannheim GmbH for outstanding and novel work in the field of biochemical analysis or biochemical instrumentation or for significant contributions to the advancement of experimental biology especially relating to clinical biochemistry. Competitors for the prize 1982 (conference 27–30th of April 1982) should submit papers concerning one theme, either published or accepted for publication between October 1st 1979 and September 30th 1981, in triplicate before November 15th 1981 to: Prof. Dr. Dr. I. Trautschold, Secretary of the prize BIOCHEMICAL ANALYSIS, Medizinische Hochschule Hannover, Karl-Wiechert-Allee 9, 3000 Hannover 61, G.F.R.

ANNOUNCEMENTS OF MEETINGS

34th CHEMISTS' CONFERENCE, SCARBOROUGH, GREAT BRITAIN

The 34th Chemists' Conference will be held at the Royal Hotel, Scarborough, England, on 9–11th June 1981. An exhibition of scientific equipment will run concurrently with the Conference, which is devoted solely to analytical problems in the steel industry.

Further information from: J. Davey, Teesside Laboratories, British Steel Corporation, P.O. Box 11, Grangetown, Middlesbrough, Cleveland TS6 6UB, Great Britain.

1982 WINTER CONFERENCE ON PLASMA SPECTROCHEMISTRY, ORLANDO, FLORIDA JANUARY 4–9, 1982

A Winter Conference featuring developments in atomic plasma spectrochemical analyses with inductively-coupled plasma, d.c. plasma and microwave plasma excitation sources will be held on January 4–9, 1982 Orlando, FL. Papers describing original work on applications, fundamentals and instrumentation developments with atomic plasmas are solicited as lectures or posters. General sessions and special symposia will be organized by internationally recognized experts. Round table discussions, manufacturer's seminars, and a plasma film festival will be featured.

Further information from: 1982 Winter Conference, c/o ICP Information Newsletter, Chemistry –GRC Towers, University of Massachusetts, Amherst, MA 01003, U.S.A.

SECOND INTERNATIONAL WORKSHOP ON TRACE ELEMENT ANALYTICAL CHEMISTRY IN MEDICINE AND BIOLOGY, NEUHERBERG NEAR MUNICH, 21–23 APRIL, 1982

This workshop is intended to guarantee effective exchange of views between analytical and biomedical specialists. It is hoped that the workshop will lead to a productive scientific dialogue between these two groups in regard to the biomedical applications of trace element analytical rssearch. The general theme will be "Essential, Toxic and Analytical Aspects of Trace Elements". Invited papers and short contributed papers will be presented.

Further information from: Dr. P. Schramel, Gesellschaft fuer Strahlen- und Umweltforschung, Institut fuer Angewandte Physik, Physikalisch-Technische Abteilung, Ingolstaedter Landstrasse 1, D-8042 Neuherberg, G.F.R.

CALENDAR OF FORTHCOMING MEETINGS

April 22–24, 1981 Noordwijkerhout, The Netherlands	**Joint NL – UK Symposium on Quantitative Organic Analysis** Contact: Dr. B. Griepink, Secretary of Analytical Chemistry Section of the Royal Netherlands Chemical Society, c/o Analytical Chemistry Laboratory, Croesestraat 77A, 3522 AD Utrecht, The Netherlands. (Further details published in Vol. 118, No. 2)
Apr. 26–May 1, 1981 Singapore, Republic of Singapore	**1st Asian & Pacific Chemistry Congress** Contact: The Congress Secretary, 1st ASPAC Congress, c/o Singapore Professional Centre, 129 B, Block 23, Outram Park, Singapore 0316, Republic of Singapore.
May 3–7, 1981 Hindenlang, (Bavarian Alps), F.R.G.	**4th International Symposium on Capillary Chromatography** Contact: Dr. J. Rijks, Laboratory of Instrumental Analysis, University of Technology, P.O. Box 513, NL–5600 MB Eindhoven, The Netherlands.
May 5–8, 1981 Gatlinburg, TN, U.S.A.	**Separation Science and Technology for Energy Applications** Contact: A.P. Malinauskas, Oak Ridge National Laboratory, P.O. Box X, Oak Ridge, TN 37830, U.S.A.
May 11–15, 1981 Avignon, France	**Vth International Symposium on Column Liquid Chromatography** Contact: Prof. G. Guiochon, Ecole Polytechnique, Laboratoire de Chimie Analytique Physique, Route de Saclay, 91128 Palaiseau Cedex, France. (Further details published in Vol. 118, No. 1)
May 18–20, 1981 Jekyll Island, Georgia, U.S.A.	**11th Annual Symposium on the Analytical Chemistry of Pollutants** Contact: Prof. Dr. Roland W. Frei, The Free University, De Boelelaan 1083, 1081 HV Amsterdam, The Netherlands.
May 20–22, 1981 Eger, Hungary	**Symposium on the Analysis of Steroids** Contact: Prof. S. Görög, c/o Hungarian Chemical Society, 1061 Budapest VI., Anker köz 1, Hungary.
June 1–5, 1981 Stresa, Lago Maggiore, Italy	**2nd European Symposium on Organic Chemistry** Contact: Prof. Giorgio Modena, Istituto di Chimica Organica, Via Marzolo, 1, 35100 Padova, Italy.
June 9–11, 1981 Scarborough, Great Britain	**The 34th Chemists' Conference** Contact: J. Davey, Teesside Laboratories, British Steel Corporation, P.O. Box 11, Grangetown, Middlesbrough, Cleveland TS6 6UB, Great Britain
June 16–17, 1981 Venice, Italy	**1st International Symposium on Chromatography in Biochemistry, Medicine and Environmental Research** Contact: Dr. A. Frigerio, Italian Group for Mass Spectrometry in Biochemistry and Medicine, c/o Istituto di Ricerche Farmacologiche "Mario Negri", Via Eritrea 62, 20157 Milan, Italy. Tel: 35.54.546.
June 18–19, 1981 Venice, Italy	**8th International Symposium on Mass Spectrometry in Biochemistry, Medicine and Environmental Research** Contact: Dr. A. Frigerio, Italian Group for Mass Spectrometry in Biochemistry and Medicine, c/o Istituto di Ricerche Farmacologiche "Mario Negri" Via Eritrea 62 20157 Milan, Italy. Tel: 35.54.546.
June 22–26, 1981 Veldhoven, The Netherlands	**4th International Symposium on Affinity Chromatography and Related Techniques** Contact: Dr. T.C.J. Gribnau, Organon Scientific Development Group, P.O. Box 20, 5340 BH Oss, The Netherlands. (Further details published in Vol. 118, No. 1)

June 23–27, 1981 Karl–Marx–Stadt, G.D.R.	**Tagung Festkorperanalytik** Contact: Dr. K. Danzer, Technische Hochschule, Karl–Marx–Stadt, Sektion Chemie und Werkstofftechnik, PSF 964, 9010 Karl–Marx–Stadt, G.D.R. (Further details published in Vol. 118, No. 2)
July 5–10, 1981 Swansea, Wales	**The Third Swansea Summer School of Automatic Chemical Analysis** Contact: Prof. D. Betteridge, Department of Chemistry, University College of Swansea, Singleton Park, Swansea SA2 8PP, Great Britain.
July 6–9, 1981 Strasbourg, France	**27th IUPAC Symposium on Macromolecules** Contact: Secretariat, Macro 1981, Société de Chimie Industrielle, 28, rue Saint-Dominique, 75007 Paris, France.
July 12–17, 1981 Exeter, Great Britain	**5th International Conference on NMR Spectroscopy** Contact: Dr. J.F. Gribnau, Royal Chemical Society, Burlington House, London W1V 0BN, Great Britain.
July 28–31, 1981 New Hampton, NH, U.S.A.	**30th Anniversary Meeting of the Gordon Research Conference on Statistics in Chemistry and Chemical Engineering** Contact: Dr. Alexander M. Cruickshank, Director, Gordon Research Conferences, Pastore Chemical Laboratory, University of Rhode Island, Kingston, RI 02881, U.S.A. Tel. (401) 783–4011.
Aug. 3–7, 1981 Denver, CO, U.S.A.	**30th Denver Conference on Applications of X-Ray Analysis** Contact: Mrs. Mildred Cain, Denver Research Institute, University of Denver, Denver, CO 80208, U.S.A. Tel: (303) 753–2141.
Aug. 16–21, 1981 Vancouver, Canada	**28th Congress International Union of Pure and Applied Chemistry** Contact: Congress Secretariat, 28th IUPAC Congress, c/o The Chemical Institute of Canada, 151, Slater Street, Suite 906, Ottawa, Ontario, Canada K1P 5H3.
Aug. 16–21, 1981 Helsinki, Finland	**Symposium on Harmonisation of Collaborative Analytical Studies** Contact: Dr. H. Egan, Laboratory of the Government Chemist, Cornwall House, Stamford Street, London SE1 9NQ, Great Britain.
Aug. 23–28, 1981 University of Auckland, New Zealand	**Golden Jubilee Conference "Chemistry in the Service of Man"** Contact: Dr. D.J. McLennan, Chemistry Dept., Univ. of Auckland, Auckland, New Zealand.
Aug. 23–28, 1981 Espoo, Finland	**Euroanalysis IV – Triennal Conference of the Federation of European Chemical Societies** Contact: Professor L. Niinistoe, Department of Chemistry, Helsinki University of Technology, SF–02150 Espoo 15, Finland. (Further details published in Vol. 109, No. 1)
Aug. 23–28, 1981 Canberra, Australia	**Sixth Australian Symposium on Analytical Chemistry** Contact: Hon. Secretary, Miss B.J. Stevenson, P.O. Box 1397, Canberra City, A.C.T. 2601, Australia.
Aug. 23–28, 1981 New York, NY, U.S.A.	**National American Chemical Society Meeting** Contact: American Chemical Society, 1155 Sixteenth Street, NW, Washington, DC 20036, U.S.A.
Aug. 30–Sep. 5, 1981 Vienna, Austria	**XI International Congress of Clinical Chemistry – IV European Congress of Clinical Chemistry** Contact: Congress Secretariat, Interconvention, P.O. Box 35, A-1095 Vienna, Austria. Tel. (0222) 42 13 52.
Sep. 1–4, 1981 Siofok, Hungary	**3rd Danube Symposium on Chromatography** Contact: Hungarian Chemical Society, H–1368 Budapest, P.O.B. 240, Hungary. Tel: Budapest 427–343. (Further details published in Vol. 115)

Sep. 1–4, 1981 Aberdeen, Scotland	**ESTA 2 – The Second European Symposium on Thermal Analysis** Contact: Dr. F.P. Glasser, Chairman of the Organising Committee, ESTA 2, Department of Chemistry, University of Aberdeen, Meston Walk, Old Aberdeen, AB9 2UE, Scotland.
Sep. 4–8, 1981 Tokyo, Japan	**9th International Conference on Atomic Spectroscopy and XXII Colloquium Spectroscopicum Internationale** Contact: The Japan Society for Analytical Chemistry, 9th ICAS/XXII CSI, Gotanda Sanhaitsu, 26-2 Nishigotanda 1-chome, Shinagawa-ku, Tokyo 141, Japan. (Further details published in Vol. 118, No. 1)
Sept. 20–25, 1981 Philadelphia, PA, U.S.A.	**8th Annual Meeting of the Federation of Analytical Chemistry and Spectroscopy Societies (FACSS)** Contact: Richard J. Knauer, Publicity Chairman, ARMCO INC., P.O. Box 1697, Baltimore, MD 21203, U.S.A.
Sep. 21–24, 1981 Loughborough, England	**Particle Size Analysis Conference** Contact: P.J. Lloyd, PSA 81 Conference, Particle Technology Group, Chemical Engineering Department, University of Technology, Loughborough, Leics. LE11 3TU, Great Britain. (Further details published in Vol. 120)
Sep. 22–25, 1981 Leipzig, G.D.R.	**Analytiktreffen 1981 – Strukturanalytische Methoden in der Stereochemie** Contact: Sektion Chemie der KMU Leipzig, Liebigstrasse 18, DDR–7010 Leipzig, G.D.R.
Sep. 28–Oct. 1, 1981 Barcelona, Spain	**16th International Symposium on Advances in Chromatography** Contact: Professor A. Zlatkis, Chemistry Department, University of Houston, Houston, Texas 77004, U.S.A.
Sep. 29–Oct. 2, 1981 Basle, Switzerland	**ILMAC'81 – 8th International Exhibition of Laboratory, Chemical Engineering, Measurement and Automation Techniques in Chemistry** Contact: D. Gammeter, Secretariat, ILMAC '81, Postfach, CH–4021 Basle, Switzerland. Tel: 061–2620 20.
Oct. 12–15, 1981 Houston, TX, U.S.A.	**"EXPOCHEM '81"** Contact: Dr. A. Zlatkis, Chemistry Department, University of Houston, Houston, TX 77004, U.S.A. Tel. (713) 749–2623.
Oct. 22–23, 1981 Montreux, Switzerland	**Workshop on Liquid Chromatography – Mass Spectroscopy** Contact: Prof. Dr. R.W. Frei, Free University, Department of Analytical Chemistry, De Boelelaan 1083, 1081 HV Amsterdam, The Netherlands
Nov. 23–25, 1981 Barcelona, Spain	**2nd International Congress on Analytical Techniques in Environmental Chemistry** Contact: Dr. J. Albaigés, General Secretary, Plaza de Espana, Barcelona–4, Spain. Tel: 223–31 01.
Dec. 2–3, 1981 Paris, France	**Journées de Chromatographie en Phase Liquide** Contact: H. Colin, Laboratoire C.A.P., Ecole Polytechnique, Route de Saclay, 91128 Palaiseau Cedex, France.
Jan. 4–9, 1982 Orlando, FL, U.S.A.	**1982 Winter Conference on Plasma Spectrochemistry** Contact: 1982 Winter Conference, c/o ICP Information Newsletter, Chemistry -GRC Towers, University of Massachusetts, Amherst, MA 01003, U.S.A. Tel. (413) 545–2294.
March 28–April 2, 1982 Las Vegas, NV, U.S.A.	**National American Chemical Society Meeting** Contact: A.T. Winstead, American Chemical Society, 1155 Sixteenth Street, NW, Washington, DC 20036, U.S.A.

ontinued from outside of cover)

hort Communications

Printed in The Netherlands

CONTENTS

(continued on inside page of cover)